Modelling the Effects of Fuel Types and Ventilation Openings on Post-Flashover Compartment Fires

---

A thesis
submitted in partial fulfilment
of the requirements for the Degree
of

Doctor of Philosophy in Fire Engineering

in the
University of Canterbury

by
Ee Hieng Yii

University of Canterbury
Christchurch, New Zealand
2002

ABSTRACT

This thesis describes the details used to model a post-flashover fire compartment as a well-stirred reactor. In particular, it examines the two foremost important variables that dictate post-flashover fire behaviour inside the fire compartment. These two variables are: (1) the mass flow rate of air into the compartment via the vent opening and (2) the fuel mass loss rate inside the compartment.

The vent flow analysis shows that the orifice analogy typically used to describe compartment vent flow is restricted to small wall opening applications. For large wall openings, such as a window occupying one whole wall, the flow rate is dictated by the plume entrainment with a flow rate ~60% of the flow rate estimated from the orifice theory.

A series of fire experiments using a reduced-scale compartment were conducted to study the vent flow behaviour in a compartment with a horizontal roof opening and a vertical wall opening. Based on the analytical and experimental studies, it is shown that in the case where the roof vent opening is not excessively large and a wall opening having a small downstand, the neutral-plane exists below the soffit of the wall opening giving outflow and inflow through the wall opening and outflow through the roof opening. In such a case, the flows through these openings can be adequately described using an extended form of the vent flow formulation that includes the roof vent opening. The area of the roof vent and the depth of the downstand between the ceiling and the soffit of the wall opening are found to be significant in determining the extra air inflow induced due to the existence of the roof vent opening.

The cellulosic and pool fuels each have different burning behaviour inside a compartment. However, compartment fire temperatures and fuel mass loss rates, from both fuel types, are strongly dependent on the available fuel surface area to ventilation opening ratio and the fuel surface to enclosure area ratio. In the case of thermoplastic

pool fires, the ratio between the heat of combustion of air for the fuel and the heat of gasification of the fuel is also found to be influential on the resulting fires.

A post-flashover fire computer program, CFIRE, has been developed that incorporates these findings. The simulation studies performed using the CFIRE computer program show that the fire time-temperature histories of wood fires are highly dependent on the remaining fuel surface area over time. In the case of thin wood, a shorter and hotter fire is expected as it has greater surface area than thick wood, even with the same fuel load. The study also shows that for small ventilation opening, a pool fire inside a fire compartment is less severe than a wood fire because the thermoplastic fuel is easily vaporised under the radiation feedback from the hot surrounding environment and discharged outside the compartment. In the case of large openings, pool fires are more likely to produce a hotter fire in the compartment than wood fires because wood fuel would not have sufficient fuel surface area to achieve ventilation controlled burning.

By comparing these simulated fires with the Eurocode parametric fires, the Eurocode parametric fires do not provide realistic decay rate. With the modified parametric fires, these fires are conservative as they provide envelopes for the simulated fire curves. However, these parametric fires do not clearly describe the fire behaviour of realistic furnishing inside the fire compartment.

ACKNOWLEDGEMENTS

The research presented in this thesis was conducted under the supervision of Associate Professor Andy Buchanan. I wish to sincerely thank Professor Buchanan for giving me the opportunity to work with him and his dedication, encouragement and support given to this project.

Dr. Charley Fleischmann, the co-supervisor of my project, for his enthusiasm and support given to this project. His advice given to my experimental works was very valuable. To Mike Spearpoint for always being available for discussion and support.

My appreciation to each and every one of the technician and secretary staff, in particular Grant Dunlop for the many hours spent on this project. Thanks to Mike Weaver for his help with the data logging systems, Melody Callahan for her help with graphics. Thanks to Graeme Harris (Mechanical Department) for the help with the wind-tunnel facility.

Special thanks to Dr. Anne Ditcher for her support and effort to proof-read this thesis.

To my past and present office mates, Jason Clement, Tony Enright, Linus Lim and Tony Parkes for their friendships, supports and laughs. To my friend, Ra Cleave, for his help with Matlab. To fellow trampers and climbers from the Canterbury University Tramping Club for the weekend adventures and to past and present postgraduates who have made this whole postgraduate-experience worthwhile.

Financial support from the University of Canterbury Doctoral Scholarship and the funding from the Foundation for Science, Research and Technology (FoRST) are very much appreciated.

Finally, to my parents and brother, for their love, encouragement and support.

TABLE OF CONTENTS

NOMENCLATURE

English Symbols

A_F	Fuel surface area (m^2)
A_T	Total internal area of the enclosure including the vent opening area (m^2)
A_t	Area of the enclosing boundaries subjected to heat transfer (m^2)
A_v	Area of the vertical wall opening (m^2)
$A_{v,roof}$	Area of the horizontal roof opening (m^2)
A_w	Area of the wall containing the vent without the downstand area above the opening (m^2)
B	The Spaulding Mass Transfer Number
b_p	Combustion mixing factor (<1) (-)
C	Coefficient constant for air inflow (Equation (3.9)) (kg s^{-1} $m^{-2.5}$)
C_{calib}	Calibration factor for the velocity probe (-)
C_d	Discharge coefficient of the wall opening including door or window (-)
$C_{d,roof}$	Discharge coefficient of the roof opening (-)
c_p	Specific heat at constant pressure (J/kg-K)
c_v	Specific heat at constant volume (J/kg-K)
D	Characteristic dimension (m)
D_c	Depth of the compartment (m)
E	Total energy content of the fuel (MJ)
e_t	Fuel load per total enclosure surface area (MJ/m^2 total surface area)
F	Shape factor (F=1, 2 and 3 for planes, sticks and cubes respectively)
Fo	Fourier number
Fr	Froude number
Fr_{flood}	Critical Froude number (Equation (7.11))
F_v	Ventilation factor (Equation (12.4))
f_i	Species mass fraction (per unit fuel mass) (g/g)
g	Gravitational constant, 9.81m/s^2

H_c	Height of the compartment (m)
H_s	Height of the soffit evaluated from the floor level (m)
H_v	Height of the vertical wall vent opening (m)
H'	The lower cold layer depth inside the compartment with respect to the sill height (m) (Figure 3.4)
H''	The height distance above the neutral plane to the soffit of the opening (m) (Figure 3.4)
h	Enthalpy of the gas species (J/kg)
h_{crib}	Crib height (m) (Equation (6.15))
h_{fg}	Enthalpy of phase change from liquid to vapour at the known pressure (J/kg)
h_{fire}	Convective heat transfer coefficient of the wall on the fire side (W/m^2-K)
h_{amb}	Convective heat transfer coefficient of the wall on the ambient side (W/m^2-K)
$\Delta h_{c,eff}$	Effective heat of combustion (J/kg)
$\Delta h_{c,i}$	Heat of combustion of incomplete combustion products (J/kg)
$\Delta h_{c,net}$	Net heat of combustion (J/kg)
J	Line plume entrainment constant
K	Dimensionless parameter (Equation (3.20))
K_{WG}	The water-gas reaction equilibrium constant (in Equation (4.10))
k	Thermal conductivity (W/m-K)
k_f	Gas absorptivity (m^{-1})
k_{growth}	T-squared fire growth constant ($s/\sqrt{MW}$) (Equation (11.32)) (k_{growth} =600, 300, 150 and 75 for slow, medium, fast and ultra-fast growth rate respectively)
L_g	Heat of gasification (J/kg)
L_m	Mean beam length (m)
M	Fire load based on wood per total enclosure area (kg/m^2) (Equation (2.21))
m	Mass (kg)
$\dot{m}_{in}$	Mass flow rate of air into the compartment (kg/s)

$\dot{m}_{out}$	Mass flow rate of hot gases out of the compartment (kg/s)
$\dot{m}_p$	Mass loss rate of fuel inside the compartment (kg/s)
P	Pressure (Pa)
ΔP	Pressure difference (Pa)
$\dot{Q}_{FB}$	Heat required to vaporise the unburned fuel per unit time (W)
$\dot{Q}_{FIRE}$	Fire heat release inside the compartment per unit time (W)
$\dot{Q}_G$	Heat loss to heating the volume of gas inside the compartment per unit time (W)
$\dot{Q}_{growth}$	T-squared fire heat release rate (MW) (Equation (11.32))
$\dot{Q}_L$	Convective heat loss rate via the outgoing flue gases per unit time (W)
$\dot{Q}_R$	Radiative heat loss via the opening per unit time (W)
$\dot{Q}_W$	Convective and radiative heat loss to the enclosing boundaries per unit time (W)
$\dot{q}''$	Heat flux (W/m^2)
$\dot{q}''_{rad}$	Radiative heat flux (W/m^2)
R	Radius of the flame cone (m) (Figure 5.2)
Re	Reynolds number
$R_{80\text{-}30}$	The average mass loss over the period when the fuel mass is reduced from 80% to 30% of its original mass (kg/s)
r	Stiochiometric air to fuel mass ratio
r_{ox}	Stiochiometric oxygen to fuel mass ratio
S	Stick clear spacing (m) (Equation (6.15))
s	Fuel-air mass ratio
T_0	Temperature of the ambient air (K)
T_H	Temperature of the hot upper layer (K)
T_g	Fire gas temperature (K)
T_v	Vaporising temperature (K)
T_{wi}	Inside wall surface temperature (K)
T_{wo}	Outside wall surface temperature (K)
t	Time (s)

t_d	Duration of the burning period for Eurocode parametric fire (hour) (Equation (12.5))
t^*	Fictitious time in parametric fire (hour) (Equation (12.2))
u	Internal energy per unit mass (J/kg)
V	Compartment volume (m^3)
v	Velocity (m/s)
v_p	Regression rate of the burning wood (m/s)
W_c	Width of the compartment (m)
W_v	Width of the vertical wall opening (m)
w	Fraction of reradiated energy that goes to the base of the flame cone (Equation (5.30))
Y	Species mass fraction (per unit mass of the outflow) (g/g)
Z_n	Height of the neutral-plane evaluated from the floor level (m)

Greek Symbols

Δ	Distance between the neutral plane and the base of the hot upper layer (m) (Figure 3.4)
Φ	Equivalence ratio
Γ	Modification factor for Eurocode parametric fire (Equation (12.3))
Γ_{DECAY}	Modification factor for modified parametric fire at decay phase (Equation (12.8))
Γ_{DESIGN}	Modification factor for modified parametric fire at fully developed phase (Equation (12.7))
Ω	Enclosure size to opening factor in the Law correlation (Equation (6.8))
Ψ	Proportionality factor (Equation (5.17))
α	Attenuation factor (Section 5.4.3)
β	$=c_p/c_v$ in Chapter 10
χ	Combustion efficiency (on the basis of unit fuel mass supplied)
δ	Sill height of the vertical wall vent opening (m)
ε_g	Gas emissivity

ε_{res}	Resultant emissivity
ε_s	Fuel surface emissivity
ε_w	Wall surface emissivity
γ	=(1+s) in Chapter 3
φ	Thermal diffusivity (m^2/s)
μ	Fraction of the fire heat release rate involved in the convection (in the line plume analysis, Equation (3.39))
θ	Temperature difference (K)
ρ	Density (kg/m^3)
ρ_0	Density of ambient air (kg/m^3)
ρ_g	Density of hot gases (kg/m^3)
$\tilde{\rho}$	Averaged density (kg/m^3)
σ	Stefan-Boltzmann constant ($W\ m^{-2}\ K^{-4}$)
τ	Mean optical path length Equation (5.29)
ω	Fire duration for the fully developed phase (minute) (Equation (2.21))
ξ	Term associated with "blockage factor" in Equation (5.6)
ψ	Semi-apex angle of the flame cone (°) (Figure 5.2)
ζ	Fuel constant for Equation (5.19)

Superscript

$'$	Per unit length
$''$	Per unit area

Chapter 1 INTRODUCTION

1.1 GENERAL

A fire that is confined in a room or an enclosure within a building is generally regarded as a "compartment fire". For a fire burning inside a compartment with no intervention, provided there is sufficient amount of fuel and ventilation, the fire can grow from a localised fire to a fully involved fire. The transition from localised burning to full room involvement is referred to as "flashover". Therefore the course of the compartment fire is generally divided into pre-flashover and post-flashover periods. The pre-flashover period generally consists of fire growth and is important for life safety. In the post-flashover period, the concern is on the structural fire performance under high thermal load, mainly for the purpose of property protection. The post-flashover fire is the main focus of this thesis.

Traditionally, the fire performance of building materials and structural elements is determined using the full size fire resistance test with standard fires such as ISO-834 (ISO, 1975) or ASTM E-119 (ASTM, 1988). Although useful when used in a grading system, standard fires are poor for representing real fires that could develop in a particular building (Franssen, 1999). Therefore, for structural fire design purposes, it is important to know the behaviour of the post-flashover fires that are likely to be encountered in the design building. Knowing about the fires will allow the selection of appropriate proprietary listed structural elements or assemblies for meeting the performance requirements. Moreover, the performance of a critical structural element in a particular building can be assessed accordingly using appropriate calculations (Buchanan, 2001).

1.2 BACKGROUND

Many compartment fire experiments have been conducted throughout the world. In early fire tests, wood cribs were frequently used as the fire source, for their repeatability and low costs. Occasionally cellulosic furniture items and combustible walls were used. For wood fires, quantitative variables that influence the severity of the expected fire were identified, notably the fuel load (Ingberg, 1928), ventilation (Kawagoe and Sekine, 1963), and the thermal properties of the compartment (Magnusson and Thelandersson, 1970). Geometry of the fuel, such as the fuel surface area and thickness, was also noted to affect the fire time-temperature history (Tsuchiya and Sumi, 1971).

Magnusson and Thelandersson derived a set of design fires largely based on wood crib fires. Their design fires are categorised using the fuel load, the ventilation and the enclosing wall properties. The exposed surface area of the fuel is not considered. The Magnusson and Thelandersson time-temperature curves appear to have the most significant influence in structural fire design worldwide as their design fires are widely used and form the basis of the Eurocode parametric fires.

However, wood cribs are seldom found inside real occupancies. Fuel loads inside typical residential and commercial occupancies are likely to include wooden furniture items such as bookshelves, desks, tables and chairs, which have vastly different geometries compared to wood cribs. Other realistic fuels could include thermoplastic materials such as mattresses and upholstered furniture that are likely to burn as pool fires. In the case of pool-like burning fuel, various studies have been done (Bullen and Thomas, 1978; Babrauskas and Wickström, 1979), and have shown that the pool fire has markedly different burning behaviour compared to woods burning inside a post-flashover compartment. Pettersson (1996), in his evaluation of the parametric time-temperature curves, indicated the importance of correct input data for the real fuel loads where these fuels could lead to substantially different fires inside the compartment than those given by the parametric design fires.

Apart from the limitation on fuel types, all the previous post-flashover fire studies neglect the possibility of roof vent openings. To the author's knowledge, most of the post-flashover fire experiments conducted around the world used a single vertical door or window vent as opening, and the extra ventilation effect provided by a roof vent opening has not been extensively studied. In New Zealand, for structural fire design, the New Zealand Building Code, C3/AS1 (BIA, 1992) provides the structural fire resistance ratings (in minutes) required in compartments with a given fire load and vertical vent opening size and horizontal roof vent area. These fire resistance ratings are derived from the Eurocode time equivalence formula (EC1, 1994). However, the origin of the Eurocode formula is not clearly stated. It is understood that the Eurocode formula is derived from the results of analysis using the MRFC (Multi-Room-Fire-Code) computer programme by Schneider et al (1990), but details have not been published.

There are other aspects that could affect the resulting post-flashover fires inside compartments, such as wind effects, cross flow and progressive burning behaviour of fuels inside a deep compartment. However, not much study has been done on these aspects.

The aforementioned scenarios represent genuine scenarios encountered in real buildings. Therefore, there is a need to broaden post-flashover fire studies to include these effects. This thesis focuses on studying the effects of different fuel types and the effects of ventilation openings including roof vent opening under still air condition. It is hoped that the improve understanding gained from the studies could provide a platform for studying scenarios such as the wind effects and the burning behaviour of fuel inside a deep compartment in the future.

1.3 RESEARCH FOCUS AND SCOPE

The objective of this research is to develop an improved post-flashover fire model that could model the post-flashover fire caused by realistic fuel types and ventilation effects with the presence of a roof vent opening.

This thesis focuses on studying the compartment ventilation and the burning behaviour of fuel inside a compartment during a post-flashover fire. The studies are largely restricted to analytical studies and modelling. In the case of a roof vent opening, a series of reduced-scale post-flashover compartment fire experiments were performed. The scenario investigated was restricted to a compartment with a horizontal roof opening and a vertical door opening. The unique case of a compartment having only a roof vent opening and no wall opening was not considered.

All the analytical studies performed in this thesis are based on the single zone compartment fire theory as described in Chapter 2.

1.4 THESIS OVERVIEW

Chapter 2 presents a background description of the single zone compartment fire theory used for modelling post-flashover fires. A review of the historical development of the post-flashover fire models is presented. Three important aspects in the single zone compartment fire theory, namely the vent flow, the combustion and the fuel mass loss rate are identified and discussed.

Chapter 3 presents the mathematical vent flow equations that describe the gas flow induced through a wall opening by a fully developed fire inside a flashed-over compartment. An analysis based on the line-plume entrainment is performed to investigate the suitability of applying these vent flow equations at a large opening that

comprises of an entire wall. The study provides an improved understanding of the vent flow behaviour at large vent openings.

Chapter 4 outlines the treatments that have been used to estimate the effective heat of combustion for the burning fuel under different ventilation conditions. The results from these different treatments are compared and their application in the well-stirred post-flashover compartment fire model is discussed.

Chapter 5 reviews a selection of pool models that have been used to describe the mass loss rate of pool fires inside a compartment. Two environmental variables that affect the mass loss rate of a pool fire are identified, namely the vitiation effect and the radiation effect. For a pool burning inside a post-flashover compartment, its mass loss rate is dominated by radiative thermal feedback from the surrounding hot environment. Experimental compartment pool fire data were used to study the mass loss rate of the pool.

Chapter 6 describes the burning mechanisms of wood. A dimensional analysis is performed to identify the influential parameters that affect the mass loss rate during the fully developed period. The models for describing the mass loss rate of wood during different burning regimes are presented and discussed. A method to describe the burning of wooden furniture is postulated.

Chapter 7 outlines the possible flow scenarios that could arise from a post-flashover compartment having both vertical and horizontal vent openings. An extended vent flow model that includes the horizontal roof vent opening is presented. The unstable phenomenon of bi-directional flow across the roof vent opening is briefly discussed.

Chapter 8 presents an outline of the fire experiments that were conducted as part of this thesis. A reduced scale compartment with two adjustable vent openings, a door vent and a circular roof vent, using a heptane pool as the fire source, was used to study the ventilation effects by the roof vents. Eleven roof vents and door vents size-combinations were tested. Details of the experimental layout, instrumentation and data reduction methods are presented.

Chapter 9 reports on the experimental observations made during the Door 1 experimental series. The experimental results from this particular test series are presented and analysed. A simplified vent flow equation for a compartment having both horizontal and vertical vent openings is deduced.

Chapter 10 describes the experimental observations for the Door 2 and Door 3 experimental series. An unexpected pulsing phenomenon was observed during these test series. This phenomenon is analysed qualitatively and focuses on identifying the possible triggering and sustaining mechanisms that result in the pulsing. The results of these experiments are not used in the development of the proposed CFIRE post-flashover fire model, but are included here for reference purposes.

Chapter 11 describes the single zone fire model-CFIRE that has been developed utilising the results from the analysis performed in the previous chapters. Verification of the model is performed by comparing the simulated results with the experimental results.

Chapter 12 presents the simulated fire time-temperature curves inside a compartment with different types of fuel at different ventilation openings using the CFIRE computer program. A steady-state analysis is also performed. The studies highlight the importance of identifying the types of fuel involved, whether the fuel is wood or thermoplastic/liquid pool, and the respective fuel surface area. It is shown that fuel with different physical and burning characteristics result in very different fires in terms of the temperature and duration, even with the same total amount of fuel load.

Chapter 13 concludes the thesis and summarises the major findings. Recommendations for future research on the area of post-flashover fires studies are given.

Chapter 2 BACKGROUND

This chapter presents a background description of the single zone compartment fire theory used for modelling post-flashover fires. A review of the historical development of post-flashover fire models is presented. Three important aspects in the single zone compartment fire theory, namely the vent flow, the combustion and the fuel mass loss rate are identified and discussed.

2.1 POST-FLASHOVER FIRES

For an uncontrolled fire inside a compartment, provided there is sufficient fuel and ventilation, the fire inside the compartment can grow from localised burning to full-room involvement. This is the stage where an intense amount of heat is released due to the ignition and burning of the available fuels, resulting in very hot gas temperatures inside the compartment. After this transition, the fire enters the post-flashover phase that consists of a fully developed stage and a decay stage. For structural fire design purposes, the fully developed stage is very important as it represents the state of ultimate burning where all the fuels available are involved to a maximum extent, with the fuel supply rate, and hence the heat release rate, subject to fuel or ventilation limitation.

The fuel supply rate is often reported as the fuel mass loss rate, which is the change in mass of the burning fuel over time measured using a load scale. It describes the release of the fuel vapour from the bulk fuel as a result of thermal feedback from the flame on top of the fuel, as well as the radiation from the surrounding hot environment. Although closely related, the fuel mass loss rate should not be confused with the burning rate, where the latter describes the amount of fuel that reacts with the oxygen per unit time. Multiplying the burning rate by the heat of combustion of the

fuel gives the fire heat release rate, which is the driving force that determines the gas temperature inside the compartment. For a compartment fire, the fuel mass loss rate could exceed the maximum burning rate restricted by the available ventilation. The excess unburned fuel is burned outside the compartment and is seen as an external flame burning outside the vent opening.

In a post-flashover fire, the temperature inside the compartment is very hot. To describe the thermal behaviour inside the compartment, the entire compartment is treated as a single control volume filled with hot gases having a uniform temperature. The temperature inside the compartment is evaluated by balancing the heat and mass that cross the control surfaces of the control volume, i.e. the compartment space. The heat release rate inside the compartment as a result of an infinitely fast reaction between the fuel vapour released and the entering air, is responsible for the elevated gas temperature inside the compartment. These are the classical treatments applied in the single zone compartment fire theory. In the section to follow, the application of the single zone compartment fire theory to post-flashover fire modelling is described.

2.2 SINGLE ZONE MODEL- THEORY AND APPLICATION

A single rectangular compartment with a single rectangular wall opening represents a classic case for studying the post-flashover compartment fires. The opening acts as the main connection between the fire within the enclosure and the outside ambient atmosphere. Typical assumptions made in a single zone model include:

- The gas temperature inside the compartment is uniform;
- The gas flows in and out of the compartment via the window opening are driven by hydrostatic pressure differences between the inside fire environment and the outside ambient air;
- The reaction between the fuel vapour released and entering air is infinitely fast;
- The fire environment is quasi-steady.

In the single zone treatment, the entire compartment is regarded as a single control volume. Conservation of energy means that the energy going into the control volume will be equal to the energy going out, such that the heat released by the fire, $\dot{Q}_{FIRE}$, equals the sum of the heat loss from the convective gas flow, $\dot{Q}_L$, the radiative losses via the opening, $\dot{Q}_R$, the convective and radiative heat loss to the enclosing boundaries, $\dot{Q}_W$, the heat feedback vaporising the excess fuel, $\dot{Q}_{FB}$, and the heat stored in the gas volume, $\dot{Q}_G$, as shown in Equation (2.1).

$$\dot{Q}_{FIRE} = \dot{Q}_L + \dot{Q}_R + \dot{Q}_W + \dot{Q}_{FB} + \dot{Q}_G \qquad \textbf{(2.1)}$$

The rate of change of energy stored in the gas volume, $\dot{Q}_G$, which is associated with the change in the fire gas temperature, T_g, has in general been neglected in most of the models, as its contribution towards the fire temperature is relatively small compared to other heat loss terms (Kawagoe, 1967). Following Kawagoe's conclusion, for engineering purposes, this heating term is dropped from the heat balance equation in Equation (2.1). This leads to the quasi-steady assumption such that the fire environment is assumed to be steady for each successive small time interval over the entire fire duration.

Continuing to invoke the quasi-steady assumption, the mass in and out of the control volume also has to be balanced with the rate of change of mass in the gas volume term being dropped. The mass balance equation is given in Equation (2.2), where $\dot{m}_{in}$ and $\dot{m}_{out}$ are the mass flow rate of outside ambient air into the compartment and mass flow rate of inside hot gases out of the compartment via the vent opening respectively; $\dot{m}_p$ is the fuel mass loss rate inside the compartment.

$$\dot{m}_{in} + \dot{m}_p = \dot{m}_{out} \qquad \textbf{(2.2)}$$

These are the two principal equations for the single zone model. The expression for each term in both the energy and the mass balance equations is described as follows.

2.2.1 Ventilation

The environments inside and outside the compartment are considered at rest with uniform temperatures, and the hydrostatic pressure in each environment varies linearly with height. The flow across the vent opening is driven by the difference between the two pressure distributions due to temperature difference. There will be a point of zero pressure difference within the vent opening, known as the neutral-plane. By knowing the pressure differences across the vent opening, Bernoulli's equation can be applied to obtain the velocity distribution from $\sqrt{2\Delta P/\rho}$. Since the pressure difference, and hence the velocity, varies with height, the mass flow in and out of the opening is obtained by integrating the velocity profile along the opening height from the neutral plane, multiplied by the discharge coefficient, C_d, the respective density (ambient air density ρ_0 or hot gas density ρ_g) and the vent width, W_v. These vent flow expressions can be found in the literature (Babrauskas and Williamson, 1978; Drysdale, 1985) and are given below as Equation (2.3) and Equation (2.4). δ and H_s denote the heights from the floor to the sill and the soffit of the opening respectively. The neutral plane height, Z_n, is solved by applying the mass balance equation (Equation (2.2)). Details of the derivation for these vent flow equations will be given in Chapter 3.

Outflow:

$$\dot{m}_{out} = \frac{2}{3} \cdot C_d \cdot W_v \cdot \rho_g \cdot \sqrt{2g\left(\frac{\rho_0}{\rho_g} - 1\right)} \cdot (H_s - Z_n)^{3/2} \qquad \textbf{(2.3)}$$

Inflow:

$$\dot{m}_{in} = \frac{2}{3} \cdot C_d \cdot W_v \cdot \rho_0 \cdot \sqrt{2g\left(1 - \frac{\rho_g}{\rho_0}\right)} \cdot (Z_n - \delta)^{3/2} \qquad \textbf{(2.4)}$$

The density of the fire gases can be estimated using the ideal gas law,

$$P = \rho RT$$

where P is the pressure (Pa), R is the specific gas constant for air (287 J kg^{-1} K^{-1}), ρ is the density (kg/m^3) and T is the temperature (K). For compartment fire application, the atmospheric pressure changes very slightly with height. By using an atmospheric pressure of 101.3kPa, the gas density can be estimated as

$$\rho = 353/T \ \ (in\ Kelvin) \tag{2.5}$$

2.2.2 Fire heat release rate

The fire heat release rate within the fire compartment, $\dot{Q}_{FIRE}$, is the cause for the elevated compartment temperature. The heat release rate from the fire inside the compartment depends on the mass loss rate of the fuel and the air inflow rate into the compartment. When the burning fuel is releasing pyrolysates greater than the amount that could be burned with the available ventilation, the fire environment inside the compartment will be fuel-rich and the heat release from the fire will be ventilation limited. If there is more air available than needed to burn all the pyrolysates released, the fire will be fuel-lean and the heat release will be fuel limited. The status of the fire inside the compartment can be described using the equivalence ratio, Φ, defined as

$$\Phi = \frac{r \cdot \dot{m}_p}{\dot{m}_{in}} \tag{2.6}$$

where r is the stoichiometric air to fuel mass ratio of the burning fuel.

The heat release rate for each fire condition can be described as:

For Φ<1 (fuel-lean):

$$\dot{Q}_{fire} = b_p \times \dot{m}_p \times \Delta h_{c,net} \tag{2.7}$$

For Φ>1 (fuel-rich):

$$\dot{Q}_{fire} = b_p \times \frac{\dot{m}_{in}}{r} \times \Delta h_{c,net} = b_p \times \frac{1}{\Phi} \times \dot{m}_p \times \Delta h_{c,net} \quad \textbf{(2.8)}$$

The combustion reaction inside the compartment is assumed to be infinitely fast with the net calorific value of the fuel being $\Delta h_{c,net}$. The factor b_p (<1.0), is used to account for mixing inefficiency. This factor is difficult to quantify and generally has a value ranging between 0.5 and 0.9 (Babrauskas, 1981).

2.2.3 Convective heat loss

The convective heat loss in the gases flowing out of the compartment window, $\dot{Q}_L$, is calculated as the product of the mass outflow rate and the enthalpy gained by the gas species due to the increase in temperature. This is shown in Equation (2.9) where Y_i is the species mass fraction per unit mass of the mass outflow and h_i is the enthalpy gained by each species due to the temperature increase.

$$\dot{Q}_L = \dot{m}_{out} \times \sum_i Y_i \cdot h_i \quad \textbf{(2.9)}$$

By definition, under constant pressure and ideal gas behaviour, the change of enthalpy for each species is given by Equation (2.10) where c_{pi} is the specific heat of individual gas species. The gas species can be estimated from the chemical equilibrium equation and the temperature dependence of specific heat for each species can be found in a thermodynamics text such as Van Wylen et al (1994).

$$h_i = \int_{T_0}^{T} c_{p_i} \cdot dT \quad \textbf{(2.10)}$$

The evaluation of the convective heat loss rate term can be simplified by using the average specific heat of the hot gases, c_p, taken approximately 1.15 kJ/kg-K (Janssens, 1992), such that

$$\dot{Q}_L = \dot{m}_{out} \cdot c_p \cdot (T_g - T_0) \quad \textbf{(2.11)}$$

where T_0 is the reference temperature taken as the ambient temperature.

2.2.4 Radiative heat loss

The term, $\dot{Q}_R$, is the heat loss from the inside fire gases to the outside ambient environment by radiation through the vent opening. The radiation heat flux from the vent opening is represented as a blackbody at temperature T_g with the expression given in Equation (2.12),

$$\dot{Q}_R = A_v \cdot \sigma \cdot \left(T_g^4 - T_0^4\right) \quad \textbf{(2.12)}$$

where A_v is the vent opening area, σ is the Stefan-Boltzmann constant, T_g is the gas temperature and T_0 is taken as the temperature of the outside ambient air.

2.2.5 Wall heat loss

The compartment consists of solid boundaries such as walls and ceiling. Unless these boundaries are adiabatic, heat will be transferred and absorbed across these solids. These solid boundaries, simply referred here as "walls", are generally treated as homogeneous solids with constant thermal properties. The heat transfer across the wall is considered to be one-dimensional. The expression for transient conduction through the wall (with no heat generation) is given by Equation (2.13), where φ is the thermal diffusivity:

$$\frac{\partial^2 T}{\partial x^2} = \frac{1}{\varphi} \cdot \frac{\partial T}{\partial t} \quad \textbf{(2.13)}$$

The convective and radiative heat transfer on both the inner and the outer wall surfaces are accounted for; such that the boundary conditions for each side of the wall are given in Equations (2.14) and (2.15).

Fire side:

$$-k\left(\frac{\partial T}{\partial x}\right)_{solid,fire} = h_{fire}\cdot\left(T_g - T_{wi}\right) + \sigma\cdot\varepsilon_{res}\cdot\left(T_g^4 - T_{wi}^4\right) \quad \textbf{(2.14)}$$

Ambient side:

$$-k\left(\frac{\partial T}{\partial x}\right)_{solid,amb} = h_{amb}\cdot\left(T_{wo} - T_0\right) + \sigma\cdot\varepsilon_{w}\cdot\left(T_{wo}^4 - T_0^4\right) \quad \textbf{(2.15)}$$

where k is the thermal conductivity of the wall material, h_{fire} and h_{amb} are the convective heat transfer coefficients on the fire side and the ambient side of the wall respectively, T_{wi} and T_{wo} are the wall surface temperatures on the fire side and ambient side respectively, and ε_{res} is the resultant emissivity between the wall inner surfaces and the fire gases. It is estimated using Equation (2.16) with ε_g and ε_w being the emissivity of fire gases and the emissivity of wall surfaces respectively.

$$\varepsilon_{res} = \left(\frac{1}{\varepsilon_g} + \frac{1}{\varepsilon_w} - 1\right)^{-1} \quad \textbf{(2.16)}$$

The convective heat transfer coefficient depends on the flow condition, whether the flow is freely induced or forced, over the surface, as well as their temperature difference. For post-flashover compartment fire application, the convection heat transfer from the hot gases to the enclosing walls is assumed to take place under free-convection. However, the application of the available correlations for convective heat transfer coefficient under specific flow conditions is restrictive due to complication arising from the large-scale turbulence where plumes, jets, boundaries and openings interact (Babrauskas and Williamson, 1975). In COMPF2, Babrauskas (1979) applied the expression of convective heat transfer coefficient as a function of temperature difference between the wall surfaces and the surrounding gases, with the convective heat transfer at the fire side ($5.0\times(\Delta T)^{1/3}$) approximately 2.7 times larger than at the ambient side ($1.87\times(\Delta T)^{1/3}$). Typical values for gaseous convective heat transfer coefficients under free convection conditions are between 2-25W/m^2-K (Incropera

and DeWitt, 2001). Kawagoe and Sekine (1963) uses a value of 23W/m^2-K at the fire side as an input value for their post-flashover fire calculations. The typical convective heat transfer coefficient for the fire side, h_{fire}, is therefore taken in the order of 25W/m^{2}K and 10W/m^{2}K for the ambient side, h_{amb}. The heat transfer across the wall is calculated using the finite difference method, solving for the wall temperature as the fire progresses.

The heat loss to the walls with a total area of A_t, is solved using Equation (2.17).

$$\dot{Q}_W = A_t \cdot h_{fire} \cdot (T_g - T_{wi}) + A_t \cdot \varepsilon_{res} \cdot \sigma \cdot (T_g^4 - T_{wi}^4) \qquad \textbf{(2.17)}$$

2.2.6 Feedback term

This is the heat required to vaporise the unburned fuel. The feedback term, $\dot{Q}_{FB}$, is evaluated as

$$\dot{Q}_{FB} = \left(\dot{m}_p - \dot{Q}_{FIRE} / \Delta h_{c,net}\right) \times L_g \qquad \textbf{(2.18)}$$

where L_g is the heat of gasification. The bracketed term refers to the fuel that has not been burned. By definition, the energy feedback required to vaporise the liquid or solid fuel has been included in the value of net heat of combustion, $\Delta h_{c,net}$. Therefore, the feedback term is to account for fuel that has been released but is not participating in the combustion.

2.2.7 Evaluation of the fire temperature

The fire gas temperature history inside the compartment is calculated by solving the energy balance equation (Equation (2.1)) at successive time interval, Δt. At time zero, the wall surface temperature is at ambient temperature; a fire gas temperature is guessed and used to calculate the air inflow rate, the fire heat release rate and the other heat loss terms. These terms are substituted into Equation (2.1). If the sum of the heat loss terms does not equate to the fire heat release rate, a new gas temperature is

tried until the equation is satisfied. The fire gas temperature is assumed to stay constant for the time interval, Δt. During this time interval, the enclosing wall will be heated by this temperature and the new wall surface temperature is calculated using Equation (2.13) with boundary conditions given in Equations (2.14) and (2.15). This new wall surface temperature will then be used to solve for the fire gas temperature at the next time interval. The calculation process continues and eventually gives the fire gas time-temperature history inside the compartment. This is summarised in Figure 2.1 below.

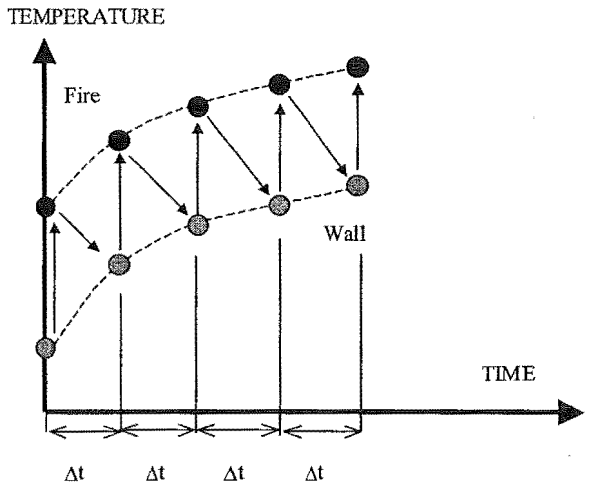

Figure 2.1 Calculation processes for wall surface temperature and fire temperature.

2.3 DEVELOPMENTS IN POST-FLASHOVER FIRE MODELS

Kawagoe and Sekine (1963) were the first to apply single zone compartment fire theory to describe post-flashover compartment fires. Their model represents the first mathematical post-flashover fire model in the world. Initially using hand calculations and graphical methods to solve for the fire gas temperature, the model was later coded as a computer program (Kawaoge, 1967). Subsequently, computational post-flashover fire models based on the single zone compartment fire theory were developed. These

fire models include: Magnusson and Thelandersson (1970) in Sweden, Tsuchiya and Sumi (1971) in Canada, the COMPF model by Babrauskas and Williamson (1978 and 1979) and later the COMPF2 model by Babrauskas (1979) in the United States, and more recently the National Research Council of Canada (NRCC) fire model by Takeda and Yung (1992) in Canada and the OZONE model by Cadorin and Franssen (1999) in Belgium. There are other post-flashover fire models developed using the same approach as reviewed by Harmathy and Mehaffey (1983) and Wade (1995). However, the first four models in particular, represent the important evolution of knowledge and concept in post-flashover fire modelling. Other single zone post-flashover fire models could generally be regarded as variants to the above four models.

In the previous section, the core equations used for modelling the post-flashover compartment fire are presented. Three major aspects that strongly affect the heat loss terms and hence the evaluated fire gas temperature are identified, that include the vent flow, the combustion, and most important of all, the fuel mass loss rate. These are the three major aspects that have been the subject of focus in the modelling during the history of the post-flashover fire models development. The treatments on these aspects by various researchers are presented in the following sections.

2.3.1 Vent flows

Vent flow is an important aspect in post-flashover fire modelling. It determines the amount of air available for combustion to take place inside the compartment and also the convective heat loss via the outgoing hot gases. Kawagoe (1958) was the first to model the flow across the vent opening using the orifice analogy, where the vent opening is treated like an orifice at the reservoir, with the hydrostatic pressure difference between the hot and cold quiescent environments converting to a velocity head driving the flow across the orifice. Bernoulli equation is used to relate the pressure difference to the flow velocity across the vent opening. A discharge coefficient of 0.68 is typically used to account for the non-idealistic flow characteristics that exist in the real flow situations, but have been ignored in theoretical flow considerations.

This treatment has been applied in almost all of the single zone fire models. However, the above treatments seem to be applicable only for small vent openings. In the case of very large openings, such as a full frontal wall opening, Babrauskas and Williamson (1978) found that the above treatment could grossly over-estimate the flow rate unless the discharge coefficient is reduced by half. However, with regard to vent opening size, no guidelines are available as to when the orifice analogy can be adequately applied to describe compartment vent flows.

Other ventilation scenarios could exist, such as a compartment with roof openings. The presence of the roof opening allows hot gases to exit through the roof opening and increases the air flowing through the wall opening. Very limited study has been performed with regard to this scenario. From the literature, the closest experimental study on this subject was that reported by Thomas et al (1963). There is also a nomogram developed by Magnusson and Thelandersson (1970) to account for the additional ventilation caused by the presence of the roof opening. However, their approach has not been experimentally validated.

Theoretical or analytical study with regard to the wind effects on the compartment ventilation is limited. Buchanan (2001) noted that for a compartment with two opposite wall openings, there is another potential flow scenario known as cross ventilation that could occur, especially when there is a wind blowing. No research has been done on this type of scenario.

2.3.2 Combustion

From the single zone compartment fire theory, the compartment is regarded as a well-stirred reactor with infinitely fast reaction between fuel and air. It is noted that the actual fire heat release rate is likely to be less than the maximum potential heat that can be released under stoichiometric conditions. This is due to inefficient mixing that results in the generation of incomplete combustion products. Kawagoe and Sekine (1963) used a value of 10.8MJ/kg as the effective heat of combustion for wood. This value is low compared with the net heat of combustion for typical dry wood which has a value of approximately 18.7MJ/kg (see Table 1C from Babrauskas (1992b)). According to Kawagoe and Sekine (1963), this lower heat of combustion is to account

for the degree of incomplete combustion, estimated from analysing the composition of combustion gases notably the carbon monoxide, during Kawagoe's (1958) fire experiments.

Tsuchiya and Sumi (1971) suggested that during the post-flashover fire, unstable combustion products might dissociate towards the reactants under the high temperature environment. They considered the "water-gas" reaction as the possible dissociation reaction illustrated below.

$$CO_2 + H_2 \Leftrightarrow CO + H_2O$$

The production of CO and H_2 is explicitly calculated via a chemical reaction equation. The production of the incomplete combustion products lowers the net heat of combustion of the burning fuel. The effective heat of combustion is calculated according to the amount of CO and H_2 produced.

The COMPF2 model by Babrauskas (1979) does not include the "water-gas" reaction for modelling the combustion reaction. Instead, a mixing efficiency factor, b_p, is introduced to account for the incomplete combustion. The fire heat release rate inside the compartment is evaluated as the lower of the fuel-limiting heat release rate ($b_p \cdot \dot{m}_p \cdot \Delta h_{c,net}$) and the ventilation-limiting heat release rate ($b_p \cdot \dot{m}_{air} \cdot \Delta h_{c,net}/r$). The mixing efficiency factor, b_p, could be interpreted as the maximum fraction of fuel involved in complete burning in the case of fuel-limited fire or the maximum fraction of air involved in complete burning in the case of ventilation-limited fire.

Other models such as OZONE do not explicitly account for any incomplete combustion and the heat of combustion for air is taken as 3000kJ/kg regardless of fuel types.

2.3.3 Fuel mass loss rate

Fuel mass loss rate modelling is the most important aspect in post-flashover compartment fire modelling. It strongly dictates the fire heat release rate, hence the temperature inside the compartment.

One of the most significant contributions by Kawagoe and his co-workers has been the mass loss rate correlation for wood crib fires, developed from their fire tests. Kawagoe and Sekine (1963) showed that the fuel mass loss rate, $\dot{m}_p$, could be correlated with the vent parameter $A_v\sqrt{H_v}$ where A_v is the area of the vertical window or door opening (m^2) and H_v is the height of the opening (m). The mass loss rate correlation is given in Equation (2.19). This mass loss rate is shown to coincide with the stoichiometric mass loss rate of wood as a result of gas phase reaction inside a compartment (Drysdale, 1985).

$$\dot{m}_{p,Kawagoe} = 5.5 \times A_v\sqrt{H_v} \quad (kg/\min) \quad or$$
$$= 0.09 \times A_v\sqrt{H_v} \quad (kg/\sec) \qquad \textbf{(2.19)}$$

In their fire modelling, Kawagoe and Sekine assumed that the mass loss rate of the burning fuel follows the correlation (Equation (2.19)) until all the fuels are exhausted. The decay phase was not explicitly treated and was assumed to be linear. Based upon their experimental experience, they suggested that for fire duration less than 60 minutes, the decay rate is 10°C per minute; for longer duration, 7°C per minute is used.

Magnusson and Thelandersson (1970) realised that the fuel mass loss rate, $\dot{m}_p$, used by Kawagoe and Sekine in Equation (2.19) was in fact the maximum rate that occurred during the ventilation controlled burning regime. During the decay phase, the fuel mass loss rate inside the enclosure will be fuel surface controlled. Sensing this inadequacy, Magnusson and Thelandersson introduced a modification factor, a, during the evaluation of the mass loss rate of fuel and hence the heat release rate $\dot{Q}_{FIRE}$. This is shown in Equation (2.20) where $0 \leq a(t) \leq 1$.

$$\dot{m}_p = a(t) \cdot 0.09 \times A_v \sqrt{H_v} \qquad (kg/\sec) \tag{2.20}$$

The $a(t)$ is a piecewise linear function which is found by matching the model fire gas temperature output, $T_g(t)$ to experimental measurements for a very large number of fire tests. A set of piecewise linear functions $a(t)$ was found for different fuel loads. Magnusson and Thelandersson defined their fire duration for the flame phase, i.e. the fully developed phase, as

$$\omega = \left(\frac{M \times A_t}{5.5 A_v \sqrt{H_v}} \right) \times \frac{\Delta h_{c,eff}}{\Delta h_{c,net}} \qquad (\min) \tag{2.21}$$

where M is the fire load based on wood per total enclosure area (kg/m^2), A_t is the total area of the bounding surfaces in the enclosure (m^2), $A_v \sqrt{H_v}$ is the vent parameter of the vent opening, $\Delta h_{c,eff}$ is the effective heat of combustion of wood fuel taken as 10.8MJ/kg and $\Delta h_{c,net}$ is the net heat of combustion for wood fuel taken as 18.8MJ/kg.

Magnusson and Thelandersson (1970 and 1974) assumed that all the fuels are released within the enclosure and excess unburned pyrolysates leaving the enclosure are negligible. Hence after the flame phase, ω, the rest of the energy would be gradually released during the decay phase. Since they used a calorific value of 10.8MJ/kg for wood during the fully developed period instead of 18.8MJ/kg, this means that 57% of fuel energy is released during the flame phase defined by ω, while the remaining 43% is released during the decay period. This has resulted in an extremely long decay period.

Unlike Kawagoe and Sekine who assumed constant ventilation controlled mass loss rate for the entire fuel load, Tsuchiya and Sumi (1971) realised that during the post-flashover period, the burning regime could switch from ventilation controlled to fuel surface controlled depending on the amount of fuel surface left during the fire. They used two mass loss rate expressions, one for each burning regime. The smaller of the two is regarded as the dominant rate and used in the fire temperature calculation.

The mass loss rate expression for ventilation controlled burning regime is represented by the stoichiometric fuel rate for the given ventilation; for wood, its expression is approximately the Kawagoe correlation (Equation (2.19)). For the fuel surface controlled burning regime, the burning is described by using a constant regression rate on the available fuel surfaces. Tsuchiya and Sumi applied Ödeen's (1963) equation to track the changes of the fuel surfaces during the fire process, hence the mass loss rate history. This equation describes the changes of the surface area for simple geometrical shapes that include plane, stick, cylinder, cube or sphere for a given regression rate. The initial amount of fuel mass, the geometrical shape, the characteristic dimension of the fuel and the regression rate are taken as inputs. This fuel surface controlled mass loss rate takes the form shown in Equation (2.22).

$$\dot{m}_{p,FC} = \frac{2v_p \cdot m(t) \cdot F}{D \cdot \left(\frac{m(t)}{M_0}\right)^{\frac{1}{F}}} \qquad \textbf{(2.22)}$$

where v_p is the regression rate (m/s), $m(t)$ is the mass of fuel (kg) at time t, M_0 is the initial mass of the fuel (kg), D is the characteristic fuel dimension (m), and F is a dimensionless geometrical factor such that F=1 represents a plane; F=2 stick or cylinder; F=3 sphere or cube.

The mass loss rate for each of these regimes is calculated at every time step and the smaller of the two rates is used. In doing so, the fuel initially having a large surface area would have a mass loss rate controlled by available ventilation until the fuel surface area decreases to a point that Equation (2.22) becomes dominant. This initiates the decay period where the mass loss rate becomes fuel surface controlled.

Babrauskas (1979) in the COMPF2 adopted the same "switching" methodology as in the Tsuchiya and Sumi model. Apart from the ventilation controlled and fuel surface controlled regimes, COMPF2 includes another regime called the porosity controlled regime for densely packed crib. This calculation is based on the formulation developed by Nilsson (1971) for wood crib fires. The smallest of the three mass loss rates is the dominant rate and is used for temperature calculation.

Other models such as OZONE do not have built-in fuel mass loss rate models and require users to input the fuel mass loss history inside the compartment.

Among the single zone fire models mentioned, only the COMPF2 and the NRCC fire model could model thermoplastic/liquid pool fires. The pool fires have very different burning behaviour compared to wood fires. Note that the NRCC fire model is designed to model post-flashover fire generated from a polyurethane slab. In the case of COMPF2 model, it is restricted to model either a wood fire or a pool fire per simulation. The co-existence of these two fuel types within the same compartment cannot be modelled.

It is also noted that the two-zone models such as FPEtool and FASTLite, which are mainly used for pre-flashover modelling, could be used to model post-flashover fires. The model descriptions for both FPEtool and FASTLite are given by Deal (1994) and Buchanan (1998) respectively. Both models also adopt the "switching" methodology between the fuel surface and the ventilation controlled burning regimes.

For a ventilation controlled fire, both FPEtool and FASTLite computer programs assume the fuel mass loss rate is at the stoichiometric rate for the given air inflow rate into the compartment. For a fuel-controlled fire, these programmes require the exposed surface area of the fuel, A_F, the heat of gasification of the fuel, L_g, the net heat of combustion of the fuel, $\Delta h_{c,net}$, and an incident heat flux, $\dot{q}''_{incident}$. The heat release rate for fuel-controlled fire takes the expression as follows,

$$\dot{Q}_{Fire,FC} = \dot{m}_{p,FC} \cdot \chi \cdot \Delta h_{c,net} = \frac{\dot{q}''_{incident} \cdot A_F}{L_g} \cdot \chi \cdot \Delta h_{c,net} \quad \textbf{(2.23)}$$

with the mass loss rate estimated by the incident heat flux, $\dot{q}''_{incident}$, on the exposed fuel surface area, A_F, divided by the heat of gasification, L_g. The incident heat flux upon the fuel has been pre-set in these programmes and usually is unalterable by the users. It has been reported that FPEtool uses a pre-set incident heat flux of 60kW/m^2 for fuel controlled fire and 80kW/m^2 during ventilation controlled fire (Deal, 1994)

whereas the incident heat flux in FASTLite is pre-set at a value of 70kW/m^2 (Buchanan, 1998). The combustion efficiency, χ, is taken as 1.0 in the FPEtool whereas χ is a user input in FASTLite. FPEtool also includes an equation to estimate the "working" heat of gasification, to account for the shielding of unpyrolysed fuel from radiation due to the presence of char (Deal, 1994). However, the origin of this equation is not cited. It can be seen that the treatments by both of these models during fuel surface controlled burning regime is restricted to fuel with a one-dimensional plane shape as the fuel surface area stays constant during the fire process. Since the heat flux is fixed, by manipulating the heat of gasification of the fuel, one could adjust the regression rate for the burning fuel.

2.4 SUMMARY

From the review, the following points are summarised:

- Post-flashover compartment is modelled using the single zone compartment fire theory, such that the entire compartment is treated as a well-stirred reactor.
- The associated vent flow theory applied in the models is based upon the orifice analogy that is only applicable for small wall openings.
- The combustion inside the compartment is assumed to be infinitely fast. The existence of incomplete combustion products hence the combustion efficiency is crudely estimated or ignored.
- In the case of modelling the mass loss rate of cellulosic fuels, the fuel characteristics such as surface area and thickness are either not considered or collectively described as plane (one-dimensional), or stick or cylinder (two-dimensional), or cube or sphere (three-dimensional). Two burning regimes are generally used that include the ventilation controlled and the fuel surface controlled regimes. The mass loss rate during the ventilation controlled regime is assumed as a result of gas phase reaction whereas as the mass loss rate during the fuel surface controlled is modelled with a prescribed regression rate on the available fuel surface. For densely packed wood cribs, there is another

burning regime known as crib porosity controlled regime, which is accounted for in some models.

- The existing single zone fire models are restricted to modelling a single fuel type, either a cellulosic fire or a pool fire, in every simulation. They cannot model the co-existence of both fuel types within the same compartment.
- Neither roof vent opening nor wind effect is considered.

These represent the current capabilities of the existing single zone post-flashover fire models. There is a need to broaden the capabilities of post-flashover fire modelling to account for many other possible scenarios in real buildings. In order to achieve this goal, focus is on studying the three important aspects identified, namely the vent flow, the combustion and the fuel mass loss rate. These are discussed in detail in the next few chapters.

Chapter 3 COMPARTMENT VENT FLOWS

This chapter presents the mathematical vent flow equations that describe the gas flow induced through a wall opening by a fully developed fire inside a flashed-over compartment. These sets of vent flow equations are derived on the assumption that the compartment has a uniform temperature from floor to ceiling. An analysis based on line-plume entrainment is performed to investigate the suitability of applying these vent flow equations at a large opening that comprises of an entire wall. The study provides an improved understanding of the vent flow behaviour at large vent openings.

3.1 GENERAL

A compartment vent flow model is an integral part of a deterministic compartment fire model. It has direct implications towards estimating the compartment fire gas temperature because it describes the amount of air flowing into the compartment for combustion and the convective heat loss through the vent opening.

Flows between a fire compartment and its immediate surroundings are termed as vent flows. The nature of the flow depends on the vent sizes and locations as well as on the temperature and pressure imposed by wind or forced ventilation effects. In a compartment subjected to only natural convection conditions, vent flows through a wall opening are a result of buoyancy forces generated from the temperature or density difference between the two quiescent environments inside and outside the compartment. Kawagoe (1958) was the first to treat the buoyancy-driven flow across the opening as an orifice problem. For the purpose of modelling a post-flashover fire, Kawagoe assumed the gas inside the compartment is at rest with uniform temperature from floor to ceiling. This is referred to as a "well-mixed" scenario. The hydrostatic

pressure distribution inside the compartment is therefore linear varying with height. Similarly, the hydrostatic pressure distribution for the outside static ambient air is linear but with different gradient compared to the inside compartment due to density difference. By having an opening at the compartment wall, the outside cold ambient air flows into the compartment because of the pressure difference and at the same time hot gases flow out of the opening to maintain the mass balance inside the compartment. There will be a point of zero pressure difference in the opening referred to as a neutral plane. Below the neutral plane, the differential pressure in the compartment is negative (compared to outside) with air flowing in; and above the neutral plane, hot gases flowing out due to positive differential pressure in the compartment. Bernoulli's equation is then used to estimate the velocity, and hence the mass flow rates across the opening. A discharge coefficient was applied, as in the orifice flow, to correct for non-idealistic flow characteristics.

The Kawagoe vent flow treatment that assumes a well-mixed fire environment with uniform temperature has been widely used to model compartments with fully developed fires. However, it appears that the Kawagoe vent flow treatment is likely to be adequate for a small wall opening application only. For a compartment with a large vent opening such as a window taking up one whole wall, the Kawagoe method could grossly overestimate the actual air inflow into the compartment (Babrauskas and Williamson, 1978).

The following sections present the vent flow equations for a post-flashover compartment assuming the entire compartment has a uniform temperature. The effects of temperature and the contribution of fuel mass loss rate on the air inflow rate are examined; and the role of the discharge coefficient is briefly discussed. A stratified two-layer flow analysis using a line-plume as a fire source is performed to study the large vent scenario.

3.2 COMPARTMENT WITH SINGLE VERTICAL VENT

In a single zone model, the environments inside and outside the compartment are considered at rest with uniform temperatures, and the hydrostatic pressure in each environment varies linearly with height. The flow across the vent opening is driven by the pressure difference between the two stagnant environments due to temperature difference. There will be a point of zero pressure difference within the vent opening, known as the neutral-plane. By knowing the pressure differences across the vent opening, Bernoulli's equation can be applied to obtain the velocity distribution from $\sqrt{2\Delta P/\rho}$. Since the pressure difference, and hence the velocity, varies with height, the mass flow in and out of the opening is obtained by integrating the velocity profile along the opening height from the neutral plane, multiplied by the discharge coefficient, C_d, the respective density (ambient air density ρ_0 or hot gas density ρ_g) and the vent width, W_v. The derivation for these vent flow expressions can be found in the literature (Babrauskas and Williamson, 1978; Drysdale, 1985). For completeness in this thesis, the derivation is repeated here.

Figure 3.1 depicts the vent flows for a compartment having a uniform temperature from floor to ceiling with a single vertical vent opening, where H_c is the height of the compartment, H_v is the height of the vertical wall vent, Z_n is the neutral plane height from floor level, δ and H_s are the sill and soffit heights of the vertical vent respectively. The hydrostatic pressure distributions and the resulting velocity distributions across the vertical vent are also shown.

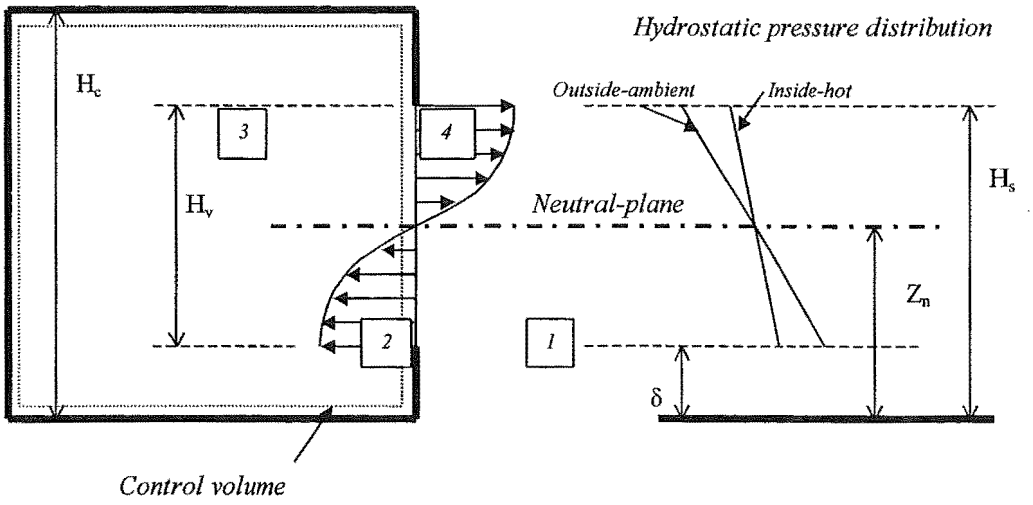

Figure 3.1 **Schematic representation of the flows and pressure distributions for a uniform temperature compartment with single vertical vent opening.**

Considering that point *1* is far away from the opening and point *2* just inside the opening, both are along an assumed streamline at the same height. The pressure at each point has a distribution related to the respective density, such as

$$P_1 = P_0 + \rho_0 g y$$

$$P_2 = P_0 + \rho_g g y$$

where subscript *0* denotes to the ambient condition, subscript g denotes the hot environment and y is the position in height from the neutral plane.

To calculate the flow, momentum conservation must be used. This is achieved by applying Bernoulli equation which has the following definition,

$$\frac{P}{\rho} + \frac{v^2}{2} + gz = const$$

The momentum equation between point *1* and *2* is therefore,

$$\frac{P_1}{\rho_1}+\frac{v_1^2}{2}=\frac{P_2}{\rho_2}+\frac{v_2^2}{2}$$

Since the assumption is made that the outside air is at rest, the velocity, $v_1 \approx 0$, and $\rho_1 = \rho_2 = \rho_0$, the ambient air density.

$$\frac{P_1-P_2}{\rho_0}=\frac{v_2^2}{2}$$

Substituting the previous equations for both P_1 and P_2 gives

$$v_2 = v_{in} = \sqrt{\frac{2\Delta P_{12}}{\rho_0}} = \sqrt{2gy\left(1-\frac{\rho_g}{\rho_0}\right)} \qquad \textbf{(3.1)}$$

Similarly, for the outflow, considering the point *3* is well inside the compartment and point *4* is just outside the opening, both are along an assumed streamline at the same height. The pressure of the issuing jet of point *4* will be the same as the ambient atmosphere pressure. The pressure at each point has the distribution of

$$P_3 = P_0 - \rho_g gy$$

$$P_4 = P_0 - \rho_0 gy$$

Applying the Bernoulli equation along the streamline between the two points with negligible velocity for hot gases inside the fire compartment, $v_3 \approx 0$, gives

$$\frac{P_3-P_4}{\rho_g}=\frac{v_4^2}{2}$$

Substituting the equations for both P_3 and P_4 gives

$$v_4 = v_{out} = \sqrt{\frac{2\Delta P_{34}}{\rho_g}} = \sqrt{2gy\left(\frac{\rho_0}{\rho_g}-1\right)} \qquad \textbf{(3.2)}$$

The inflow and outflow velocities at the opening are shown to vary with height from the neutral plane. To obtain both the inflow and outflow mass flow rates, the velocity distributions are integrated along the height from the neutral plane to the sill and to the soffit respectively. The mass inflow rate and outflow rates are as follow.

$$\dot{m}_{in} = C_d \cdot \rho_0 \cdot W_v \cdot \int_0^{Z_n-\delta} v_{in} \cdot dy \qquad \textbf{(3.3)}$$

$$= C_d \cdot \rho_0 \cdot W_v \cdot \int_0^{Z_n-\delta} \sqrt{2gy\left(1-\frac{\rho_g}{\rho_0}\right)} \cdot dy$$

$$= \frac{2}{3} \cdot C_d \cdot W_v \cdot \rho_0 \cdot \sqrt{2g\left(1-\frac{\rho_g}{\rho_0}\right)} \cdot (Z_n - \delta)^{3/2}$$

Similarly, for the mass outflow rate,

$$\dot{m}_{out} = C_d \cdot \rho_g \cdot W_v \cdot \int_0^{H_s-Z_n} v_{out} \cdot dy \qquad \textbf{(3.4)}$$

$$= \frac{2}{3} \cdot C_d \cdot W_v \cdot \rho_g \cdot \sqrt{2g\left(\frac{\rho_0}{\rho_g}-1\right)} \cdot (H_s - Z_n)^{3/2}$$

There are now two equations and three unknowns, namely the mass flow rates in and out and the neutral plane height. Since the compartment is regarded as a single zone, the entire inner compartment space is treated as a single control volume. Under steady conditions, conservation of mass implies that the sum of masses flowing into the control volume has to equal the masses flowing out of the control volume. The mass balance equation is given in Equation (3.5) and it provides the additional equation necessary to solve for the mass flow rates.

$$\dot{m}_p + \dot{m}_{in} = \dot{m}_{out} \qquad or \qquad \textbf{(3.5)}$$

$$\dot{m}_{out} = \dot{m}_{in} \cdot \left(1+\frac{\dot{m}_p}{\dot{m}_{in}}\right)$$

where $\dot{m}_p$ is the fuel mass loss rate, $\dot{m}_{in}$ is the air inflow rate and $\dot{m}_{out}$ is the mass flow of hot gases out of the compartment. The mass flow rates in and out of the compartment and the neutral plane height are solved simultaneously using Equations

(3.3), (3.4) and (3.5). By substituting Equations (3.3) and (3.4) into Equation (3.5), the neutral plane height, Z_n, can be expressed as

$$Z_n - \delta = \frac{H_v}{1+\left[\left(\frac{\rho_0}{\rho_g}\right)^{1/3} \cdot \left(1+\frac{\dot{m}_p}{\dot{m}_{in}}\right)^{2/3}\right]} \quad \textbf{(3.6)}$$

where the height of vertical wall vent opening is $H_v = H_s - \delta$, shown in Figure 3.1.

3.2.1 Discharge coefficient

The above mass flow rate equations are derived based on the assumption that the compartment has a uniform temperature with linear hydrostatic pressure distribution varying along the height of the compartment, such as inside a reservoir. The vent opening is like an orifice at the reservoir with the hydrostatic pressure difference between the hot inside compartment and cold outside ambient converting to a velocity head driving the flow across the orifice. For an opening which is small compared to the cross section of the compartment space, the fluid approaching the orifice converges towards it. Because the streamlines cannot instantaneously change direction, they continue to converge beyond the orifice until they become parallel. This section of minimum area is known as vena contracta (Massey, 1989) and the discharge coefficient accounts primarily for this decrease in cross-section (Thomas, 1995).

Various researchers have determined this discharge coefficient experimentally. Notable are the small-scale kerosene water experiments by Prahl and Emmons (1975) where the discharge coefficient of 0.68 for both inflow and outflow was found to be sufficiently accurate for most fire purposes. Steckler et al (1984) from their compartment fire experiments found that the mean value of the inflow coefficient is 0.68 and 0.73 for the outflow coefficient, whereas Nakaya et al (1986) in their compartment fire experiments found that both inflow and outflow coefficients are approximately 0.68.

3.2.2 Simplified equation

The vent flows deduced from the well-mixed assumption, which assumes the hot upper layer has reached the floor level and there is no cold layer inside the compartment, is the maximum possible for a given gas temperature through the opening (Rockett, 1976). Substituting the neutral plane expression (Equation (3.6)) into the mass inflow equation (Equation (3.3)) gives

$$\dot{m}_{in} = \frac{2}{3} \cdot C_d \cdot \rho_0 \cdot \sqrt{2g} \cdot A_v \sqrt{H_v} \cdot \sqrt{1 - \frac{\rho_g}{\rho_0}} \cdot \left\{ \frac{1}{\left[1 + \left(\rho_0 / \rho_g \right)^{\frac{1}{3}} \cdot \left(1 + s \right)^{\frac{2}{3}} \right]} \right\}^{\frac{3}{2}} \qquad \textbf{(3.7)}$$

where $s = \dfrac{\dot{m}_p}{\dot{m}_{in}}$, referred as the fuel-air ratio.

Assuming the gases behave ideally, the density is inversely proportion to the temperature, given by

$$\rho = 353 / T \left(in\ Kelvin \right)$$

Rockett (1976) showed that the temperature effect on the mass flow rate of air is minimal over the entire temperature range of fire interest from 150°C to 2325°C. For convenience, he suggested that Equation (3.7) could be considered in the form of Equation (3.8).

$$\dot{m}_{in} \approx C \cdot A_v \sqrt{H_v} \qquad \textbf{(3.8)}$$

where C is a coefficient that lumps all the constants and temperature dependent terms from Equation (3.7). It is expressed as

$$C = \frac{2}{3} \cdot C_d \cdot \rho_0 \cdot \sqrt{2g} \cdot \sqrt{1 - \frac{T_0}{T_g}} \cdot \left\{ \frac{1}{\left[1 + \left(T_g / T_0 \right)^{\frac{1}{3}} \cdot \left(1 + s \right)^{\frac{2}{3}} \right]} \right\}^{\frac{3}{2}} \qquad \textbf{(3.9)}$$

Figure 3.2 plots the coefficient C-value for various compartment temperatures using C_d=0.68, ρ_0=1.2kg/m^3 and g=9.81m/s^2 for the constants. Since Equation (3.9) also depends on the fuel to air mass ratio, s, two typical values of s are used. It includes s=0 where the fuel mass loss rate is negligible compared to the air inflow rate and s=0.2 where the fuel mass loss rate is 20% of the air inflow rate. This s=0.2 is related to the stoichiometric burning of wood where the stoichiometric fuel to air mass ratio is approximately 20%.

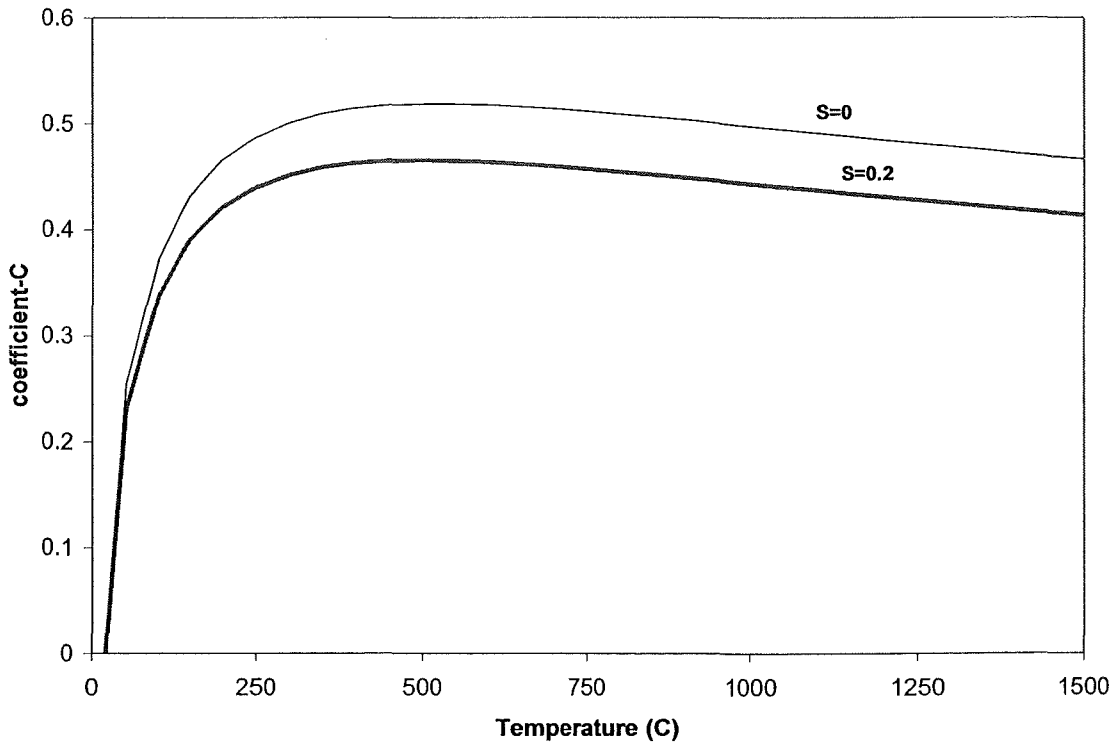

Figure 3.2 Coefficient C-value (Equation (3.9)) at various temperatures.

Figure 3.2 shows that the C-values calculated for the two different s values are reasonably constant over the post-flashover temperature range of interest (600°C to

1200°C). It is also clear that the fuel-air mass ratio, s, has an impact on the mass flow rate, such that increasing s decreases the air inflow. Over the temperature range between 600°C and 1200°C, the C-value for s=0 is 0.5±3%; and for s=0.2, the C-value is 0.45±4%. In post-flashover fires, large amount of fuels are expected to vaporise under the high temperature especially when liquid fuel or thermoplastics are involved. The significance of s to the mass flow rates should not be neglected.

3.3 VERY LARGE WALL OPENING

The vent flow equations presented above have assumed a well-mixed fire environment with uniform temperature inside a compartment with a small vent opening. The vent flow under such a condition is at the maximum flow rate (Rockett, 1976). For a large vent opening such as a window taking up one whole wall, the actual air inflows appear lower than predicted by Equation (3.9). Babrauskas and Williamson (1978) stated that a value of about one half the normally used discharge coefficient value is necessary to fit the data. It seems that this one half factor applied to the discharge coefficient is an arbitrary factor to account for the flow rate being much lower than the maximum rate, because of the less well defined fire environment inside a compartment with a large wall opening.

Figure 3.3 (a) shows a photograph of a compartment fire with an opening occupying an entire side of the wall, i.e. a full wall-size opening (Thomas and Heseldan, 1972). Suppose that the fire environment inside the compartment is not very well mixed and could be represented as a stratified two-layered environment with cool air being entrained into fire plume and a hot layer flowing out, as depicted in Figure 3.3 (b). Consider the fuels are uniformly distributed over the floor area inside the compartment, the flame engulfs the plane of the opening, such that the fire cuts off access of airflow from the opening to the space "behind" the fire, leading to a two-dimensional line plume scenario with its line source spanning the width of the compartment. The plume will only be entraining the air from its "front" side and flow entrained by the "rear" side would simply stir the gas behind the fire. All incoming air

is entrained via the opening into the line-plume and the hot gases flow out as the hot layer. In this scenario, the flow across the opening is an entrainment problem. Assuming the hot layer has reached the floor level as in Kawogoe's treatment would result in an over-estimation of the buoyant forces and hence the mass flow rates across the opening.

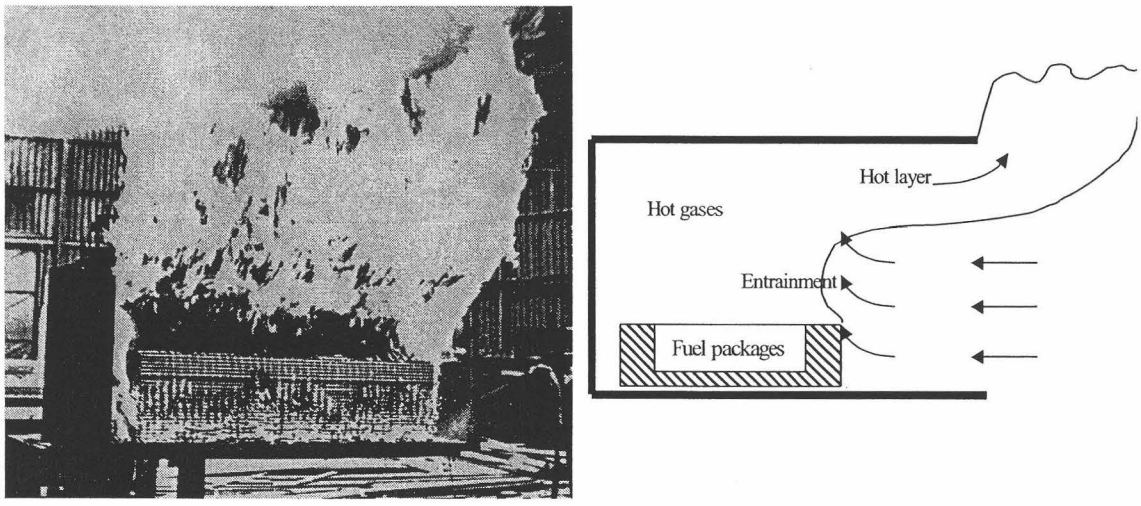

(a) Compartment fire- Full wall-size opening. (Photo taken from Thomas and Heseldan (1972))

(b) Schematic representation of a compartment with full wall-size opening.

Figure 3.3 Compartment fire with full wall-size opening.

In the analysis to follow, we shall consider a line-plume connecting a stratified two-layer fire environment inside the compartment. The intention of the analysis is to (1) better understand the one half factor applied on Equations (3.3) and (3.4) for an opening occupying one whole wall; and (2) to investigate the adequacy of applying the flow equations (Equations (3.3) and (3.4)) subjected to various opening sizes.

3.3.1 Line plume analogy

Thomas (1992) has performed analytical studies on the vent flows using a two-dimensional line plume as a fire source. His study focussed on the vent flows across a full frontal wall opening. In the analysis to follow, Thomas's treatment is extended and expressed in a generalised form for various wall opening geometry.

Consider a two-layer flow system as depicted in Figure 3.4. The system has a hot upper layer and a cold lower layer separated by a thermal discontinuity, and a plume acting as a link between the two layers. Air from the outside flows into the compartment due to the pressure difference and is entrained into the plume. The mass flux from the plume entrainment and the fuel flux from the plume cross the interface into the hot layer. A positive pressure is generated pushing the hot layer out to maintain the mass balance. The pressure distributions between the compartment and outside ambient are also shown in the figure. The mass flow equations for a stratified two-layered environment have been given by Rockett (1976). Expressed in term of the mass flow rates per unit vent width, $\dot{m}'$, the inflow and the outflow rates at the vent opening are given in Equations (3.10) and (3.11) respectively. Note that these equations are expressed in slightly different form than Equations 1 and 2 given by Rockett (1976), where Equations (3.10) and (3.11) are expressed in terms of the height above the neutral plane to the soffit of the opening, H'', the lower cold layer depth inside the compartment with respect to the sill height, H', and the distance between the base of inside hot layer and the neutral plane in the opening, Δ. For the opening having no sill and extending to the floor level, δ, is equal to 0. The effect of sill height is discussed later in the analysis.

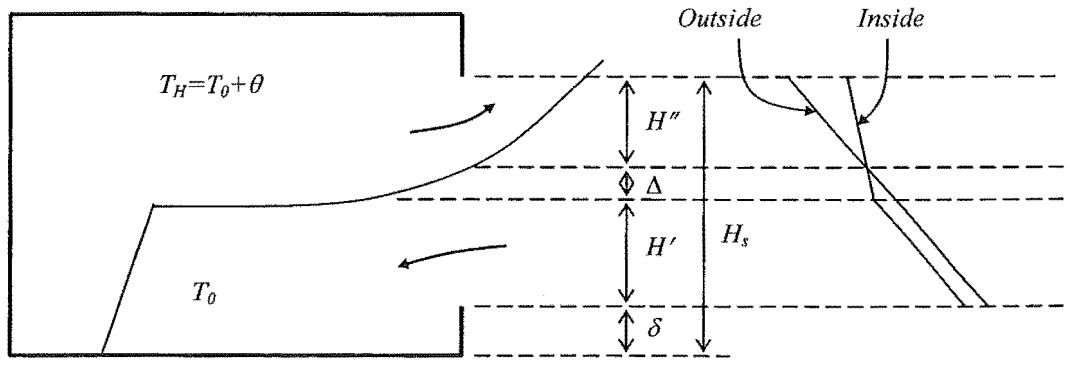

Figure 3.4 Schematic representation of hot layer flowing across vent opening.

$$\dot{m}'_{in} = \dot{m}_{in} / W_v = \rho_0 C_d \sqrt{2g \frac{\theta}{T_H}} \left(\frac{2}{3} \Delta^{\frac{3}{2}} + \Delta^{\frac{1}{2}} H' \right) \qquad \textbf{(3.10)}$$

$$\dot{m}'_{out} = \dot{m}_{out} / W_v = \frac{2}{3}\rho_0 C_d \left(\frac{T_0}{T_H}\right)\sqrt{2g\frac{\theta}{T_0}}(H'')^{\frac{3}{2}} \quad \textbf{(3.11)}$$

To account for the mass loss rate of fuel, $\dot{m}_p$, from the fire, let

$$\dot{m}_p = (\gamma - 1)\dot{m}_{in} \quad \textbf{(3.12)}$$

where

$\gamma = 1+s$

and s is the fuel-air mass ratio

$$s = \frac{\dot{m}_p}{\dot{m}_{in}}$$

Hence

$$\dot{m}_{out} = \gamma \cdot \dot{m}_{in} \quad \textbf{(3.13)}$$

For the fire plume inside the compartment, consider a line plume spanning the full width of the compartment, W_c, with two full wall-size openings, one at the front and one at the back, shown schematically in Figure 3.5. Since the interest is on the "one-sided" line plume with entrainment into one side of the plume, an imaginary frictionless wall closing one fully open end at the plane of symmetry of the plume is considered. The "one-sided" plume is therefore represented by half of its plume strength of $2\dot{Q}'$ and the entrainment by the line plume per unit of its line source is (after Thomas (1992)):

$$\dot{m}'_{plume} = \dot{m}_{plume} / W_c = \rho_0 J \left(\frac{g\dot{Q}'}{\rho_0 c_p T_0}\right)^{\frac{1}{3}} (H' + \delta) \quad \textbf{(3.14)}$$

where J is the entrainment constant that varies with plume "types". Note that for an opening with a sill height, δ, it would provide the plume with an additional entraining height of δ to H'. Thomas (1992) reported that for the free line-plume, J=0.365 (after Lee and Emmons, 1961) and for the wall line-plume, J=0.214 (after Grella and Faeth, 1975); the lower J value in the wall plume was attributed to the wall stabilising the plume and to a lesser extent by the wall friction effect (Thomas, 1992).

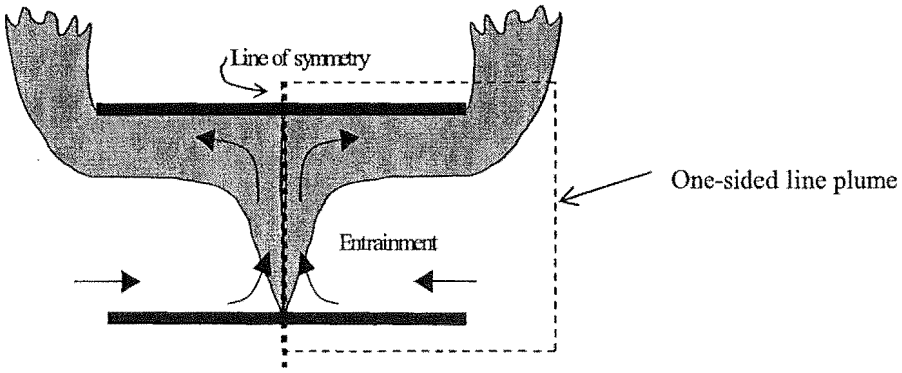

Figure 3.5 Schematic representation of line plume inside a compartment.

Assuming the same discharge coefficient, C_d, for both inflow and outflow, the heat released from the fire convected away by the flow via the opening can be expressed as

$$\begin{aligned} \mu\dot{Q} &= \dot{m}_{out} c_p \theta \\ &= \gamma \dot{m}_{in} c_p \theta \end{aligned} \qquad \textbf{(3.15)}$$

where μ is a factor that describes the fraction of the fire heat release rate involved in the convection. For negligible energy loss to the boundaries as well as radiation loss via opening, μ is equalled to unity; otherwise, μ is less than unity.

Expressing in term of the heat release per unit length of the line source, $\dot{Q}'$, where the length of the line source is assumed to equal the width of the compartment, W_c, Equation (3.15) becomes

$$\mu\dot{Q}' = (\dot{m}_{out}/W_c)c_p\theta = (\gamma\dot{m}_{in}/W_c)c_p\theta \quad \textbf{(3.16)}$$

By substituting Equation (3.16) into Equation (3.10) to eliminate θ, and using Equation (3.13) to express Equation (3.10) as outflow per unit vent width, $(\dot{m}_{out}/W_v)$, gives

$$(\dot{m}_{out}/W_v)\left(\frac{1}{\gamma}\right)^{\frac{2}{3}} = \rho_0\left(\frac{g\dot{Q}'}{\rho_0 c_p T_0}\right)^{\frac{1}{3}}(2\mu)^{1/3}(C_d)^{2/3}\left(\frac{T_0}{T_H}\right)^{\frac{1}{3}}\left(\frac{W_c}{W_v}\right)^{\frac{1}{3}}\left(\frac{2}{3}\Delta^{3/2} + \Delta^{1/2}H'\right)^{\frac{2}{3}} \quad \textbf{(3.17)}$$

Similarly, by substituting Equation (3.16) into Equation (3.11) gives

$$(\dot{m}_{out}/W_v) = 2\left(\frac{C_d}{3}\right)^{\frac{2}{3}}\left(\frac{T_0}{T_H}\right)^{\frac{2}{3}}\rho_0\left(\frac{g\dot{Q}'}{\rho_0 c_p T_0}\right)^{\frac{1}{3}}(\mu)^{1/3}\left(\frac{W_c}{W_v}\right)^{\frac{1}{3}}H'' \quad \textbf{(3.18)}$$

Assuming there is no mixing between the two layers, from the conservation of mass, the sum of the entrainment into the plume and the fuel rate has to equal the outflows through the opening. Expressed in term of outflow per unit vent width, $(\dot{m}_{out}/W_v)$, Equation (3.14) can be expressed as

$$H' = \frac{(\dot{m}_{out}/W_v)}{\rho_0\left(\frac{g\dot{Q}'}{\rho_0 c_p T_0}\right)^{\frac{1}{3}}}\cdot\frac{1}{\chi J}\cdot\left(\frac{W_v}{W_c}\right) - \delta \quad \textbf{(3.19)}$$

Defining a dimensionless parameter, K, as

$$K = \frac{(\dot{m}_{out}/W_v)}{H_v\rho_0\left(\frac{gQ'}{\rho_0 c_p T_0}\right)^{\frac{1}{3}}} \quad \textbf{(3.20)}$$

Rewrite Equations (3.17), (3.18) and (3.19) in term of K, as follows:

$$K = \gamma^{\frac{2}{3}}\left(\frac{1}{H_v}\right)(2)^{1/3}(\mu)^{1/3}(C_d)^{2/3}\left(\frac{T_0}{T_H}\right)^{\frac{1}{3}}\left(\frac{W_c}{W_v}\right)^{\frac{1}{3}}\left(\frac{2}{3}\Delta^{3/2}+\Delta^{1/2}H'\right)^{\frac{2}{3}} \tag{3.21}$$

$$= a\left(\frac{1}{H_v}\right)(\mu)^{1/3}\left(\frac{W_c}{W_v}\right)^{\frac{1}{3}}\left(\frac{2}{3}\Delta^{3/2}+\Delta^{1/2}H'\right)^{\frac{2}{3}}$$

$$K = 2(\mu)^{1/3}\left(\frac{C_d}{3}\right)^{\frac{2}{3}}\left(\frac{T_0}{T_H}\right)^{\frac{2}{3}}\left(\frac{W_c}{W_v}\right)^{\frac{1}{3}}\left(\frac{1}{H_v}\right)H'' \tag{3.22}$$

$$= b(\mu)^{1/3}\left(\frac{1}{H_v}\right)\left(\frac{W_c}{W_v}\right)^{\frac{1}{3}}H''$$

$$K = \chi J\left(\frac{W_c}{W_v}\right)\left(\frac{1}{H_v}\right)(H'+\delta) \tag{3.23}$$

$$K = c\left(\frac{W_c}{W_v}\right)\left(\frac{1}{H_v}\right)(H'+\delta)$$

where

$a = \gamma^{\frac{2}{3}}(2)^{1/3}(C_d)^{2/3}\left(\frac{T_0}{T_H}\right)^{\frac{1}{3}}$, $b = 2\left(\frac{C_d}{3}\right)^{\frac{2}{3}}\left(\frac{T_0}{T_H}\right)^{\frac{2}{3}}$ and $c = \chi J$.

Since the opening height, H_v, as shown in Figure 3.4 is

$$H_v = H'' + \Delta + H' \tag{3.24}$$

Substituting Equations (3.22) and (3.23) into Equation (3.24), to obtain an expression for Δ, where

$$\Delta = H_v + \delta - \left[\frac{K}{c} H_v \left(\frac{W_v}{W_c}\right)\right] - \frac{K}{b} H_v \left(\frac{W_v}{W_c}\right)^{\frac{1}{3}} \left(\frac{1}{\mu}\right)^{\frac{1}{3}} \quad \textbf{(3.25)}$$

Substituting Equation (3.25) into Equation (3.21) gives an expression for K in terms of geometry variables that include the opening width fraction, W_v/W_c, the sill height to opening height ratio, δ/H_v, and the associating constants, a, b and c for the given temperature ratio, T_H/T_0, discharge coefficient, C_d, the fuel-air mass ratio, γ, and the plume entrainment constant, J, (as given in Equations (3.21), (3.22) and (3.23) respectively), where

$$K = a(\mu)^{\frac{1}{3}} \left(\frac{W_c}{W_v}\right)^{\frac{1}{3}} \left\{ \begin{array}{l} \frac{2}{3}\left[1 + \frac{\delta}{H_v} - \frac{K}{c}\left(\frac{W_v}{W_c}\right) - \frac{K}{b}\left(\frac{W_v}{W_c}\right)^{\frac{1}{3}}\left(\frac{1}{\mu}\right)^{\frac{1}{3}}\right]^{\frac{3}{2}} \\ + \left[1 + \frac{\delta}{H_v} - \frac{K}{c}\left(\frac{W_v}{W_c}\right) - \frac{K}{b}\left(\frac{W_v}{W_c}\right)^{\frac{1}{3}}\left(\frac{1}{\mu}\right)^{\frac{1}{3}}\right]^{\frac{1}{2}} \left[\frac{K}{c}\left(\frac{W_v}{W_c}\right) - \frac{\delta}{H_v}\right] \end{array} \right\}^{\frac{2}{3}} \quad \textbf{(3.26)}$$

For a uniform well-mixed fire environment, where the hot layer has reached the floor level, $H' = 0$, (which is the assumption made by Kawagoe), the flow is at the maximum for the given layer temperature. Similarly, this maximum flow can be expressed in term of K. Using Equation (3.21) with $H' = 0$ to obtain the expression for Δ, and Equation (3.22) for H'', substituting these expressions into Equation (3.24), gives

$$K_{\max} = \frac{\left(\frac{W_c}{W_v}\right)^{\frac{1}{3}}}{\left(\frac{1}{\mu}\right)^{\frac{1}{3}}\left[\frac{1}{a}\left(\frac{3}{2}\right)^{\frac{2}{3}} + \frac{1}{b}\right]} \quad \textbf{(3.27)}$$

This is the condition for the maximum flow, hence a subscript of max for K.

The term K is written in term of mass outflow, $\dot{m}_{out}$. Since the present analysis is to investigate the air inflow rate across the vent opening, the K-term, $(\dot{m}_{out}/W_v)/\rho_0\left(g\dot{Q}'/\rho_0 c_p T_0\right)^{1/3} H_v$, can be rearranged and reduced to give the air inflow per unit opening width, $(\dot{m}_{in}/W_v)$, by substituting Equations (3.13) and (3.16) into Equation (3.20) giving

$$\dot{m}_{in}/W_v = \frac{1}{\gamma}\cdot(\rho_0 K)^{\frac{3}{2}}\cdot\sqrt{\frac{g\theta}{\mu\rho_0 T_0}}\cdot\sqrt{\frac{W_v}{W_c}}\cdot H_v^{3/2} \qquad \textbf{(3.28)}$$

The right hand terms in Equation (3.28) excluding the term, $H_v^{3/2}$, can be lumped into the coefficient, C, given as follows:

$$\dot{m}_{in}/W_v = C\cdot H_v^{3/2} \qquad \textbf{(3.29)}$$

or

$$\dot{m}_{in}/A_v\sqrt{H_v} = C = \frac{1}{\gamma}\cdot(\rho_0 K)^{\frac{3}{2}}\cdot\sqrt{\frac{g\theta}{\mu\rho_0 T_0}}\cdot\sqrt{\frac{W_v}{W_c}}$$

where the coefficient C can be regarded as the air inflow per unit vent parameter, $(\dot{m}_{in}/A_v\sqrt{H_v})$; and the K for the stratified two-layer environment, $H'>0$, is given in Equation (3.26).

For a uniform well-mixed fire environment, where the hot layer has reached the floor level (for a door) or the sill level (for a window), $H'=0$, the flow is at the maximum. The expression of coefficient, C_{max}, is given in Equation (3.9) as derived by Rockett (1976), where the subscript, max, denotes the maximum flow. Note that Equation (3.9) can also be derived from substituting the $K_{\max}$ expression in Equation (3.27) into Equation (3.28).

3.3.2 Vent without sill (Door)

Equation (3.26) is a generalised flow equation for a stratified two-layer flow system coupled by a line plume at various vent geometry characterised by the opening width

fraction, W_v/W_c, and the sill height to opening height ratio, δ/H_v. Consider a wall opening with no sill, δ =0, i.e. a door opening. Assuming adiabatic boundaries and negligible radiative heat loss through the opening, where all the heat released by the fire being convected away by the flow, i.e. μ =1; using a layer temperature of 900°C as an example, Figure 3.6 (a) shows the calculated C-value for the free and the wall line plume at various opening width fractions, W_v/W_c. The C_{max}-value for the maximum flow condition (from Equation (3.9)) is also shown. The constants used in the calculations include: ρ_0 =1.2kg/m^3, g =9.81m/s^2, γ=1.2, C_d =0.68 and T_0 =293K.

It can be seen that at large W_v/W_c, the air inflow per unit vent parameter, $(\dot{m}_{in} / A_v\sqrt{H_v})$, i.e. the coefficient C, from the line plume entrainment is less than the prediction made by using Kawagoe treatment that assumes uniform well-mixed temperature inside the compartment. Figure 3.6 (b) show the corresponding C/C_{max} ratio for the free line-plume and the wall line-plume at various opening width fractions. It can be seen that over this temperature range, at the full width opening, i.e. W_v/W_c =1, the air inflow per unit vent parameter, C, from the free and wall line plumes entrainment is approximately 80% and 60% respectively of the maximum value predicted by assuming a uniform well-mixed fire environment with H'=0 (as by Kawagoe). As the opening width fraction decreases, the C-value by the line plumes approaches the Kawagoe prediction. This is expected because with the reduction of the opening width fraction, the outflow through the opening is reduced. In order to maintain the mass balance in the system, which requires the entrainment into the plume plus the fuel rate to equal the outflow through the opening, the system adjusts itself lowering the hot layer towards the floor level. This decreases the clear height, H', between the floor and the hot layer, hence the plume entrainment rate. Continuing to decrease the opening width will lead to the lowering of the hot layer towards the floor level approaching a uniform well-mixed environment.

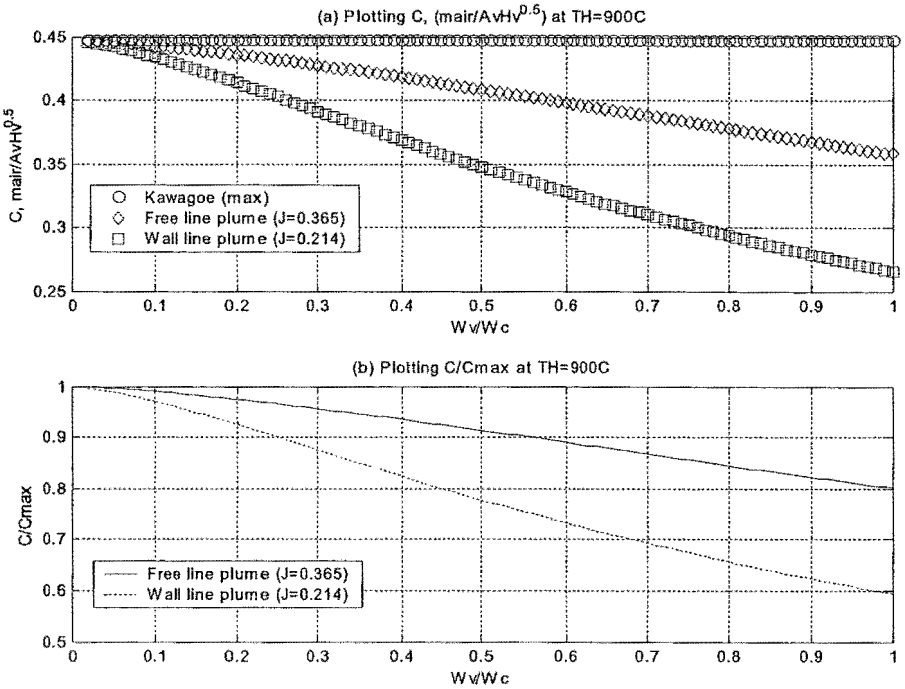

Figure 3.6 **The air inflow behaviours at various opening width fractions predicted using the line-plume analogy and the Kawagoe treatment at a layer temperature of 900°C.**

Figure 3.7 shows the C-value calculated from the uniform well-mixed temperature assumption, i.e. the Kawagoe treatment (Equation (3.9)) and from the two line plumes (Equation (3.28)) plotted against the hot layer temperature for a full width opening with no sill. The constants used in the equations are as follows: ρ_0 =1.2kg/m^3, g = 9.81m/s^2, γ=1.2, C_d =0.68 and T_0 =293K.

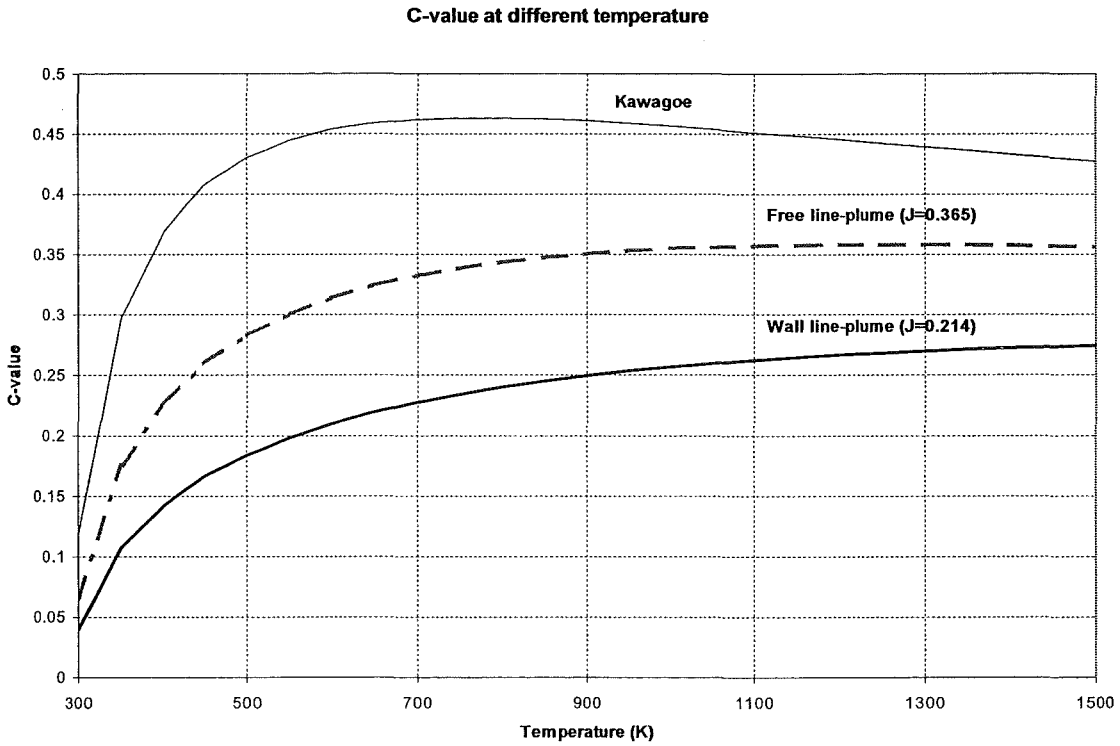

Figure 3.7 **C-value as a function of temperature for different types of flow across a vent with a full width opening and no sill.**

For the range of temperature (800K to 1500K) of most interest, it can be seen that in Figure 3.7 that the C-value is almost constant for the three cases, varying up to approximately ±7% of their values within this temperature range. The approximate C-values for each case are given in Table 3.1. Note that for the Kawagoe case which assumes a uniform well-mixed environment with $H'=0$, the C-value is approximately 0.45, the same as previously deduced (shown in Figure 3.2).

Table 3.1 **C-values for approximate air inflow equation for temperature ranges from 800K to 1200K at a full opening.**

	C-value	Approximate air inflow equation	
Kawagoe (H'=0)	C=0.45±3%	$\dot{m}_{in} / A_v\sqrt{H_v} \approx 0.45$	**(3.30)**
Free line-plume (J=0.365)	C=0.35±2%	$\dot{m}_{in} / A_v\sqrt{H_v} \approx 0.35$	**(3.31)**
Wall line-plume (J=0.214)	C=0.26±7%	$\dot{m}_{in} / A_v\sqrt{H_v} \approx 0.26$	**(3.32)**

Consider an opening having no sill and with opening width equal to the compartment width (i.e. W_v=W_c), taking the practical maximum line source length equal to the compartment width, the air inflow through the opening into the compartment due to plume entrainment are $0.35\,A_v\sqrt{H_v}$ and $0.26\,A_v\sqrt{H_v}$ for a free line plume and a wall line-plume respectively and both are smaller than the maximum of $0.45\,A_v\sqrt{H_v}$. A wall line plume will have a flow rate of approximately 60% of the maximum flow rate predicted by assuming a uniform fire environment with H'=0 (as by Kawagoe). This finding is in line with the observation by Babrauskas and Williamson (1978), that for a large vent opening such as a window taking up one whole wall, the actual air inflows appear to be ~50% lower than predicted by Kawagoe's method.

The lower flow rate estimated from a line plume in a stratified two-layer environment compared to Kawagoe's uniform well-mixed assumption can be comprehended by comparing the hydrostatic pressure distributions from the two assumptions. Figure 3.8 schematically depicts the hydrostatic pressure distribution for both the uniform (H' =0) and the stratified (H'> 0) cases.

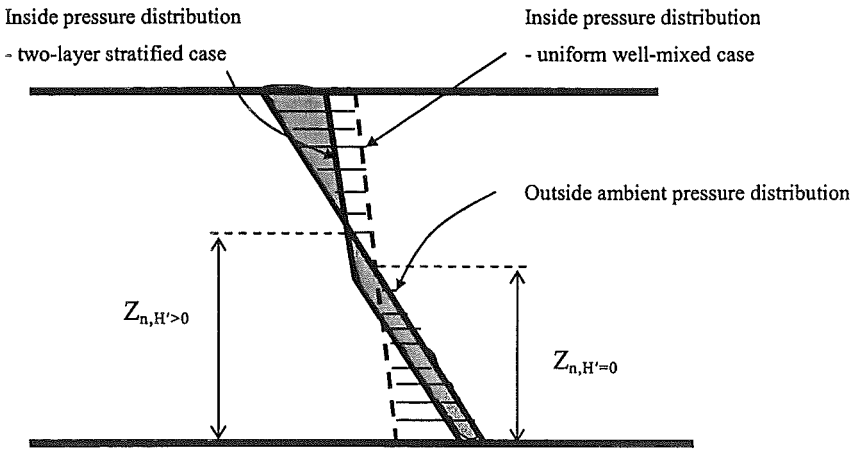

Figure 3.8 Schematic representation of pressure distribution at the opening.

The pressure gradient of the inside gas layer for both cases are indicated in the figure. From the mass balance, the mass flow above the neutral-plane height plus the fuel mass loss rate equal the mass flow below the neutral plane height. The buoyancy head across the vent opening is represented by the hydrostatic pressure difference between the inside and outside environment. It can be seen that the single zone uniform assumption (with $H'=0$) produces the maximum buoyancy head across the opening indicated by the large "area" between the hydrostatic pressure distributions. Since the vent flows are the result of buoyancy, the "one-half factor" mentioned is simply used to adjust the flow rate so it matches with the plume entrainment rate. It is noted that due to the nature of the assumption, the neutral-plane height from the uniform well-mixed assumption with $H'=0$ is expected to be lower than the neutral-plane height evaluated from the stratified assumption with $H'>0$.

3.3.3 Vent with sill (Window)

As discussed before, reducing the opening width will lower the hot layer towards the floor level. For a window opening with a given sill height, there exists a limiting opening width fraction where the hot layer is at the sill level. At this stage, the flow across the opening is at the maximum and is restricted by the opening geometry. Further decrease in the opening width would mean that the plume is trying to entrain

more air than allowed through the opening, resulting in a lot of circulation and mixing.

Figure 3.9 plots the C/C_{max} ratio of a wall line-plume in a compartment at various opening width ratios, W_v/W_c, for different sill height, δ/H_v, at a layer temperature of 900°C. It can be seen that for a window with a high sill, the maximum flow condition (C/C_{max} =1) is achieved at a larger width ratio compared to a window with a low sill.

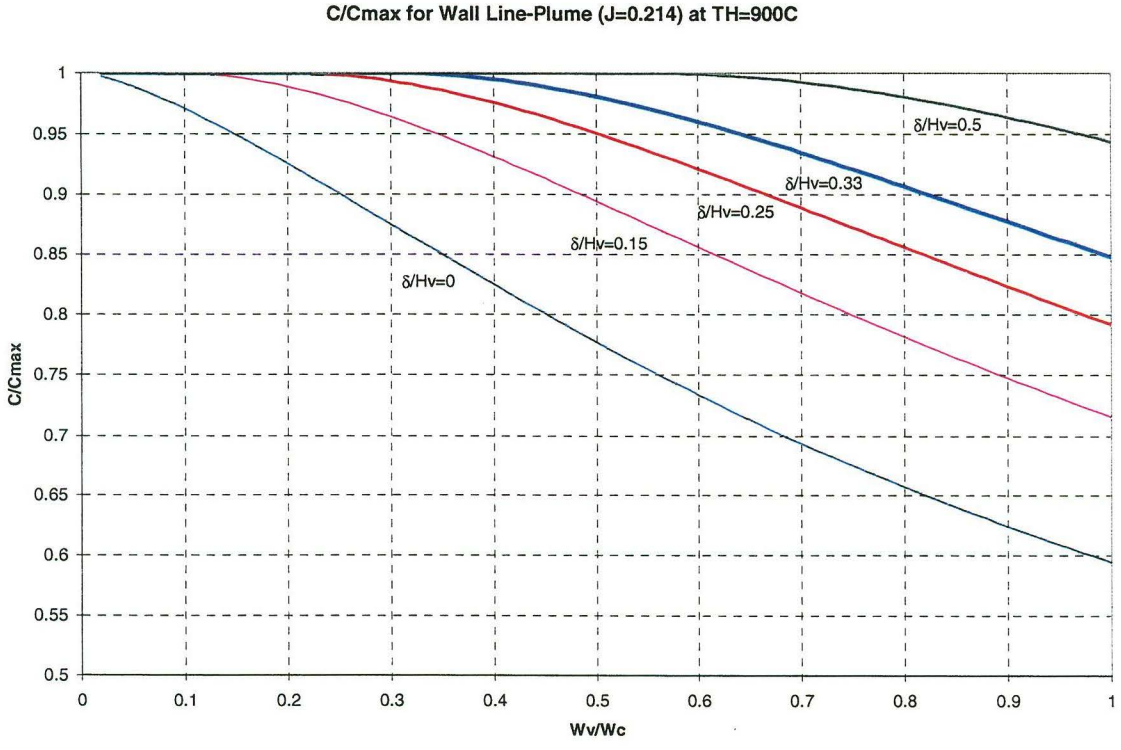

Figure 3.9 **The flow behaviour of a wall line-plume (J=0.214) at various opening width ratios, W_v/W_c, for different sill heights, δ/H_v, at a layer temperature of 900°C.**

This limiting opening width fraction, $(W_v/W_c)_{\lim}$, for a given sill height, δ/H_v, can be deduced by equating Equation (3.23) to Equation (3.27), with $K_{\max}$ describing the maximum flow condition at H'=0. This is given in Equation (3.33).

$$\left(\frac{W_v}{W_c}\right)_{\lim} = \frac{\gamma J}{K_{\max}} \cdot \frac{\delta}{H_v} \qquad (3.33)$$

Figure 3.10 plots the critical geometry combinations, W_v/W_c against δ/H_v for the two different line plumes using Equation (3.33). For the actual vent opening geometry (defined by the combination of W_v/W_c and δ/H_v) smaller than the critical value, i.e. below the critical line to the right hand side in the plot in Figure 3.10, the hot layer is expected to drop below the sill height of the opening, and the flow is at the maximum. The Kawagoe vent flow treatment would be appropriate in these scenarios.

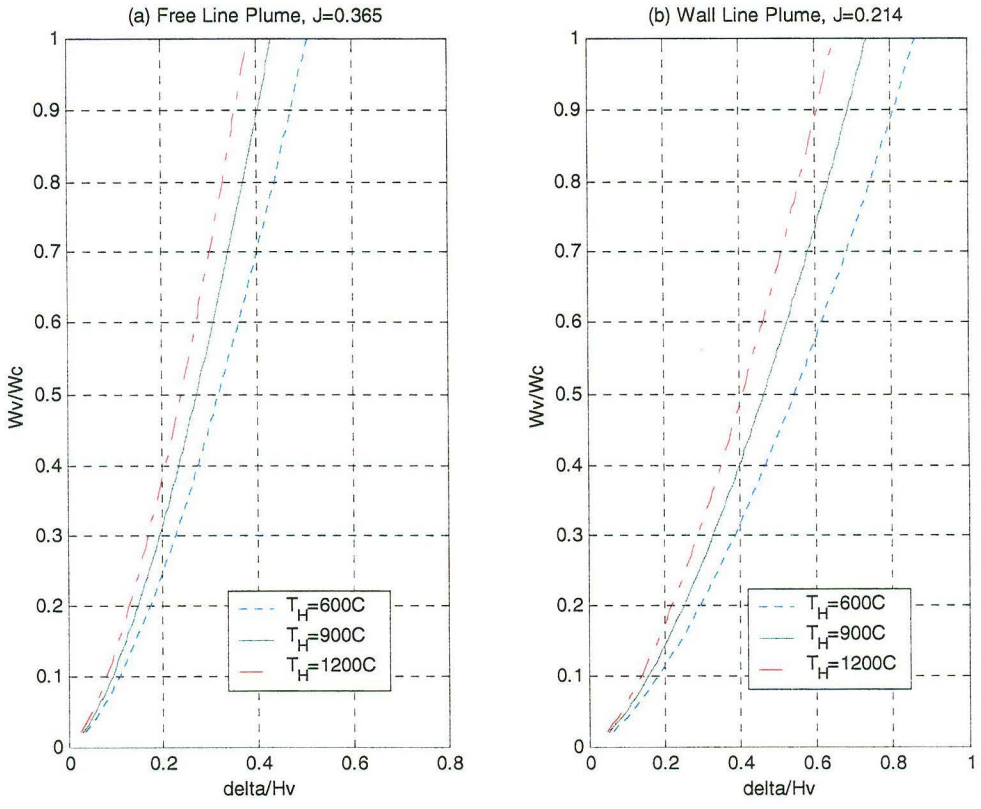

Figure 3.10 Critical geometry combinations between W_v/W_c and δ/H_v.

Both W_v/W_c and δ/H_v are geometrical variables that describe the geometry of a vent opening. They can be combined to give a single variable, termed as the opening fraction, A_v/A_w, where A_v is the vent opening area and A_w is the area of the wall that contains the vent without the downstand area above the opening. Defining the opening height fraction as the ratio between the opening height, H_v, to the height from the floor level to the soffit height of the opening, H_s, and expressed in term of the sill height, δ, gives

$$\frac{H_v}{H_S} = \frac{1}{(1+\delta/H_v)} \tag{3.34}$$

The opening fraction, A_v/A_w, is then expressed as

$$\frac{A_v}{A_w} = \frac{W_v H_v}{W_c H_S} = \frac{W_v}{W_c}\frac{1}{(1+\delta/H_v)} \tag{3.35}$$

This is a useful parameter for estimating the flow conditions through the opening. For example, from the plot in Figure 3.10, for W_v/W_c =1, the limiting δ/H_v for the free and the wall line plumes is 0.43 and 0.74 respectively at 900°C. This corresponds to a critical opening fraction, A_v/A_w, of 0.7 and 0.6 respectively. Hence, for a compartment with a full width opening, provided the opening fraction is smaller than the critical opening fraction defined by Equation (3.33), the plume would be trying to entrain more air than allowed through the opening, resulting in a lot of circulation and mixing. The flow will be at the maximum with the flow rate limited by the given environment and vent geometry. In such conditions, the Kawagoe vent flow treatment will be adequate as the hot layer will be at or below the sill.

3.3.4 Effects of heat losses

The above analysis is performed on the assumption that all the energy released in the fire is convected away by the flow via the opening with negligible heat losses to the enclosure ceiling and walls as well as radiation loss to the outside, i.e. μ taken as 1 in Equation (3.15). The heat loss terms can be presented in such a form by linearising with the temperature rise, θ, such that the heat loss to the enclosure boundaries is estimated as $h_w A_t \theta$, where h_w is the overall heat transfer coefficient to the ceiling and walls, A_t is the area associated with the heat transfer. For radiation loss through vent opening, this loss term can be estimated as $A_v \sigma T_H^3 \theta$ where $T_H^4 \approx T_H^3 \theta$ for $T_H >> T_0$. Equation (3.15) can be rewritten as

$$\dot{Q} \approx \gamma \dot{m}_{in} c_p \theta + h_w A_t \theta + A_v \sigma T_H^3 \theta \tag{3.36}$$

Normalised by the convection term, $\gamma \dot{m}_{in} c_p \theta$, Equation (3.36) becomes

$$\dot{Q} \approx \gamma \dot{m}_{in} c_p \theta \left(1 + \frac{h_w A_t}{\gamma \dot{m}_{in} c_p} + \frac{A_v \sigma T_H^3}{\gamma \dot{m}_{in} c_p} \right) \tag{3.37}$$

Since the air inflow takes the form of Equation (3.29), where $\dot{m}_{in} \approx C \cdot A_v \sqrt{H_v}$, Equation (3.37) becomes

$$\dot{Q} \approx \gamma \dot{m}_{in} c_p \theta \left(1 + \frac{h_w A_t}{\gamma c_p C A_v \sqrt{H_v}} + \frac{A_v \sigma T_H^3}{\gamma c_p C A_v \sqrt{H_v}} \right) \tag{3.38}$$

Equation (3.38) is similar to the expression given by Quintiere (2002) in his analysis of the heat loss terms inside a compartment. Following the definition in Equation (3.15), μ is represented as

$$\mu \approx \left(1 + \frac{h_w A_t}{\gamma c_p C A_v \sqrt{H_v}} + \frac{A_v \sigma T_H^3}{\gamma c_p C A_v \sqrt{H_v}} \right)^{-1} \tag{3.39}$$

The overall heat transfer coefficient, h_w, depends on the convection (h_{conv}), radiation (h_{rad}) and conduction (h_{cond}) into the wall. For boundaries with semi-infinite thickness, the heat loss to the boundaries, $\dot{q}''_w$, can be written as follows

$$\begin{aligned} \dot{q}''_w &= (h_{conv} + h_{rad})(T_H - T_{wi}) = h_{cond}(T_{wi} - T_0) \\ &= h_w (T_H - T_0) \end{aligned} \tag{3.40}$$

where

$$1/h_w = 1/(h_{conv} + h_{rad}) + 1/h_{cond}$$

Quintiere (2002) has given the typical range for these heat transfer coefficients, where h_{conv} ~10-30W/m^{2}K, h_{rad} ~5-100W/m^2-K, and $h_{cond} \sim \sqrt{k\rho c/t}$ ~5-60W/m^2-K, with

h_{cond} decreases over time. For the purposes in estimating the boundary heat loss term in Equation (3.39), the overall heat transfer coefficient, h_w, is taken to be 20W/m^2-K as a first approximation. By taking $A_t = A_T - A_v$ with A_T being the total internal surface area, for a square compartment with a height of 3m having a vent opening comprising one full wall, $A_t / A_v\sqrt{H_v}$ ranges from 4m$^{-0.5}$ to 5m$^{-0.5}$ for the respective compartment length ranging from 5m to 10m. Using the wall line-plume analogy for a full wall opening, $C \approx 0.26$, with $\gamma = 1.2$ and $c_p = 1150$J/kg-K, the boundary heat loss term in Equation (3.39) is approximately 0.3. This value will be even smaller for larger vent openings. To estimate the radiation loss term in Equation (3.39), for the vent opening height equals to the wall height of 3m, using $T_H = 1500$K, the radiation loss term is approximately 0.3. This loss term will be smaller for a lower layer temperature, T_H. Hence the value of μ is likely to range between ~0.6 and 1.

The effects of heat losses (μ<1) on the calculated C values for different types of flow across a vent with a full width opening and no sill are shown in Figure 3.11.

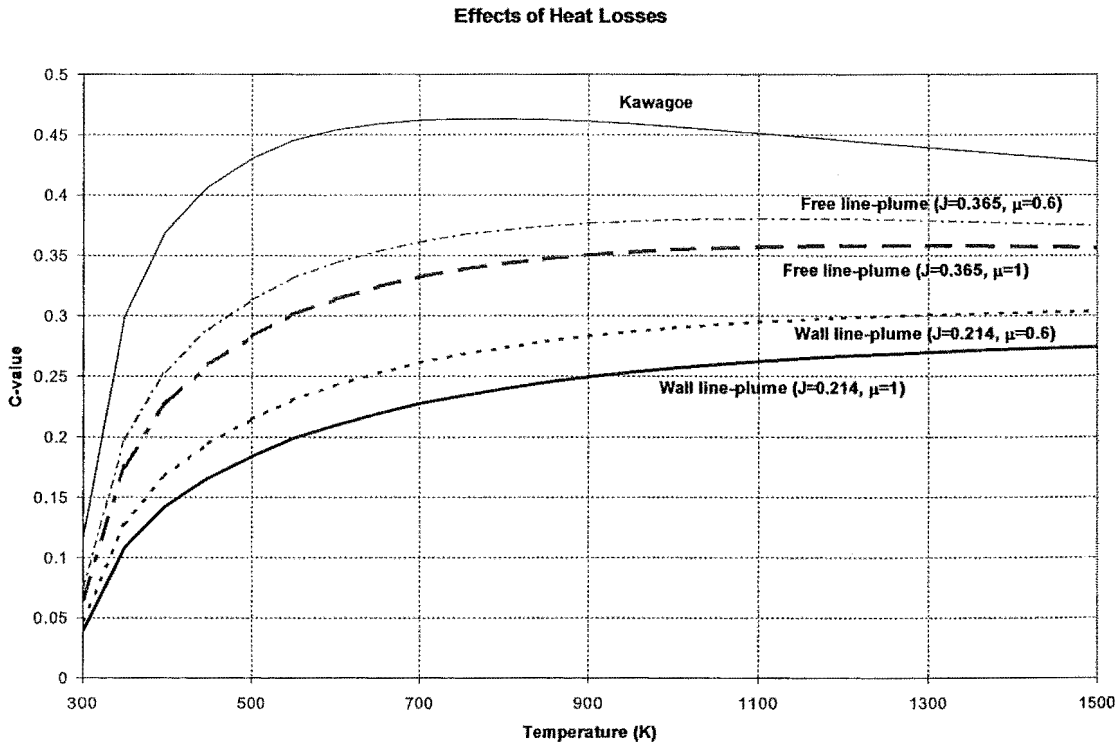

Figure 3.11 Effects of heat losses (μ<1) on the calculated C values for different types of flow across a vent with a full width opening and no sill.

From Figure 3.11, it can be seen that the for μ between 0.6 and 1.0, the calculated C-values vary only slightly, raising from approximately 0.26 to 0.29 for a wall line-plume; and from approximately 0.35 to 0.37 for a free line-plume over the temperature range from 800K to 1500K. Equation (3.15) expresses the heat release rate, $\dot{Q}$, in term of the layer temperature rise, θ. With the inclusion of the heat loss terms, i.e. μ <1, to maintain a given θ requires a higher value of heat release rate $\dot{Q}$. This translates to a greater entrainment rate, as the plume entrainment is a function of $\dot{Q}$ (Equation (3.14)). The limiting vent geometry defined in Equation (3.33) will be affected by $\mu^{-1/3}$, as K_{max} is a function of $\mu^{1/3}$ given in Equation (3.27), such that

$$\left(W_v/W_c\right)_{\text{lim},\mu<1} = \mu^{-1/3} \cdot \left(W_v/W_c\right)_{\text{lim},\mu=1} \qquad \textbf{(3.41)}$$

In the case of μ =0.6, for a given sill height, the limiting opening width ratio, $(W_v/W_c)_{lim,\mu=0.6}$, is approximately 1.2 times larger than the limit evaluated for μ =1, i.e. $(W_v/W_c)_{lim,\mu=1}$, which means achieving the maximum flow condition at a larger opening geometry than the case of μ =1.

3.4 SUMMARY

The above analysis has shown that for a compartment with a full frontal opening, the Kawagoe method is likely to overestimate the vent flows because the environment inside is not very well-mixed. It appears that using the line-plume analogy to emulate the flows in the full opening condition can yield a result in line with the findings reported in the literature. The critical opening fraction for a given sill height found in the analysis that separates the well-mixed and the stratified conditions should be regarded only as an indicative value. This is because the vent flow analysis performed is idealistic in that it assumes a cold ambient lower layer below a hot upper layer with no mixing which may not be true in an actual post-flashover fire environment. It should also be noted that in actual fires the outflow could be subjected to potential

momentum influences from the flame or ceiling jet that would have an effect on the resulting vent flows. Future research is needed to study these effects.

For engineering application purposes, it is useful to introduce a correction factor, $\Lambda=C/C_{max}$, on the vent flow equations (Equations (3.3) and (3.4)) to account for the less well-mixed environment encountered at large openings. For a full wall opening, i.e. full width with no sill (A_v/A_w =1), based on the wall line plume analogy, $\Lambda\approx 0.6$. For partial wall openings (A_v/A_w <1), from Figure 3.9, for window type openings with high sill, δ/H_v, $\Lambda\approx 1$; whereas for door type openings with low or no sill, $0.6<\Lambda<1.0$. As mentioned before, Figure 3.9 presents the results obtained from an idealistic study based on wall line-plume analysis assuming stratified layers without mixing. Further analysis with reference to experimental fires is necessary to deduce practical correction factors for the various opening geometries.

In the proposed CFIRE model, the vent flows equations (Equations (3.3) and (3.4)) derived from the assumption of uniform temperature are retained. A correction factor, Λ, of 0.6 is introduced for a full opening, A_v/A_w =1, to account for the less well-mixed environment encountered based on the wall line plume analogy. Equations (3.3) and (3.4) are rewritten as Equations (3.42) and (3.43).

$$\dot{m}_{in} = \frac{2}{3}\cdot\Lambda\cdot C_d\cdot W_v\cdot\rho_0\cdot\sqrt{2g\left(1-\frac{\rho_g}{\rho_0}\right)}\cdot(Z_n-\delta)^{3/2} \qquad \textbf{(3.42)}$$

$$\dot{m}_{out} = \frac{2}{3}\cdot\Lambda\cdot C_d\cdot W_v\cdot\rho_g\cdot\sqrt{2g\left(\frac{\rho_0}{\rho_g}-1\right)}\cdot(H_s-Z_n)^{3/2} \qquad \textbf{(3.43)}$$

where Λ is taken as 1 for A_v/A_w <1, and Λ as 0.6 for A_v/A_w =1 as first approximations. It should also be noted that the use of the correction factor, Λ, in Equations (3.42) and (3.43) at the full opening only corrects for the flow rates. The would-be neutral-plane height, Z_n, associated with the stratified flow is underestimated as depicted in Figure 3.8.

Chapter 4 COMBUSTION

This chapter outlines the treatments that have been used to estimate the effective heat of combustion for the burning fuel under different ventilation conditions. The results from these different treatments are compared and their application in the well-stirred post-flashover compartment is discussed.

4.1 INTRODUCTION

The heat release from the fire is the result of the combustion reaction between the fuel vapour and air where the fuel and air molecules are broken up and converted to new molecules, giving off energy from releasing the binding forces that hold the molecules together. The term, *heat of combustion*, represents the energy released from a unit mass of fuel after complete combustion, producing carbon dioxide and water as the combustion products. Depending on the state of water, whether it is in liquid or in vapour form, the heat of combustion is represented by the *gross* heat of combustion, $\Delta h_{c,gross}$, and the *net* heat of combustion, $\Delta h_{c,net}$ respectively. For fire applications the net heat of combustion is used. However, for a burning fuel inside a compartment, the effective heat release per unit mass of the burning fuel, $\Delta h_{c,eff}$, is likely to be less than the net heat of combustion, $\Delta h_{c,net}$. This is due to inefficient mixing that results in the generation of incomplete combustion products such as carbon monoxide, hydrogen, soot and unburned hydrocarbon. The ratio between these two quantities is the combustion efficiency, χ, given in Equation (4.1).

$$\chi = \frac{\Delta h_{c,eff}}{\Delta h_{c,net}} \qquad \textbf{(4.1)}$$

Hess's law of constant heat summation can be used to estimate the effective heat of combustion provided the composition of the combustion products are known (Drysdale, 1985). Equation (4.2) is a generalised equation for estimating the effective heat release per unit mass of fuel, $\Delta h_{c,eff}$,

$$\Delta h_{c,eff} = \Delta h_{c,net} - \sum_{i}^{p} f_i \Delta h_{c,i} \qquad \textbf{(4.2)}$$

where f_i is the mass yield of incomplete combustion products per unit mass of fuel (kg/kg) and $\Delta h_{c,i}$ is the net heat of combustion of the incomplete combustion products (J/kg). From Equation (4.2), it can be seen that if there are incomplete combustion products being generated, the effective heat of combustion will be less than the net heat of combustion. Kawagoe and Sekine (1963), in their post-flashover fire modelling, used an effective heat of combustion of 10.8MJ/kg for wood rather than the net heat of combustion of 18.7MJ/kg. They attributed the reduction in the heat of combustion was due to the high carbon monoxide presence in the outflow observed during the experiments (Kawagoe, 1958). This contributes to a combustion efficiency of χ=0.6.

The condition inside the environment where combustion takes place can be described using a dimensionless number known as the equivalence ratio, Φ. It provides a relative measure over the condition in the fire environment with respect to the stoichiometry condition. The equivalence ratio is defined as

$$\Phi = \frac{\dot{m}_p \times r}{\dot{m}_{in}} \qquad \textbf{(4.3)}$$

where r is the stoichiometric air to fuel mass ratio for the fuel involved. The equivalence ratio has a value greater than 1 for a fuel-rich environment and a value less than 1 for a fuel-lean environment.

4.2 ESTIMATING THE EFFECTIVE HEAT OF COMBUSTION

The single zone compartment fire theory assumes that the compartment behaves as a well-stirred reactor with infinitely fast reaction. The fire heat release rate is therefore evaluated as the product between the fuel supply rate, $\dot{m}_p$, and the effective heat of combustion, $\Delta h_{c,eff}$. Since the fire heat release rate is the main force that drives the temperature inside a post-flashover compartment, the effective heat of combustion per unit mass of fuel supplied is an important parameter. In the sections to follow, the available treatments and correlations that have been used to estimate the effective heat of combustion under different ventilation conditions are presented. The application of these treatments in post-flashover compartment modelling is discussed.

4.2.1 Complete reaction model

This is the simplest combustion model that has been used in the post-flashover compartment fire model. During the well-ventilated condition, $\Phi<1$, all the available fuel is assumed to be burned completely; for ventilation limited condition, $\Phi>1$, all the air available is assumed to be burned completely and the remaining fuel is simply regarded as incomplete combustion products. The combustion products consist of CO_2, H_2O, N_2 and O_2 for fuel-lean condition, i.e. $\Phi<1$, and CO_2, H_2O, N_2 and unburned fuel for fuel-rich condition, i.e. $\Phi>1$. The chemical reaction formula for each of these conditions is presented in Equations (4.4) and (4.5) respectively. Generic fuel $C_xH_yO_zN_v$ is used for illustrative purpose.

For fuel-lean condition, $\Phi < 1$,

$$C_xH_yO_zN_v + \frac{m_s}{\Phi}(O_2 + 3.76N_2) \rightarrow xCO_2 + \frac{y}{2}H_2O + m_s\left(\frac{1}{\Phi} - 1\right)O_2 + \left(\frac{v}{2} + \frac{3.76m_s}{\Phi}\right)N_2 \qquad \textbf{(4.4)}$$

where $m_s = x + y/4 - z/2$; which is the mole of the air for stoichiometric combustion of a unit mole of fuel.

For fuel-rich condition, $\Phi > 1$,

$$C_xH_yO_zN_v + \frac{m_s}{\Phi}(O_2 + 3.76N_2) \rightarrow \frac{x}{\Phi}CO_2 + \frac{y}{2\Phi}H_2O + \left(1 - \frac{1}{\Phi}\right)C_xH_yO_zN_v + \left(\frac{v}{2} + \frac{3.76m_s}{\Phi}\right)N_2 \quad \textbf{(4.5)}$$

Since this simple model assumes complete combustion, for the fuel-lean condition ($\Phi<1$), the effective heat of combustion equals the net heat of combustion as no incomplete combustion products have been generated ($\chi=1$). For the fuel-rich condition ($\Phi>1$), the effective heat that could be released per unit mass of fuel being supplied depends on the available ventilation. Since the excess unburned fuel is regarded as the incomplete combustion product, by using Equation (4.2), the effective heat release per unit mass of fuel supplied during fuel-rich condition ($\Phi>1$) is:

$$\Delta h_{c,eff} = \Delta h_{c,net} - \left(1 - \frac{1}{\Phi}\right)\Delta h_{c,net} \quad \textbf{(4.6)}$$

Hence, the combustion efficiency is $\chi = 1/\Phi$.

The complete reaction model yields the same results as the correlations given by Gottuck et al (1992), giving the maximum combustion efficiency. This is presented in Equation (4.7).

$$\begin{aligned} &\chi = 1; && \text{for } \Phi<1; \quad \text{(fuel lean)} \\ &\chi = 1/\Phi; && \text{for } \Phi>1; \quad \text{(fuel rich)} \end{aligned} \quad \textbf{(4.7)}$$

Babrauskas (1979) in the COMPF2 applied a similar approach, but introduced a b_p factor to further reduce the combustion efficiency such that

$$\begin{aligned} &\chi = b_p \times 1; && \text{for } \Phi<1; \quad \text{(fuel lean)} \\ &\chi = b_p \times 1/\Phi; && \text{for } \Phi>1; \quad \text{(fuel rich)} \end{aligned} \quad \textbf{(4.8)}$$

The b_p factor has a range from 0.5 to 0.9 and is to account for the "unmixness" during the combustion inside the compartment (Babrauskas, 1979 and 1981).

4.2.2 Water-gas reaction model

This model assumes that the carbon monoxide, carbon dioxide, hydrogen and water vapour are the sole products from the combustion. It does not assume that the more reactive hydrogen will be fully oxidised in preference of carbon, but recognises dissociation only to the extent of sharing the limited oxygen available between CO_2 and CO (Goodger, 1977). The chemical reaction equation can be presented as follow.

$$C_xH_yO_z + m_s(O_2 + 3.76N_2) \rightarrow n_1CO_2 + n_2H_2O + n_3CO + n_4H_2 + n_5N_2 \qquad \textbf{(4.9)}$$

where $m_s = x + y/4 - z/2$; which is the number of moles of oxygen required for complete combustion of 1 mole of fuel. The "water-gas" dissociation reaction is

$$CO_2 + H_2 \Leftrightarrow CO + H_2O$$

Tsuchiya and Sumi (1971) used this combustion model to estimate the effective heat of combustion for the burning fuel inside a post-flashover compartment fire. They assumed that during the flaming phase of the post-flashover fire, the temperature is hot enough to initiate the water-gas reaction. However, from the literature (Goodger, 1977) the temperature required to cause instability, giving rise to dissociation back towards the reactant forms of CO and hydrogen, is above 1800K (1527°C) which is much hotter than the typical post-flashover fire.

To solve for the amount of the combustion products in Equation (4.9) requires the water-gas reaction equilibrium constant, K_{WG}, and the molecular balance equations. The K_{WG} is defined as

$$K_{WG} = \frac{n_3 n_2}{n_1 n_4} \qquad \textbf{(4.10)}$$

The value of K_{WG} can be found in Table 3 in Goodger (1977) (derived from Stull and Prophet (1971) *JANAF Thermodynamical Tables*). The molecular balance equations are as follow:

carbon balance

$$n_1 + n_3 = x \tag{4.11}$$

hydrogen balance

$$n_2 + n_4 = y/2 \tag{4.12}$$

oxygen balance

$$2n_1 + n_2 + n_3 = 2m_s + z \tag{4.13}$$

nitrogen balance

$$n_5 = 3.76m_s \tag{4.14}$$

Since both linear and non-linear equations are involved, solution requires iteration. The procedure can be found in Goodger (1977).

With the inclusion of both CO and H_2 through the dissociation reaction, the effective heat of combustion, $\Delta h_{c,eff}$, is evaluated as in Equation (4.15).

$$\Delta h_{c,eff} = \Delta h_{c,net} - \Delta h_{c,CO}(f_{CO}) - \Delta h_{c,H_2}(f_{H_2}) \tag{4.15}$$

where $\Delta h_{c,CO}$ and $\Delta h_{c,H2}$ are the net heat of combustion of carbon monoxide (10,100 kJ/kg CO) and hydrogen (130,800 kJ/kg H_2) respectively, with f_{CO} and f_{H2} the mass yield of carbon monoxide (kg/kg), and hydrogen (kg/kg) per unit mass of fuel reacted.

4.2.3 Yamada and Tanaka model

Yamada and Tanaka (1994) have proposed an empirical combustion model with the species production based on the correlations developed by Beyler (1986). In their combustion model, the combustion products include CO_2, H_2O, CO, C, H_2, N_2 and unburned fuel. Although the correlation parameters are obtained using propane as fuel, Yamada and Tanaka (1994) suggest the model could be extended to generic fuels. The basic structure of their combustion model is illustrated in Figure 4.1. The portion r undergoing complete combustion is set as $1-(1-0.75)^{(1/\Phi)^2}$ for $\Phi<1$, and 0.75 for $\Phi\geq 1$. From this combustion model, indication of incomplete combustion starts as early as $\Phi = 0.6$ (Tanaka and Yamada, 1994).

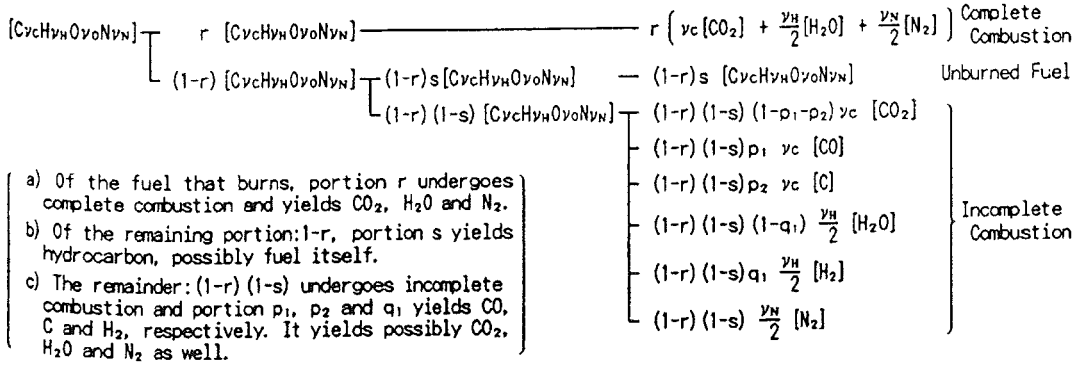

Figure 4.1 Combustion model from Yamada and Tanaka (1994).

The incomplete combustion products consist of unburned fuel, carbon monoxide, hydrogen and carbon. The effective heat of combustion is therefore evaluated as

$$\Delta h_{c,eff} = \Delta h_{c,net}\left(1 - f_{fuel}\right) - \Delta h_{c,CO}\left(f_{CO}\right) - \Delta h_{c,H_2}\left(f_{H_2}\right) - \Delta h_{c,C}\left(f_C\right) \qquad \textbf{(4.16)}$$

where f_{fuel} and f_C is the unburned fraction of fuel and the mass yield of carbon (kg/kg) per unit mass of fuel reacted respectively, and $\Delta h_{c,C}$ is the net heat of combustion of carbon (32,800 kJ/kg C).

4.2.4 Tewarson model

Based on experiments performed using the Factory Mutual Research Corporation (FMRC) flammability apparatus, Tewarson (1995) found that the effective heat of combustion for non-halogenated materials at different ventilation conditions can be estimated using the correlation given in Equation (4.17) as follows:

$$\frac{\Delta h_{c,eff}}{\Delta h_{c,net}} = 1 - \frac{0.97}{\exp\left(\frac{\Phi}{2.15}\right)^{-1.2}} \qquad \textbf{(4.17)}$$

Lin and Mehaffey (1997) adopted this correlation in their compartment fire modelling. Note that the ratio between the effective heat of combustion and the net heat of combustion gives the combustion efficiency (as given in Equation (4.1)).

4.3 ANALYSIS

In the analysis to follow, the effective heats of combustion evaluated from the aforementioned models at various ventilation conditions are compared. The effective heat of combustion is presented in terms of the combustion efficiency, χ, defined as the ratio between the effective heat of combustion and the net heat of combustion given in Equation (4.1). The different ventilation conditions are characterised using the equivalence ratio, Φ. Since the water-gas reaction model and the Yamada and Tanaka model require the fuel composition to evaluate the species productions, two different fuel types, namely dry wood and heptane are used as examples. Their properties are presented below.

Fuel	Composition	Net heat of combustion (MJ/kg)
Dry Wood (Drysdale, 1985)	$CH_{1.5}O_{0.7}$	18.2[†]
Heptane (Tewarson, 1995)	C_7H_{16}	44.6

†Note: the gross heat of combustion for dry wood ($CH_{1.5}O_{0.7}$) is given as 19.3MJ/kg (Drysdale, 1985), where the state of water, a product after combustion, is in liquid form; the net heat of combustion is equal to the gross heat of combustion minus the latent heat of water at 298K, where the state of water is in gaseous form. This is the quantity that is much more commonly used in fire applications than the gross heat of combustion (Babrauskas, 1992b).

For the complete reaction model and the Tewarson model, the combustion efficiencies at different equivalence ratios are given by Equations (4.7) and (4.17) respectively. The results are presented in Figure 4.2 and Figure 4.3 for dry wood and heptane respectively. For wood, an equivalence ratio up to 1.4 is plotted since wood does not burn more than 30 to 40 percent fuel rich (Babrauskas, 1995). For heptane, an equivalence ratio up to 2 is plotted as it can burn in a highly fuel-rich manner.

Figure 4.2 and Figure 4.3 show that the evaluated combustion efficiencies from the water-gas reaction model and the Yamada and Tanaka model is less than the combustion efficiency evaluated from the complete reaction model. This is expected as those two models account for the incomplete combustion products generated during the combustion. However, it is surprising to see the Tewarson model exceeding the maximum possible value given by the complete reaction model.

From the figures, it can be seen that the combustion efficiency evaluated from the Yamada and Tanaka model in fuel-rich conditions ($\Phi>1$) could be approximately matched by multiplying the maximum efficiency ($1/\Phi$) with a b_p factor of 0.85 as in Equation (4.8). This suggests that the application of the b_p factor with the maximum efficiency presented in Equation (4.8) is a simplistic way of accounting for the presence of incomplete combustion products.

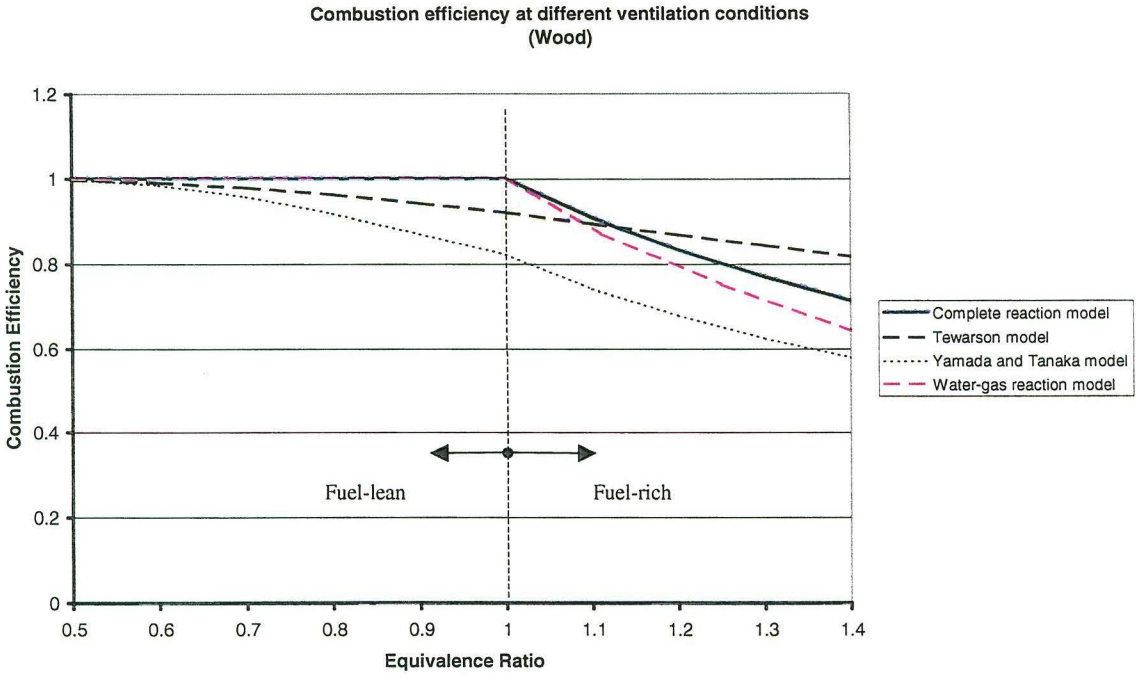

Figure 4.2 **Combustion efficiency for wood evaluated using various models at different ventilation conditions.**

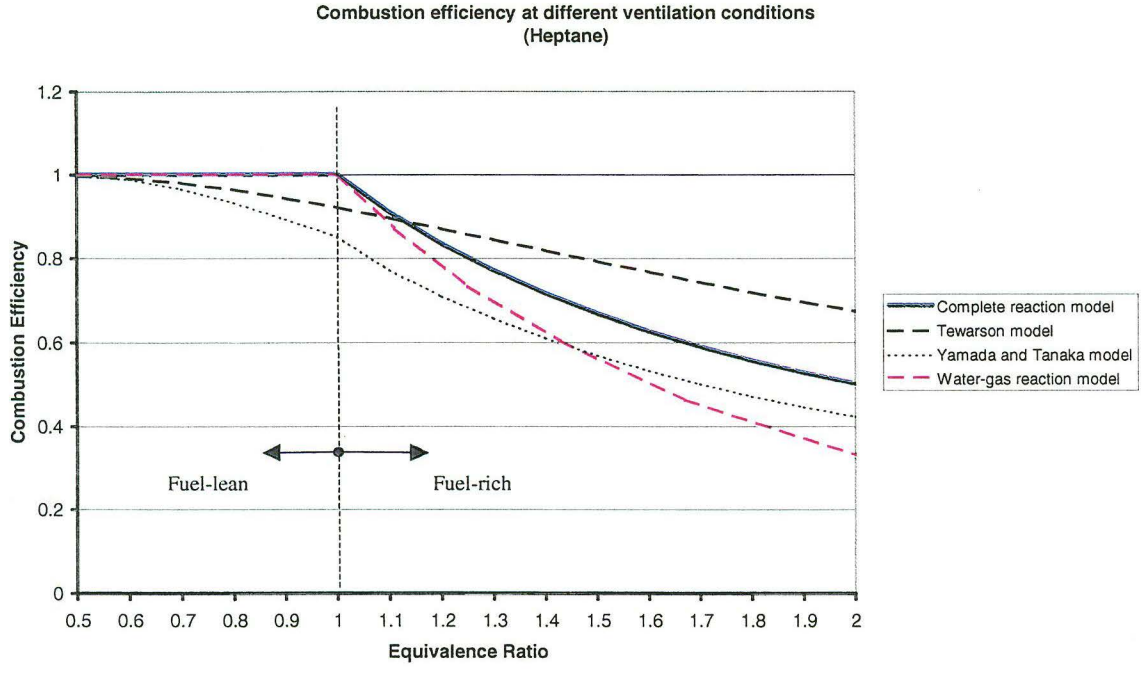

Figure 4.3 **Combustion efficiency for heptane evaluated using various models at different ventilation conditions.**

4.4 SUMMARY

Various treatments that have been used to model the combustion inside a well-stirred fire compartments are presented. These models attempt to estimate the effective heat of combustion of the burning fuel at various ventilation conditions by estimating the amount of incomplete combustion products being produced. Although correlations of species production at different ventilation conditions are available (as used in the Yamada and Tanaka model), the application of these correlations in post-flashover compartment fires remains uncertain. This is because these correlations are derived from hood tests (Beyler, 1986), where conditions are vastly different compared to post-flashover fires inside a compartment. For the water-gas reaction model used by Tsuchiya and Sumi, this model appears to be rather restrictive as dissociation temperature is much higher than the typical post-flashover fire. Furthermore, apart from carbon monoxide and hydrogen, other incomplete combustion products could also be generated during the combustion. Currently there is no practical experimental technique available for measuring the fire heat release rate inside a post-flashover compartment that excludes the external burning. Hence the actual combustion efficiency within the post-flashover compartment remains largely unknown. For the purpose of estimating the fire heat release rate inside the compartment, it appears that Babrauskas's method (Equation (4.8)) remains the best option at present. Therefore Equation (4.8) is used in the proposed CFIRE model for estimating the fire heat release rate inside the compartment. The value of b_p is to be estimated from its effect on the calculated gas temperature.

Chapter 5 POOL FIRES

This chapter reviews a selection of pool models that have been used to describe the mass loss rate of pool fires inside a compartment. Two environmental variables that affect the mass loss rate of a pool fire are identified, namely the vitiation effect and the radiation effect. For a pool burning inside a post-flashover compartment, its mass loss rate is dominated by radiative thermal feedback from the surrounding hot environment. Experimental compartment pool fire data were used to study the mass loss rate of the pool.

5.1 INTRODUCTION

The term "pool" used in this thesis refers to non-charring fuel such as liquid fuels with a highly exposed fuel surface configuration. The mass loss rate per unit area of the pool is a function of the net heat flux received on the surface and the energy required to vaporise the fuel. This energy required to release the fuel vapour from the pool is known as the heat of gasification, L_g, and is a thermodynamic property called the latent heat of evaporation for liquid fuels. For a free burning pool, the principal heat flux to the fuel surface comes directly from the flame in the mode of convection and radiation. The magnitude of the heat flux on the pool surface could be augmented by other external radiant heat sources. For pool burning inside a compartment, these external radiant sources could come from the hot gases and the heated walls inside the compartment. The magnitude of the augmentation by the compartment can produce a fuel mass loss rate up to four times the free-burning rate (Fleischmann and Parkes, 1997).

The study of pool fire behaviour inside a compartment is important as it resembles the behaviour of non-charring thermoplastics that melt and burn like a pool on the floor

during the fire (Babrauskas and Wickström, 1979). These thermoplastic materials are widely used in furniture making and end up in real occupancies. When modelling a post-flashover pool fire, simply using the free-burn mass loss rate as input in the post-flashover fire model would underestimate the actual mass loss rate. A pool model that accounts for the augmentation from the hot environment inside the compartment is crucial for determining the resulting fire gas temperature inside the compartment as well as the fire duration.

5.2 BACKGROUND

To consider the burning pool in mathematical terms, it is easiest to consider a one-dimensional vaporising pool surface undergoing heat and mass transfer. This is depicted in Figure 5.1 below:

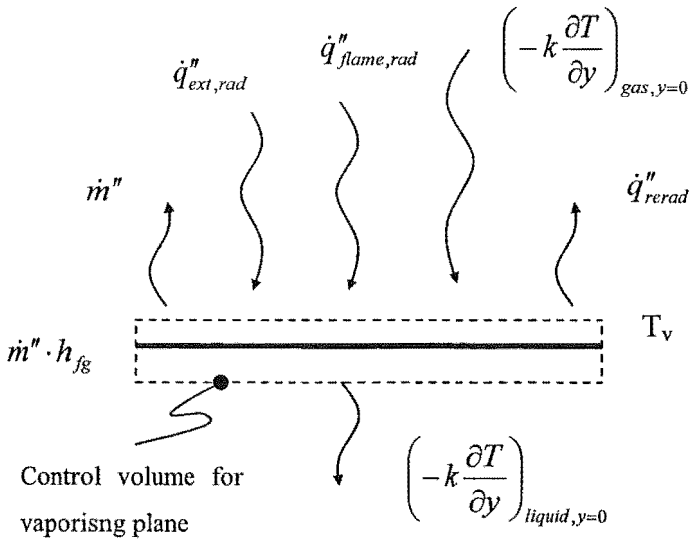

Figure 5.1 Schematic representation of heat and mass transfer at a pool surface.

Applying the conservation of energy equation on the vaporising plane control volume, in terms of per unit surface area of the pool, yields the following equation:

[Rate of energy to vaporise] = [Rate of flame convection] + [Rate of flame radiation] + [Rate of external radiation] – [Rate of re-radiation] – [Rate of energy loss to heating the bulk liquid]

In equation form,

$$\dot{m}'' \cdot h_{fg} = \left(-k \frac{\partial T}{\partial y} \right)_{gas,y=0} + \left(\dot{q}''_{flame,rad} + \dot{q}''_{ext,rad} \right) - \varepsilon_s \sigma T_v^4 - \left(-k \frac{\partial T}{\partial y} \right)_{liquid,y=0} \quad \textbf{(5.1)}$$

where h_{fg} is the enthalpy of phase change from liquid to vapour at the known pressure.

During the vaporisation process, the pool surface temperature is at the vaporising temperature, T_v. Underneath the vaporising plane, the bulk liquid would be at its bulk temperature, T_0. The energy required to heat up the bulk liquid from T_0 to T_v is

$$\left(-k \frac{\partial T}{\partial y} \right)_{liquid,y=0} = \dot{m}'' c_{p,l} \left(T_v - T_0 \right) \quad \textbf{(5.2)}$$

where $c_{p,l}$ is the specific heat for the liquid. Substituting Equation (5.2) into Equation (5.1) gives

$$\left(-k \frac{\partial T}{\partial y} \right)_{gas,y=0} = \dot{m}'' \cdot \left\{ h_{fg} + c_{p,l} \cdot \left(T_v - T_0 \right) - \frac{1}{\dot{m}''} \left[\left(\dot{q}''_{flame,rad} + \dot{q}''_{ext,rad} \right) - \varepsilon_s \sigma T_v^4 \right] \right\} \quad \textbf{(5.3)}$$

or

$$\left(-k \frac{\partial T}{\partial y} \right)_{gas,y=0} = \dot{m}'' \hat{L}$$

where $\hat{L}$ is regarded as an effective heat of gasification that includes the radiative effect.

As shown by Kanury (1992), by assuming a unit Lewis number, at the vaporising fuel surface, with or without combustion, the mass flux can be calculated using Equation (5.4), which represents the steady state pure convective condition.

$$\dot{m}'' = \frac{h}{c_{p,gas}} \cdot \ln(1+B) \tag{5.4}$$

where h is the convective heat transfer coefficient, $c_{p,gas}$ is the specific heat of the gas, and B is the Spalding Mass Transfer number, which is a ratio of the driving force for the heat transfer across the gas phase to the demand of liberating and heating of the fuel. For open burning, the B number can be defined as

$$B = \frac{Y_{ox,\infty} \cdot \dfrac{\Delta h_{c,net}}{r_{ox}} + c_{p,gas}(T_\infty - T_v)}{\hat{L}} \tag{5.5}$$

where $Y_{ox,\infty}$ and T_∞ are the oxygen mass fraction and the temperature at "ambient" condition.

Combining Equations (5.3), (5.4) and (5.5) yields the following expression, which is similar to the one obtained by Iqbal and Quintiere (1994).

$$\dot{m}'' = \frac{\dfrac{h}{c_{p,gas}}\left(\dfrac{\xi}{e^{\xi}-1}\right)\cdot\left[Y_{ox,\infty}\cdot\dfrac{\Delta h_{c,net}}{r_{ox}} + c_{p,gas}(T_\infty - T_v)\right] + \left[\left(\dot{q}''_{flame,rad} + \dot{q}''_{ext,rad}\right) - \varepsilon_s \sigma T_v^4\right]}{h_{fg} + c_{p,l}(T_v - T_0)} \tag{5.6}$$

where

$$\xi = \frac{\dot{m}'' \cdot c_{p,gas}}{h}$$

The denominator denotes the heat of gasification for the liquid fuel, L_g, i.e.

$$L_g = h_{fg} + c_{p,l}(T_v - T_0) \tag{5.7}$$

whereas the first term in the numerator denotes the convective heat flux, i.e.

$$\dot{q}''_{flame,conv} = \frac{h}{c_{p,gas}} \cdot \left(\frac{\xi}{e^{\xi}-1}\right) \cdot \left[Y_{ox,\infty} \cdot \frac{\Delta h_{c,net}}{r} + c_{p,gas} \cdot (T_\infty - T_0)\right] \tag{5.8}$$

The term $\left(\frac{\xi}{e^{\xi}-1}\right)$ is regarded as the "blocking factor", effectively reduces the convective heat transfer coefficient, h, from its pure heat transfer value as the mass transfer increases (Iqbal and Quintiere, 1994). Therefore, the flame convective heat flux component diminishes with the increases in the fuel vaporisation rate.

However, Equation (5.6) cannot be readily used to estimate the mass loss rate of the pool because both the flame convective and radiative heat flux components are not known.

Babrauskas (1992a) presents a correlation for the mass loss rate of large pool (diameter greater than 0.2m) in the form of

$$\dot{m}'' = \dot{m}''_{\infty}\left(1 - e^{-k\beta D}\right) \tag{5.9}$$

where $\dot{m}''_{\infty}$ and $(k\beta)$ are empirical factors for each different fuel and D is the diameter of the pool. This correlation can be used to estimate the free-burning mass loss rate without any external heating.

5.3 COMPARTMENT POOL FIRE MODELS

For pool fire burning inside a compartment, apart from receiving the flame flux from its fire plume, the pool will also receive additional heating from the upper hot layer

and surrounding walls. Various compartment pool fire models can be found in the literature. Only a selection of models is reported here with the intention to show the variables considered during the modelling.

5.3.1 Mitler

In the Harvard compartment fire model, Mitler (1978) considered the fire plume on top of the vaporising fuel to take a shape of a cone such that the flame is modelled as a grey, homogenous, "solid" cone of uniform gas temperature, T_f, of 1150K and gas absorptivity, k_f, of 1.55m^{-1}. By default, the cone is assumed to have a semi-apex angle, ψ, of 30° as shown in Figure 5.2.

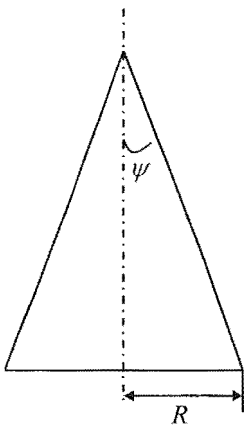

Figure 5.2 Flame cone in Mitler's model.

The radiant heat flux from the "flame cone" alone is spatially averaged across the base of the cone. The average radiative flame heat flux at the base, $\dot{q}''_{fl}$, is calculated as (Mitler, 1978),

$$\dot{q}''_{fl,rad} = \sigma T_f^4 \left[1 - \exp\left(-0.7755 \hat{\phi} k_f R\right)\right] \qquad \textbf{(5.10)}$$

where R is the radius of the flame cone, 0.7755 is a factor resulting from spatially averaging the radiant flux across the base area of the flame cone, and $\hat{\phi}$ is the factor giving the mean beam length in the conical flame defined as

$$\hat{\phi} = 2\cos\psi\left\{\sin\psi + \cos\psi + \sin\psi\cos\psi \cdot \ln\left[\frac{\sin\psi(1-\sin\psi)}{\cos\psi(1+\cos\psi)}\right]\right\} \qquad \textbf{(5.11)}$$

The convective flame heat flux is not explicitly treated in the flame cone model. It is artificially accounted for by lumping it into the re-radiation term from the hot surface, such that for a small flame in the growth phase, i.e. small R, the re-radiation term is adjusted so that the overall pyrolysis matches the observed rate from experiment.

With the pool fire burning inside a compartment, the vaporising surface is subjected to external radiation heating from the hot layer and the heated walls. Due to the presence of the flame cone, the incident heat flux has to pass through the gas medium in the cone before reaching the base of the fire. Since the gas medium is assumed to have absorptivity, the incident flux would be attenuated. The general equation for the attenuation is described as follows (after Mitler, 1978):

$$\dot{q}''_{res} = \dot{q}''_{target}\left[\frac{\exp(-k_f R)+\sin\psi}{1+\sin\psi}\right] \qquad \textbf{(5.12)}$$

where $\dot{q}''_{res}$ is the resultant heat flux that reaches the vaporising fuel surface at the base of the flame cone; the $\dot{q}''_{target}$ is the incident heat flux from either the hot layer or the heated walls; and the expression in the square bracket is the attenuation term. The expressions of $\dot{q}''_{target}$ for both layer and walls to the target (the burning surface) can be found in Cox (1995).

The net heat flux on the pyrolysing pool surface is the sum of the radiative flame heat flux, the incident heat fluxes from the hot layer and the walls that reached the fuel surface after attenuation minus the reradiation from the vaporising surface. This is given as follow.

$$\dot{q}''_{net} = \dot{q}''_{fl,rad} + \dot{q}''_{res,layer} + \dot{q}''_{res,walls} - \dot{q}''_{rerad} \quad \textbf{(5.13)}$$

The mass loss rate of the burning pool is therefore calculated as

$$\dot{m}'' = \frac{\dot{q}''_{net}}{L_g} \quad \textbf{(5.14)}$$

5.3.2 Babrauskas

Babrauskas (1979) in the COMPF2 post-flashover fire model modelled the pool fire in a slightly different way. The pool is assumed to receive the radiation from the hot gas directly, where the view factor between the pool and the room is taken as 1. The wall radiation is considered small and its effect can be included into the gas emissivity term, ε_g. Assuming the emissivity from the pool surface is the same as ε_g, the mass loss rate of the pool by the hot gas radiation is regarded as a "far field" term where

$$\dot{m}''_{p,rad} = \frac{\varepsilon_g \sigma \left(T_g^4 - T_v^4\right)}{L_g} \quad \textbf{(5.15)}$$

The heat flux contribution from the fire plume is accounted for by using an empirical relationship derived from limited experimental data. The mass loss rate due to the fire plume is described as

$$\dot{m}''_{p,fire\,plume} = 0.0014 \frac{\Delta h_c}{L_g} \quad \textbf{(5.16)}$$

The effect of the fire plume radiation on vaporising the fuel is considered to decrease with the increase in room radiation from the hot gases. This is obtained by multiplying the fire plume term by a proportionality factor, Ψ, before adding to the far-field term. The proportionality factor, Ψ, is set as

$$\Psi = 1.0 - \frac{T_g^4 - T_v^4}{1700^4 - T_v^4} \tag{5.17}$$

This implies that the fire plume contributes to the mass loss rate of the pool in a diminishing fashion until the gas temperature inside the compartment gets greater than 1700K. This is when the pool will be totally driven by the radiation from the surrounding hot gases (Equation (5.15)).

5.3.3 Takeda and Yung

In the NRCC fire model developed by Takeda and Yung (1992) in the National Research Council of Canada, they considered the mass loss rate of the pool fire to be influenced by the radiation from the surrounding hot environment as well as the fire plume. The treatment for describing the mass loss rate of the pool by the hot environment is similar to that in the COMPF2, except that the radiation from the hot inner compartment walls is treated separately rather than lumping it into the emissivity term as in COMPF2, such that,

$$\dot{m}''_{p,rad} = \frac{\varepsilon_g \sigma T_g^4 + (1-\varepsilon_g)\sigma T_{wi}^4 - \sigma T_v^4}{L_g} \tag{5.18}$$

where the surface emissivity of the compartment walls and the burning object is assumed to be 1.

The fire plume term is considered to depend on the oxygen concentration inside the compartment, described as:

$$\dot{m}''_{p,fire\ plume} = \left(\frac{\zeta}{L_g}\right) N_{oxy} \tag{5.19}$$

where ζ is a constant and is fuel dependent, and N_{oxy} is the oxygen mole fraction. This is to account for the vitiation effect such that a decrease in the oxygen concentration decreases the plume term. The total mass loss rate of the pool inside the compartment

fire environment is the sum of the radiation and fire plume terms. There are other models (such as Takeda and Akita, 1982; Takeda, 1983) that adopt similar treatments to that in the NRCC fire model, except that the fire plume term is replaced by the free burning rate of the pool.

5.4 POOL MODEL FOR POST-FLASHOVER APPLICATION

5.4.1 Background

From the literature review, two environmental terms are identified to affect the vaporisation rate of pool fires inside a compartment. These environmental terms include the oxygen concentration in the surrounding environment, i.e. the vitiation effect, and the radiation from the surrounding sources, i.e. the radiation effect.

Quintiere (1984) provides a generalised fuel mass loss rate expression that includes both the vitiation and the radiation effects. This expression is given in Equation (5.20) below. The free burning mass loss rate, $\dot{m}''_{freeburn}$, under normal ambient condition with oxygen concentration of 0.233 (by mass) is used as a datum. In the expression, the vitiation effect on the free burning mass loss rate is linearly approximated using the local oxygen concentration in the environment where burning takes place. For the radiation effect from the surroundings, this additional radiation driven mass loss rate is represented by the net heat flux imposed on the fuel surface from the external sources, $\dot{q}''_{rad,net}$, divided by the heat of gasification of the fuel, L_g. The summation of the fire plume term and the "far field" radiation term gives the overall mass loss rate of the burning item.

$$\dot{m}''_p = \dot{m}''_{freeburn}\left(\frac{Y_{ox}}{0.233}\right) + \frac{\dot{q}''_{rad,net}}{L_g} \qquad \textbf{(5.20)}$$

Figure 5.3 compares the predicted mass loss rate using Equation (5.20) with the experimentally measured data from the tests by Tewarson et al (1981), Santo and

Tamanini (1981) and Mulholland et al (1992). All of these tests were conducted in a controlled environment with different oxygen concentration in the supply air stream. The tests by Tewarson et al (1981) and Santo and Tamanini (1981) were performed in a reduced oxygen concentration environment with no external irradiance heat flux being imposed upon the burning fuels, whereas the tests by Mulholland et al (1992) involved different level of irradiant heat flux at different oxygen concentration environments. The experimental data and calculations are presented in Appendix A. The plot shows that Equation (5.20) is reasonably effective in describing the vitiation and radiation effects on the mass loss rate of the burning pool.

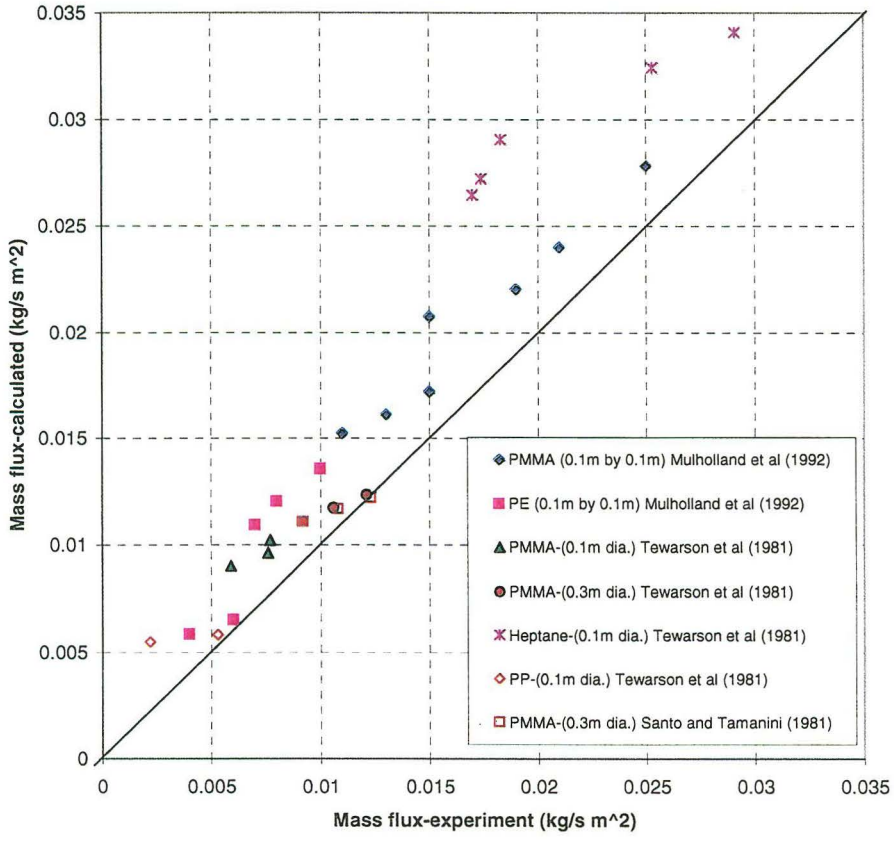

Figure 5.3 **Comparing the experimental results from literature to the calculated values for fuel mass loss.**

The fire environment inside a post-flashover compartment is very hot and well-mixed. Considering it to behave as a single zone well-stirred reactor with the entire compartment as a single control volume, at steady state, the mass balance and the oxygen balance equations are:

The mass balance

$$\dot{m}_{in} + \dot{m}_p = \dot{m}_{out} \tag{5.21}$$

The oxygen balance

$$\dot{m}_{out} \cdot Y_{ox} = \dot{m}_{in} \cdot (0.233) - \dot{m}_p \cdot r \cdot (0.233) \tag{5.22}$$

where the last term in the oxygen balance equation is the amount of oxygen used in the reaction with the fuel. By substituting the mass balance equation into the oxygen equation, the oxygen mass fraction inside the compartment is

$$Y_{ox} = 0.233 \cdot \frac{(1-\Phi)}{(1+\Phi/r)} \tag{5.23}$$

where Φ is the equivalence ratio.

For $\Phi<1$, $r>>1$, the term Φ/r becomes negligible, therefore Equation (5.23) can be simplified to

$$Y_{ox} \approx 0.233 \cdot (1-\Phi) \tag{5.24}$$

Hence Equation (5.20) can be written as follows in Equation (5.25) as given by Quintiere (2002).

$$\dot{m}''_p \approx \dot{m}''_{freeburn}(1-\Phi) + \frac{\dot{q}''_{rad,net}}{L_g} \tag{5.25}$$

During the ventilation controlled burning with $\Phi>1$, therefore, the plume term diminishes, with the mass loss rate being strongly driven by the "far field" radiation such that

$$\dot{m}_p'' \approx \frac{\dot{q}_{rad,net}''}{L_g} \tag{5.26}$$

where $\dot{q}_{rad,net}''$ is the net radiative heat flux that reaches the pool surface from the hot surrounding gases.

5.4.2 External radiation heat flux reaching pool surface

For a post-flashover compartment fire, the gas temperature is high and reasonably uniform within the compartment. Following the assumption that the entire compartment has a uniform temperature and the view factor between the pool and the room is unity, the radiation heat flux from the surrounding hot gases to the pool surface is estimated by

$$\dot{q}_{rad}'' = \varepsilon_g \sigma T_g^4 \tag{5.27}$$

It is noted that for a burning pool, especially a large pool, there exists a cool fuel vapour zone just above the centre of the pool surface, where air is not been able to reach and be reacted with. Such a vapour zone has been reported by Gritzo et al (1998) in their studies on large jet-fuel pool fire. Brosmer and Tien (1987) performed an analytical study on the radiative energy blockage effect by the vapour zone on the free burning pool, and found that it could attenuate the radiant flux to surface by 25 to 35 percent. Imagine a burning pool being exposed to external heating, the incoming radiation would have to pass through the flame envelope as well as the vapour zone before reaching the pool surface. The flame and the cool vapour zone just above the fuel surface could absorb some of the radiation, and therefore decrease the actual heat flux that reaches the fuel surface.

To include the attenuation by the flame and the vapour zone above the pool surface, a gas column with an arbitrary shape having an absorption coefficient above the pool surface is considered. This gas column would absorb some of the incoming radiation, and at the same time its temperature increases due to the absorption. Following the same treatment by Mitler (1978), the attenuation is represented by an exponential

attenuation factor, $e^{-\tau}$, and the absorbed radiation is simply reradiated. The actual radiation from the hot gases, expressed in term of heat flux, $\dot{q}''_{actual,rad}$, reaching the pool surface is equal to the radiation after attenuation plus the re-radiation from the gas column due to radiation absorption raising its temperature. This is given in Equation (5.28).

$$\dot{q}''_{actual,rad} = \dot{q}''_{rad}\left[e^{-\tau} + \left(1 - e^{-\tau}\right)w\right] \tag{5.28}$$

where τ is the mean optical path length approximated as the product of absorption coefficient, k_f, and the mean beam length, L_m.

$$\tau \approx k_f L_m \tag{5.29}$$

The term, w, in Equation (5.28) is the fraction of reradiated energy that goes to the base. Assuming isotropic radiation, this fraction is the ratio of the areas between the base, A_{base}, and the surface area of the gas column, $A_{gas\ column}$, (Mitler, 1978), given as follows,

$$w \approx \frac{A_{base}}{A_{gas\,column}} \tag{5.30}$$

The term in the square bracket of Equation (5.28) determines the amount of radiation reaching the pool surface. It can be seen that this term depends on the absorption coefficient of the gas column, k_f, and the shape of the gas column, which determines the mean beam length, L_m, and the term, w. An increase in the absorption coefficient and the mean beam length, by means of changing the shape and volume of the gases, would increase the blockage of the incoming radiation reaching the pool surface. However, both the absorption coefficient and the shape of the gas column are unknowns.

In order to apply the radiation blockage concept on the pool model, a more useful form of Equation (5.28) can be obtained by replacing the attenuation term in the

square bracket with a single factor, α. By substituting Equation (5.27) into Equation (5.28) and introducing α, the actual radiative heat flux from the hot gases to reach the pool surface can be approximated as

$$\dot{q}''_{actual,rad} = \alpha \varepsilon_g \sigma T_g^4 \qquad \textbf{(5.31)}$$

The attenuation factor, α, is to be empirically determined from post-flashover experimental data.

5.4.3 Determining the attenuation factor α

During vaporisation, the pool surface is at vaporising temperature, T_v, and the re-radiation from the surface is

$$\dot{q}''_{rerad} = \varepsilon_s \sigma T_v^4 \qquad \textbf{(5.32)}$$

Assuming the emissivity on the fuel surface, ε_s, is unity (typically for liquids and char (Tien et al, 1995)), the *net* heat flux that on the pool surface, $\dot{q}''_{rad,net}$ is

$$\dot{q}''_{rad,net} = \alpha \varepsilon_g \sigma T_g^4 - \sigma T_v^4 \qquad \textbf{(5.33)}$$

Recalling Equation (5.26), the mass loss rate per unit area of the pool in a post-flashover compartment is approximated by the net heat flux on the pool surface divided by the heat of gasification. Substituting Equation (5.33) into Equation (5.26) gives

$$\dot{m}''_p = \frac{\alpha \varepsilon_g \sigma T_g^4 - \sigma T_v^4}{L_g} \qquad \textbf{(5.34)}$$

and rearranging gives

$$\left(\dot{m}_p'' L_g + \sigma T_v^4\right) = \alpha\left(\varepsilon_g \sigma T_g^4\right) \qquad \textbf{(5.35)}$$

The term on the left hand side is the net heat flux required to vaporise a specific pool with properties of L_g and T_v at a rate of $\dot{m}_p''$. The bracketed term on the right is the radiation intensity from the surrounding hot gases, and α represents the fraction of this incoming flux that reaches the pool surface resulting in the mass loss rate of $\dot{m}_p''$.

The attenuation factor, α, is empirically determined using experimental results from post-flashover compartment tests by Fleischmann and Parkes (1997) and by the author. In the Fleischmann and Parkes (1997) experiments, single small window openings with different heights and widths were investigated, whereas in the author's experiments, different door and roof vent openings were investigated. Both the test series were conducted in a similar size compartment having the approximate dimensions of 1m high by 1m wide by 1.5m deep, lined with kaowool insulation, and using heptane as a fire source. The fuel pan was located at the centre back of the compartment and the heptane liquid fuel was supplied via a header tank system, to maintain the fuel level inside the pan during the course of the fire. This allowed the fire environment inside the compartment to dictate the mass loss rate of the fuel. The size of the fuel pan used by Fleischmann and Parkes (1997) and by the author differed slightly, with the former using a fuel pan of 0.2m in diameter and the author using a fuel pan of 0.3m in diameter. Figure 5.4 presents the compartment setup for the Fleischmann and Parkes (1997) experiments. The temperature inside the compartment was monitored using two bare bead thermocouple trees located at the front and the back corners of the compartment. Each tree consisted of 10 thermocouples spaced 100mm vertically apart. Details of these experiments can be found in the research report by Parkes (1996). Details of the author's experiments are presented in Chapter 8. Note that the compartment temperatures in the author's experiments were monitored using three bare bead thermocouple trees with an addition thermocouple tree at the centre of the compartment.

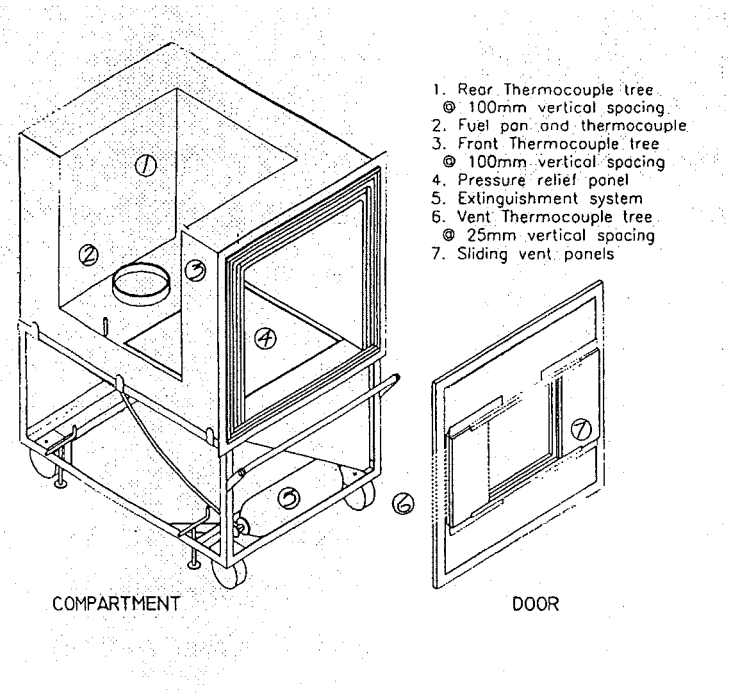

Figure 5.4 Test compartment setup in Fleischmann and Parkes (1997) experiments.

Table 5.1 presents the average results measured during the quasi-steady period for the tests by Fleischmann and Parkes (1997) and by the author. These results include the average gas temperature inside the compartment, the fuel mass loss rate, the air inflow rate and the calculated global equivalence ratio inside the compartment. The last two columns in the Table are the two terms in Equation (5.35). For heptane fuel, the heat of combustion and heat of gasification are 44500 kJ/kg and 500 kJ/kg respectively; and the stoichiometric air to fuel mass ratio, r, is 15.1. For a pool vaporising under a very high surrounding temperature compared to the boiling point temperature of the liquid, the vaporising pool surface temperature is only slightly smaller than the boiling temperature (Kanury, 1992). For heptane fuel, its boiling temperature is 98°C. The emissivity of the gas inside the compartment is unknown. The radiation of the hot gases inside the compartment comes from the discrete pocket of radiation of fuel and combustion products such as CO_2 and H_2O and a full spectrum of radiation frequencies from the soot particles (Quintiere, 1997). Assuming the fire gas inside the compartment is represented by a homogeneous isothermal gas volume, the emissivity can be estimated as

$$\varepsilon = 1 - \exp(-k_f L_m) \tag{5.36}$$

where k_f is the absorption coefficient and L_m is the mean beam length. The mean beam length of the hot gases inside the compartment is estimated as (after Tien et al, 1995)

$$L_m = 3.6\frac{V}{A} \tag{5.37}$$

where V and A are the volume and the area of the boundary surface of the gas body. For the compartment involved, with internal dimensions of 1m high by 1m wide by 1.5m deep, the mean beam length is estimated as 0.675m. However, to the author's knowledge, no absorption coefficient for heptane fuel has been reported. As a first approximation, the absorption coefficient of $1m^{-1}$ is used. This gives an estimation of gas emissivity of 0.5. If the actual absorption coefficient is greater than $1m^{-1}$, the gas emissivity would increase and vice versa. The unknown absorption coefficient for the heptane, coupled with the radiation effect from the wall, is to be lumped into this emissivity term for total radiation estimation, so a value of 0.7 is used. This value is lower than the 0.9 often used in full-scale compartments, simply to account for the small-scale nature of the compartment.

Note that the author's data presented in the Table 5.1 is from the Door 1 experimental series where the door vent opening is 450mm high by 250mm wide, i.e. a ventilation parameter at the door of $0.0755m^{2.5}$ tested against different roof vent opening sizes. The D1R0, D1R150, D1R250 and D1R300 denote the door vent opening with roof vent opening of 0mm (no roof vent), 150mm, 250mm and 300mm in diameter as given in the parentheses.

Table 5.1 Summary of the experimental data and calculated results for the reduced-scale compartment fires.

Test#	Ventilation parameter $A_v\sqrt{H_v}$ ($m^{2.5}$)	Average temp T_{gas} (°C)	Expt-mass loss rate $\dot{m}_{p-exp}$ (kg/s)	Expt-air inflow rate $\dot{m}_{air-exp}$ (kg/s)	Calculated equivalence ratio Φ	$\left(\varepsilon_g \sigma T_g^4\right)$ (kW/m^2)	$\left(\dot{m}_p'' L_g + \sigma T_v^4\right)$ (kW/m^2)
Fleischmann and Parkes (1997)[1]							
1	0.0442	884	0.0023	0.0251	1.4	71	38
2	0.0221	726	0.0017	0.0124	2.1	40	28
3	0.011	576	0.001	0.0058	2.6	21	17
4	0.0287	786	0.0022	0.0207	1.6	50	36
5	0.0144	614	0.0012	0.0103	1.8	25	20
7	0.0156	611	0.0012	0.0119	1.5	24	20
8	0.0078	504	0.0007	0.0059	1.8	14	12
11	0.0156	618	0.0012	0.0118	1.5	25	20
12	0.011	583	0.0012	0.0058	3.1	21	20
13	0.0072	577	0.0009	0.0048	2.8	21	15
14	0.0442	961	0.0023	0.025	1.4	92	38
16	0.0707	1045	0.0043	0.0334	1.9	120	70
Yii (Author)[2]							
D1R0	0.0755 (0mmϕ)	907	0.007	0.033	3.2	77	50
D1R150	0.0755 (150mmϕ)	962	0.010	0.044	3.4	92	72
D1R250	0.0755 (250mmϕ)	1048	0.012	0.070	2.6	121	86
D1R300	0.0755 (300mmϕ)	1059	0.012	0.074	2.4	125	86

[1] The reported average temperature is represented by the averaged temperature measured from the front thermocouple-tree inside the compartment.

[2] The reported average temperature is represented by the averaged temperature measured from the three thermocouple-trees inside the compartment.

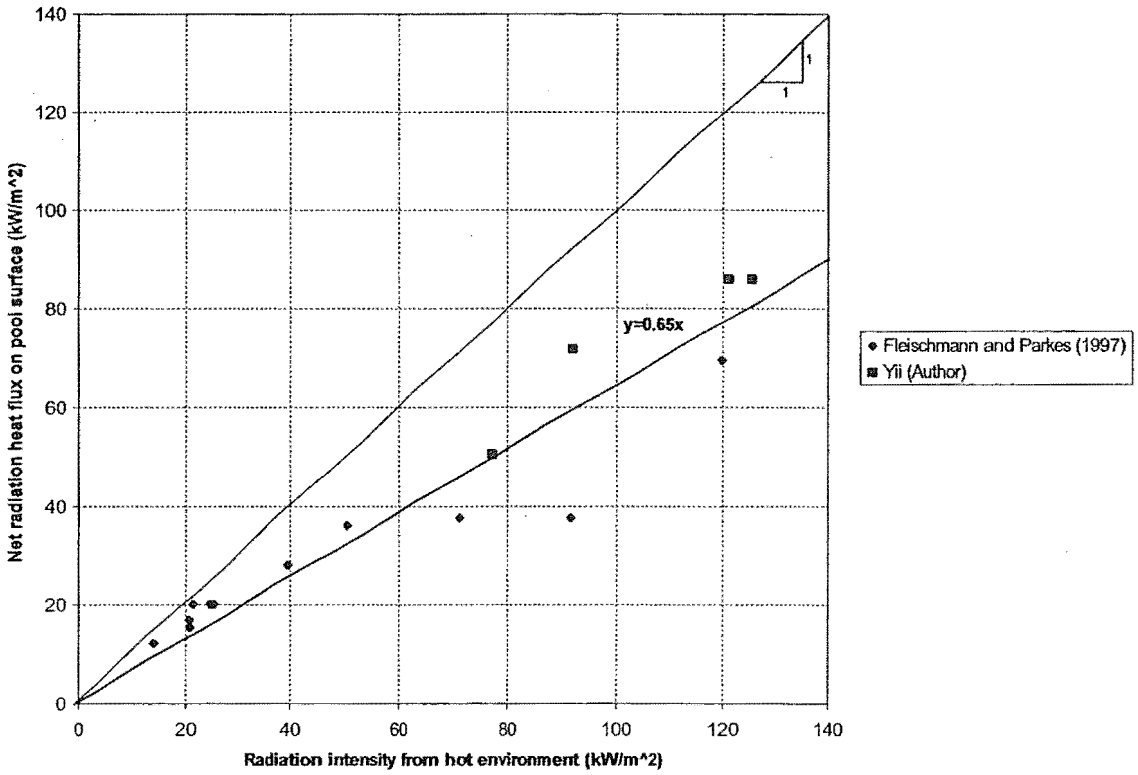

Figure 5.5 **The radiation intensity from the hot gases, $\left(\varepsilon_g \sigma T_g^4\right)$, versus the net radiation heat flux on the pool surface required to achieve the mass loss rate, $\left(\dot{m}_p'' L_g + \sigma T_v^4\right)$.**

Figure 5.5 plots the radiation intensity from the hot gases, $\left(\varepsilon_g \sigma T_g^4\right)$, against the net radiation heat flux on the pool surface required to achieve the mass loss rate, $\left(\dot{m}_p'' L_g + \sigma T_v^4\right)$. The ratio between these two terms is the attenuation factor, α, (Equation (5.35)). By fitting a straight regression line through the origin, α is found to be approximately 0.65. This suggests that not all of the radiation from the hot gases has reached the pool surface, otherwise the regression line would have a gradient of 1.0. The attenuation factor, α, of 0.65 serves only as an indicative value, because the emissivity of the fire gases in these heptane tests is unknown and has been assumed to be 0.7 in the analysis. For the range of gas emissivity between 0.9 and 0.5, following the same analysis as before, the attenuation factor α is found to be between 0.5 and 0.9 respectively. Although the above analysis is based only on heptane fires, its

implication in estimating the pool mass loss rate should be noted, especially when estimation of fire duration is concerned.

5.5 SPECIAL POOL- THERMOPLASTIC FURNITURE

Thermoplastics are widely used in furniture making. In particular, polyurethane foam is commonly used to manufacture upholstered furniture that ends up inside real occupancies. These non-charring thermoplastics tend to melt and burn like a pool during the fire. To model thermoplastics as a pool fire, the fuel burning surface area is required.

Thermoplastics in the form of upholstered furniture generally come in two configurations that include (1) the open and exposed configuration in the form of a slab such as a mattress and (2) the ornate and convoluted configuration such as upholstered armchairs. For plain slab configuration such as mattress, provided there is no dripping, the fuel burning surface area would be approximately the fuel footprint area. However, the same cannot be applied to upholstered armchairs. Observations made during the burning of upholstered armchairs show that the burning will involve individual components of the chair such as backrest, armrest and seats as well as a pool accumulated from the dripping of the melting foam underneath the furniture (Enright, 1999; Denize, 2000). Hence, the burning surface area will be greater than the furniture's own footprint area. There is very little study being done on quantifying the burning surface area of upholstered armchairs. So the modelling of upholstered furniture inside a post-flashover compartment is restricted to plain slab configuration with a known exposed burning surface area. Further research is necessary to estimate the equivalent pool area for upholstered armchairs, so that their effects on post-flashover fires can be studied.

5.6 REMARKS

The analysis performed above is based on a single pool with fixed surface area burning inside a compartment having a uniform temperature; and the total pool area is subjected to the thermal feedback from the surrounding hot environment. In the event of multiple pools inside a compartment with extreme geometry, such as a long narrow compartment, experimental observation has shown that the pool closest to the vent opening burns first until exhaustion before progressing to the next pool (Thomas and Bennetts, 1999). Therefore the overall available exposed fuel surface decreases as the fire progresses. The temperature inside the compartment was found to be non-uniform during the course of the fire, as the temperature at the back of the compartment was cooler than the temperature at the front where the pool was burning. These issues represent the limitation of the single zone model. It is envisaged that dividing a compartment into multiple zone along its depth could perhaps account for these issues. However, it would require knowledge of the conditions necessary to ignite the fuel at the back. Investigations of these aspects are outside the scope of this thesis. Parkes (2002) in the University of Canterbury is presently conducting fire experiment with multiple pools inside a test compartment of 2.4m wide by 1.2m high by 3.6m long. The compartment will have at least three fuel sources located evenly throughout the compartment with each fuel source monitored by individual load cell. Radiant heat flux inside the compartment will be monitored and one side of the compartment will have a fire rated window to facilitate observation. His research will lead to a better understanding of the multiple pools scenario.

5.7 SUMMARY

The fuel mass loss rate from pool fires are affected by both vitiation and radiation effects. With regard to pool fires burning in a post-flashover environment, its mass loss rate will be dominated by the radiation thermal feedback from the surrounding hot environment. It is also found that not all of the incoming radiation would reach the fuel surface, as the vaporising vapour above the fuel surface could attenuate a fraction

of the incident flux. In the proposed CFIRE model, Equation (5.34) with α=0.65 is used for modelling the pool mass loss rate under post-flashover condition where the pool surface area is required as an input. It should be noted that the input pool surface area would be a fixed value where the progressive burning effect that leads to the reduction of exposed pool surface area over the duration of the fire is not considered.

Chapter 6 WOOD FIRES

This chapter describes the burning mechanism of wood. A dimensional analysis is performed to identify the influential parameters that affect the mass loss rate during the fully developed period. The models for describing the mass loss rate of wood during different burning regimes are presented and discussed. A method for describing the burning of wooden furniture is postulated.

6.1 INTRODUCTION

Ever since it was realised that realistic compartment fire temperatures can be very different from standard test fire, intensive studies have been done on compartment fires with wood based fuels. In particular, the mass loss rate of wood fuels inside a compartment fire has long been the principal target in compartment fire studies. This is because the fuel release rate represents the foremost important parameter with regard to compartment modelling, as it dictates the heat release inside the compartment and hence the resultant gas temperature as well as the fire duration.

Most of the time, wood fuels in the form of cribs are used in compartment fire tests. Apart from measuring the fire gas temperature inside the test compartment, the overall mass loss of the burning cribs is also monitored. Kawagoe et al (1972) suggested that a mean rate of mass loss is an important statistic to be derived from the rate of mass loss data, because it provides a direct indicator of the fire duration for a given fire load. This mean mass loss rate for wood cribs fires is generally reported as $R_{80\text{-}30}$, which represents the average mass loss over the period when the fuel mass is reduced from 80% to 30% of its original mass. This is a practical quantity to describe the average mass loss rate during the period of fully developed fire (Harmathy, 1972). Using data from various sources, Harmathy (1972) showed that the wood fire inside a

compartment could be classified into two categories, namely the ventilation controlled fire and the fuel surface controlled fire. At small ventilation openings, the fuel mass loss rate increases proportionally to the vent parameter, $A_v\sqrt{H_v}$, similar to that shown by Kawagoe and Sekine (1963), with a proportionality constant of 0.09kg s^{-1} $m^{-2.5}$. At this regime, the fire is classified as a ventilation controlled fire. However, this proportional relationship breaks down at large values of vent parameter, such that continuing to increase the vent parameter would not increase the mass loss rate, and the fire is now classified as a fuel surface controlled fire. This is summarised in the plot shown in Figure 6.1.

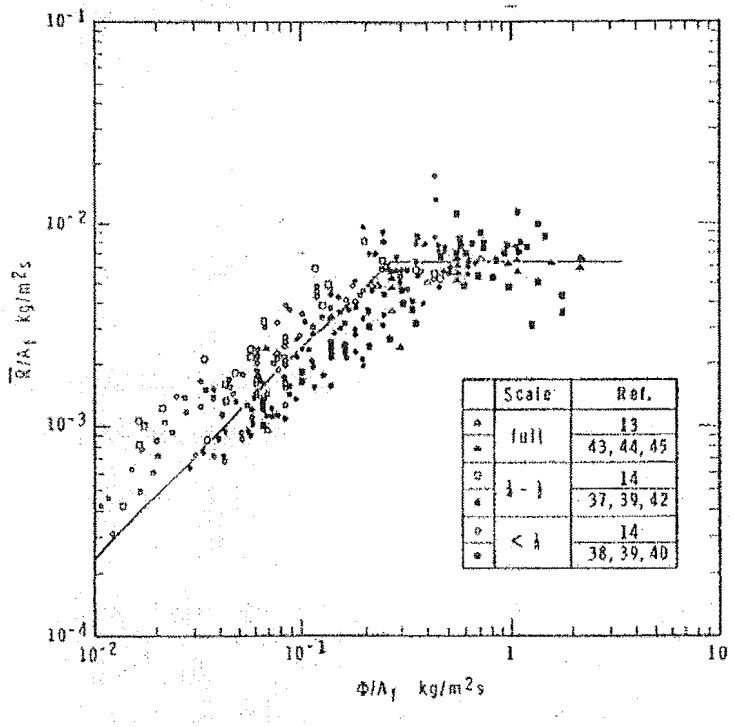

Figure 6.1 **Correlation of experimental data on the rate of burning of cellulosic fuels in compartments (Harmathy, 1972).**

Harmathy (1972) showed that the mass loss rate of the cellulosic fuel for these two burning regimes could be represented by the following two equations:

Ventilation controlled

$$\dot{m}_p = 0.09 A_v \sqrt{H_v} \qquad \text{if } \frac{A_v \sqrt{H_v}}{A_F} < 0.071 \qquad \textbf{(6.1a)}$$

Fuel surface controlled

$$\dot{m}_p = 0.0062 A_F \qquad \text{if } \frac{A_v \sqrt{H_v}}{A_F} \geq 0.071 \qquad \textbf{(6.1b)}$$

Note: Harmathy used ventilation parameter, "Φ", which is equal to $\rho_0 \sqrt{g}\left(A_v \sqrt{H_v}\right)$ as characterising parameter. The equation above lumps the term, $\rho_0 \sqrt{g}$, into the correlating constants with ρ_0=1.18kg/m^3, and g=9.81 m/s^2, thereby expressing the equation in terms of vent parameter $A_v \sqrt{H_v}$. Equation (6.1a) is effectively the Kawagoe correlation.

Equations (6.1a) and (6.1b) suggest that mass loss rate of wood depends on either the ventilation or the fuel surface area, and is unaffected by the potential radiation effect from the surrounding environment. However, these two correlations are rather simplistic, in particular, the use of a constant fuel surface area, A_F, in the Equation (6.1b) is rather odd because a substantial amount of the fuel surface would have been burned away over the fire duration. Also, the use of the Kawagoe correlation, $0.09 A_v \sqrt{H_v}$, for describing the mass loss rate could only be effective for certain compartment and ventilation geometry (Thomas, 1974 and 1995).

In this chapter, the burning behaviours of wood are described and discussed. Further analysis is performed using the $R_{80\text{-}30}$ data to identify other parameters that could affect the mass loss rate of wood.

6.2 BURNING OF WOOD

Quintiere (1992) developed a semi-quantitative model for wood burning under heat flux. His model presents a useful insight to the wood burning characteristics. It is known that when wood is ignited and burned, a char layer is formed and thickened over the duration with a pyrolysis front moving towards the virgin core of the solid. In Quintiere's model, three entities are considered over the entire solid, and each is treated as separate control volume. These include the char layer, the virgin core and a vaporising plane between the char layer and the virgin core, as shown in Figure 6.2.

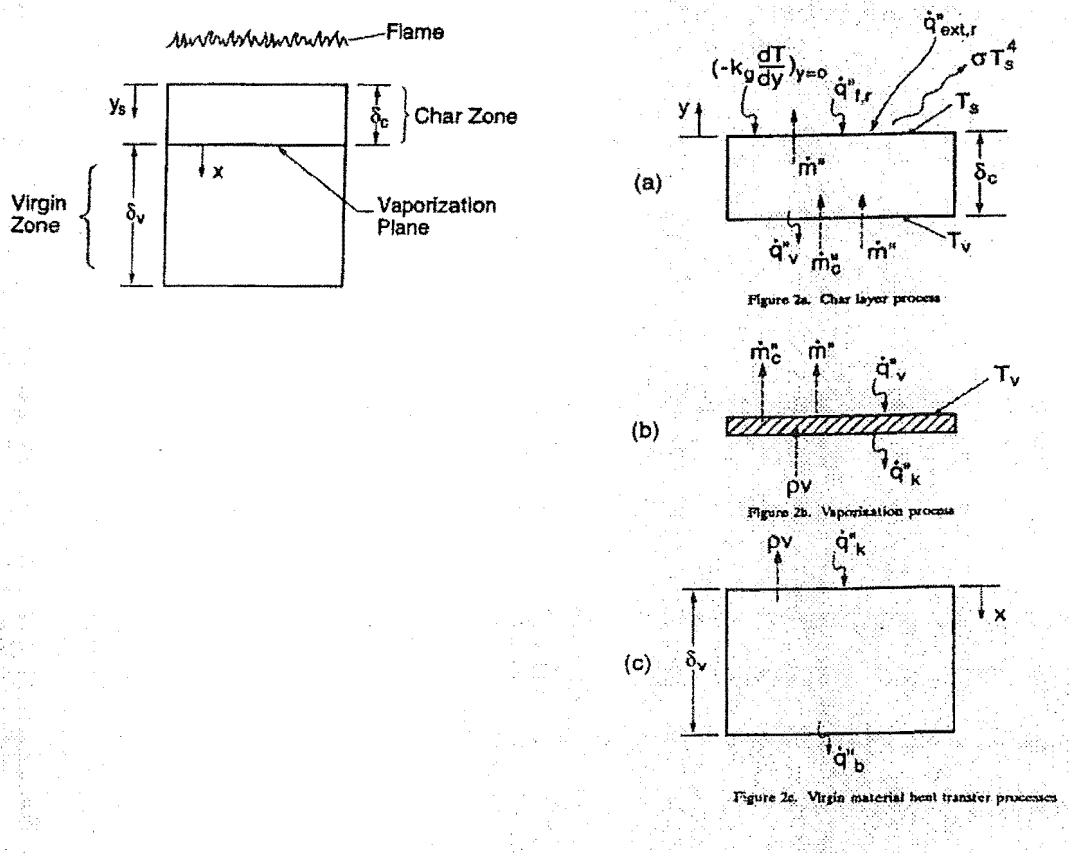

Figure 6.2 Quintiere's wood model (Quintiere, 1992).

It is assumed that the original solid thickness does not change and that only the char layer is thickened over time. The pyrolysates from the virgin core go straight through the char layer unimpeded and burned in the gas phase. The oxidation of char is

ignored. By applying conservation heat and mass equations to each control volume, the following equation can be obtained (after Quintiere, 1992 Equation (21b)).

$$\beta \dot{m}'' L_g = \left(-k\frac{\partial T}{\partial y}\right)_{y=0} + \dot{q}''_{fl,rad} + \dot{q}''_{ext,rad} \qquad \textbf{(6.2)}$$

convective heat transfer *flame radiation* *external radiation*

$$-\sigma T_s^4 \qquad -\rho_c c_c \frac{d}{dt}\int_0^{\delta_c}(T-T_0)dy_s$$

surface re-radiation *energy storage due to charring*

$$-\dot{m}'' c_g (T_s - T_v) + \beta \dot{m}'' \rho_c c_c (T_v - T_0)/\rho \qquad -\dot{q}''_b$$

energy flow through char *back face heat loss*

$$-\rho c \frac{d}{dt}\int_{\delta_c}^{\delta_c+\delta_v}(T-T_0)dy_s$$

virgin solid energy storage

where

$$\beta = \rho/(\rho - \rho_c)$$

Equation (6.2) reveals an interesting aspect of wood burning. At the initial period when wood is ignited and the char layer is thin, by neglecting all the char terms, and ignoring the rate of temperature change in the virgin solid and the back face heat loss, the mass loss rate has an expression similar to that in the pool (Equation 5.6). Thus the mass loss rate depends on the convective and radiative flame heat flux components, the external irradiance flux minus the surface re-radiation. However, as the char layer thickens, the surface temperature, T_s, increases and all the char terms increase. As a consequence, the mass loss rate is reduced. It should be noted that for wood with finite thickness, the back face effect could be felt when the back face substrate fails to dissipate the heat in the solid. The bulk temperature in the entire solid could increase considerably leading to an increase in mass loss rate.

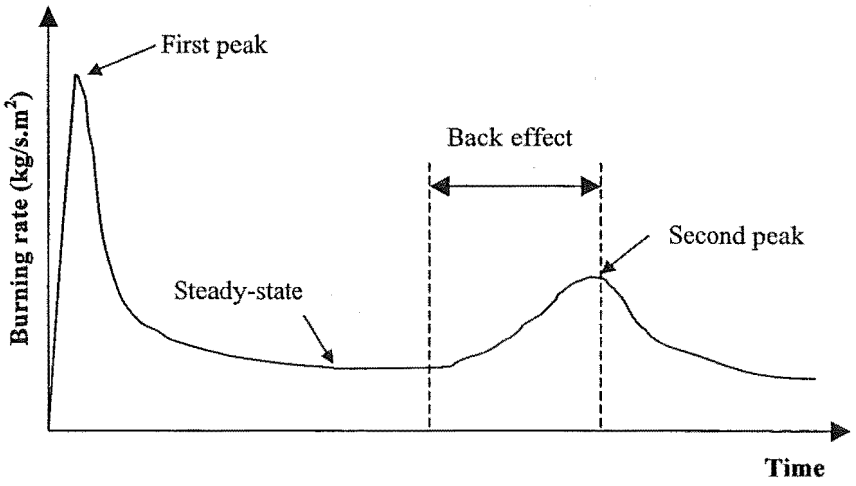

Figure 6.3 **Schematic representation of the burning rate of wood under cone-calorimeter.**

Figure 6.3 is a schematic representation of the burning behaviour of wood. The first peak represents the condition where the char layer is thin. The decrease in the burning rate after the peak is due to char building-up, thereby increasing the thermal resistance between the surface area and the vaporising front. The second peak occurs as a result of back effect. However, it would not exist if attached to a substrate acting as a heat sink (Tran, 1992).

Quintiere's (1992) model has been further developed by Spearpoint (1999) and shown to produce favourable results compared with experimental data from cone-calorimeter tests (Spearpoint and Quintiere, 2000). There are other mathematical models available for describing the burning of wood, notably the numerical model by Parker (1988 and 1992). Although these models have shown promising results, they are considered to be too cumbersome for use in conjunction with a compartment fire model.

6.2.1 Burning regression rate of wood

Generally, the burning of wood is described by a constant rate regressing from the surface. An empirical value of 1/40″ per minute, i.e. 0.0106 mm/s, is normally quoted. However, as noted by Thomas (1995), this value originates from large wood specimen tested in a furnace with a standard fire, and therefore is reasonable only for behaviour in a standard furnace test.

Babrauskas and Williamson (1978) reported on the study by Schaffer (1966 and 1967) for which Schaffer studied the effect of furnace temperatures other than the standard curves. For three constant furnace temperatures 538°C, 815°C and 926°C, Schaffer obtained regression velocities of 25mm/hr (0.0069mm/s), 45mm/hr (0.012mm/s) and 53mm/hr (0.015mm/s) respectively. In the furnace test, the specimens are generally thick enough to establish a nearly steady regression rate. Babrauskas (1981) suggested that for thick cellulosic slabs with a thickness, D, greater than 0.05m, a steady regression rate can be assumed to be in the range of

$$v_p = 8.5 - 10 \times 10^{-6} \text{ (m/s)} \quad \textbf{(6.3)}$$

For slabs with thickness less than 0.05m, i.e. $D \leq 0.05$m, the bulk temperature in the specimen could heat up considerably during the course of a fire, resulting a faster regression velocity. The regression rate for the thin slabs can be estimated as (Babrauskas, 1981):

$$v_p = 2.2 \times 10^{-6} \times D^{-0.6} \text{ (m/s)} \quad \textbf{(6.4)}$$

Spearpoint (1999) analysed a large amount of small-scale wood burning data from cone-calorimeter tests. The tests included four wood species, namely Douglas fir, Maple, Red oak and Redwood, tested in two orientations, one along the grain (L) and the other across the grain (X), under various irradiance heat fluxes. All of the wood samples had a nominal thickness of 50mm. Observations made during the tests were reported to have similar trend to that presented in Figure 6.3, where there exists a peak and decrease to a state close to steady-state (Spearpoint, 1999).

Figure 6.4 plots the steady-state regression rate versus the irradiance heat flux using the data obtained from Spearpoint's study (1999). The regression rate is estimated by dividing the steady-state mass loss rate per unit area with the wood density. Such a treatment represents the extreme case which assumes that the char above the pyrolysis front burns away immediately as the front progress into the virgin core. Using another extreme, which assumes the original solid thickness does not change and that only the char layer is thickened over time, the regression rate would be calculated by dividing

the mass loss rate per unit area by the density difference between the wood and the char, as this is the mass that is vaporised. In reality, during the actual burning of wood, part of the char at the surface would burn away. The regression rate that describes the actual burning is likely to have a value between the two extremes.

From Figure 6.4, it can be seen that increasing the irradiance heat flux imposed upon the wood samples increases the regression rate; this is in-line with Schaffer's findings. The density of wood also seems to have an effect on the increment in the regression rate, possibly due to its relevancy towards the thermal inertia ($k\rho c$) of the sample. For example, for softwood species such as Redwood, the increment is more obvious. These results show that the wood mass loss rate is affected by the irradiance heat flux, with the steady-state regression rate ranging from approximately 0.0075mm/s to 0.015mm/s over the irradiance flux of 25kW/m^2 to 75kW/m^2. Although the results from the cone-calorimeter tests have shown that the regression rate is a function of irradiance heat flux, there are still uncertainties involved over its application in post-flashover fire conditions. In particular, the high heat flux with the potential of being greater than 100kW/m^2 during post-flashover fires, is outside the range of cone-calorimeter test range. Furthermore, the vitiating effects inside the post-flashover compartment as well as the thickness of the wood fuels could well affect the burning hence the resulting regression rate. Recalling Harmathy's equation (Equation (6.1b)) for the fuel surface controlled burning regime, assuming wood has a density of 500 kg/m^3, gives a regression rate of 0.012mm/s. This value is comparable to the averaged regression rate of 0.0115mm/s from Spearpoint's data for all the wood species over heat flux ranging from 25kW/m^2 to 75kW/m^2. Therefore, as a first approximation, this value could be regarded as typical for wood burning over a range of irradiance fluxes.

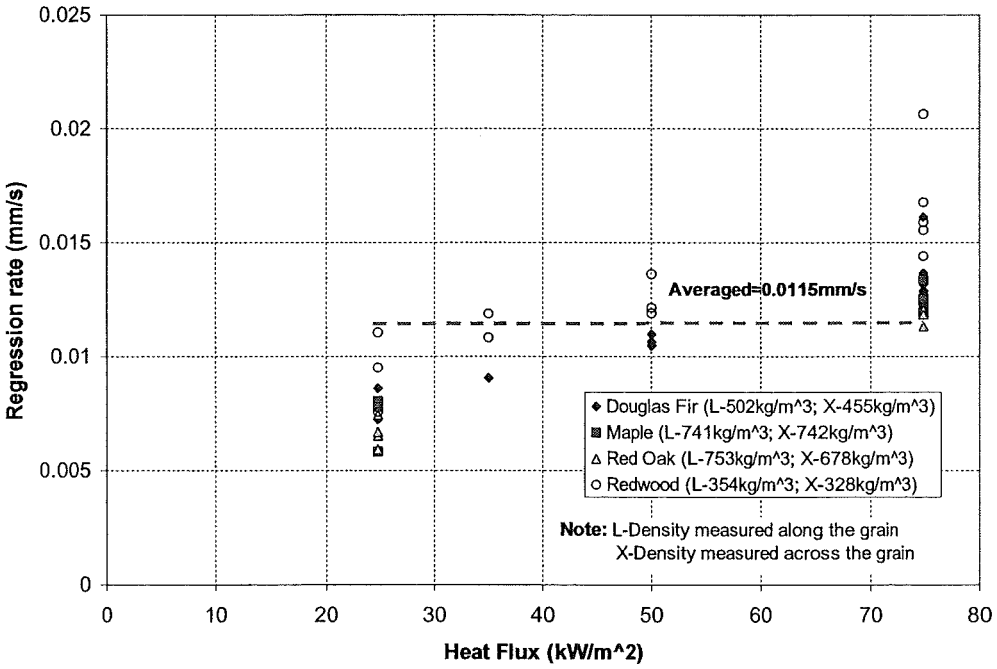

Figure 6.4 Heat flux versus regression rate (Data from Spearpoint (1999)).

6.2.2 Fuel with shape

For fuel having a shape other than a one-dimensional plane, such as a stick (a two-dimensional shape) or a cube or sphere (a three-dimensional shape), the constant regression rate cannot be applied to all the surfaces, as the corners would be counted twice. Ödeen (1963) postulated a method that describes the change of volume and hence the surface area of the fuel, given the initial fuel dimension and a constant regression rate. In term of mass loss rate, this is given as follows:

$$\frac{\dot{m}_p}{M_0} = \frac{2v_p F}{D} \cdot \left(\frac{m(t)}{M_0}\right)^{1-\frac{1}{F}} \tag{6.5}$$

with

$$m(t) = M_o - \sum_i^t \dot{m}_p(t_i)\Delta t$$

where:

M_0 =The initial mass before fire (kg)

$m(t)$ =The remaining mass at time t (kg)

F =The shape factor

F=1 for an infinite plane

F=2 for cylinders and rectangular sticks

F=3 for spheres and cubes

D = The characteristic dimension (m)

v_p = The regression rate (m/s)

According to the model, the mass loss rate is constant for an infinite plane, decreases linearly for two-dimensional objects such as sticks and cylinders, and decreases more rapidly for three-dimensional objects such as cubes and spheres.

Ödeen's method could alternatively be stated as

$$\dot{m}_p = v_p \times \rho_{wood} \times A_F(t) \qquad \textbf{(6.6)}$$

The mass loss rate is the product of the regression rate, v_p, the density of the fuel, ρ_{wood} and the remaining fuel surface area at time t, $A_F(t)$. The total exposed surface area depends on the initial shape of the fuel as well as the amount of the fuel. As the burning progresses, as described by the regression rate, v_p, the remaining fuel surface area will decrease with time due to the fuel burning away.

6.2.3 Modelling wooden furniture

Babrauskas (1976) showed that Ödeen's method could be used to describe the burning of wood crib. With regard to modelling furniture items inside post-flashover compartments, he suggested that Ödeen's approach could still be used by assigning equivalent geometrical properties to the actual fuel. This requires estimating the total fuel load and the average thickness of the fuel elements to provide the required inputs for Equation (6.5).

However, this presents a few difficulties as the geometrical properties between furniture items, as well as the components that make up a single piece of furniture, could vary markedly. In order to avoid the difficulty of trying to specify a single geometrical dimension and shape as required in Equation (6.5), the alternative form of Ödeen's equation, Equation (6.6) is used instead. This allows measuring each furniture item in detail and manually calculating the change in surface area over time using a constant regression rate. Yii (2000) surveyed and measured the geometry of typical furniture items including bookshelves, cupboards, desks, tables and chairs. Each furniture item was divided into individual components of different geometrical shape. A regression rate of 0.011mm/s is chosen as it is considered to be a practical representative value for different wood species at different heat fluxes (Figure 6.4). This regression rate is applied to all the exposed surface areas. The change of the remaining surface area of the furniture over time is manually evaluated by summing the remaining surface area of each component over time. The mass loss rate history of the furniture item over time due to surface regression is therefore obtained via Equation (6.6), i.e. by multiplying the regression rate (0.011mm/s), the density of wood (450 kg/m^3) and the remaining fuel surface area, $A_F(t)$.

For example, Figure 6.5 and Figure 6.6 show the mass loss rate for a desk and a bookshelf, respectively, calculated using the constant regression rate of 0.011mm/s on all exposed surfaces.

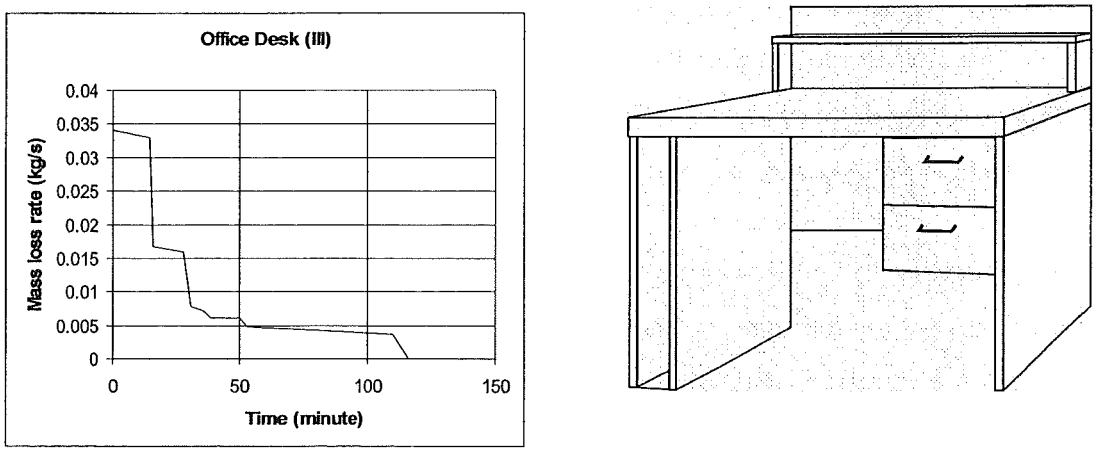

Figure 6.5 **The mass loss rate of a desk evaluated using the measured surface area and a regression rate of 0.011mm/s.**

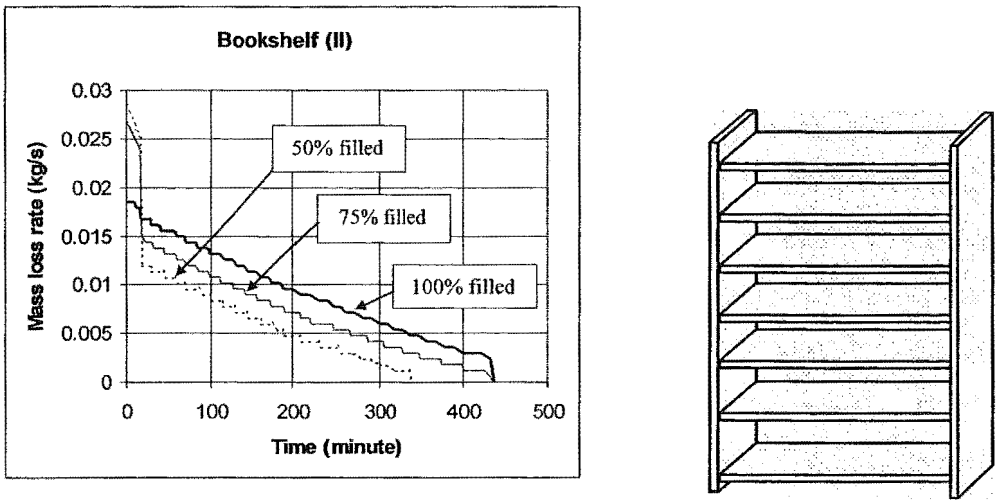

Figure 6.6 The mass loss rate for a bookshelf (50%, 75% and 100% full of books) using the measured surface area and a regression rate of 0.011mm/s.

The mass loss history of the desk presented in Figure 6.5 shows a steep drop in the mass loss rate after about 15 minutes, resulting from the thin components with large surface area burning away. The duration of burning depends on the thickness of the thickest component of the furniture, such as a filled drawer. For the bookshelf shown in Figure 6.6, the books are modelled as solid blocks in the bookshelf. The regression is from all directions except the back. From the mass loss rate histories shown, it can be seen that for non-fully filled bookshelves, the initial mass loss rates are larger than the fully filled bookshelf, followed by a large drop in the mass loss rate. This is largely due to the burning of the exposed thin components in non-fully filled bookshelves. These exposed thin components provide greater initial surface areas for burning, and after these thin components are consumed, the mass loss rate drops as to represent the burning of solid blocks of books. The bookshelf tends to burn for a long time because of the thickness of the books.

Since the burning behaviour among wooden furniture items is different, the types of furniture are categorised into two categories namely (1) "thick" and (2) "thin". This classification is arbitrary and is based upon the furniture respective mass loss rate curve. Wood-based furniture items that present a rapid drop in mass loss rate during the first 30 minutes, and burn away completely in less than three hours, are classified as "thin". Wood-based furniture items that do not exhibit any rapid drop in the mass loss rate, or burn for three hours or more, are classified as "thick".

Appendix B presents the furniture items surveyed and measured by Yii (2000) with their respective mass loss rate history. By having a catalogue of furniture items with vastly different geometry, a selection of these items could be picked to represent the fuel load inside a compartment, therefore studying the resultant fire. This will be further discussed in Chapter 12.

It is acknowledged that the furniture model assumes that the entire mass of wood is consumed by flaming combustion where no char is left behind the pyrolysis front (described by the regression rate). Therefore the fire heat release rate is evaluated as the product between the mass loss rate and the net heat of combustion for wood (~19MJ/kg for dry wood (Babrauskas, 1992b)). Such treatment represents a general first approximation to describe the burning of wood. In realistic wood burning process, apart from burning the volatile released from the virgin core, char will also be produced and burned later. The heat of combustion for the volatile can be estimated depending on the fraction of char yield per unit mass of wood burned, which could range from ~10-17MJ/kg for char yield for dry wood of 33% to 15% of the original mass (after Harmathy, 1972; Spearpoint and Quintiere, 2002); and the heat of combustion for char is approximately two to three times the value for volatile of ~33MJ/kg (Harmathy, 1972). By ignoring the char oxidation, the furniture model is likely to underestimate the heat release especially during the later stage of the fire where the burning is dominated by the burning of char. Further comparative study between the furniture model and experimental studies is needed to evaluate the adequacy of the model and to study the effects of char oxidation.

6.3 ANALYSING R80-30 DATA

The mean mass loss rate for wood cribs in compartment test fires is generally reported as $R_{80\text{-}30}$ which represents the average mass loss over the period when the fuel mass is reduced from 80% to 30% of its original mass. This is a practical quantity to describe the mass loss rate of wood during the period of fully developed fire (Harmathy, 1972).

Kawagoe and Sekine (1963) were the first to show that the mass loss rate of wood inside the compartment could be correlated using the vent parameter, $A_v\sqrt{H_v}$, such that

$$\dot{m}_p = 0.09 A_v \sqrt{H_v} \qquad \textbf{(6.7)}$$

Later, Thomas and Heselden (1972) analysed a large number of small scale fire test results from a co-operative research programme of the Conseil International Du Batiment on fully developed fires (known as the CIB tests) and found that the mass loss rate of wood in fully developed fires is not only dependent upon the vent parameter, $A_v\sqrt{H_v}$, but also on the size of the vent opening relative to the compartment size, Ω, and the compartment aspect ratio, (D_c/W_c). The resulting correlation is shown in Equation (6.8) (Law, 1983). This correlation is referred to as the Law correlation.

$$\dot{m}_p = 0.18 \cdot A_v \sqrt{H_v} \cdot \left(\frac{W_c}{D_c}\right)^{\frac{1}{2}} \cdot \left(1 - e^{-0.036\Omega}\right) \qquad \textbf{(6.8)}$$

where $\Omega = \dfrac{(A_T - A_v)}{A_v\sqrt{H_v}}$

and A_T is the total internal surface area including the vent opening area, W_c is the compartment width and D_c is the compartment depth. The main feature of the Law correlation is that a deep compartment would result a lower mass loss rate than a wider compartment. The mass loss rate could be even smaller with small Ω.

Recent studies at Victoria University of Technology (VUT) (Thomas and Bennetts, 1999; Thomas, 1999a and 1999b) showed that the vent width ratio, W_v/W_c, which is the ratio of the vent opening width to the width of the compartment, is influential over the mass loss rate. It was observed that the flow within the enclosure was two-dimensional for W_v/W_c =1 compared to three-dimensional for W_v/W_c <1 (Thomas and

Bennetts, 1999). Based on the CIB data and experiments conducted in VUT, a correlation is derived by Thomas (1999b) and is given by:

$W_v/W_c < 1$ $$\dot{m}_p = 0.199 W_v^{0.543} H_v^{1.31} \quad \textbf{(6.9a)}$$

$W_v/W_c = 1$ $$\dot{m}_p = 0.026 W_v^{1.17} H_v^{1.69} \quad \textbf{(6.9b)}$$

Estimates made by the above correlations for the mass loss rate of wood in a fully developed fire vary markedly when involving very large vent opening such as a window occupying a full wall. For example, for a compartment 2.4m x 3.6m x 2.4m (width x depth x height), fully open at one of the long ends (2.4m by 2.4m opening), the Law correlation predicts a mass loss rate of 0.205kg/s, compared with 0.845kg/s predicted by the Kawagoe correlation. For the same compartment with a door opening of 2.03m high by 0.76m wide, however, both correlations provide similar predictions with 0.172kg/s by Law and 0.198 by Kawagoe. It has been suggested that the Kawagoe correlation is only applicable for certain combinations of vent and compartment geometries (Thomas, 1974 and 1995) although there are no guidelines available.

The various correlations presented above show that the mass loss rate of wood inside a compartment may depend on the vent parameter, $A_v\sqrt{H_v}$, the compartment aspect ratio, D_c/W_c, the compartment internal area, A_T, and the vent width ratio, W_v/W_c. The objective of the following analysis is to investigate and identify the influential geometrical parameters that could affect the mass loss rate of wood burning inside the compartment. This would allow a better understanding of the mechanism that controls and affects the burning of wood inside a compartment.

6.3.1 Dimensional analysis

In order to identify the parameters that affect the mass loss rate inside the compartment, dimensional analysis is performed. The analysis uses the data sets from the test programmes conducted by the Conseil International Du Batiment (CIB), the British Steel Corporation (BSC), the Joint Fire Research Organisation (JFRO) and the Centre Technique Industriel de la Construction Métallique (CTICM), extracted from

Thomas (1999a, 1999b) and the published data from Gross and Robertson (1965) tests. The geometrical parameters considered in the analysis include those in the existing correlations such as vent parameter, $A_v\sqrt{H_v}$, compartment aspect ratio, D_c/W_c, compartment internal area, A_T, and the vent width ratio, W_v/W_c. The opening fraction, A_v/A_w, which characterises the vent size in the wall, is also included in the analysis. Table 6.1 presents the variables for the dimensional analysis. The gravitational constant, g, and the air density, ρ_0, are both included, as they are terms involved in describing the buoyancy driven flow across the vent opening.

Table 6.1 Variables for correlation analysis.

Quantity	Symbol	Unit	Dimensions
Mass loss rate	$\dot{m}_p$	kg/s	MT^{-1}
Density of air	ρ_0	kg/m^3	ML^{-3}
Vent parameter	$A_v\sqrt{H_v}$	$m^{2.5}$	$L^{2.5}$
Gravitational constant	g	m/s^2	LT^{-2}
Total enclosed boundary surface areas- including vent opening area	A_T	m^2	L^2
Enclosure aspect ratio- "depth to width ratio"	D_c/W_c	-	-
Vent width to compartment width ratio- "vent width ratio"	W_v/W_c	-	-
Fraction of vent opening area to the area of the wall containing the vent- "opening fraction" Note: the height of *Aw* is evaluated from the floor level to the soffit of the opening.	A_v/A_w	-	-

In order to correlate the geometric parameters with the mass loss rate, these parameters are arranged into dimensionless groups, such that when correlation is made between these terms the correlation coefficient does not carry any units. Since geometrical variables such as D_c/W_c, W_v/W_c and A_v/A_w are already dimensionless, attention is on reducing $\dot{m}_p$, ρ_0, $A_v\sqrt{H_v}$, g and A_T into dimensionless terms.

With three different reference dimensions (mass, length, time) and five variables ($\dot{m}_p$, ρ_0, $A_v\sqrt{H_v}$, g, A_T) there will be two dimensionless π groups. These groups are derived by choosing ρ_0, g and $A_v\sqrt{H_v}$ as repeating variables (as these three variables contain all three reference dimensions). These two dimensionless π groups are found in the form of $\dot{m}_p/(\rho_0 \cdot \sqrt{g} \cdot A_v\sqrt{H_v})$ and $A_T/(A_v\sqrt{H_v})^{0.8}$. Since the other four variables involved are already in dimensionless form, there are a total of 6 dimensionless π groups involved.

$$f_1\left(\frac{\dot{m}_p}{\rho_0 \cdot \sqrt{g} \cdot A_v\sqrt{H_v}}, \frac{A_T}{\left(A_v\sqrt{H_v}\right)^{0.8}}, \frac{D_c}{W_c}, \frac{W_v}{W_c}, \frac{A_v}{A_w}\right)$$

$$\pi 1: \frac{\dot{m}_p}{\rho_0 \cdot \sqrt{g} \cdot A_v\sqrt{H_v}} = f_2\left(\pi 2: \frac{\left(A_v\sqrt{H_v}\right)^{0.8}}{A_T}, \pi 3: \frac{D_c}{W_c}, \pi 4: \frac{W_v}{W_c}, \pi 5: \frac{A_v}{A_w}\right)$$

Note that since the analysis involves the mass loss rate of wood during the fully developed period, the data having temperatures less than 600°C are neglected.

6.3.2 Outcomes and findings

$\pi 1$ is the dimensionless group that defines the mass loss rate. In order to find the relationship between the mass loss rate and other parameters, $\pi 1$ is plotted against every other π group using the data from the aforementioned sources.

Figure 6.7 is a plot between $\pi 1$ and $\pi 2$. From the plot, although there is a lot of scatter in the data, a trend could still be observed, such that increasing $\pi 2$ would decrease $\pi 1$. In other words, for similar compartment size, A_T, increasing the ventilation opening would result in a decrease in the mass loss rate for the given opening. A logarithm relationship is used to fit data. The Kawagoe correlation is also shown in Figure 6.7 where the coefficient of 0.09 in Equation (6.7) has an equivalent value of 0.024, i.e. $0.09/(\rho_0 * \sqrt{g})$, in the figure due to the convention used in the y-axis. The plot

suggests that the Kawagoe correlation gives a crude approximation to the mass loss rate from these scattered data points. Noticeably, the Kawagoe correlation over-estimates the mass loss rate of fuel for large windows (at the high end of $\pi 2$) and under-estimates the mass loss rate for small windows (at the low end of $\pi 2$).

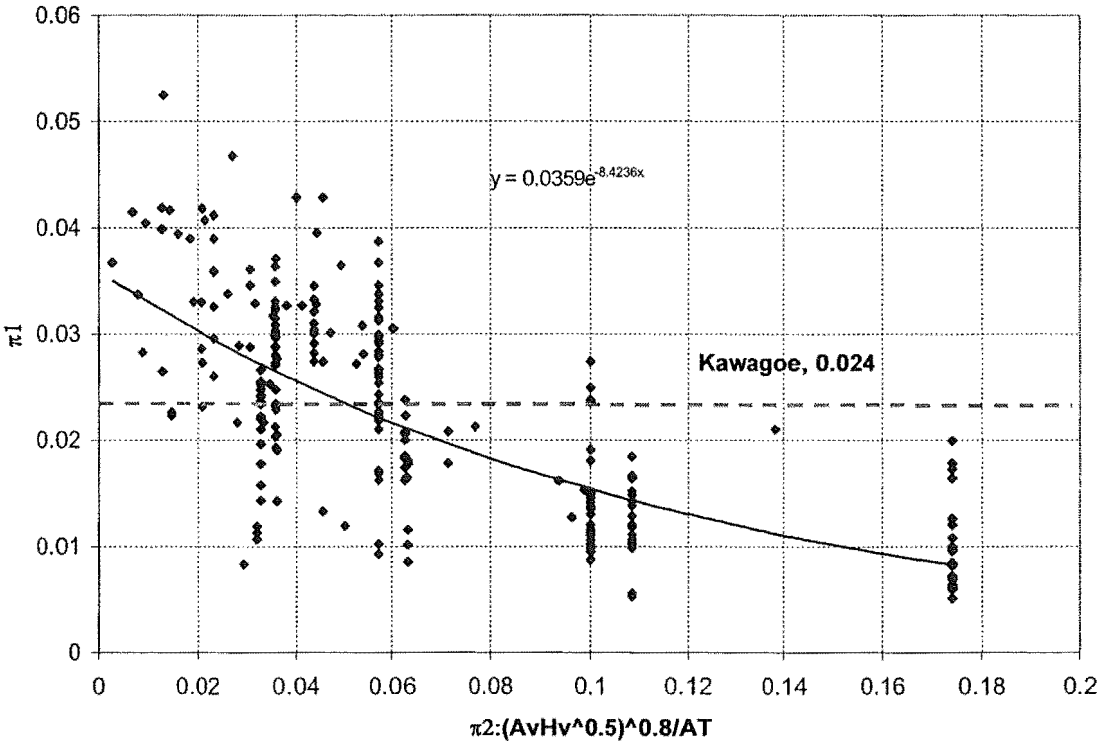

Figure 6.7 Dependence of Variation of $\pi 1$ on $\pi 2$.

Figure 6.8 is a plot of $\pi 1$ against $\pi 3$ (D_c/W_c). No noticeable trend can be observed. In the plot, the CIB test data have been distinguished from the overall data used; a slight trend can be observed despite the scatter in the data points. The CIB data shows that increasing D_c/W_c decreases the fuel mass loss rate. This could be the reason that this term is included in the Law correlation. However, when other test data are included, this trend is not obvious.

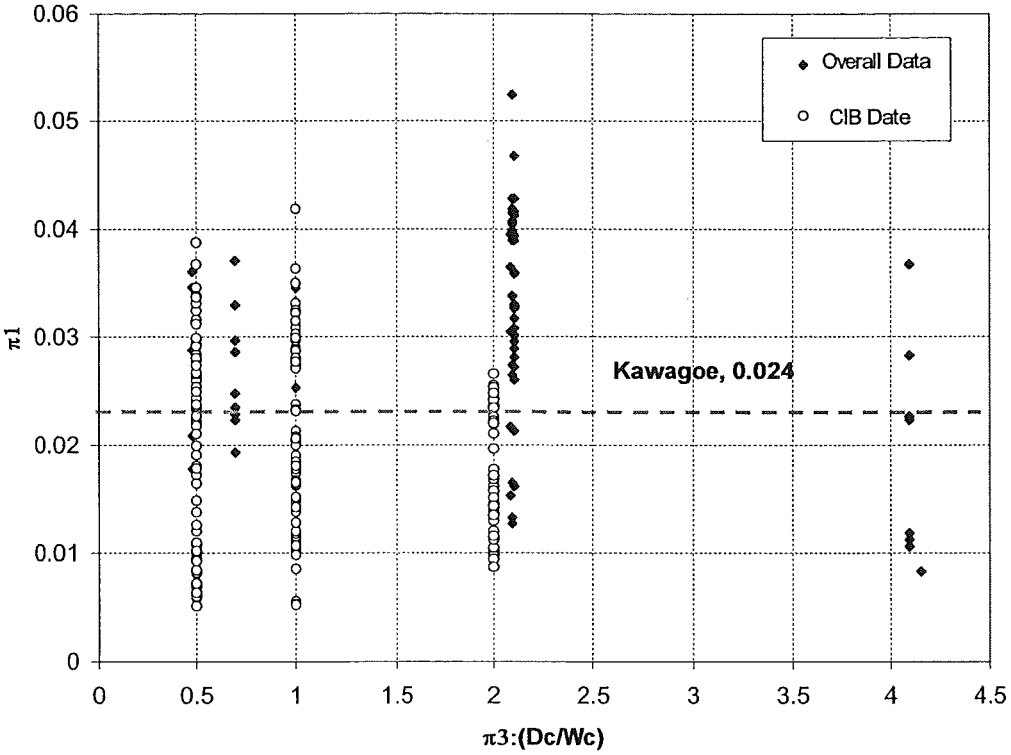

Figure 6.8 Dependence of Variation of π1 on π3.

Figure 6.9 is a plot of π1 against π4 (W_v/W_c). There is no noticeable trend observed. In the plot, data with openings extending to the floor level (i.e. a door-type opening with zero sill height, δ=0) are distinguished from the overall data. A trend can be observed from the door-type opening data, such that increasing the door opening width fraction, W_v/W_c, could result in a reduction in the fuel mass loss rate for the given ventilation opening ($\dot{m}_p / A_v\sqrt{H_v}$). For door width equal to the width of the compartment, i.e. W_v/W_c =1, the mass loss rate is approximately half Kawagoe's value. Recalling the vent flow analysis in Chapter 3, similar trend can be seen for door type opening (δ=0) where $\dot{m}_{in} / A_v\sqrt{H_v}$ decreases with increasing W_v/W_c. Using a wall line-plume as an analogy, at the full opening width, W_v/W_c =1, the entrained air inflow per unit vent parameter, $\dot{m}_{in} / A_v\sqrt{H_v}$, is approximately 60% of the maximum flow, mirroring the trend seen in Figure 6.9.

Figure 6.10 is a plot of π1 against π5, (A_v/A_w). A clear trend could be observed in the plot showing that the fuel mass loss rate for the given ventilation opening,

($\dot{m}_p / A_v\sqrt{H_v}$), decreases with increasing opening fraction, A_v/A_w, though there is very little data in the range between $0.5< A_v/A_w<1.0$. It is acknowledged that the trend in the plot is largely shaped by the data from the tests having an opening without sill. However, it can be seen that by using the parameter, A_v/A_w, it helps to provide a general overall characterisation of data for tests having opening with and without sill. Recalling the line plume analysis in Chapter 3, the air inflow per unit vent parameter approaches the maximum with small openings. The close similarity between the trends observed in the air inflow ($\dot{m}_{in} / A_v\sqrt{H_v}$) from the line plume analysis and the mass loss rate ($\dot{m}_p / A_v\sqrt{H_v}$) observed in Figure 6.9 and Figure 6.10 strongly indicates that the mass loss rate of wood during the fully developed period is related to the air inflow.

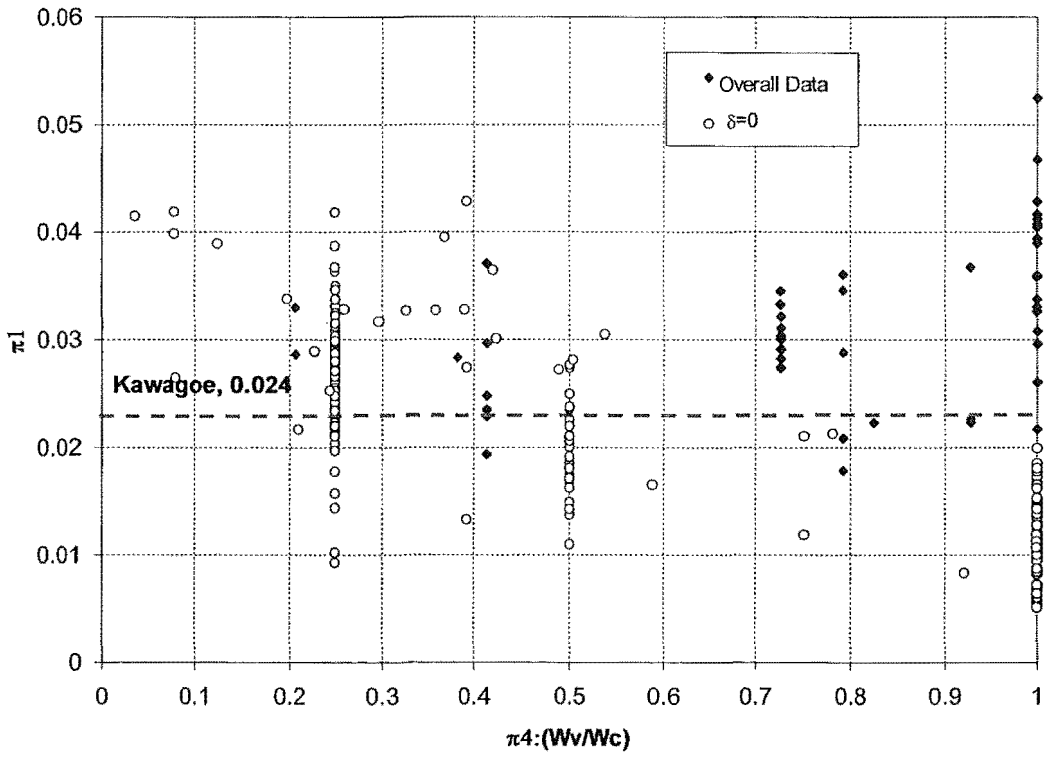

Figure 6.9 Dependence of Variation of π1 on π4.

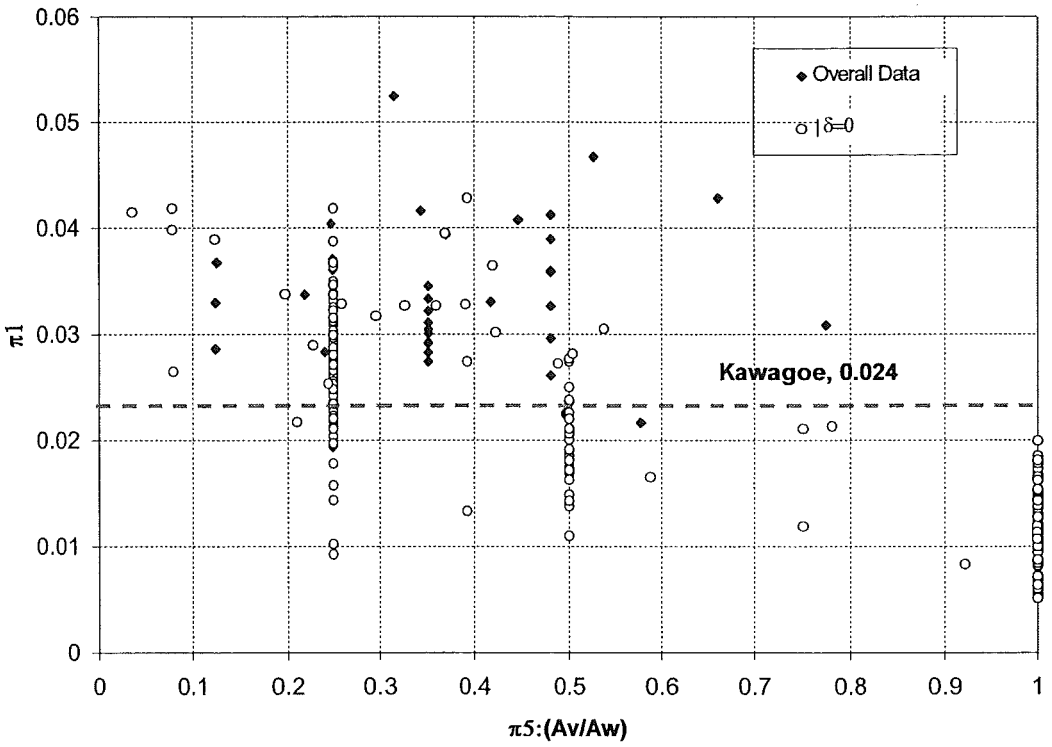

Figure 6.10 Dependence of Variation of π1 on π5.

The dimensional analysis to this point shows that π1 is dependent upon π2 and π5, such that:

$$\pi 1: \frac{\dot{m}_p}{\rho_0 \cdot \sqrt{g} \cdot A_v \sqrt{H_v}} = f_3\left(\pi 2: \frac{\left(A_v \sqrt{H_v}\right)^{0.8}}{A_T},\quad \pi 5: \frac{A_v}{A_w}\right)$$

Figure 6.11 combines these three parameters (π1, π2 and π5) into a single summary plot, with π2 plotted on the x-axis and π1 plotted on the y-axis. An exponential relationship was used to describe π2 and π1, hence the natural logarithm LN(π1) is used on the y-axis. Data points with three different values of π5 are categorised separately (0.25, 0.5 and 1.0). Other π5 values are not included due to the very small number of data points available. A straight-line linear regression is fitted to each of the π5 category. The Kawagoe correlation is also shown in the Figure 6.11. It seems that the Kawagoe correlation provides reasonable prediction for $0.25 < A_v/A_w < 0.50$ and $(A_v\sqrt{H_v})^{0.8}/A_T$ between 0.02 and 0.10 (Figure 6.11).

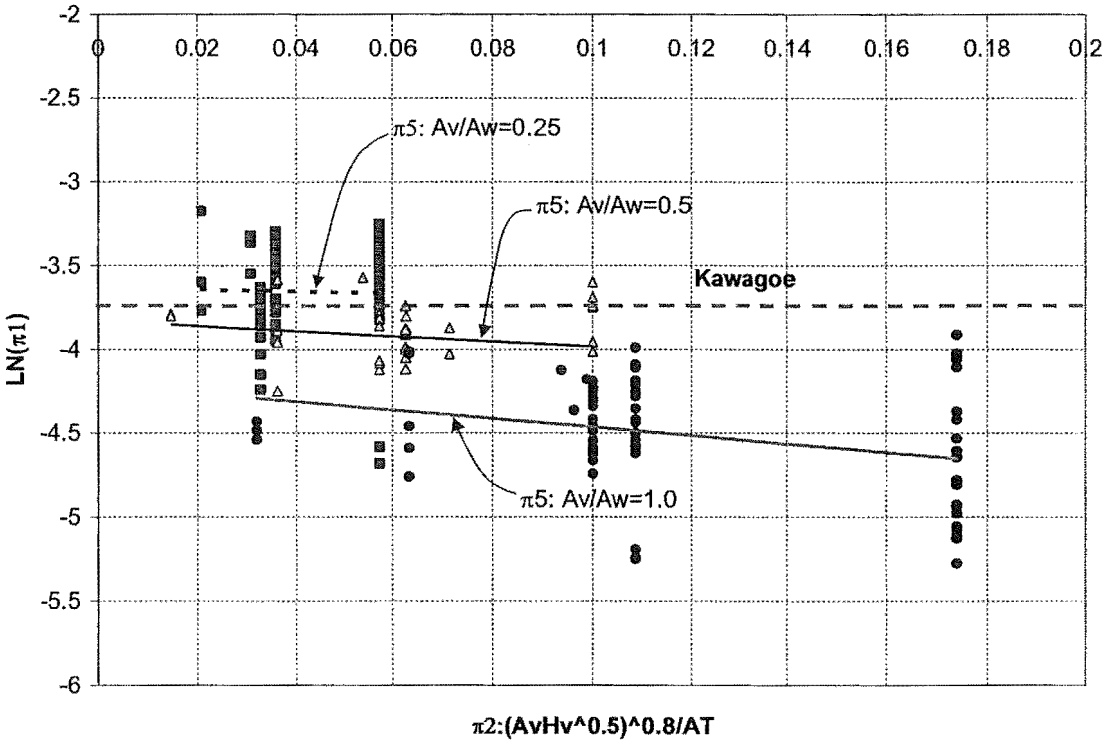

Figure 6.11 A summary plot for the relationships between π1, π2 and π5

A mathematical relationship between π1, π2 and π5 can be developed from the information shown in Figure 6.11. The relationship has the following form:

$$\pi 1 = c_1 \cdot e^{C_2[\pi 2]}$$

where c_1 and c_2 are functions of π5 obtained from the individual regression lines, with values given in the table below for three values of A_v/A_w

	A_v/A_w=0.25	A_v/A_w=0.50	A_v/A_w=1.0
c_1	0.027	0.022	0.015
c_2	-0.640	-1.536	-2.526

When π1 and π2 are expanded, the relationship between them becomes:

$$\frac{\dot{m}_p}{\rho_0 \cdot \sqrt{g} \cdot A_v \sqrt{H_v}} = c_1 \cdot e^{C_2\left[\frac{\left(A_v\sqrt{H_v}\right)^{0.8}}{A_T}\right]} \quad \textbf{(6.10)}$$

By developing an expression for c_1 and c_2 in terms of A_v/A_w, Equation (6.10) can be re-written as:

$$\frac{\dot{m}_p}{\rho_0 \cdot \sqrt{g} \cdot A_v \sqrt{H_v}} = \left(0.030 - 0.016\frac{A_v}{A_w}\right) \cdot e^{\left[-2.515\left(\frac{A_v}{A_w}\right)-0.011\right]\frac{\left(A_v\sqrt{H_v}\right)^{0.8}}{A_T}} \quad \textbf{(6.11)}$$

Equation (6.11) is the correlation of $\pi 1$ with $\pi 2$ and $\pi 5$.

6.3.3 Effects of opening fraction

The above dimensional analysis has identified the opening fraction, A_v/A_w, as one of the parameters that affects the mass loss rate of wood burning inside the compartment. It is found that at large opening fraction, such as A_v/A_w =1, the mass loss rate per unit vent parameter, $\dot{m}_p / A_v\sqrt{H_v}$, is much smaller than at small opening fractions, A_v/A_w <1. This trend coincides with the findings from the vent flow analysis in Chapter 3, which shows a small air flow rate per unit vent parameter, $\dot{m}_{in} / A_v\sqrt{H_v}$, at large opening fraction where A_v/A_w =1. This indicates that the mass loss rate of wood inside the compartment is strongly related to the air inflow rate.

The Kawagoe correlation for mass loss rate is usually interpreted as the result of the gas phase reaction, defining the equivalence ratio, Φ, as

$$\Phi = \frac{\dot{m}_p \cdot r}{\dot{m}_{in}} \quad \textbf{(6.12)}$$

Assuming the "typical" wood in compartment fires consists of some moisture, taking wood with 12% moisture content by weight as an indicative value with a chemical formula of $CH_{1.455}O_{0.645}\bullet 0.18H_2O$ (c.f. $CH_{1.455}O_{0.645}\bullet 0.233H_2O$ with 15% moisture content by weight as given by Harmathy (1972)), where r is approximately 5.3. With

$\dot{m}_{in} \approx 0.45 A_v \sqrt{H_v}$, at stoichiometric combustion, Φ=1, substituting the expression for air inflow and r into Equation (6.12) gives the Kawagoe correlation. Following the same argument, using the airflow expressions obtained from the wall line-plume analogy, the corresponding respective mass loss rate expressions could be deduced. These are given as follows:

Φ=1.0

$A_v/A_w < 1$ $\quad \dot{m}_{in} \approx 0.45 A_v \sqrt{H_v} \quad \dot{m}_p = 0.09 A_v \sqrt{H_v}$ **(6.13a)**

$A_v/A_w = 1$ $\quad \dot{m}_{in} \approx 0.26 A_v \sqrt{H_v} \quad \dot{m}_p = 0.05 A_v \sqrt{H_v}$ **(6.13b)**

6.3.4 Comparison of correlations

The above analysis has shown the relationships between different geometrical variables and the mass loss rate. Comparison between the new correlation developed from the analysis and existing correlations including the Kawagoe, Law and Thomas correlations are made by comparing the fuel mass loss rate predictions made from each correlation with experimental results. These experimental results are the same as those used in the above analysis. The comparative plots are given in Figure 6.12.

From the comparative plots, among the existing correlations, the Law correlation (plot (b)) produces the best prediction to the fuel mass loss rate compared to correlation by Kawagoe (plot (a)) and Thomas (plot (c)). In general, the Kawagoe correlation provides a reasonably good prediction on the fuel mass loss rate at small vent opening but over-predicts at the very large vent opening. The Thomas correlation does not provide good prediction as it tends to over-estimate most of the data. Plot (d) shows that the new correlation developed (Equation (6.11)) provides a better prediction for the mass loss rate compared with the other existing correlations. Plot (e) compares the prediction made by the Equations (6.13a) and (6.13b) with the experimental data. Noted that at small opening, Equation (6.13a) is effectively the same as the Kawagoe correlation except that modification was made at a full opening ($A_v/A_w = 1$) according to the wall line-plume entrainment analogy. Therefore, it provides the same prediction as the Kawagoe correlation at small openings and an improved prediction than the

Kawagoe correlation at the full opening. The comparison between the experimental measurements and the predictions made by Equations (6.13a) and (6.13b) are good given the simplicity of the correlation.

It is noted that there are a few data points that are insensitive to the correlation variables used in all the aforementioned correlations. In particular, the data points measured between 1.4kg/s and 1.8kg/s, as shown in all plots (a) to (e). Since these correlations include the vent geometry as part of the correlation, the insensitiveness of these data points to the vent opening geometry indicates the likelihood of fuel-surface controlled burning. The fuel surface area for each experiment would be a useful parameter for differentiating between the ventilation and the fuel-surface controlled regime as shown in the study by Harmathy (1972), (Figure 6.1). However, this parameter is often not reported.

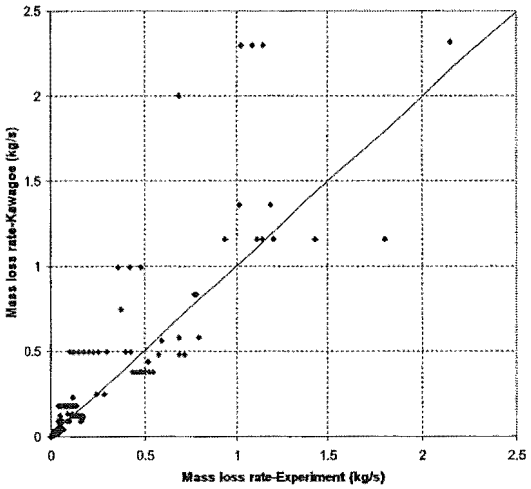

(a) The Kawagoe correlation

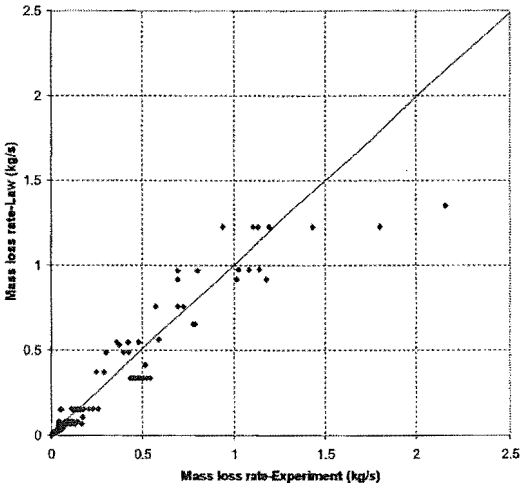

(b) The Law correlation

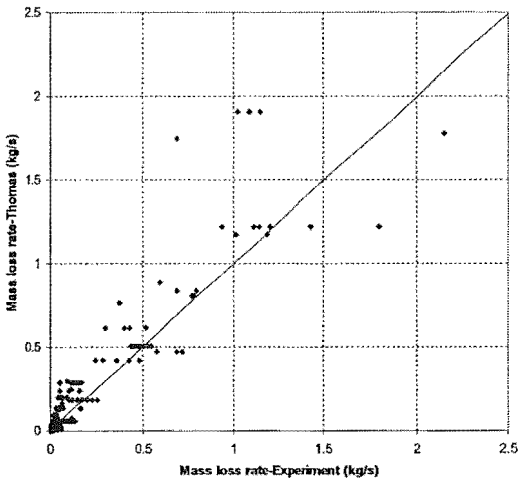

(c) The Thomas correlation

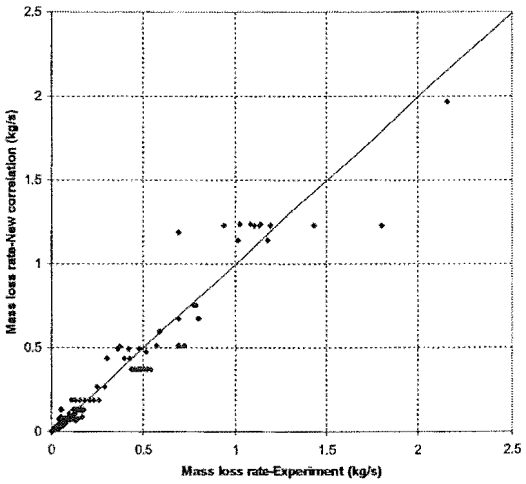

(d) The new correlation-Full

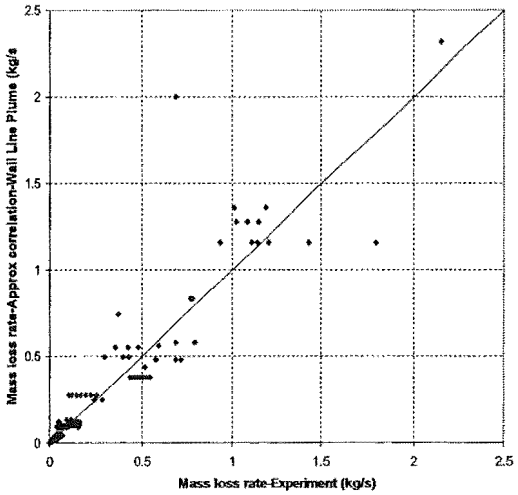

(e) The new correlation-Approximated

Figure 6.12 Comparison of experimental mass loss rate with different correlations.

6.3.5 Remarks

The dimensional analysis of a large number of historical test results has confirmed that the Kawagoe correlation for mass loss rate of wood is a good approximation for only a limited range of ventilation conditions.

Two influential parameters on the mass loss rate per unit vent parameter, $\dot{m}_p / A_v\sqrt{H_v}$, are identified. These two parameters include: A_v/A_w and $(A_v\sqrt{H_v})^{0.8}/A_T$. The vent flow analysis has shown that the air inflow per unit vent parameter, $\dot{m}_{in} / A_v\sqrt{H_v}$, is conditional to the opening fraction, A_v/A_w, decreasing with increase A_v/A_w. The low $\dot{m}_{in} / A_v\sqrt{H_v}$ at large A_v/A_w is attributed to a less uniform, stratified fire environment, with vent flows driven by the fire plume entrainment. This trend is mirrored in the mass loss rate analysis which shows the mass loss rate per unit vent parameter, $\dot{m}_p / A_v\sqrt{H_v}$, decreases with increasing A_v/A_w. This mirroring trend suggests the mass loss rate is strongly coupled with the air inflow rate into the compartment. It is rather interesting to see that the Law correlation fits the data well. The use of the compartment aspect ratio, D_c/W_c, could have accounted for the less uniform, stratified fire environment, which would usually be associated with a deep compartment. The parameter, $(A_v\sqrt{H_v})^{0.8}/A_T$, can be interpreted as the opening to enclosure size ratio. It is also found in Law's correlation but in slightly different form of $(A_T\text{-}A_v)/ A_v\sqrt{H_v}$ (as Ω in Equation (6.8)). At the moment, no rationale can be offered to explained the dependency between the mass loss rate and $(A_v\sqrt{H_v})^{0.8}/A_T$.

It should be noted that the mass loss rate data used in the dimensional analysis are the $R_{80\text{-}30}$ data which represent the average mass loss over the period when the fuel mass is reduced from 80% to 30% of its original mass. These data are used as the practical quantities that describe the mass loss rate of wood during the period of fully developed fires. Therefore, the mass loss rate correlations derived represent the average mass loss rate during the fully developed period.

6.4 MODELLING MASS LOSS HISTORY

As shown in Figure 6.1, there are generally two possible burning regimes for wood fuels burning inside a compartment. The first is the fuel surface controlled burning regime, where there is sufficient ventilation available and where the fuel mass loss rate depends on the burning of the exposed surface area. The second is the ventilation controlled burning regime, where there are more fuel surfaces available than can be burned with the available ventilation and the fuel mass loss rate is restricted by the ventilation. Although Harmathy (1972) provided the criteria and correlations for both the ventilation controlled and the fuel surface controlled burning regimes (Equations (6.1a) and (6.1b)), these correlations are rather simplistic. In particular, the use of a constant fuel surface area, A_F, for differentiating between the two regimes and in the calculation for the mass loss rate during the fuel controlled regime. As shown in Ödeen's model, unless the fuel is a one-dimensional plane, its surface area would be burned away over the fire duration and hence would decrease with time. Therefore, Harmathy's correlations seem to represent the average mass loss rate over the fully developed period. Babrauskas (pers. comm.) insisted that in post-flashover fire modelling, it is important to allow the fire to switch from ventilation controlled to fuel controlled during the fire process. This could provide a better representation of the fire behaviour over its duration.

Analysing the $R_{80\text{-}30}$ data has shown that the mass loss rate of wood fire is strongly related to the ventilation. Harmathy (1972, 1978 and 1979) argued that the coupling between the fuel mass loss rate and the air inflow rate is related via the oxidation of char rather than the gas phase reaction. He suggested that it is the airing and hence the oxidation of char on the wood surfaces that provides the necessary heat for pyrolysing the fuel. Although the relation between the fuel mass loss rate and the ventilation might not be related to the gas phase reaction as argued by Harmathy, the gas phase interpretation could be useful in setting an upper limit. Babrauskas (1981 and 1995) suggested that wood crib fires do not burn more than 35% fuel-rich. By setting Φ=1.35, and r=5.3 for wood, substituting the appropriate expressions for the air inflow rate at various vent opening fractions into the equivalence ratio equation (Equation (6.12)), the ventilation controlled mass loss rate expressions are given as

follows in Equation (6.14a and b). These represent the maximum mass loss rate from the wood fuel for the given ventilation opening. Note that the mass loss rate expression in Equation (6.14a) is the same as given by Babrauskas (1981 and 1995).

Φ=1.35

A_v/A_w <1 $\quad \dot{m}_{in} \approx 0.45 A_v \sqrt{H_v} \quad \dot{m}_p = 0.12 A_v \sqrt{H_v}$ **(6.14a)**

A_v/A_w =1 $\quad \dot{m}_{in} \approx 0.26 A_v \sqrt{H_v} \quad \dot{m}_p = 0.07 A_v \sqrt{H_v}$ **(6.14b)**

The mass loss rate for the fuel surface controlled regime is modelled according to Ödeen's model (Equation (6.6)). The smaller of the two rates (Equations (6.6) and (6.14)) is regarded as the governing mass loss rate in the compartment. If the fuel surface controlled mass loss rate is greater than the ventilation controlled rate, the actual mass loss rate will be ventilation controlled until the surface area diminishes to a level that will cause the mass loss rate to be governed by fuel surface control, as shown in Figure 6.13. The two cross-hatched areas are equal, hence the thick black line represents the actual mass loss rate history inside the compartment. If the fuel surface controlled mass loss rate is less than the ventilation controlled rate, the actual mass loss rate history inside the compartment is the same as the fuel surface controlled mass loss rate curve.

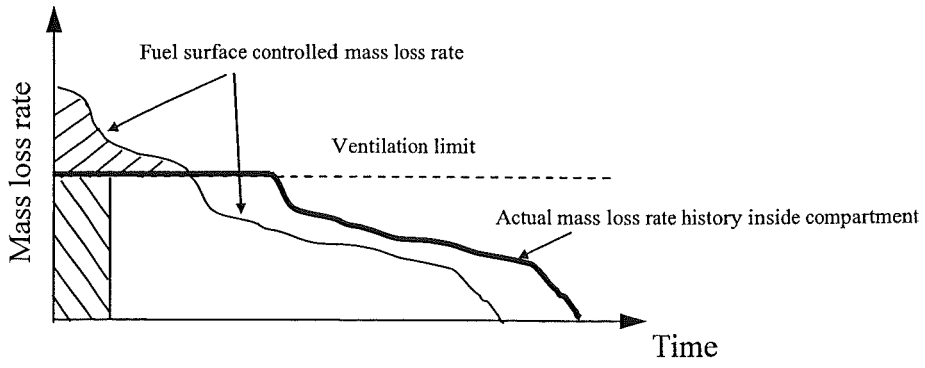

Figure 6.13 Actual mass loss rate for a fire which is initially ventilation controlled.

The above treatments account for two burning regimes. For fuel in the form of densely packed crib, there exists another burning regime called the porosity controlled regime. The mathematical representation for this burning regime is (Babrauskas, 1979)

$$\dot{m}_p = 4.4\times10^{-4}\left(\frac{S}{h_{crib}}\right)\left(\frac{M_0}{D}\right) \qquad \textbf{(6.15)}$$

where $\left(\frac{S}{h_{crib}}\right)$ is the ratio of stick clear spacing to crib height.

In the case of simulating a wood crib fire, the smallest of the three rates (Equations (6.6), (6.14) and (6.15)) is regarded as the governing mass loss rate in the compartment. Because this correlation involves the crib characteristic dimension, it is not used when considering the wooden furniture.

6.5 DISCUSSION

The sections above have reviewed the available treatments for modelling the mass loss rate of wood inside a fire compartment. In general, two main burning regimes could occur in wood fires inside a compartment; these are a fuel surface controlled regime and a ventilation controlled regime (for densely packed cribs this would include a porosity controlled regime).

For fuel surface controlled burning, the mass loss rate is modelled by using a constant regression rate where the mass loss rate is calculated as the product of the regression rate, the fuel density and the exposed surface area. Hence, both the surface area and thickness of the fuel are important parameters that determine the burning inside the compartment. Buchanan (1998) presented a single compartment fire study using the FASTlite computer program. Using the same regression rate, the same fuel load and the same vent opening for fuel with different thicknesses and surface areas, he showed

that the resultant compartment fire temperature profiles varied markedly. For fuel with a large exposed surface area and small thickness, the compartment fire is short and hot. For fuel with a small exposed surface area and larger thickness, the fire is likely to be longer and slightly cooler.

For real occupancies, the furniture inside the compartment will have a variety of different surface areas and thicknesses. Following the above argument, furniture with a different geometry and shape is likely to produce different fires inside the compartment. For example, for the same regression rate, a desk that is made of thin panels will have a large exposed surface area and a small thickness resulting in a faster and shorter mass loss rate history than a fully filled bookshelf that has a much smaller exposed surface area and a large thickness. This phenomenon has been observed in actual fire sites where tables and chairs are burned away during the fire while bookshelves full of books are heavily charred but remain intact after the fire. From the modelling point of view, in order to produce a representative fire, a representative mass loss rate history of the burning fuel needs to be known. By applying a constant regression rate to model each individual furniture item, the general characteristic of the mass loss rate history pattern determined by the surface area and thickness can be accounted for. This presents the opportunity to study compartment fires with realistic wooden furniture other than wood cribs, which are not normally found in real occupancies. This will allow a more representative prediction of the fire gas temperature inside real occupancies.

6.6 SUMMARY

There are generally two burning regimes that could occur for wood burning inside a compartment. These regimes include (1) the fuel surface controlled regime, during which there is sufficient ventilation to burn all the available fuel, and the fuel mass loss rate is restricted by the available fuel surfaces, and (2) the ventilation controlled regime, during which there is insufficient ventilation available and the fuel mass loss rate as well as the burning rate are restricted by the available ventilation. For fuel

packages with finite shape and thickness, the fuel surfaces will be burned away during the course of the fire. This means a reduction in the remaining fuel surface area over time and hence a reduction in the mass loss rate. With the fuel surface area reducing over time, the fire could switch from being ventilation controlled to being fuel surface controlled. Hence an accurate description of the change of fuel surface area over time is important as it ultimately describes the mass loss rate history and hence the fire time-temperature history. Because realistic furniture has a complex shape and thickness, there is no simple way of describing the change of surface area over time. It is necessary to manually calculate the change of the surface area of individual components that makes up the furniture. In the CFIRE computer program, various realistic furniture items with their change of surface area and hence mass loss rate histories (such as shown in Figure 6.5 and Figure 6.6) are stored in the program library. The user can call upon these individual furniture mass loss rate histories for fire simulations. The maximum mass loss rate of wood during the ventilation controlled burning regime is set in accordance with Equations (6.14a) and (6.14b). The smaller of the fuel surface controlled and the ventilation controlled mass loss rates is used to evaluate the fire temperature. By accounting for the shapes and thicknesses of different furniture items, the behaviour of furniture fires can be studied. This will lead to a more representative prediction of the fire gas temperature inside real occupancies.

Chapter 7 COMPARTMENT WITH ROOF VENT OPENING

This chapter outlines the possible flow scenarios that could arise from a post-flashover compartment having both vertical and horizontal vent openings. An extended vent flow model that includes an additional horizontal roof vent opening is presented. The unstable phenomenon of bi-directional flow across the roof vent opening is briefly discussed.

7.1 INTRODUCTION

Previous compartment fire studies largely focussed on compartments with a single vertical door or window opening. However, in real occupancies, the compartment may have both horizontal and vertical vent openings. Horizontal vents can exist in the form of openings left by the melting of skylights, or the roof being burned through during the fire.

There exist three possible flow scenarios for compartments with both horizontal and vertical vent openings. These scenarios are schematically shown in Figure 7.1. Scenarios (a) and (b) represent the stable flow scenarios arising due to pressure differences resulting from temperature fields between the two stagnant environments under natural convection conditions. Scenario (c) represents unstable flow across the roof vent opening when the very small vertical opening is unable to provide adequate inflow to maintain the unidirectional outflow via the roof vent. A bi-directional flow occurs at the roof vent opening when the pressure difference across the roof vent opening is less than a critical value, such that the light hot gases do not have enough pressure exerted on them to counter the weight of the dense air above, thereby resulting in air flowing in through the roof vent opening.

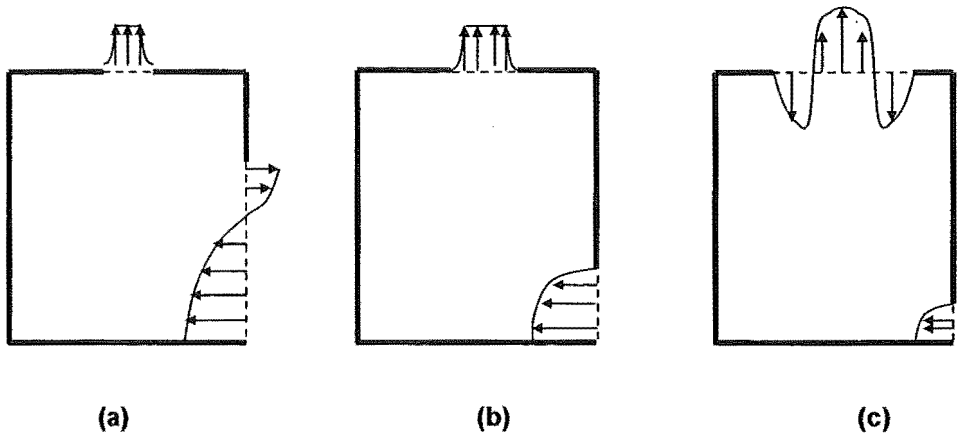

Figure 7.1 **Possible compartment vent flow scenarios with the existence of both horizontal and vertical vent openings.**

7.2 RESEARCH IMPETUS

The existence of a roof vent opening is common in real buildings. Because it affects the overall ventilation to the compartment, a roof vent will have great implications on the post-flashover fire temperature and fire severity.

There are very limited vent flow studies for post-flashover compartments with both vertical (wall) and horizontal (roof) openings. From the literature, the closest experimental study on this subject is that reported by Thomas et al (1963). Their tests involved a small-scale compartment of 0.76m by 0.46m by 0.46m high constructed with 12mm thick asbestos board. The compartment was open entirely at one end and could be partially closed with a sliding roof screen. On top of the compartment, the rectangular roof vent opening had a fixed width of 0.38m across the compartment; its other dimension as well as its position on the roof could be varied. A fully developed fire was simulated using town gas which was distributed over the floor by jets broken up by fire brick. The objective was to find the depth of roof screen necessary to prevent the spilling of flame from a fully developed fire beneath the screen for different sizes and positions of the roof vent. The authors were effectively testing the

limiting condition for scenario (a), for which is also the onset of scenario (b), such that the outflow via the vertical opening vent just diminished. Only the fuel gas flow rate and the height of the opening beneath the roof screen were recorded in their tests. Magnusson and Thelandersson (1970) provided a nomogram to estimate air inflow rate for a compartment having both horizontal and vertical opening. The flow scenario they considered is restricted to flow scenario (a) in Figure 7.1. However, their approach has not been validated with any experimental data.

Before the impact of the roof vent on the resultant fire severity inside the compartment can be modelled and studied, a vent flow model that is capable of describing vent flows at different combinations of horizontal and vertical vent openings has to be established.

7.3 ROOF VENT FLOW FORMULATIONS

To establish a vent flow model for modelling a post-flashover compartment having both horizontal and vertical vent openings, the vent flow model for a single vertical wall vent opening (as given in Chapter 3) is extended to include an additional horizontal roof vent opening.

Consider a well-mixed compartment with a wall opening as described in Chapter 3. Under natural convection conditions, vent flows arise due to pressure differences resulting from temperature fields between the two stagnant environments. By having an opening at the compartment wall, the outside cold ambient air flows into the compartment because of the pressure difference, and at the same time hot gases flow out of the opening to maintain the mass balance inside the compartment. There will be a point of zero pressure difference in the opening, referred to as the neutral plane. Below the neutral plane, the differential pressure in the compartment is negative (compared to outside) with air flowing in; and above the neutral plane, hot gases flowing out due to positive differential pressure in the compartment. If there is a roof vent opening, the positive differential pressure at the roof level will push the hot gases

out through the roof opening; the neutral plane will rise to allow more air inflow to match the increase in the outflows. Figure 7.2 depicts the flows for a compartment with both vertical and horizontal vent openings. The hydrostatic pressure distributions and the resulting velocity distributions across the vertical and horizontal vents are also shown, with the pressure difference across the roof vent being the hydrostatic pressure difference at the roof level, denoted as ΔP_{roof}. The geometrical terms used in the figure are as follows: H_v is the vertical vent opening height, i.e. distance between the soffit and sill, $(H_s\text{-}\delta)$; Z_n is the neutral-plane height evaluated from the floor; and H_c is the compartment height evaluated from the floor to the roof.

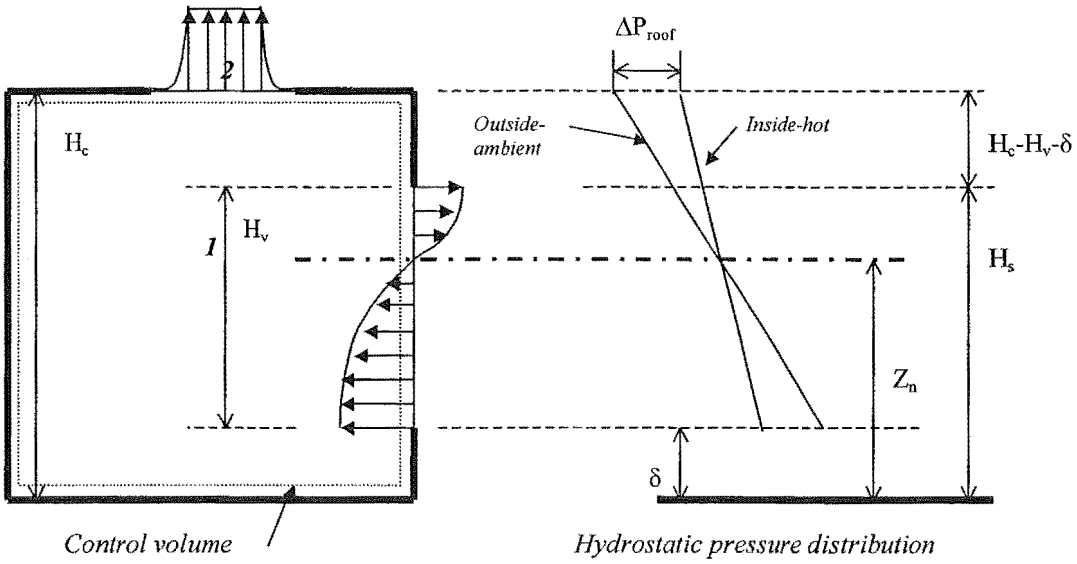

Figure 7.2 **Schematic representation of buoyancy flows for compartment with both roof and window opening.**

Considering the point *1* is level with the neutral-plane height and point *2* is just outside the roof opening, both are along an assumed streamline with a height different of $H_c\text{-}Z_n$. The pressure at each point is

$$P_1 = P_0$$
$$P_2 = P_0 - \rho_0 g(H_c - Z_n)$$

where P_0 is the atmospheric pressure at the neutral-plane level.

Applying the Bernoulli equation along the streamline between the two points with negligible velocity for hot gases inside the fire compartment, $v_2 \approx 0$ and $\rho_1 = \rho_2 = \rho_g$,

$$\frac{v_2^2}{2} = \frac{\rho_0 g(H_c - Z_n)}{\rho_g} - g(H_c - Z_n)$$

or

$$v_2 = v_{out,roof} = \sqrt{\frac{2\Delta P_{roof}}{\rho_g}} \qquad \textbf{(7.1)}$$

where the pressure difference across the roof vent, ΔP_{roof}, is given in Equation (7.2), which is the hydrostatic pressure difference between the hot compartment and the outside ambient at the roof level.

$$\Delta P_{roof} = (\rho_0 - \rho_g) \cdot g \cdot (H_c - Z_n) \qquad \textbf{(7.2)}$$

The mass flow rate through the roof vent opening is therefore the product of the discharge coefficient of the roof vent, $C_{d,roof}$, the area of the roof vent, $A_{v,roof}$, the density of the gas flow, ρ_g, and the velocity, $v_{out,roof}$ (Equation (7.1)). This is given in Equation (7.5).

For a compartment with a single vertical window opening and a single horizontal roof opening, the mass flow rates for both inflow and outflow via the vertical window opening and the outflow via the horizontal roof opening are expressed as follows.

$$\dot{m}_{in,window} = \frac{2}{3} \cdot C_d \cdot W_v \cdot \rho_0 \cdot \sqrt{2g\left(1 - \frac{\rho_g}{\rho_0}\right)} \cdot (Z_n - \delta)^{\frac{3}{2}} \qquad \textbf{(7.3)}$$

$$\dot{m}_{out,window} = \frac{2}{3} \cdot C_d \cdot W_v \cdot \rho_g \cdot \sqrt{2g\left(\frac{\rho_0}{\rho_g} - 1\right)} \cdot (H_s - Z_n)^{\frac{3}{2}} \quad \textbf{(7.4)}$$

$$\dot{m}_{out,roof} = C_{d,roof} \cdot \rho_g \cdot A_{v,roof} \cdot \sqrt{2g\left(\frac{\rho_0}{\rho_g} - 1\right)} \cdot (H_c - Z_n)^{\frac{1}{2}} \quad \textbf{(7.5)}$$

Equations (7.3) and (7.4) are the mass flow rate expressions for the inflow and outflow via the vertical window vent. They are the same expressions for a compartment with a single vertical window vent. Equation (7.5) is the mass flow rate for the outflow through the roof vent opening. There are four unknowns in these three equations, namely the neutral-plane height and the three mass flow rates. The steady-state mass balance equation given in Equation (7.6) provides the additional equation for solving these four unknowns.

$$\dot{m}_{in,window} + \dot{m}_p = \dot{m}_{out,window} + \dot{m}_{out,roof} \quad \textbf{(7.6)}$$

It can be seen that a limiting condition could be reached when the neutral-plane is at the soffit of the window opening, i.e. $Z_n=H_v+\delta$. In this condition, there will be no outflow through the window vent and Equation (7.4) becomes zero. By substituting the remaining two vent flow equations (Equations (7.3) and (7.5)) into the mass balance equation (Equation (7.6)) with $Z_n=H_v+\delta$, the condition necessary for the neutral-plane to be at the soffit of the window opening is

$$H_v = (H_c - \delta) - \left[\left(\frac{2}{3}\right)^2 \cdot \left(\frac{C_d}{C_{d,roof}}\right)^2 \cdot \left(\frac{A_v\sqrt{H_v}}{A_{v,roof}}\right)^2 \cdot \frac{\rho_0}{\rho_g} \cdot \left(1 + \frac{\dot{m}_p}{\dot{m}_{in}}\right)^2\right] \quad \textbf{(7.7)}$$

Equation (7.7) represents the limit for the flow scenario (a), which is also the onset of the flow scenario (b) as depicted in Figure 7.1. This is the condition where the incoming air flows through the entire window opening area and all the hot gases are vented out through the roof vent opening. Note that when the right hand term of Equation (7.7) is greater than the vertical vent height, H_v, the neutral-plane will be

above the soffit of the opening. For $C_d \approx C_{d,roof}$ and $\dot{m}_p << \dot{m}_{in}$, the flow scenario (b) of Figure 7.1 occurs when

$$\frac{2}{3} \cdot A_v \sqrt{H_v} \cdot \sqrt{\frac{\rho_0}{\rho_g}} \leq A_{v,roof} \sqrt{H_c - (H_v + \delta)} \qquad \textbf{(7.8)}$$

or

$$A_v \sqrt{H_v} \leq \frac{3}{2} \cdot \sqrt{\frac{\rho_g}{\rho_0}} \cdot A_{v,roof} \sqrt{H_c - (H_v + \delta)}$$

In this case, the hot gases outflow through the roof is still described using Equation (7.5), whereas the air inflow via the vertical opening is estimated as

$$\dot{m}_{in,window} = \frac{2}{3} \cdot C_d \cdot W_v \cdot \rho_0 \cdot \sqrt{2g\left(1 - \frac{\rho_g}{\rho_0}\right)} \cdot \left\{ (Z_n - \delta)^{3/2} - [(Z_n - \delta) - H_v]^{3/2} \right\} \qquad \textbf{(7.9)}$$

where the inflow is driven by the hydrostatic pressure difference along the vent height as depicted in Figure 7.3 below.

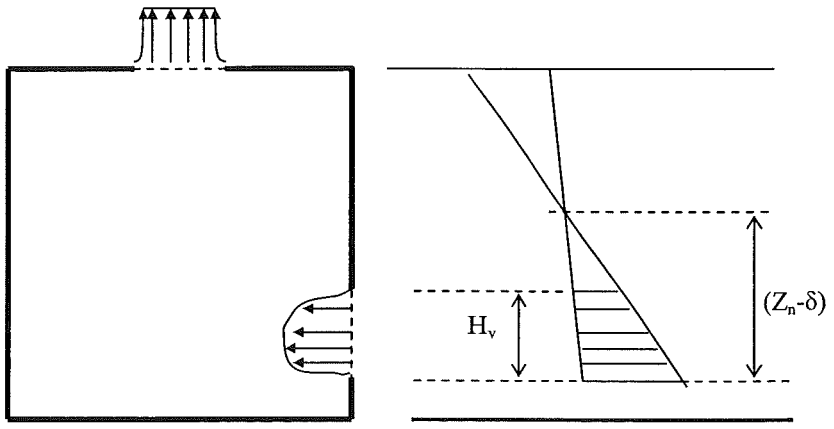

Figure 7.3 **Schematic sketch showing the hydrostatic pressure difference profile at the vertical vent opening.**

For a given vertical vent geometry and location relative to the roof vent opening, increasing the roof vent opening area increases the ventilation rate to the compartment. The neutral-plane height will rise accordingly so as to allow greater air inflow through the vertical window opening to match the outflow through the roof vent. According to the vent flow model, the maximum possible flow across the vertical wall opening for a given compartment gas temperature occurs when the neutral-plane height is close to the roof level, such that the hydrostatic pressure difference and hence the inflow across the vertical wall vent is at a maximum. However, with a high neutral-plane position, the pressure difference across the roof vent opening will be small (see Equation (7.2)). A critical pressure could be reached where the flow across the roof vent becomes unsteady, and air starts to flow into the compartment via the roof vent opening, i.e. the flow scenario (c) in Figure 7.1.

7.3.1 Flood limit at roof vent

The critical pressure difference that defines the boundary between unidirectional and bi-directional flow across the horizontal vent opening is referred as the critical flood pressure, ΔP_{flood}. Research studies by Emmons (1997) and Yamada (1997) have shown that this critical condition could be characterised using the Froude number at the roof vent opening. Following the definition by Yamada, the Froude number is defined as

$$Fr = \frac{v_{out,roof}}{\sqrt{2gD \cdot \frac{\Delta\rho}{\tilde{\rho}}}} \qquad (7.10)$$

where $v_{out,roof}$ is the velocity across the roof vent opening, g is the gravitational constant, D is the diameter of the roof vent opening, $\Delta\rho$ is the density difference between the hot gases and cold ambient air and $\tilde{\rho}$ is the average density between the hot gases and cold ambient air.

Based on the data obtained from small-scale compartment fire experiments, Yamada (1997) gave the critical Froude number as

$$Fr_{flood} = 0.274 \exp\left(0.6987 \frac{\Delta\rho}{\tilde{\rho}}\right) \quad \textbf{(7.11)}$$

This critical Froude number defines the boundary between the unidirectional flow regime and the bi-directional flow regime across the roof vent opening, such that for a Froude number at the roof vent greater than the critical value, Fr_{flood}, the flow across the roof vent is unidirectional.

Substituting the critical Froude number correlation (Equation (7.11)) into the Froude number expression (Equation (7.10)), a critical velocity across the roof vent opening can be obtained; it is the minimum velocity required to maintain a unidirectional flow across the roof vent opening.

$$\left(v_{out,roof}\right)_{flood} = Fr_{flood} \times \sqrt{2gD\frac{\Delta\rho}{\tilde{\rho}}} \quad \textbf{(7.12)}$$

Substituting Equation (7.12) into Equation (7.1) gives the critical flood pressure, ΔP_{flood}, necessary to force a unidirectional outflow through the roof vent. This is given in Equation (7.13).

$$\Delta P_{flood} = Fr_{flood}^2 gD\rho_g \frac{\Delta\rho}{\tilde{\rho}} \quad \textbf{(7.13)}$$

However, it should be noted that the flood limit given by Yamada (1997) should be regarded as indicative only because the temperature associated in his experiment was low (maximum temperature approximately 300°C) compared to post-flashover fire temperatures. Further research is needed to investigate the high temperature effect on the critical flood limit.

7.4 SUMMARY

A compartment having both horizontal and vertical vent openings is a practical scenario that exists in real buildings. However, in the past very limited study has been done on this problem. A vent flow model for post-flashover compartment having both horizontal and vertical vent openings is presented here. Three geometrical parameters that affect the vent flows through the openings can been identified, namely the vent parameter, $A_v\sqrt{H_v}$ for the vertical vent opening, the roof vent opening area, $A_{v,roof}$, and the square root of the depth of the downstand, i.e. the distance between the roof vent and the soffit height of the vertical vent, $\sqrt{H_c-(H_v+\delta)}$.

To the author's knowledge, mathematical vent flow models with a roof opening have not been extensively studied or verified. Since the presence of a roof vent opening could increase the air inflow into the compartment, it will have great implications for post-flashover fire temperatures and fire severity. Its importance has been shown in the New Zealand Building Code, such that AS1/C3 (BIA, 1992) provides the minimum structural fire resistance rating required for different combinations of vertical and horizontal vent openings. Experimental study of post-flashover compartment fires having both vertical and horizontal vent openings will provide better understanding of the effects on the fire by the roof vent opening. This will provide the first step towards the study of the fire severity inside a compartment with both types of opening.

In the following chapters, the application of the vent flow equations (Equations (7.3), (7.4) and (7.5)) is examined using the results obtained from fire experiments.

Chapter 8 EXPERIMENTAL METHOD

This chapter outlines the context and scope of the experimental study performed. Details of the experiment layout, instrumentation and data reduction methods are presented.

8.1 CONTEXT OF THE EXPERIMENTAL WORKS

Compartments having both vertical and horizontal vent openings are practical scenarios that exist in real buildings. Vertical openings are usually windows or doors. Horizontal vents can exist in the form of openings left by the melting skylights or the roof being burned through during the fire. Currently, post-flashover compartment fire models such as COMPF2 and OZONE allow only vertical openings. To study post-flashover compartment fires, the ability to model practical ventilation openings is desirable. The vent flow formulations for a compartment having both vertical and horizontal vent openings have been presented in the Chapter 7. The experimental studies performed were used to verify these vent flow formulations, so that they could be incorporated into the proposed CFIRE post-flashover fire model.

8.2 SCOPE OF THE STUDY

The primary objective of the experimental work was to obtain a series of vent flow data from various combinations of wall and roof openings. In particular, data for the air inflow through the wall vent into the compartment with the presence of a roof vent were required. These data sets are used to verify the vent flow formulations developed in Chapter 7.

As mentioned in Chapter 7, there are three possible flow scenarios that could occur in a compartment having both vertical and horizontal vent openings. The first two scenarios (Figure 7.1 (a) and (b)) are scenarios that are likely to be encountered in real buildings where the roof vent opening is not excessively large compared to the vertical wall opening. For this reason, the experimental work focussed on examining these vent flow scenarios. No attempt was made to study the third scenario (Figure 7.1 (c)) which involves bi-directional flow across the roof vent opening, and which is a large research topic in its own right.

The experiments were conducted using a reduced scale compartment having internal dimensions of 1m high by 1m wide by 1.5m deep. This scale was used because, firstly, it was easier to manage in the sense of experimental safety and secondly, it would create a "well stirred" fire environment inside the compartment, closer to the assumption made in the derivation of the vent flow formulations. The compartment was fitted with a centrally located adjustable roof vent and a door vent flush with the floor level. Three sizes of door vent were used in the test programme. These three door vents all had a width of 250mm but with different heights, ranging from 450mm (Door 1), 250mm (Door 2) and 125mm (Door 3). Each of these doors was tested against different roof vent sizes. The tests conducted are presented in Table 8.1. Only one test was made for each setup except D1R400, which was tested twice.

Table 8.1 Testing matrix.

Door vent	Depth of the down-stand between the roof and the soffit	Roof vent opening diameter					
		0mm	150mm	250mm	300mm	350mm	400mm
Door 1 H:450mm W:250mm	550mm	✓ (DIR0)	✓ (D1R150)	✓ (D1R250)	✓ (D1R300)		✓✓ (D1R400)
Door 2 H:250mm W:250mm	750mm		✓ (D2R150)	✓ (D2R250)	✓ (D2R300)		
Door 3 H:125mm W:250mm	875mm			✓ (D3R250)	✓ (D3R300)	✓ (D3R350)	

It was envisaged that the Door 1 experimental series would produce the flow scenario as depicted in Figure 7.1 (a) where the neutral-plane was in the door opening with inflow and outflow occurring at the door vent and outflow through the roof vent; the Door 3 experimental series would produce the flow scenario as depicted in Figure 7.1 (b) where the neutral-plane was high above the door opening with inflow through the entire door vent and outflow through the roof vent; and the Door 2 experimental series would produce the intermediate condition between the two scenarios where the neutral-plane height was close to the soffit of the door vent. By covering the possible flow conditions across the spectrum between flow scenario (a) and (b), thus provided a platform to verify the vent flow formulations.

A heptane pool was used as the fire source. The compartment temperature measurements were made with bare-wire thermocouple trees inside the compartment and the vent flow was measured using type-S pitot tubes located at the openings. The measurements were logged during the entire fire duration in every test. The tests were conducted inside the Fire Engineering Laboratory at the University of Canterbury.

Details of the test compartment and instrumentation are described in the following sections.

8.3 EXPERIMENTAL LAYOUT

8.3.1 Test compartment

The fire experiment was conducted using a reduced-scale compartment with an internal dimension of 1m wide by 1m high by 1.5m deep. The entire compartment was lined with two layers of kaowool blanket sandwiched between a layer of kaowool vacuum board on the fire side and a thin stainless steel sheet on the ambient side; with the exception of the floor and the front door panel where these two boundaries were lined with two layers of kaowool vacuum board on the stainless steel sheet. Both the kaowool vacuum board and the stainless steel sheet acted to hold the lining in place inside the compartment. This is shown schematically in Figure 8.1. Both the kaowool blanket and the vacuum board had a thickness of 25mm per layer.

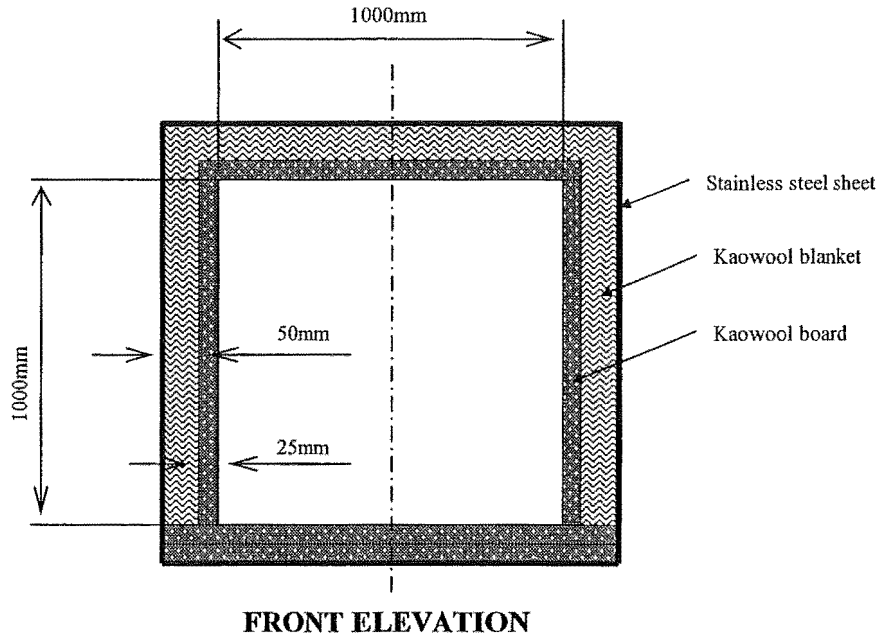

Figure 8.1 Cross section of the test compartment.

The test compartment had two adjustable vent openings, a door vent and a circular roof vent. The door vent was placed at the front end of the compartment flush with the floor; and the roof vent was placed at the centre of the roof. The height of the door vent was adjusted using an extra piece of kaowool board to block part of the opening, thereby changing the size of the door vent.

Since the roof vent opening was located at the centre of the roof, in order to facilitate the change of roof vent sizes during different tests, an adjustable roof vent was designed. This involved a series of 75mm deep stainless steel rings being cut to form the passage for the roof vent. The depth of these rings was the same as the thickness of the roof. The size difference between each ring was a 50mm increment in diameter. An additional lip was welded on the outer edge of the ring forming a flange. When these rings were slotted into one another, an adjustable circular vent was formed such that taking out the smallest ring increased the circular vent size by one ring size, i.e. an increment of 50mm in diameter. Kaowool ropes were used to wrap around the outside of each ring along the ring depth. This produced a tight-fit between rings to prevent leakage, as well as ensuring central positioning for every opening size. The largest roof vent opening for the fire experiment was 400mm in diameter, and the smallest was 150mm in diameter. This adjustable roof vent opening is shown in Figure 8.2. The test compartment layout is shown in Figure 8.3.

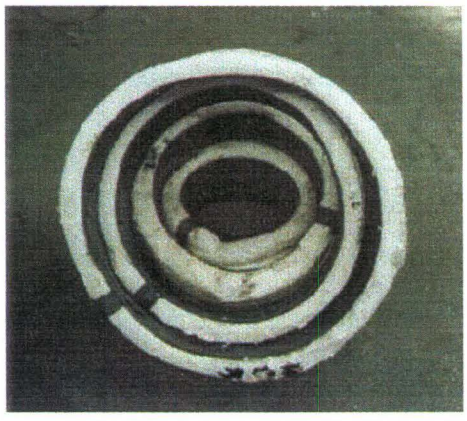

Figure 8.2 Adjustable roof vent.

Figure 8.3 The test compartment layout.

8.3.2 Fire source

A pan of 300mm diameter with a lip of 50mm was employed. This corresponded to the large pool scenario, i.e. the diameter exceeding 200mm, where the radiation from the flame becomes the dominant mode of heat transfer to the pool surface. Kaowool rope was wrapped around the outside circumference of the pan up to the lip height to minimise edge effects. The pan was placed at the centre-back of the compartment.

Heptane (C_7H_{16}) liquid fuel was used to produce the fire. The fuel was fed to the pan from two fuel tanks outside the compartment via a header tank system. The header tank system had two tubes, where the inner tube was connected directly to the underside of the fuel pan, and the level height of the inner tube corresponded to the fuel level inside the pan, was set as 20mm from the bottom of the pan. To maintain the fuel level inside the pan during the experiment, a pump was used to constantly fill the inner tube of the header tank with fuel from the fuel tanks. The excessive fuel was drained back into the fuel tank via a return tube. This is shown schematically in Figure 8.4.

The two fuel tanks were placed on an electronic load scale that was connected to the data logging system. The mass of fuel remaining inside the tanks was continuously logged during the experiment.

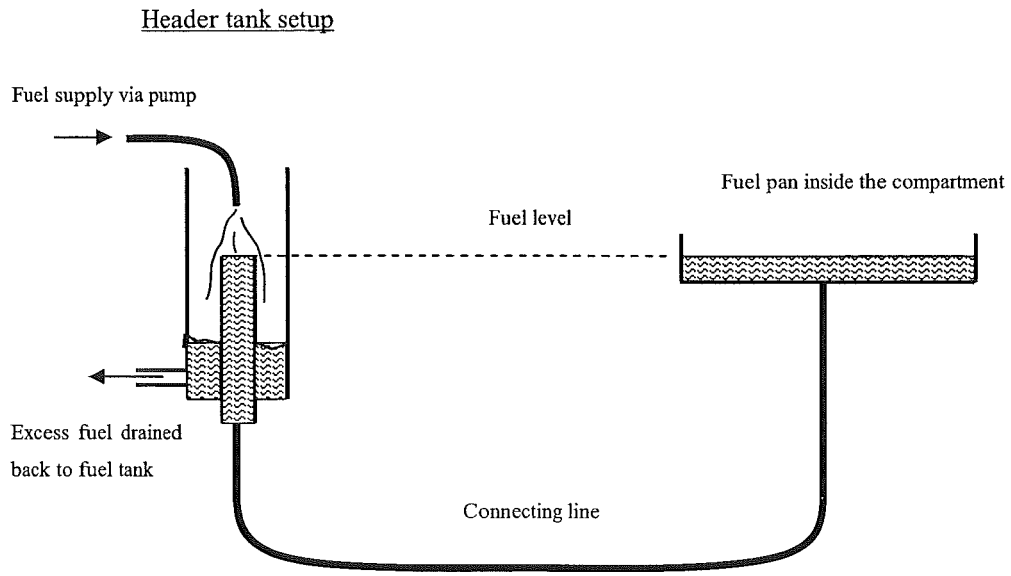

Figure 8.4 Schematic representation of the header tank system.

8.4 INSTRUMENTATION AND DATA ACQUISITION

8.4.1 Universal Data Logging System

The Universal Data Logging (UDL) system was designed and built at the University of Canterbury. It is a general-purpose data logging system with the ability to log various sensing devices ranging from strain gauges to thermocouples. The logging system consists of both hardware and software components. The hardware component includes the multiplexing plug-in boxes for the different sensing devices, and the software component includes the UDL programme where the appropriate calibration factors and the sampling interval for these different sensing devices are set.

In this experimental series, the UDL programme was run from a Pentium notebook computer running under Windows 98. The data sampling-interval was set as 1 second, i.e. data was logged every second.

8.4.2 Temperature measurements

The compartment temperature measurements were made with 0.5mm diameter bare-bead wire thermocouples. Type-K wire was used, as its operating temperature is between -250°C and 1100°C (Childs, 2001). Three thermocouple trees each consisting of 10 equally spaced thermocouples along the height of the compartment were used to measure the fire gas temperature inside the compartment. The vertical displacement between each thermocouple was 100mm, with the highest and the lowest thermocouples 50mm from the roof and the floor respectively. One thermocouple tree was positioned in the front corner 80mm away from the front door panel, the other thermocouple tree in the middle of the longitudinal plane of the compartment and the third thermocouple tree in the back corner 40mm from the back wall. The thermocouples on the two corner trees were held using 6mm diameter steel tubes with the thermocouple bead protruding 10mm outside the protective tube which extended 100mm from the wall boundary. The thermocouples for the middle tree were held using 3mm stainless steel tubes that extended 500mm from the side wall to the centre of the compartment. Because of the large distance from the wall, a supporting tube placed 150mm from the wall was used to hold the thermocouple in place. It was noted that during the experiment, due to the high temperatures inside the compartment, the stainless steel tubes holding the thermocouples in the middle tree sagged substantially. In particular, a vertical displacement of up to 100mm was observed for tubes at the top portion of the tree. Therefore, care should be exercised when interpreting the respective position of the temperature measured in the middle of the compartment. For the thermocouple trees at the corners, no sagging was observed. Figure 8.5 shows the locations of the thermocouple trees inside the compartment.

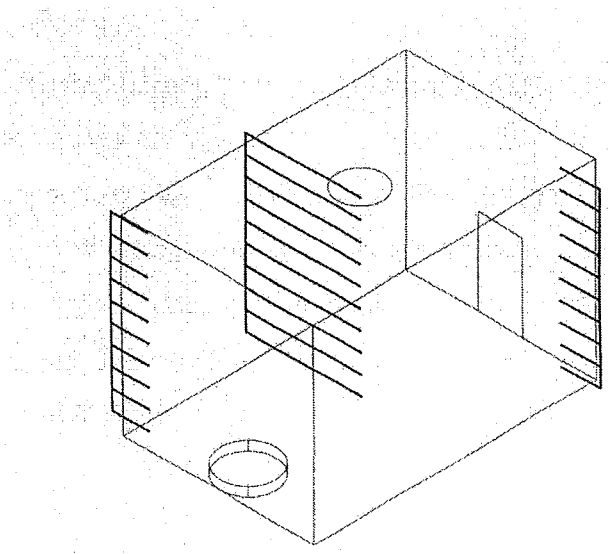

Figure 8.5 Locations of thermocouple trees inside the compartment.

Pitts et al (1998) have shown that a bare-bead thermocouple is likely to experience a measurement error due to radiation exchange between the surrounding and the thermocouple. To reduce the effect of external radiative exchange on a thermocouple, the thermocouple has to be shielded from the radiation, while increasing the convective exchange between the gas and the thermocouple; in doing so, the temperature indicated by the thermocouple would be closer to the true gas temperature (Blevins and Pitts, 1999). An aspirated thermocouple is a sophisticated version of the bare wire thermocouple that employs this idea. It has a thermocouple shielded inside a steel tube, with the gas to be measured being pulled axially through the tube using a pump. ASTM (1998) recommends that the gas flow inside the tube be maintained near 5m/s, to allow accurate temperature measurement. This velocity is disputed by Blevins and Pitts (1999) but no practical guidance is given.

A reversed air blower was used as a suction pump to pull the air through the aspirated thermocouples. Using a mounting with ten aspirated thermocouples, each with an internal diameter of 5mm, the suction capability of the air blower was tested using a flow meter. Under ambient condition, the blower was found to provide a velocity of approximately 6.7m/s through each aspirated thermocouple, which was sufficient to meet the ASTM recommendation. Initially, five aspirated thermocouples were installed inside the compartment for measuring the compartment gas temperature; two

were installed at the back corner, two at the front corner and one right at the centre of the compartment space. The two aspirated thermocouples installed at each corner were located adjacent to the second highest and the second lowest positions of the respective bare-bead wire thermocouple tree. Three aspirated thermocouples were placed at the door vent and two at the roof vent for measuring the temperature at the vent flows. Copper tubes were used to connect the aspirated thermocouples to the inlet port of the air blower acting as a suction pump. A water bath was used to cool the hot gases in the copper tubes before entering the blower. This is schematically shown in Figure 8.6.

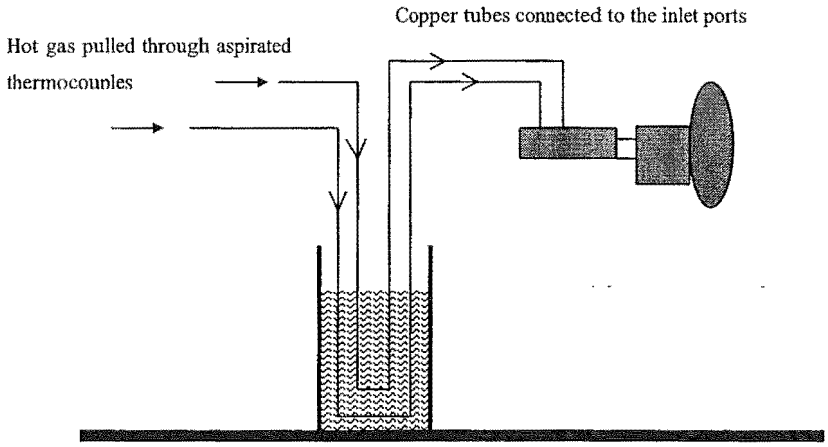

Figure 8.6 Schematic representation of aspirated thermocouple setup.

During the course of the experiments, three aspirated thermocouples inside the compartment at the back corner and the centre, together with the two aspirated thermocouples at the roof vent were damaged and were not replaced. With regard to the compartment fire temperature, since the aspirated temperature data set was partial, bare-bead wire temperature measurement was taken to represent the fire gas temperature inside the compartment. The three aspirated thermocouples at the door vent were operational and their measurements were used for velocity measurement purposes.

8.4.3 Vent flow measurements

To measure the mass flow rates across the vent openings, temperature and velocity measurements at the vent are required. Traditionally, the velocity in fluid flow is measured using the standard pitot-static tube that gives accurate velocity measurement. However, in a compartment fire experiment, the standard pitot-static tube has two primary limitations: (1) it has small impact or sensing holes; and (2) it is a single direction measuring instrument. In the compartment fire situation, soot is a concern as it could block the small holes on the standard pitot-static tube, which could result in erratic velocity measurements. Apart from this, the flow direction across the vent could change during the course of fire. Since the standard pitot-static tube is a single direction measuring instrument, it will not be able to respond to the change of the flow direction. The robustness of the standard pitot-tube in the fire environment is also a concern.

The standard McCaffrey and Heskestad (1976) bi-directional probe is typically used in compartment fire experiments. It has a size of 7/8 inch or 22mm probe diameter. For the purpose of measuring the vent flows in the scaled down fire compartment, the standard McCaffrey and Heskestad (1976) bi-directional probe was considered too big because it could interfere with the actual flow when multiple probes are positioned at the vent openings. Scaling down the standard bi-directional probe would involve labour intensive work in manufacturing, such as welding the joint between the supporting tubes and the pressure taps on the sensing tubes. The joint would also have to be reasonably clean of burr to ensure minimal disturbance in the pressure differential measurements.

The type-S pitot tube is a type of velocity probe that has been used in stack gas velocity measurement in duct systems. It consists of two stainless steel tubes with impact or sensing holes orientated at 180° angles to one another. Its basic operating principal is similar to the bi-directional probe, having a sensing hole facing upstream measuring the stagnation pressure and a sensing hole facing downstream measuring the static pressure. However, the manufacturing of the type-S pitot tube is more straightforward than the bi-directional probe, as the type-S pitot tube does not require wielding between the support tubes and the sensing tube. Rather, the end edges of

support tubes are bent such that they form pressure taps themselves. The manufacturing specifications for the type-S pitot tube allow a minimum external tubing diameter down to 3/16 inch or 4.8mm which is much smaller than the standard bi-directional probe. With these attributes, the type-S pitot tube presents an attractive alternative for reduced-scale compartment fire application. The manufacturing specifications for the type-S pitot tube can be found from the Emission Measurement Center- Codes of Federal Regulations (EMC-CFR) promulgated test methods for type-S pitot tube on the United States Environmental Protection Agency (USEPA) website: http://www.epa.gov/ttn/emc/tmethods.html.

The type-S pitot tube used in this experiment was fabricated using a 1/4 inch or 6.35mm external diameter stainless steel tube as shown in Figure 8.7. Two thermocouples were mounted on the probe by tacking smaller hollow tubes between the upper and lower sides of the two support tubes, which thermocouple wires were run through and correctly located at the sensing point. The calibration was done in the wind tunnel. The probe correction factor, C_{calib}, is defined as

$$\Delta P = C_{calib} \times \frac{\rho v^2}{2}$$

where ΔP is the pressure differential measured between the stagnation and static pressure measured by the probe, and ρ and v are the density and velocity of the flow. From the calibration exercise, it was found that the calibration factor, C_{calib}, varied with the Reynolds number (based on the diameter of the probe), such that at low Reynolds number, Re<700, $C_{calib} \approx 1.59$, and for high Reynolds number, Re>1000, $C_{calib} \approx 1.90$. Details on probe testing and calibration can be found in Appendix C.

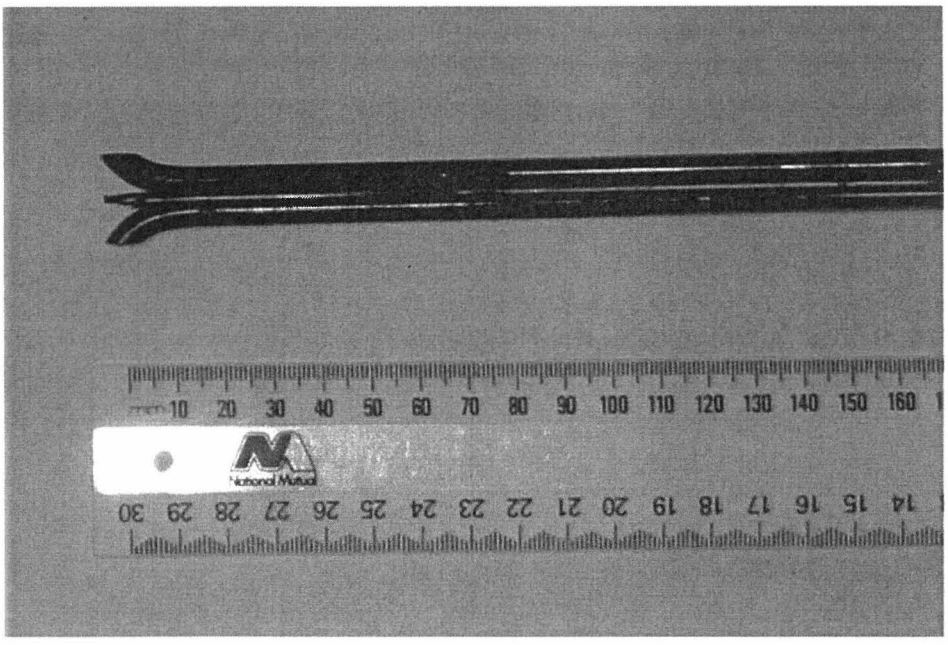

Figure 8.7 Type-S pitot tube used in the experiment.

The type-S pitot tubes were positioned on a rack mounted at each vent opening. Since the rack was mounted flush on the face of the vent, offset by the rack thickness, the actual probe position (from the centre between the two support tubes) was 15mm away from the face of the vent. The typical position of the type-S pitot tubes at the door vent and roof vent are shown in Figure 8.8 (a) and (b) respectively. At the largest door vent (Door 1), seven type-S pitot tubes were located at positions traversing vertically along the centre of the opening, they were spaced 63mm apart vertically with the 1st probe (i.e. the bottom probe at floor level) and the 7th probe (i.e. the top probe) approximately 35mm from the respective boundary. Three aspirated thermocouples were installed at the locations of the 2nd, 4th and 6th probes. (Note that at D1R400 test, only two aspirated thermocouples at the locations of the 2nd and 6th probes were operational). For the intermediate door vent setting (Door 2), four type-S pitot tubes were used with two aspirated thermocouples installed at the locations of the 2nd and 4th probes; for the small door vent (Door 3), two type-S pitot tubes were used with one aspirated thermocouple at the 2nd probe position. At the roof vent, the type-S pitot tubes were placed along the longitudinal direction of the compartment on top of the opening. The number and position of these type-S pitot tubes placed at the roof vent varied according to the size of the roof vent involved. Details of the type-S pitot tube positions for each test can be found in Appendix D.

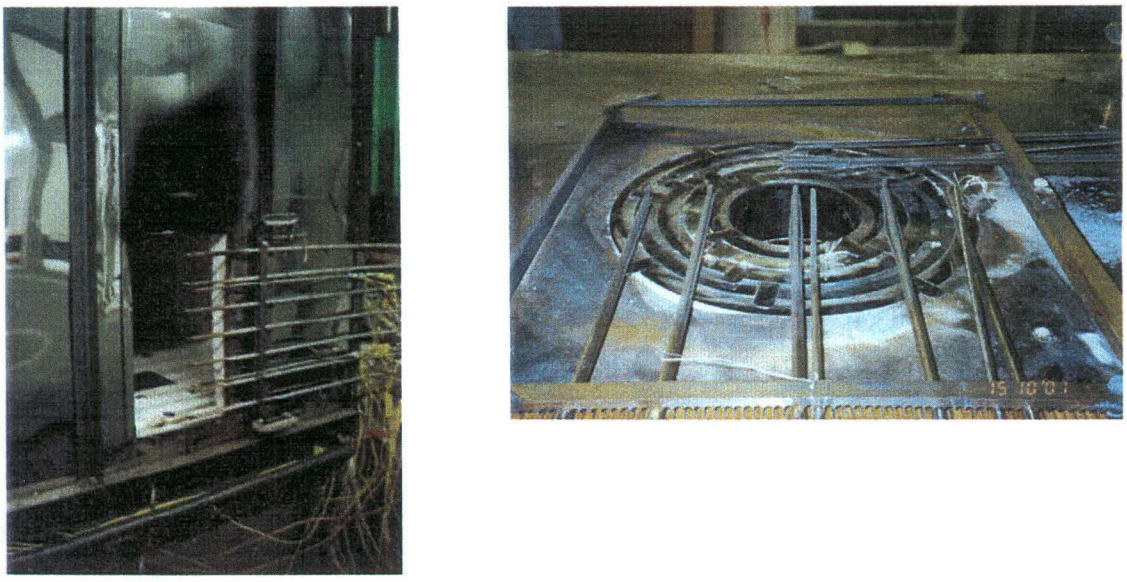

(a) At door vent opening

(b) At roof vent opening

Figure 8.8 Velocity probes placement at the vent openings.

Each velocity probe, (the type-S pitot tube), was connected to a pressure transducer for pressure differential measurement. The pressure transducers used were MKS Baratron Type 223B bi-directional pressure transducer. The pressure transducers were mounted at the same level as the respective velocity probes to minimise the possible error incurred in pressure readings due to hydrostatic pressure difference. The pressure transducer layout is shown in Figure 8.9. These transducers were orientated in such a way that a positive pressure differential measured on the probe denoted flow into the compartment (i.e. +ve velocity) and a negative differential denoted flow out of the compartment (i.e. -ve velocity).

Figure 8.9 **Layout of the pressure transducers.**

8.4.4 Final layout

The experiments were conducted in the Fire Engineering Laboratory in the University of Canterbury. The final experimental layout is shown schematically in Figure 8.10.

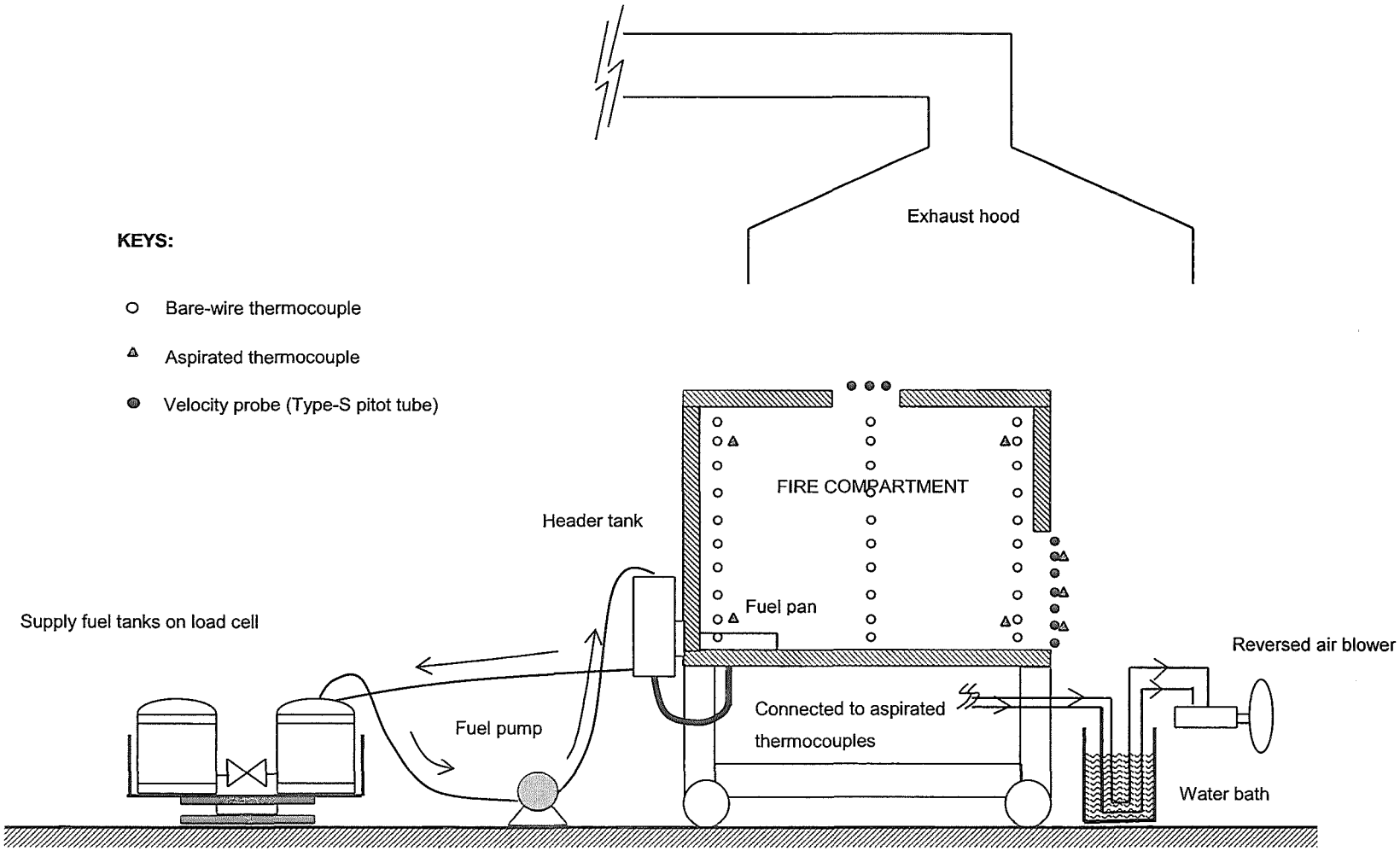

Figure 8.10 General layout of the experiment.

8.5 DATA REDUCTION PROCEDURES

8.5.1 Vent flows

The directional coordinates used in the data analysis are shown in Figure 8.11: x is the direction along the width of the compartment; y along the height of the compartment; and z along the depth of the compartment. For convenience, the coordinate origin is taken at the centre of the door at the sill level.

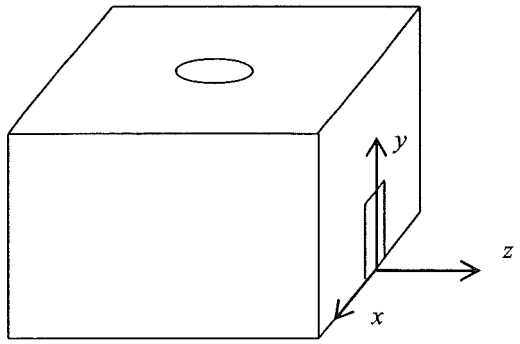

Figure 8.11 The definition of the directional convention used.

The mass flow rates across the vents were determined using the gas flow velocity profiles measured at the openings. In the case of a door vent, a neutral plane could exist separating the inflow and outflow across the opening. The neutral plane height, Z_n, was the position of zero pressure differential, i.e. zero velocity. It was estimated by interpolating between the two velocity probes that registered opposite flow directions. Both the mass inflow and outflow rates were determined by integrating the mass centreline velocity, ρv, over the height of inflow (Z_n) and outflow (H_v-Z_n) respectively. The flow density, ρ, was calculated assuming ideal gas behaviour by using the temperature measured from the aspirated thermocouples interpolated to the respective positions of the velocity probes. The density and temperature relationship based on the ideal gas behaviour is as follows:

$$\rho = 353/T \ (in\ Kelvin) \tag{8.1}$$

The experimental mass flows are (after Quintiere and DenBraven, 1978)

$$\dot{m}_{in,door} = W\int_0^{Z_n} \rho(y)v(y)dy \tag{8.2}$$

$$\dot{m}_{out,door} = W\int_{Z_n}^{H_v} \rho(y)v(y)dy \tag{8.3}$$

Because the vertical spacing between each velocity probe in the opening was small, i.e. ~63mm, a simple rectangle rule (or one point rule) was used for the integration. The approximation for Equations (8.2) and (8.3) are given in Equations (8.4) and (8.5) respectively where i stands for the particular i-th velocity probe with the corresponding flow velocity, v_i, and density, ρ_i measured. The y_i is the distance interval between adjacent velocity probes. This is schematically shown in Figure 8.12.

$$\dot{m}_{in,door} = W\int_0^{Z_n} \rho(y)v(y)dy \approx W\sum \rho_i v_i y_i \tag{8.4}$$

$$\dot{m}_{out,door} = W\int_{Z_n}^{H_v} \rho(y)v(y)dy \approx W\sum \rho_i v_i y_i \tag{8.5}$$

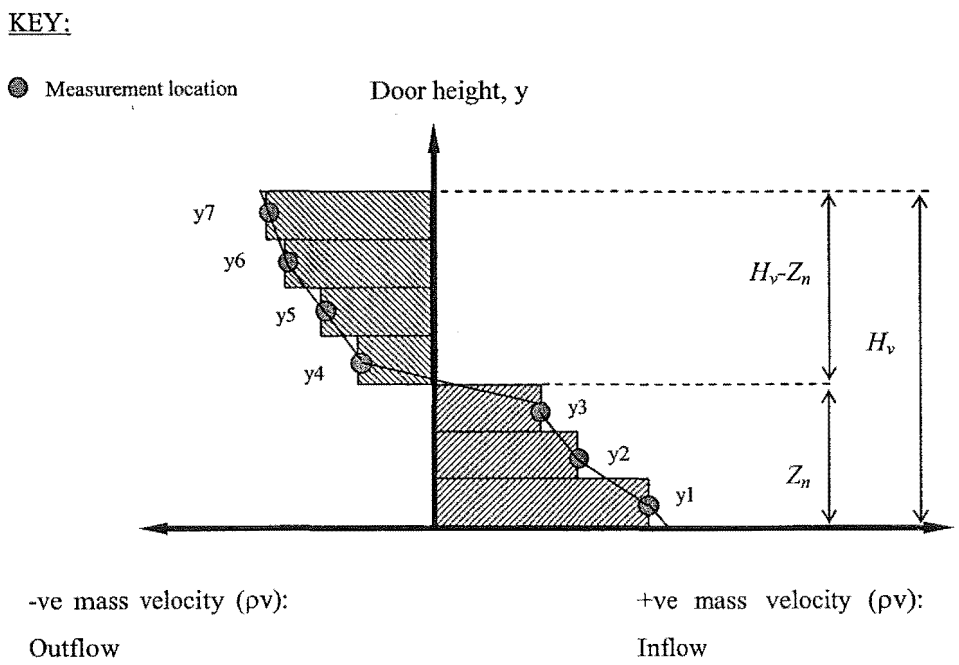

Figure 8.12 Schematic representation for mass flow rates calculations.

Graphically, it is the same as assigning a coverage area for each probe, such that the flow across the assigned area was assumed to have the same velocity and temperature (density) as measured by that particular probe. This is shown in Figure 8.13.

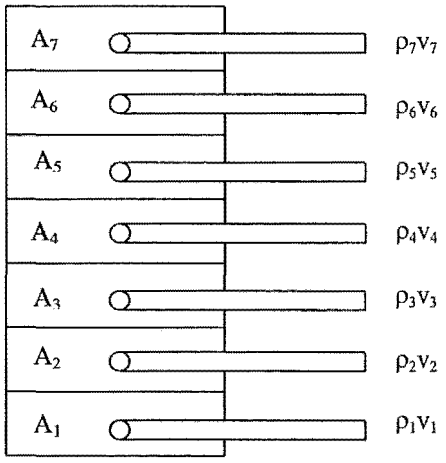

Figure 8.13 Velocity probes and coverage areas at the door vent opening.

The velocity probes placed in the roof vent opening were to gather information on the velocity distribution across the opening, which has not been documented in the literature. At the roof vent openings, typically four velocity probes were used for measuring the velocity distribution across the opening, except that the smallest opening (150mmϕ) used only one probe to prevent potential interference with the flow. Because the velocity distribution across the roof vent was unknown and could be different from that in a pipe flow, the measuring technique used in the pipe flow measurement such as the "log-linear" method was not used. Three of the probes were positioned along the z-direction; one at the centre of opening and the remaining two equally spaced from the centre along the z-axis. The fourth probe was placed at some distance off the centre along the x-axis. This is shown schematically in Figure 8.14. In order to make a first approximation of the roof vent mass flow rate from the velocities measured, with the four probes setup, the circular roof opening was divided into 5 equal areas such that three probes covered one-fifth of the opening area each. The fourth probe along the x-axis was assumed to cover two-fifths of the opening area, assuming symmetry along the z-axis. The flow density at the roof vent was estimated using the bare-bead thermocouples mounted on the velocity probes. The total mass flow rate across the roof vent opening was calculated using Equation (8.6). This treatment assumes that the velocity measured by each probe is a representative velocity over the assigned "coverage area". Details of the probe placements for each test can be found in Appendix D.

$$\dot{m}_{out,roof} = \sum_i v_i \rho_i A_i \qquad \textbf{(8.6)}$$

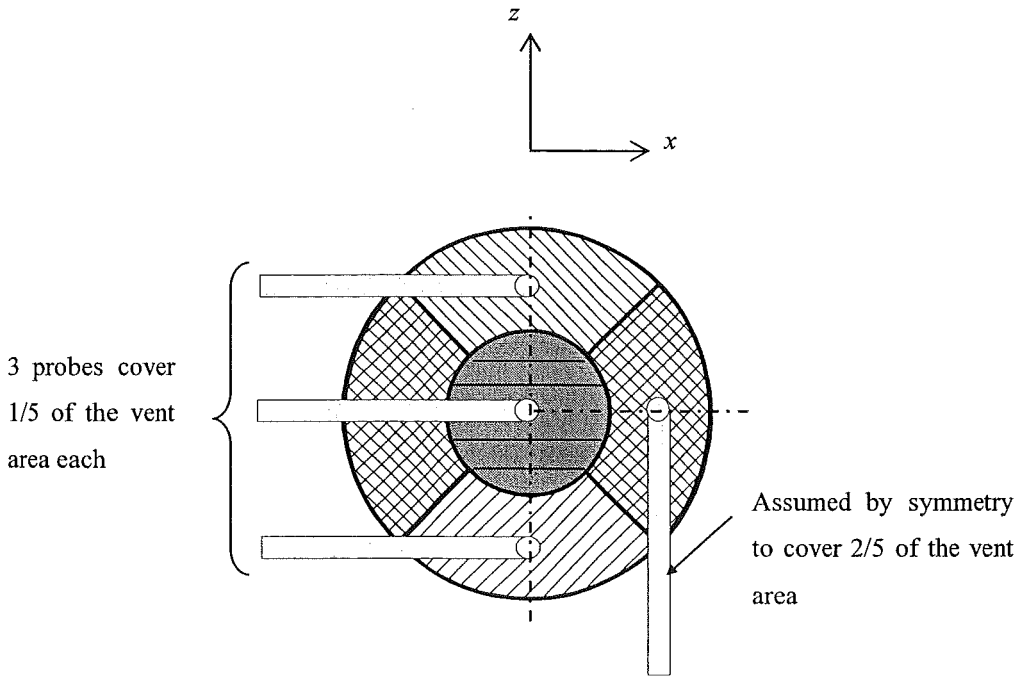

Figure 8.14 Velocity probes and coverage areas at the roof vent opening.

Note that these mass flow rates across the roof vent, $\dot{m}_{out,roof}$, were not used in the subsequent analysis of the results. This is because the velocity measured at each of the probe location does not seem to represent the averaged value over the assigned "coverage area" due to the small number of sampling points. Apart from the measurement locations, there were also problems with the data resulting from soot building up on the velocity probes and uncertainties due to the very high temperature of the velocity probes. New techniques for measuring gas flows across roof vent openings at very high temperatures need to be addressed by future research.

8.5.2 Fuel mass loss rate

Fuel mass loss history was monitored continuously using the load cell. The instantaneous mass loss rate at some time t_i, $\dot{m}(t_i)$, was calculated using a 5-point least squares fit of the mass loss data given in Equation (8.7) where i is a given measured data point, m is the mass at i and t is the time at i.

$$\dot{m}_i = \frac{5\sum_{n=i-2}^{i+2}(m_n t_n) - \sum_{n=i-2}^{i+2}(m_n)\sum_{n=i-2}^{i+2}(t_n)}{5\sum_{n=i-2}^{i+2}(t_n)^2 - \left(\sum_{n=i-2}^{i+2}(t_n)\right)^2} \quad (8.7)$$

8.6 EXPERIMENTAL PROCEDURES

Before every experiment, compressed air was used to clean the soot on the velocity probes and to purge the residue inside the aspirated thermocouples and their respective suction lines. The velocity probes were then positioned at the openings, followed by zeroing the relevant pressure transducers. The data logging channels were checked to make sure they were registering appropriate readings. Two filled fuel tanks were placed on the load cell, and the fuel pan inside the compartment was then filled. The fan in the exhaust hood and the air blower for the aspirated thermocouples was then switched on.

The data logging system was activated three minutes before the fuel pan was lit to include pre-fire data. After the pan was lit, the fuel pump was activated to maintain a constant head in the header tank, and therefore the fuel level inside the fuel pan. The fire experiments generally ran for 30 to 40 minutes duration. It is acknowledged that the tests did not reach steady state after this duration. The experimental fire duration was limited by the capacity of the fuel tanks as well as by the precautions taken to prevent permanent structural damage to the test compartment due to the high gas temperatures generated during the experiments.

Chapter 9 DOOR 1 EXPERIMENTAL RESULTS AND ANALYSIS

This chapter describes the observations made during the Door 1 experimental series. The summarised experimental results from this particular test series are presented and analysed. A simplified vent flow equation for a compartment having both horizontal and vertical vent openings is deduced. Complete experimental data is available in a separate report by Yii (2002).

9.1 DOOR 1 EXPERIMENTAL SERIES

As shown in Table 8.1, the Door 1 experimental series involved a door vent opening of 450mm high by 250mm wide tested against five different sizes of roof vent openings. The diameters of roof vent opening tested include: 0mm (no roof vent, D1R0), 150mm (D1R150), 250mm (D1R250), 300mm (D1R300) and 400mm (D1R400).

Of these experiments, D1R400 was conducted twice during the preliminary compartment and equipment setup. It was found that for both of these experiments, the initial header tank feeding system did not produce adequate fuel supply into the fuel pan, such that the fuel mass loss rate was dictated by the pumping rate of the fuel pump rather than at a rate that was driven by the fire environment inside the compartment. This problem was later rectified by replacing the initial supply tube that connected the header tank and the fuel pan with a larger diameter tube and a larger hole at the bottom of the pan. D1R400 was not repeated with the improved fuel supply system due to time constraint. The fuel supply for the rest of the Door 1 series experiments was expected to keep up with the rate imposed by the fire environment inside the compartment, therefore producing the natural compartment enhancing fires.

9.1.1 Observations

The pattern of the growth phase was very similar for all the tests in the Door 1 experimental series. Typically, after the pan was lit, smoke was seen flowing out of the roof vent, and all the air was flowing into the compartment via the door vent, i.e. no outflow at the door vent was observed. A smoke layer was seen to gradually build-up inside the compartment descending towards the soffit of the door opening. Flame was occasionally observed at the roof vent and at the same time smoke started to spill out of the door vent. Continuous flame was seen at the roof vent before the flame extended out of the door vent. This was the scenario where the neutral-plane was in the vertical door opening with inflow and outflow occurring at the door vent and outflow through the roof vent, i.e. the flow scenario (a) in Figure 7.1. Figure 9.1 is a photo of the D1R150 experiment showing the aforementioned flow scenario with the neutral-plane in the door vent opening.

Figure 9.1 Photo of the D1R150 experiment.

A trend could be observed over this experimental series. With the increase in roof vent size, an increased amount of hot gases in the form of flame was vented out of the compartment through the roof opening. Consequentially, a reduction of outflow was

observed at the door vent indicating a rise in the neutral-plane position at the door. Therefore, increased air inflow through the door was expected with the increase in roof vent size.

For all of the Door 1 experiments with the roof vent opening, the upper hot layer for each experiment was observed to descend close to the floor level. Of these experiments, the D1R400 experiments were seen to have a "brighter" fire environment compared to the "yellowish-brown" fire environment observed in the rest of the Door 1 experiments. This bright fire environment appeared to be a result of a hotter fire environment due to the combination of a larger vent opening and a lower fuel supply rate (due to fuel system not keeping up) resulting in more efficient combustion inside the compartment.

During the Door 1 experimental series, bundles of soot were found to attach to the velocity probes placed in the roof vent and to the velocity probes in the door vent. The effects of soot on the vent flow measurements are discussed in the section to follow.

9.1.2 Temperatures inside the compartment

Figure 9.2, Figure 9.3 and Figure 9.4 show the temperature histories measured from the three bare-bead wire thermocouple trees for experiment D1R250 as an example. The temperatures are plotted for 5 of the 10 thermocouples from each tree starting from 150mm off the floor and spaced 200mm apart. The temperature histories are typical of the Door 1 experimental series with a roof vent opening. It can be seen that after the ignition of the pool, the temperature inside the compartment rises quickly within the first five minutes. The temperature continues to rise as the fire progresses and becomes reasonably well established after 10 minutes, as indicated by smaller temperature changes over time compared to the period before 5 minutes. As the fire progresses, the temperature begins to plateau. However, in the Door 1 experimental series, the steady state condition was not achieved over the test duration (the duration is limited by either the fuel tank capacity or precautions taken to prevent structural damage to the test compartment due to the high gas temperature generated during the experiments). The overall compartment temperature history is represented by

averaging the 30 thermocouple measurements from the three bare-bead wire thermocouple trees inside the compartment.

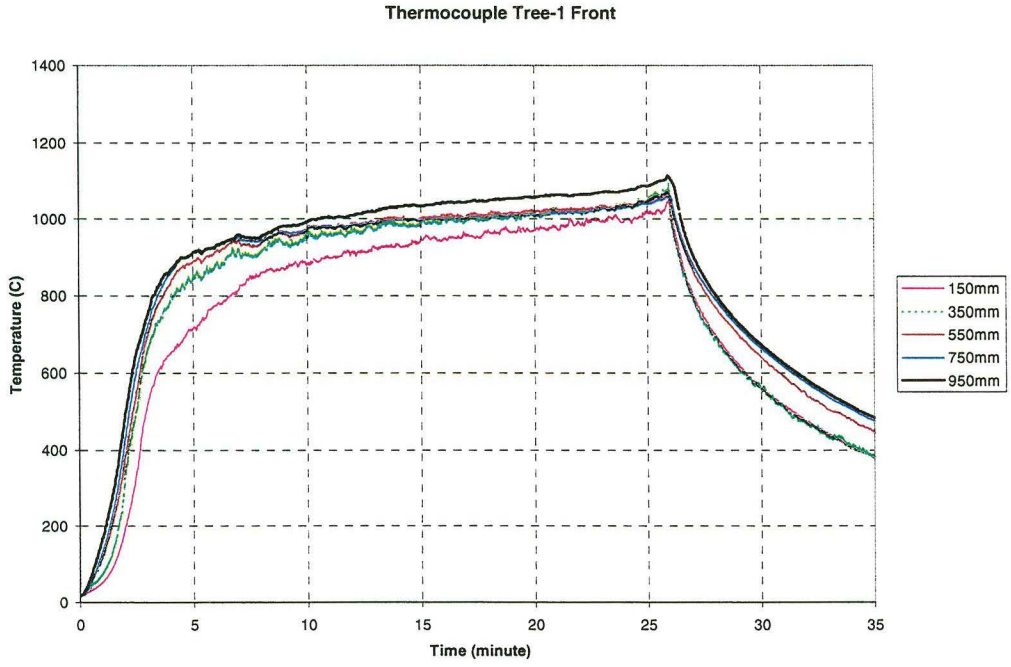

Figure 9.2 **Temperature history for the front thermocouple tree closest to the door vent for the D1R250 experiment. The legend gives the height of each respective thermocouple measured from the floor.**

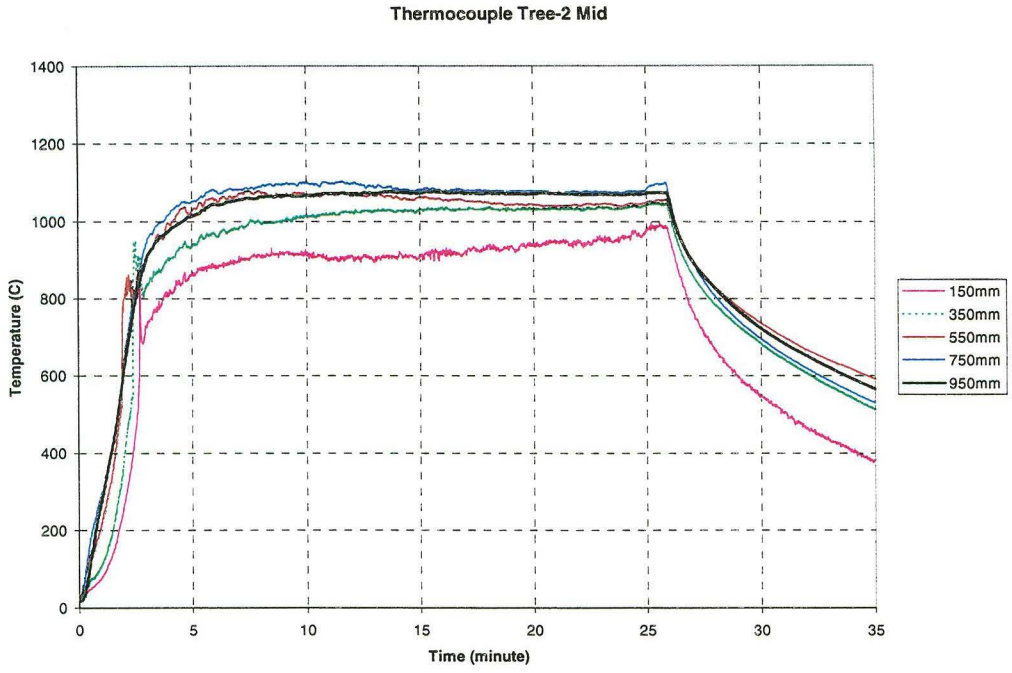

Figure 9.3 Temperature history for the middle thermocouple tree for the D1R250 experiment. The legend gives the height of each respective thermocouple measured from the floor.

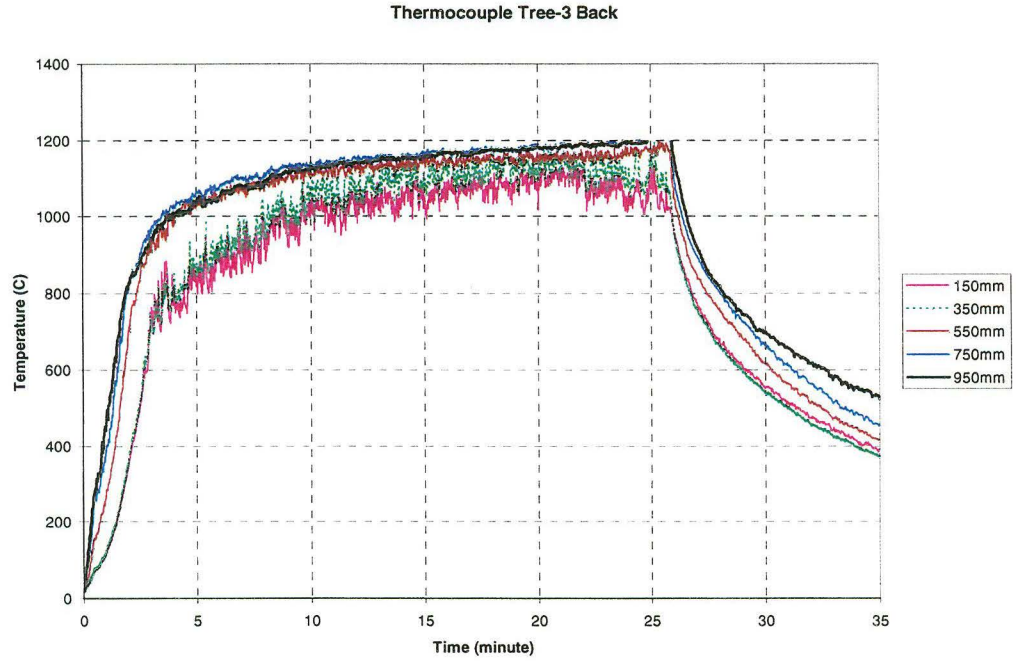

Figure 9.4 Temperature history for the back thermocouple tree furthest away from the door vent for the D1R250 experiment. The legend gives the height of each respective thermocouple measured from the floor.

Reviewing the logged temperature data, it was found that in experiments D1R350, D1R400a and D1R400b, some thermocouples at the back thermocouple tree furthest away from the door vent were registering 0°C. This was due to the temperature exceeding 1200°C, which was the maximum temperature setting in the UDL data logging system. Figure 9.5 shows the temperature history for the back thermocouple tree furthest away from the door vent, for the D1R400b experiment as an example. The legend gives the height of each respective thermocouple measured from the floor. It can be seen that the four thermocouples at a height greater than 650mm would have exceeded the maximum temperature setting of 1200°C set in the UDL data logging system. Since the compartment fire temperature is represented by the averaged temperature using the 30 thermocouple measurements from the three bare-bead wire thermocouple trees inside the compartment, these 0°C reading were manually changed to 1200°C rather than being ignored. This was to obtain a more representative average temperature.

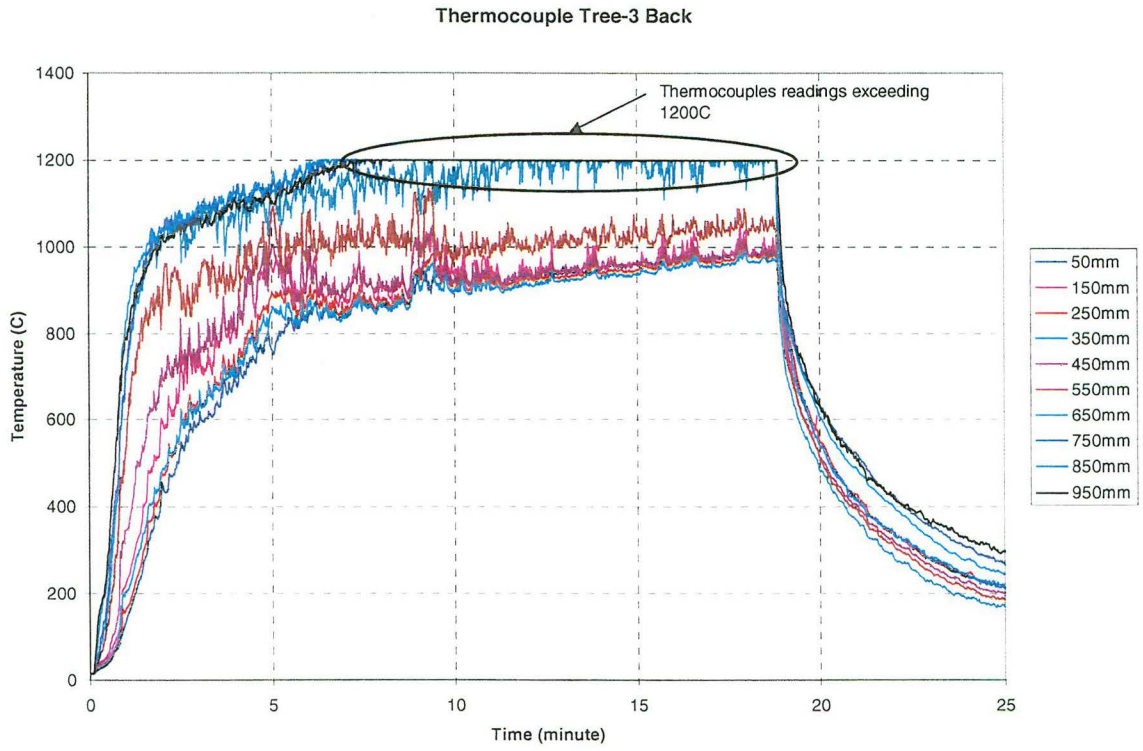

Figure 9.5 Temperature history for the back thermocouple tree furthest away from the door vent for the D1R400b experiment. The legend gives the height of each respective thermocouple measured from the floor.

9.1.3 Vent flows at door

Vent flows across the openings were calculated using the velocity and the temperature profiles measured at the openings. At the Door 1 opening (450mm high by 250mm wide), seven equally spaced velocity probes with vertical displacements of 63mm between each probe were placed along the centreline of the door. Because the environment inside the compartment was very hot, the bare-bead thermocouples mounted on the velocity probes were expected to experience significant radiation effects. Therefore, the temperature at each probe location was interpolated using the temperature measured by the aspirated thermocouples mounted on the door. The mass flow rates were calculated using the rectangular mid-point integration rule as described in Chapter 8. Note that over the entire Door 1 opening series, the Reynolds numbers at the door opening (based on the diameter of the velocity probe, 6.35mm), ranges from close to 0 (for the probe close to the neutral plane) to about 700 (for the probe at the lowest position of the door). This is within the calibration range and the calibration constant, $C_{calib} \approx 1.59$, is appropriate for data reduction purposes.

Figure 9.6 shows the mass flow rate history for the D1R0 experiment without a roof vent, which is the base case scenario. The averaged air inflow rate via the door vent over the period between 20 and 30 minute was 0.033kg/s with a fuel mass loss rate of 0.007kg/s. This is the period where the temperature rise inside the compartment over time was small, i.e. not yet steady but plateauing towards the steady state.

For a compartment with a single vertical vent opening, the air inflow rate can be estimated using the following approximated equation:

$$\dot{m}_{in,door} \approx C \cdot A_v \sqrt{H_v}$$

Since the fuel-air mass ratio in this test was approximately 0.2, i.e. 0.007/0.033, from the vent flow analysis performed in Chapter 3, for a fuel-air mass ratio of 0.2 and the discharge coefficient at the door, C_d, taken to be 0.68, the coefficient C-value is about 0.45 over the temperature range between 600°C and 1200°C. The experimental result compares well with the air inflow rate of 0.034kg/s predicted by the equation. It was

therefore concluded that the data reduction procedure used for analysing the door vent flow was sound.

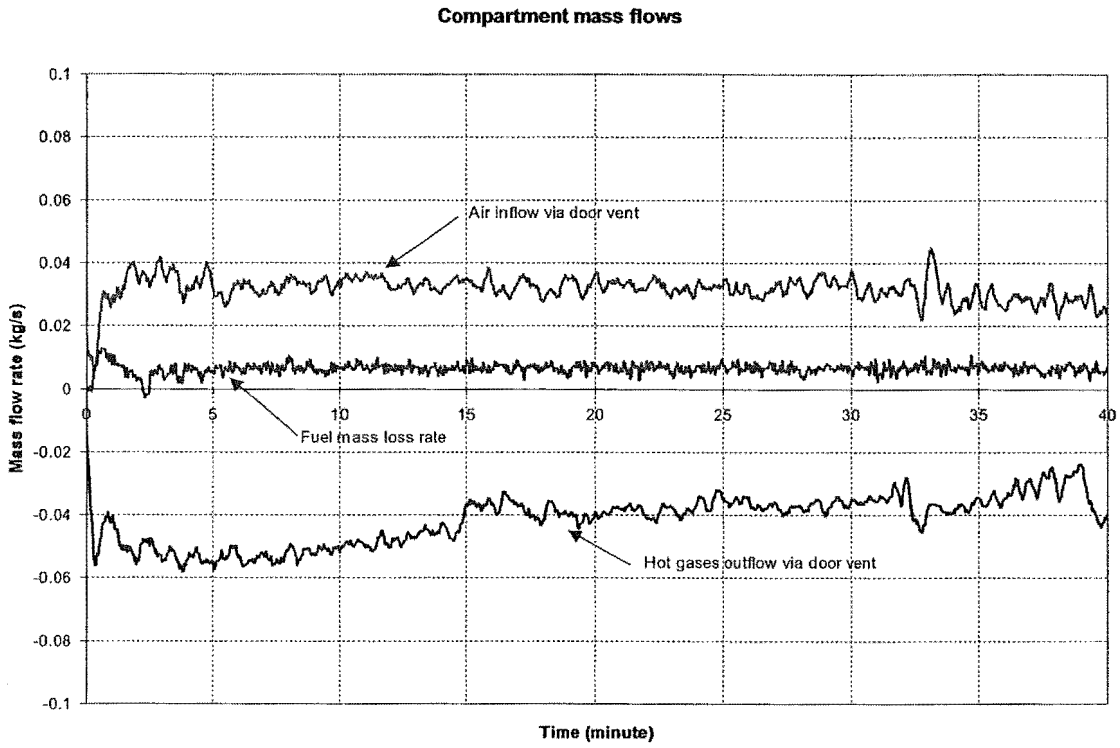

Figure 9.6 Mass flows histories for the D1R0 experiment.

Note that Figure 9.6 shows a slight decrease in the outflow after 15 minutes. Closer examination of the data suggested that the top velocity probe at the door opening was affected by the soot accumulating on the probe. The effects of soot on the vent flow measurements are discussed in the following section.

9.1.4 Effects from soot build-up

Visual observations had found that soot could attach and accumulate along the length of the velocity probes which protruded into the perimeter of the vent opening, in particular, on the top two probes at the door opening and the probes at the roof opening. Analysing the data shows that the soot build up on the probes could affect the vent flow measurement in two different ways. In some cases, the soot could block the sensing holes of the velocity probes resulting in lower pressure differential readings than expected. In other cases, especially for probes located at the roof vent

opening, the accumulation of the soot on the probe could physically block the flow through the roof vent and the air inflow through the door vent was restricted as a consequence. These effects are described below.

For the velocity probes at the door vent, using the D1R0 experiment as example, Figure 9.7 presents the pressure readings recorded at probe P-7 (the velocity probe located at the highest position at the door). The low pressure differential measurements after the 15 minute period could be attributed to soot blocking the impact sensing hole on the velocity probe. Therefore the measurement of the mass flow rate out of the door vent was slightly lower than expected from the mass balance as shown in Figure 9.6.

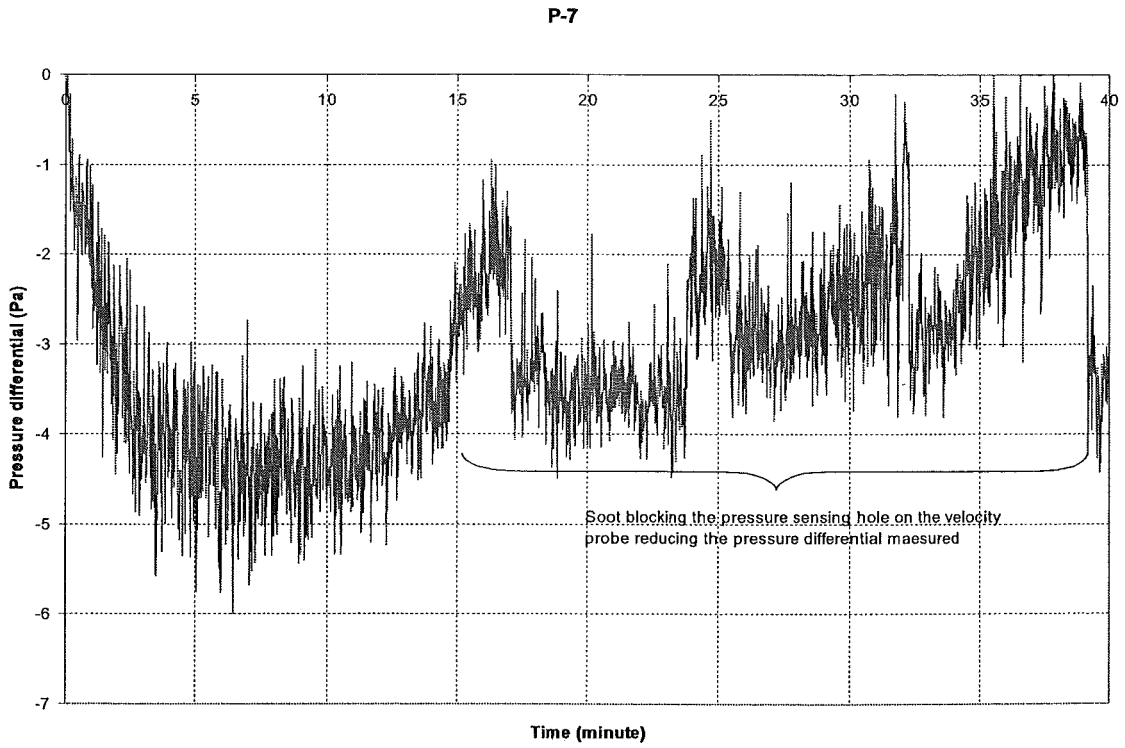

Figure 9.7 Pressure differential reading on P-7 (at the door vent) during the D1R0 experiment.

For the velocity probes at the roof vent, the accumulation of soot on the probes not only affected the pressure differential measurements, but it also affected the air inflow via the door vent as a consequence. Using the D1R300 experiment for example, Figure 9.8 presents the pressure readings recorded at probe P-13 (the velocity probe

located off centre along the x-direction at the roof vent). This figure shows that soot was clogging on probe P-13 from approximately 20 minutes onwards, where the pressure differential measured was close to zero. The positive pressure differential seen during the soot blockage period was likely to be the result of the bi-directional behaviour of the velocity probe rather than an inflow through the roof vent as continuous outflow through the roof vent opening was observed during this period. With soot blocking the impact sensing hole of the probe facing into the vent opening, any fluctuation downstream could be picked up by the reverse facing sensing hole, thereby registering the positive pressure differential readings. Figure 9.9 presents the mass flow rates measured across the door vent during the D1R300 experiment. The soot accumulated on the velocity probes at the roof vent appeared to reduce the effective roof vent opening area, thereby forcing more outflow through the door vent. This can be seen in Figure 9.10 where the neutral plane (estimated by interpolating between the two velocity probes that registered opposite flow direction at the door opening) was lowered at about the same time. As a consequence, the air inflow rate was reduced.

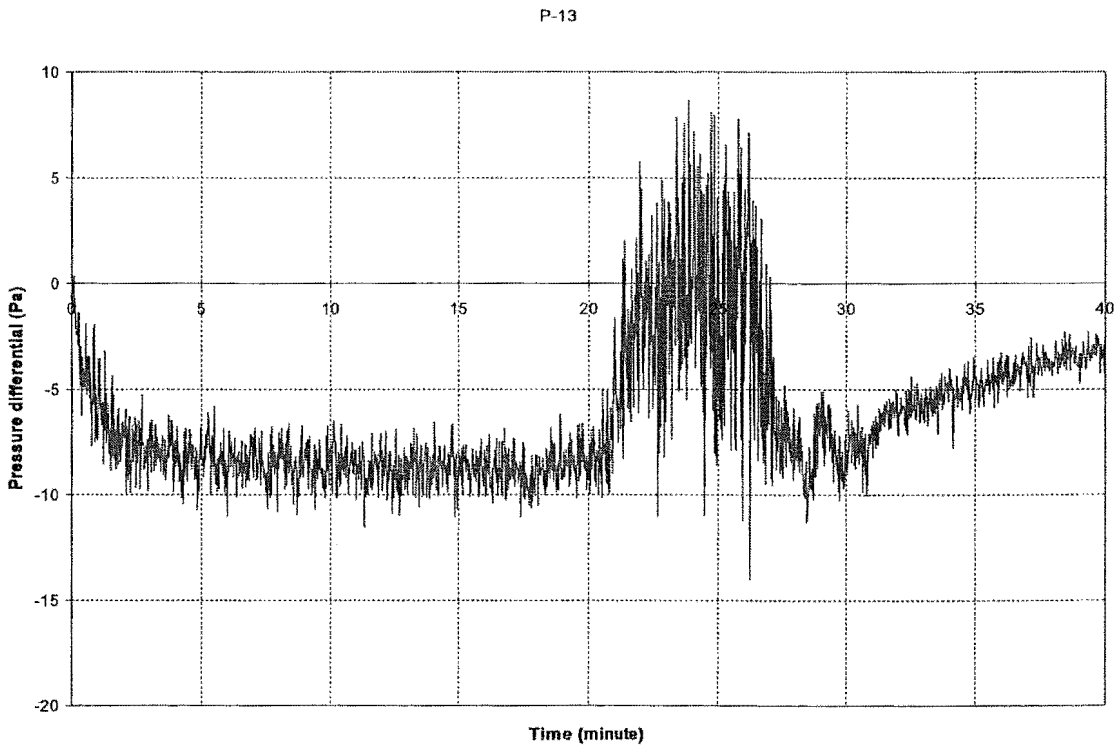

Figure 9.8 **Pressure differential reading on P-13 (at the roof vent) during the D1R300 experiment.**

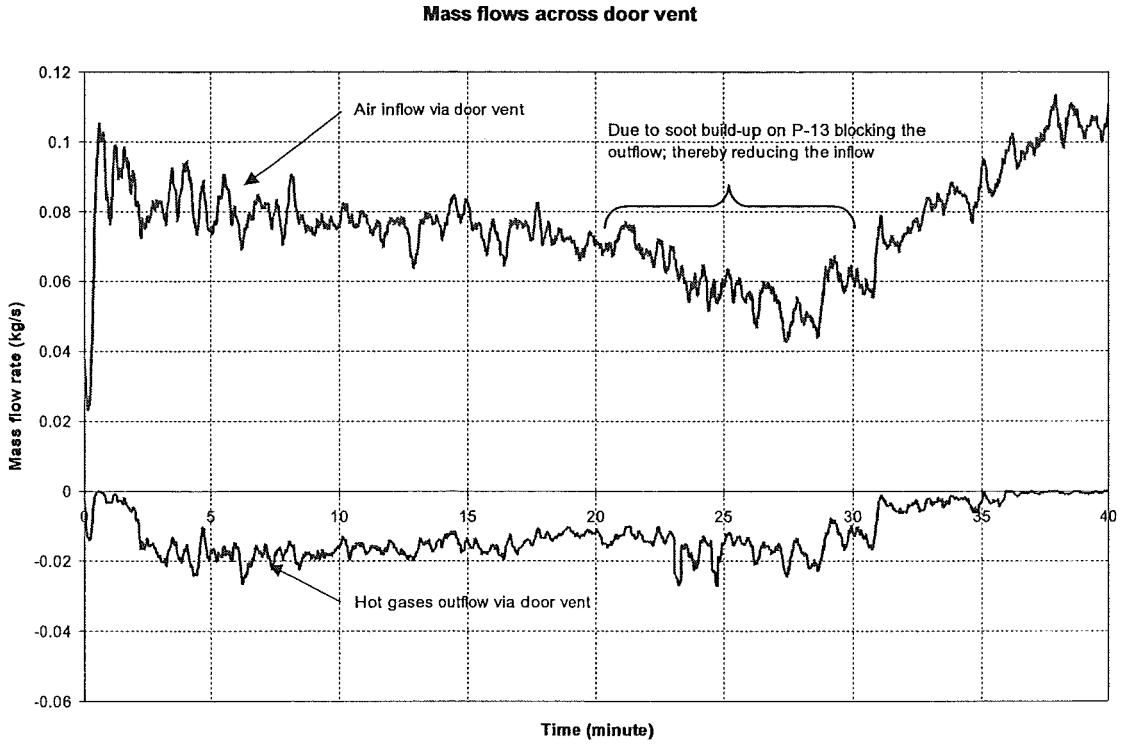

Figure 9.9 Mass flow rates measured at door vent during the D1R300 experiment.

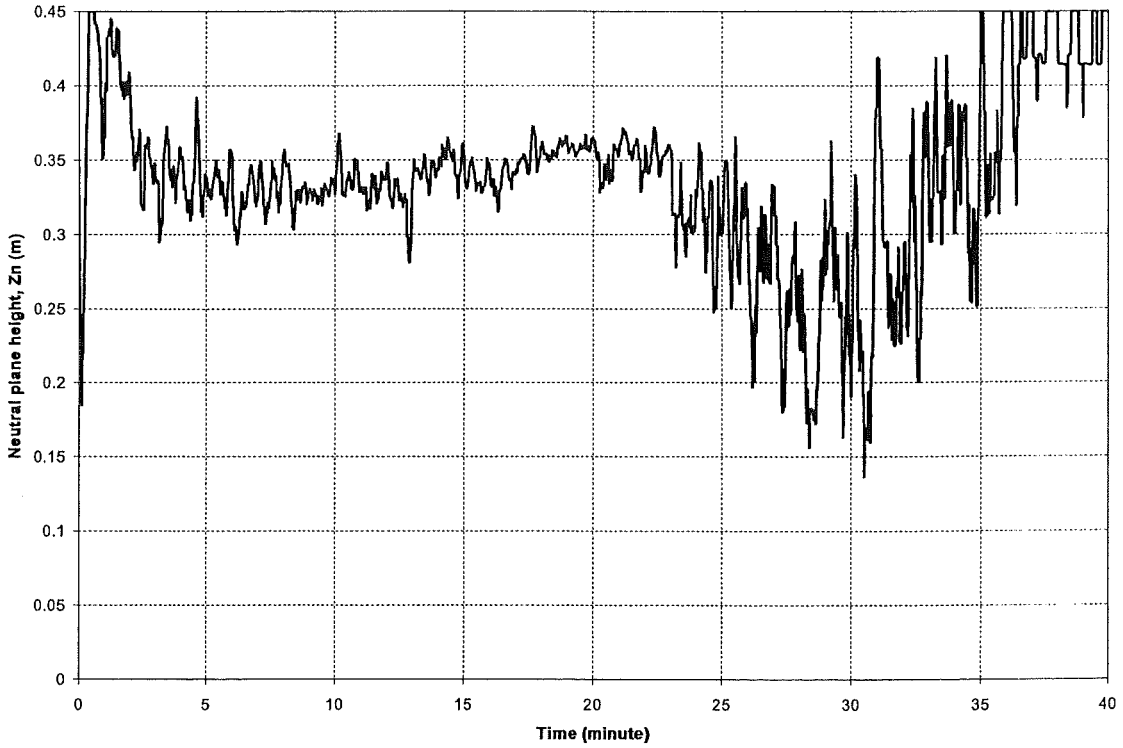

Figure 9.10 Neutral-plane height measured during the D1R300 experiment.

9.1.5 Vent flow at roof vent

For all the Door 1 experimental tests, the fire environment was well mixed and the vent flows across the openings were stable and well established. Under such conditions, the compartment as a system was approaching a quasi-steady state and the mass flowing into and out of the compartment had to be balanced. The mass balance equation requires the net mass flow across the door vent opening plus the fuel mass flow to equal the mass flow leaving via the roof vent. This is given in Equation (9.1) as follows:

$$\dot{m}_{in,door} - \dot{m}_{out,door} + \dot{m}_p = \dot{m}_{out,roof} \quad \textbf{(9.1)}$$

However, analysing the roof vent flow data showed that in all Door 1 cases tested, $\dot{m}_{out,roof}$ (evaluated using Equation (8.6)) was greater than ($\dot{m}_{in,door} - \dot{m}_{out,door} + \dot{m}_p$). A factor in the order of 0.5 to 0.7 would have to be applied to $\dot{m}_{out,roof}$ in order to satisfy the mass balance (Equation (9.1)).

The reason for this discrepancy is not clear, but it is likely to relate to the data reduction method used as well as a combination of several factors associated with the velocity measurements. The data reduction method employed has assumed that the velocity measured by each probe on the roof vent opening is the representative velocity for the assigned "coverage area" in the opening. However, since there were a limited number of probes being placed in the roof vent and the outside probes were not placed close to the edge of the opening, the whole velocity distribution over the roof vent opening remains unknown. The overestimation of roof vent flow rate seems likely to stem from using the velocities measured by those outside probes as representative velocities for the "coverage areas" around the edge of the opening.

Apart from the data reduction method, there are several other factors associated with the velocity measurements which could have contributed to this discrepancy. The main differences in the measurement of mass flow across the roof vent compared with the wall vent include the shape of the opening, i.e. the circular roof vent versus the rectangular door vent, the location of the velocity probes at these openings; and the

temperatures involved. Since the velocity probes were positioned on a rack mounted at the vent opening, they were not positioned exactly in the opening. The velocity probes at the roof vent were placed in the downstream side of the exit gases, whereas the velocity probes at the door vent were placed in the upstream side. This might have some effect on the area integration procedures taken to deduce the mass flow rate. Also, there were uncertainties in the velocity measurements made by the velocity probes placed at the roof vent. This is because the velocity probes at the roof vent were subjected to a very high temperature gas stream, subsequently, the probe temperature was very high (seen glowing red during the experiments). This high temperature effect on the pressure differential measurements was unknown. Furthermore, the gas temperature measurements of the discharge gas stream were also questionable as these measurements were made by bare-bead wire thermocouples that could well be affected by the radiation from the hot velocity probes. Compounding the potential soot effect on the probe, the velocity measurement made under such harsh conditions was suspect. Therefore, the roof vent flow data was not used to evaluate the mass flow rate out of the roof vent. Instead, $\dot{m}_{out,roof}$ was calculated using Equation (9.1) with the measured mass flow rates across the door vent, $\dot{m}_{in,door}$ and $\dot{m}_{out,door}$, and the measured fuel mass loss rate, $\dot{m}_p$.

9.1.6 Door 1 results summary

The primary objective of the experimental study was to obtain the air inflow data through a door vent with different roof vent openings. The data is required for verifying the vent flow model derived in Chapter 7. Ideally, steady-state mass flow rates were preferred for these purposes. However, this was not achievable since soot build-up on the velocity probes at the roof vent affected the mass flow rate of air into the compartment as previously mentioned. From the mass flow rate data, it was found that typically over the period between 10 minutes to 20 minutes after ignition, the fire environment inside the compartment was well-established and the velocity probes were experiencing minimal soot build-up. As a compromise, the mass flow rates over this period were used as representative data for the tests.

Table 9.1 summarises the experimental results for the Door 1 experimental series. The results presented are the time average values over the 10-20 minutes period after ignition. Except for experiments D1R400a and D1R400b, both of which were run for less than 20 minutes (to avoid structural damage to the test compartment caused by the high temperatures generated), the results for these two tests are represented by the time average values over the 10-15 minutes period. Column 1 gives the test number for each specific test. Column 2 gives the time average temperature over the 10-20 minute period, which is represented by averaging the 30 thermocouple measurements from the three bare-bead wire thermocouple trees inside the compartment. Columns 3 to 5 give the corresponding mass inflow and outflow rates at the door vent and the fuel mass loss rate respectively. Column 6 gives the mass flow rates through the roof calculated using the flow rates measured at the door vent and the fuel mass loss rate (Equation (9.1)). Column 7 gives the neutral plane height estimated by interpolating between the two velocity probes that registered opposite flow directions at the door opening, and Column 8 gives the calculated equivalence ratio, Φ, inside the compartment for each experiment. The equivalence ratio is evaluated as

$$\Phi = \frac{\dot{m}_p \times r}{\dot{m}_{in,door}} \qquad (9.2)$$

where the stoichiometry air to fuel mass ratio, r, for heptane is 15.1. This equation provides an indication of the fire environment inside the compartment, where $\Phi>1$ indicates the fire is fuel-rich, having more fuel available than can be burned with the ventilation available, and $\Phi<1$ indicates the fire is fuel-lean with sufficient ventilation.

The plots in Figure 9.11 show the trends of vent flow behaviours for the Door 1 experiments at various sizes of roof vent opening. It can be seen that increasing the roof vent opening area increases the rate of outflow through the roof opening, and as a consequence, the rate of airflow into the compartment increases. This raises the neutral-plane height and reduces the amount of the hot gases discharged through the door.

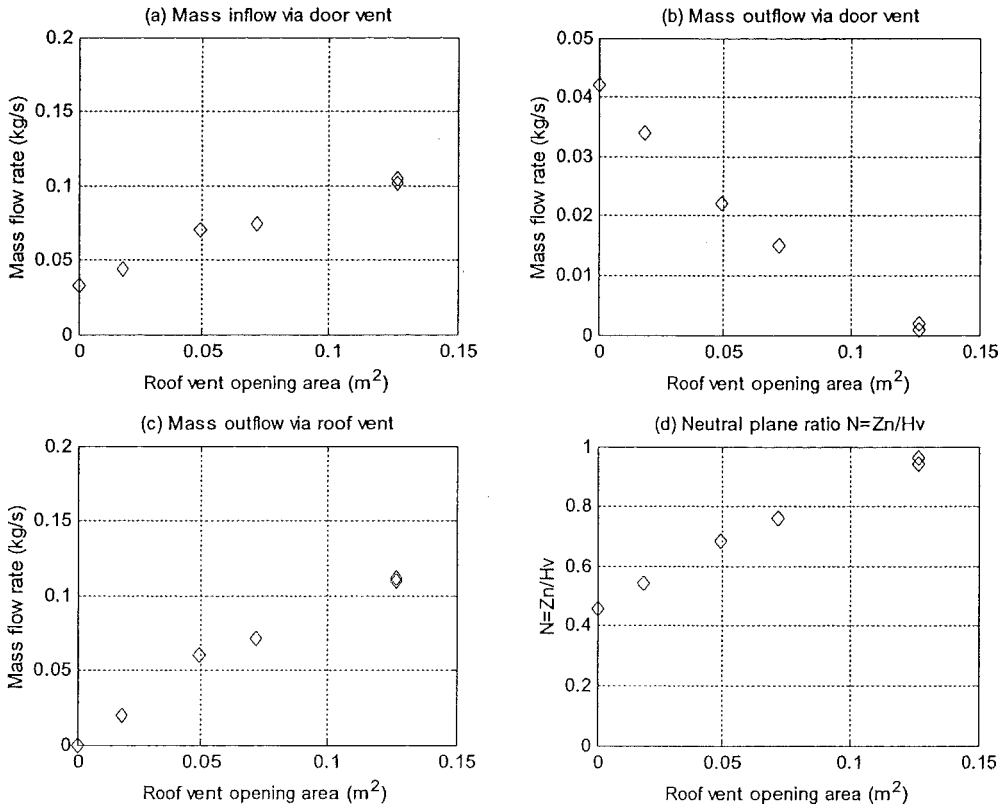

Figure 9.11 Summary data plot for the Door 1 experimental series.

Table 9.1 Data summary for the Door 1 experimental series.

Test	T_g (°C)	$\dot{m}_{in,door}$ (kg/s)	$\dot{m}_{out,door}$ (kg/s)	$\dot{m}_p$ (kg/s)	$\dot{m}_{out,roof} = \dot{m}_{in,door} - \dot{m}_{out,door} + \dot{m}_p$ (kg/s)	Z_n (m)	Φ (calculated)
D1R0	838	0.033	0.042	0.007	N/A	0.206	3.2
D1R150	912 (962)[1]	0.044	0.034	0.010	0.020	0.244	3.4
D1R250	1031 (1048)[1]	0.070	0.022	0.012	0.060	0.307	2.6
D1R300	986 (1059)[1]	0.074	0.015	0.012	0.071	0.343	2.4
D1R400a[2]	1039	0.105	0.002	0.009[3]	0.112	0.424	1.3
D1R400b[2]	1002	0.102	0.001	0.009[3]	0.110	0.432	1.3

Note:

[1]The temperature inside the bracket () is the averaged value over the last 10 minute of the fire state, i.e. approaching the steady state value.

[2]D1R400a and b: data averaged over 10-15 minute period. Both of these fires did not reach steady state yet during the 10-15 minute period.

[3]Fuel mass loss rate restricted by supply system.

9.2 ANALYSIS

The primary objective of the experimental study was to obtain a set of vent flow data at different opening combinations to verify the mathematical vent flow model for a compartment with a roof vent opening. Two flow scenarios were targeted in the experimental investigation: the first involved the neutral-plane in the door vent (Figure 7.1(a)); and the second involved the neutral-plane above the soffit of the door vent (Figure 7.1(b)). The experimental results presented in Table 9.1 from the Door 1 series are used to study the former scenario.

9.2.1 Vent flow model with roof opening

The mathematical vent flow formulations that involved the neutral-plane in the door vent (Figure 7.1(a)) are presented as Equations (7.3), (7.4), (7.5) and (7.6) in Chapter 7. These formulations are used to calculate the vent flow rates and the neutral plane height for each Door 1 test. The gas temperature and the fuel mass loss rate for each Door 1 experiment as presented in Table 9.1 were used as inputs in the vent flow formulations. Typical flow coefficient values, $C_{d,door}$=0.68 for door opening (Prahl and Emmons, 1975) and $C_{d,roof}$=0.60 for circular roof vent opening (Zukoski, 1995) were used in the calculations; ambient air density was taken as 1.2kg/m^3 and the hot gas density was evaluated as in Equation (9.3) assuming ideal gas behaviours.

$$\rho_g = \frac{353}{T_g(in\,Kelvin)} \qquad (9.3)$$

Note that the Door 1 experimental setting had a door vent flush with the floor level, so the sill height is zero, δ=0, and the soffit height equals the door height, H_s=H_v.

Figure 9.12 compares the Door 1 experimental measurements with the predictions from the vent flow formulations (Equations (7.3), (7.4), (7.5) and (7.6)). Comparisons were made between the mass flow rates via the door and roof vent openings, as well as the neutral-plane height at the door vent. From the comparative plots shown in Figure 9.12, the mass flow rates predictions made by the vent flow model compare

well with the experimental results. It can be seen that the neutral plane height measured during the experiment (estimated by interpolating between the two velocity probes that registered opposite flow direction at the door opening) is slightly higher compared to the model prediction. This discrepancy between model prediction and experimental measurement can be attributed to the fire environment inside the compartment. In the model, it is assumed that the fire environment inside the compartment has a uniform temperature from floor to ceiling. However, inside the actual fire compartment, the environment is not perfectly uniform. The temperature close to the floor level would be slightly lower than the average temperature inside the compartment with a lower buoyancy head for the inflow across the door opening. To maintain the mass balance inside the compartment, the compartment as a system adjusted itself by allowing the inflow to flow through a greater portion of the door opening. As a consequence, the actual neutral plane height measured is higher than the model prediction. It is noted that for the D1R400 experiments, the model calculates a slightly greater mass flow rate of air into the compartment than the measurements. This discrepancy might be the result of having only two operational aspirated thermocouples at the locations of the 2^{nd} and 6^{th} probes during the D1R400 experiments. Since the velocity and temperature measurements at the door were deduced from interpolation between the two aspirated thermocouples, because of the large interpolation distance, the temperature in between might not be as representative. It was likely that the temperature in between was over-estimated that lead to slightly lower air inflow measurements.

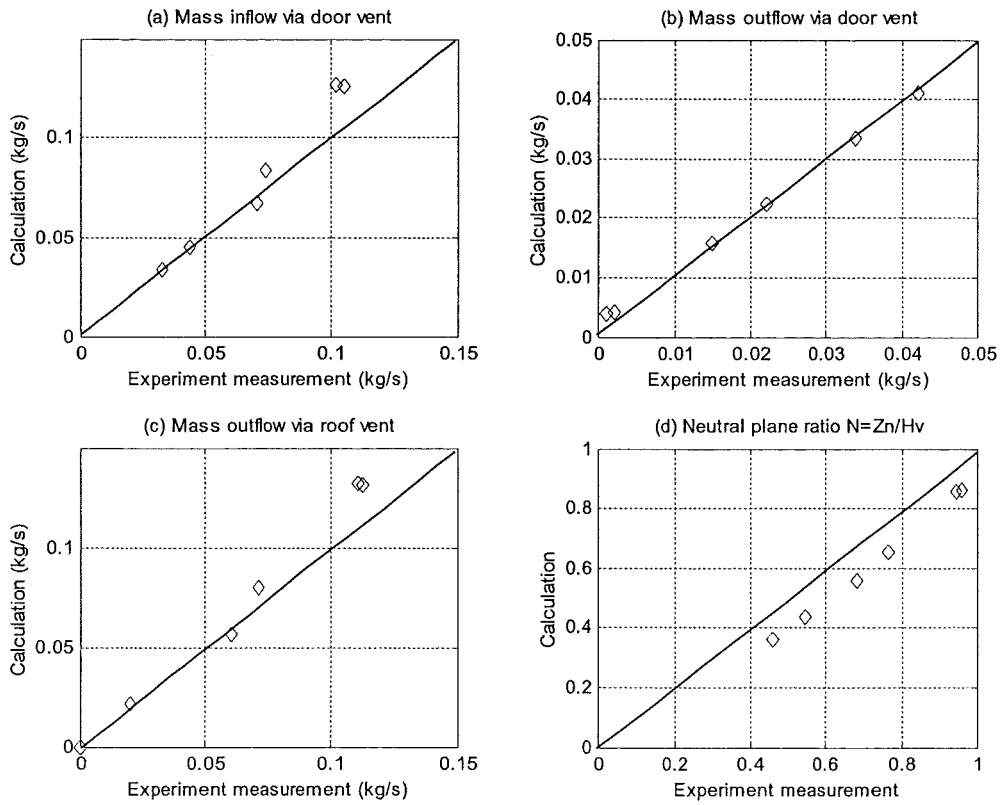

Figure 9.12 Comparison between the experimental results and predictions made from vent flow model.

The above results show that the vent flow model (described by Equations (7.3), (7.4), (7.5) and (7.6)) is adequate for predicting the vent flows for a compartment with both horizontal and vertical openings under the circumstance that the neutral-plane is in the door vent opening.

9.2.2 Simplified equation

Due to the nature of the equations (Equations (7.3), (7.4), (7.5) and (7.6)), solving the respective mass flow rates by hand is not straightforward. Often in compartment fires, the mass flow rate of air into the compartment is important as it provides an estimate for the maximum heat that can be released inside the compartment. It could also serve to estimate the mass loss rate of wood during the ventilation controlled burning regime.

For a compartment with a single vertical vent opening, the air inflow rate can be estimated using the following approximated equation.

$$\dot{m}_{in} \approx C_{(Av,roof=0)} \cdot A_v \sqrt{H_v} \qquad \textbf{(9.4)}$$

The full expression for $C_{(Av,roof=0)}$ (no roof vent opening) has been presented in Equation (3.9) in Chapter 3. As shown in Chapter 3, the coefficient C (which is the air inflow rate per unit vent parameter, $\dot{m}_{in} / A_v \sqrt{H_v}$) is relatively constant over the post-flashover temperature ranges between 600°C and 1200°C having a value of approximately 0.45 for the fuel-air ratio s=0.2. Since the value C is approximately a constant, it provides a convenient way to estimate the air inflow through the given opening, such that

$$\dot{m}_{in} / A_v \sqrt{H_v} = C \qquad \textbf{(9.5)}$$

For a compartment having both vertical and horizontal vent openings, a simplified equation similar to Equation (9.5) is desirable as to provide a first estimation for the mass flow rate of air through the vertical wall opening for a given roof vent size.

From the experimental results and the model calculations presented, it can be seen that for a compartment with a given vertical wall opening, provided the roof vent is not excessive large, increasing the roof vent opening area will increase the air inflow through the vertical wall opening, as seen in Figure 9.11(a). Therefore, the air inflow rate per unit vent parameter of the vertical wall vent, $\dot{m}_{in} / A_v \sqrt{H_v}$, represented by C as in Equation (9.5), will increase with increasing roof vent opening area.

There exists a limit where the neutral-plane height is at the soffit where the air flowing into the compartment through the entire wall opening and out through the roof opening. For a given vertical wall opening, the maximum roof vent opening, $A_{v,roof,\max}$, that will result in the neutral plane height being at the soffit level is given in Equation (9.6).

$$A_{v,roof,\max,(Zn=Hs)} = \frac{2}{3} \cdot \frac{C_{d,door}}{C_{d,roofv}} \cdot \frac{A_v\sqrt{H_v}}{\sqrt{H_c - (H_v + \delta)}} \cdot \sqrt{\frac{\rho_0}{\rho_g}} \cdot (1+s) \qquad \textbf{(9.6)}$$

The variables follow those depicted in Figure 7.2 and the fuel-air mass ratio is denoted as s. Note that Equation (9.6) is the same as Equation (7.7) presented in a different form. This is the condition where air is flowing into the compartment through the entire vertical wall vent and out through the roof vent.

Figure 9.13 shows the schematic representation of C varying with roof vent opening area. Starting from no roof vent opening, C has the same value as $C_{(Av,roof=0)}$ given in Equation (3.9), increasing to a value up to $C_{(Av,roof=max)}$ at the maximum roof vent opening defined by Equation (9.6). The variation between $C_{(Av,roof=0)}$ and $C_{(Av,roof=max)}$ over the opening area is taken as linear as a first approximation (see Figure 9.11(a)).

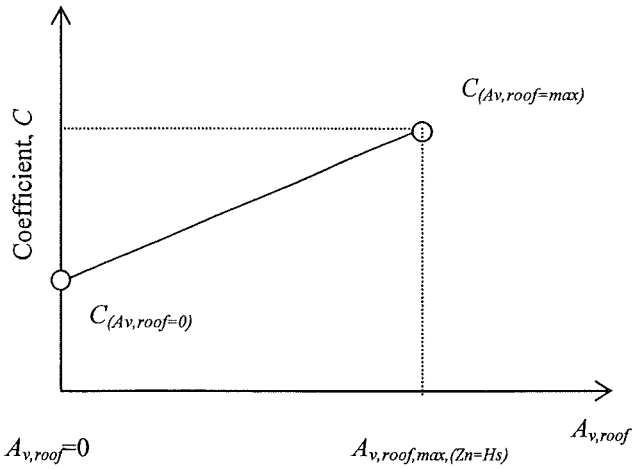

Figure 9.13 Schematic representation for the relationship between coefficient C and roof vent opening area.

The relationship between the coefficient C and the roof vent opening area, $A_{v,roof}$, over the range from no roof vent opening to the maximum roof vent opening, is

$$C = gradient \times A_{v,roof} + C_{(Av,roof=0)} \qquad \textbf{(9.7)}$$

Substituting Equation (9.5) into Equation (9.7) to eliminate C, gives

$$\dot{m}_{in} / A_v \sqrt{H_v} = gradient \times A_{v,roof} + C_{(Av,roof=0)} \tag{9.8}$$

For a linearly varying C, with increasing roof vent opening area, $A_{v,roof}$, the *gradient* is

$$gradient = \frac{\Delta C}{\Delta A_{v,roof}} = \frac{C_{(Av,roof=\max)} - C_{(Av,roof=0)}}{A_{v,roof,\max,(Zn=Hs)}} \tag{9.9}$$

From Equation (7.3), the expression for $C_{(Av,roof=max)}$ at the maximum roof vent opening when the neutral-plane is levelled at the height of the soffit of the vertical vent, i.e. $(Z_n - \delta)^{3/2} = H_v^{3/2}$, can be written as Equation (9.10).

$$C_{(Av,roof=\max)} = \frac{2}{3} \cdot C_{d,door} \cdot \rho_0 \cdot \sqrt{2g} \cdot \sqrt{1 - \frac{\rho_g}{\rho_0}} \tag{9.10}$$

By substituting Equation (3.9) for $C_{(Av,roof=0)}$, Equation (9.6) for $A_{v,roof,max,(Zn=Hs)}$, and Equation (9.10) for $C_{(Av,roof=max)}$ into Equation (9.9), and replacing the density terms with temperature terms using the ideal gas law (Equation (9.3)), the *gradient*, i.e. the change of the C-value over the roof vent opening area, is given as follow.

$$gradient = \frac{\sqrt{H_c - (H_v + \delta)}}{A_v \sqrt{H_v}} C_{d,roof} \rho_0 \sqrt{2g} \times \frac{\sqrt{1 - \frac{T_0}{T_g}} \cdot \left\{ 1 - \left[\frac{1}{1 + (T_g/T_0)^{\frac{1}{3}} \cdot (1+s)^{\frac{2}{3}}} \right]^{\frac{3}{2}} \right\}}{\sqrt{\frac{T_g}{T_0}} \cdot (1+s)} \tag{9.11}$$

The last term in Equation (9.11) is regarded as the *temperature factor*. It defines the temperature dependence of the gradient and is shown in Figure 9.14 for two fuel-air ratios. Over the temperature range of interest, from 800K to 1500K for post-flashover

fires, this temperature function is reasonably constant, giving 0.33±7% for s=0 and 0.285±7% for s=0.2.

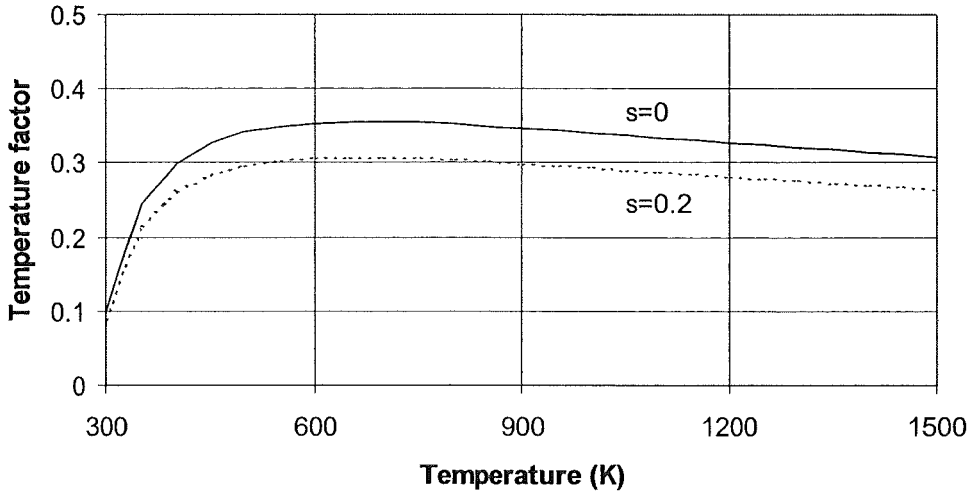

Figure 9.14 Temperature factor of Equation (9.11).

For $C_{d,roof}$=0.6, ρ_0=1.2kg/m^3 and g=9.81m/s^2, the gradient expression in Equation (9.11) can be expressed as follows:

$$gradient \approx 1.05 \frac{\sqrt{H_c - (H_v + \delta)}}{A_v \sqrt{H_v}} \quad \text{(for } s=0\text{)} \tag{9.12}$$

and

$$gradient \approx 0.91 \frac{\sqrt{H_c - (H_v + \delta)}}{A_v \sqrt{H_v}} \quad \text{(for } s=0.2\text{)} \tag{9.13}$$

For post-flashover fires, the fuel mass contribution to the vent flows is more significant than for pre-flashover fires. For fuel air mass ratio, s=0.2, by substituting the gradient expression (Equation (9.13)) and the $C_{(Av,roof=0)}$=0.45 (for s=0.2) into Equation (9.8), the simplified equation for the air inflow through the vertical vent opening is

$$\dot{m}_{in} \approx 0.45 A_v \sqrt{H_v} + 0.91 A_{v,roof} \sqrt{H_c - (H_v + \delta)} \quad \textbf{(9.14)}$$

The first term in the simplified equation is the typical expression used to estimate the mass flow rate of air through a vertical wall vent opening. The later term adds the extra ventilation effect due to the existence of the roof vent opening. Note that the term (H_c-(H_v+δ)) represents the depth of the downstand, which is the portion of the wall between the soffit of the vertical wall opening and the ceiling. The square root of the downstand depth, i.e. $\sqrt{H_c - (H_v + \delta)}$, is significant as it dictates the extra buoyancy head generated for the discharge through the roof vent opening. It should be noted that before applying Equation (9.14), one needs to ensure that the roof vent opening area is within the maximum value defined in Equation (9.6) and the temperature range is between 800K and 1500K.

Figure 9.15 compares the mass inflow rate of air estimated using Equation (9.14) with the data from the Door 1 experimental series. It can be seen that the simplified equation provides satisfactory estimations for the air inflow rates over the various sizes of roof opening tested in the Door 1 series.

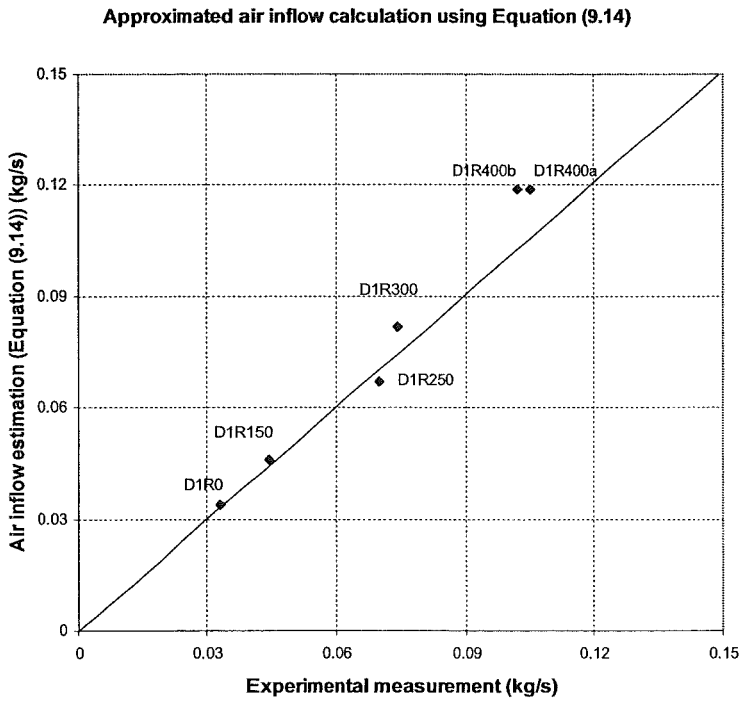

Figure 9.15 **Comparison of mass flow rates of air estimated using the simplified Equations (9.14) to the experimental measurements.**

9.2.3 Simplified equation without downstand

The above analysis has shown that the simplified Equation (9.14) based on the vent flow formulations (Equations (7.3), (7.4), (7.5) and (7.6)) is adequate for predicting the mass flow rate of air into the compartment with a roof vent opening. It has also identified the significance of the depth of the downstand over the resultant air inflow rate. It can be seen that Equation (9.14) is applicable only for wall openings with downstands, i.e. $(H_c-(H_v+\delta))>0$. For a wall opening having its soffit at the ceiling level, i.e. $H_c=H_s=(H_v+\delta)$, there will be no downstand effect, and the air inflow is dependent only on the roof vent opening area. The following analysis investigates the scenario for wall openings without any downstand. It is an analytical study and no experimental verification is made as all the tests conducted were with a finite downstand depth.

From Equations (7.3), (7.4), (7.5) and (7.6), for a wall opening having its soffit at the ceiling level, i.e. $H_c=H_s=(H_v+\delta)$, the following equation can be deduced

$$\sqrt{\frac{\rho_0}{\rho_g}}(1+s)=\left(\frac{1-N}{N}\right)^{\frac{3}{2}}+\frac{3}{2}\frac{C_{d,roofv}}{C_{d,door}}\frac{A_{v,roof}}{A_v}\left(\frac{1-N}{N^3}\right)^{\frac{1}{2}} \quad \textbf{(9.15)}$$

where N is defined as $(Z_n-\delta)/H_v$. N can be solved for a given density (or in terms of temperature assuming ideal gas behaviour, Equation (9.3)) and a vent opening ratio, $A_{v,roof}/A_v$. The corresponding air inflow rate through the vertical wall opening can be solved using Equation (7.3). Expressed in term of N, Equation (7.3) can be written as follows

$$\dot{m}_{in}=\frac{2}{3}C_d\rho_0\sqrt{2g\left(1-\frac{\rho_g}{\rho_0}\right)}\left(N^{3/2}\right)A_v\sqrt{H_v} \quad \textbf{(9.16)}$$
$$=C_{(Hc=Hs)}\cdot A_v\sqrt{H_v}$$

Figure 9.16 plots the calculated N and the corresponding C over the temperature range from 300K to 1500K at various $A_{v,roof}/A_v$ ratio with s=0.2. For illustrative purposes, $A_{v,roof}/A_v$ ratios from 0 to 5 are plotted. It can be seen that an increase in $A_{v,roof}/A_v$ ratio results in an increase in N, such that the neutral plane height approaches the roof height asymptotically. The increase in N increases the air inflow and hence C.

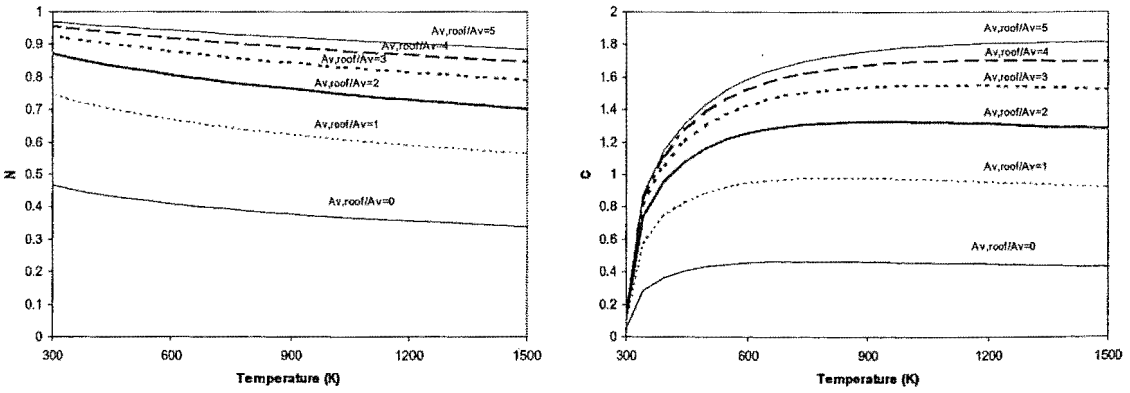

Figure 9.16 The effects of $A_{v,roof}/A_v$ ratios to the N and C values for wall vent with no soffit.

For a vertical wall vent without any downstand, the air inflow rate through the opening could be approximated using the C-value plot presented in Figure 9.16. The

C values for the $A_{v,roof}/A_v$ ratios plotted are reasonably constant at high temperature. By representing the air inflow for each $A_{v,roof}/A_v$ ratio using the respective C value averaged over the temperature range between 800K and 1500K, the relationship between C and $A_{v,roof}/A_v$ ratio can be plotted, as shown in Figure 9.17.

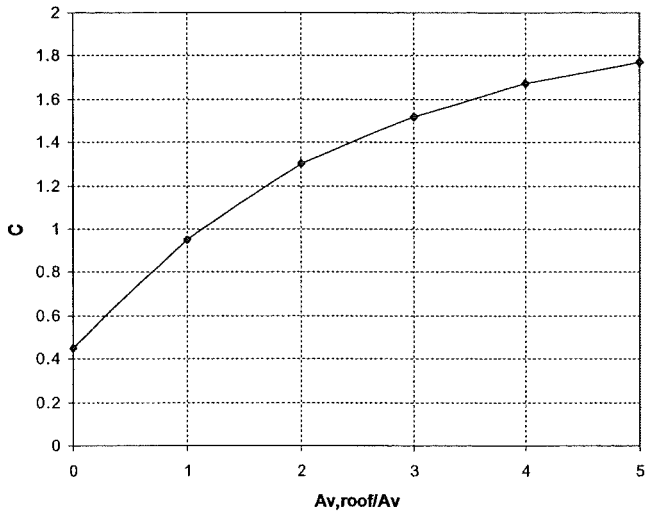

Figure 9.17 Relationship between C and $A_{v,roof}/A_v$ ratio for vertical wall vent without soffit.

A curve fit to these point can be made to describe the relationship between C and $A_{v,roof}/A_v$ ratio, such that

$$C \approx -0.05\left(A_{v,roof}/A_v\right)^2 + 0.5\left(A_{v,roof}/A_v\right) + 0.5 \qquad \textbf{(9.17)}$$

Substituting into Equation (9.16) gives:

$$\dot{m}_{in} \approx 0.5 A_v \sqrt{H_v} \cdot \left(1 + \left(A_{v,roof}/A_v\right) - 0.1\left(A_{v,roof}/A_v\right)^2\right) \qquad \textbf{(9.18)}$$

Equation (9.18) is an approximated equation derived to estimate the air inflow through the vertical wall opening that has no downstand. It shows that in such a case, the air inflow into the compartment can be characterised by the relative vent sizes using $A_{v,roof}/A_v$.

It should be noted that both Equations (9.14) and (9.18) are deduced from the natural convection flow model that assumes uniform temperature inside the compartment, and that the flow across the roof vent opening is unidirectional. To fulfil these assumptions, the vent sizes for both openings should not be excessively large and the fire environment inside the compartment has to be well-mixed with a uniform temperature. In cases where these assumptions may be violated, such as excessive large openings, where bi-directional flow could occur at the roof opening, or entrainment dominates the inflow through the wall opening or in cases where the inside compartment temperature is not uniform, the vent flow model and its derivatives (Equations (9.14) and (9.18)) are not expected to produce adequate results.

9.3 SUMMARY

From the results of Door 1 experiments, it can be seen that increasing the roof vent opening area increases the rate of outflow through the roof opening; and the rate of air inflow into the compartment follows the increase as a consequence. This raises the neutral-plane height and reduces the amount of the hot gases discharged through the door. These behaviours are predicted in the vent flow model. The vent flow model is shown to produce favourable flow estimations to the experimental results. In the proposed CFIRE post-flashover fire model, Equations (7.3), (7.4), (7.5) and (7.6) are used to describe the vent flows that involve both horizontal and vertical vent openings. The simplified equations for estimating the mass flow rate of air into a compartment with both horizontal and vertical vent openings with and without downstand are developed. These simplified air inflow expressions (Equations (9.14) and (9.18)) are used in the CFIRE model to estimate the mass loss rate of wood during the ventilation controlled burning regime under these ventilation conditions.

Chapter 10 DOOR 2 AND 3 EXPERIMENTAL RESULTS AND ANALYSIS

This chapter describes the experimental observations for the Door 2 and the Door 3 experimental series. An unexpected pulsing phenomenon was observed during these tests. This phenomenon is analysed qualitatively and focus is on identifying the possible triggering and sustaining mechanisms that result in the pulsing. The results of these experiments are not used in the development of the proposed CFIRE post-flashover fire model, but are included here for reference purposes. Complete experimental data is available in a separate report by Yii (2002).

10.1 INTRODUCTION

The Door 3 experimental series was designed to produce the flow scenario such that the neutral-plane was high above the door opening, with the ambient air flowing into the compartment through the entire door vent, and hot gases flowing out through the roof vent opening. The Door 2 experimental series was designed to produce the transitional condition where the neutral-plane height was close to the soffit of the door vent. It was initially envisaged that the Door 2 and the Door 3 setups could produce a stable quiescent thermal environment inside the test compartment, such that the vent flows were solely driven by the pressure difference from the temperature fields. However, an unexpected pulsing phenomenon was observed in all of the Door 2 and Door 3 experiments (except the D3R350 experiment). This phenomenon was a sustained pulsing action once started, and consisted of charging and discharging phases. During the charging phase, air entered the compartment via the door opening, followed by the discharging phase where hot gases puffed out through the door vent. The vent flow at the door vent followed the cycle of the pulsing action. This was a transient behaviour and therefore the vent flow formulations derived in Chapter 7,

which assumed that vent flows were driven solely by the hydrostatic pressure difference between two quiescent environments under steady conditions, were not applicable in this situation. To the author's present knowledge, this pulsing phenomenon has not been reported in the literature. In the following sections, the pulsing phenomenon observed is described, and qualitative discussion on the likely mechanism that causes the pulsing action is provided.

10.2 EXPERIMENTAL OBSERVATIONS AND RESULTS

The experimental setup for the Door 2 and Door 3 experiments were the same as in the Door 1 experiments; only the door geometry was altered. During the Door 2 and Door 3 experimental series, each experiment was initiated by lighting the fuel pan; smoke was seen to flow out of the roof vent with all the air flowing into the compartment via the door vent. As the fire progressed, flame was seen occasionally at the roof vent opening with the hot layer deepening inside the compartment. For experiments D2R150 and D2R250, smoke was observed to spill out of the door vent, an indication of neutral-plane height in the door. The hot layer inside the compartment then dropped close to the floor level. Through the door vent opening, the layer close to the floor level was initially seen as a black sooty smoke layer. As the fire progressed, its colour changed from black to reddish black, accompanied with light puffing of the black smoke out of the door vent. When the layer colour got to orange red, flame puffed out of the door vent triggering a continuous pulsing action. The pulsing action consisted of charging and discharging phases. During the charging phase, air flowed into the compartment via the entire door vent area after the exit of the flame at the door; this airflow seemed to reach the fuel pan before igniting, as indicated by a flash observed at the fuel pan. This initiated the discharging phase with a flame front moving towards the door opening and ending with a fireball outside the door vent. Simultaneously, the ejection of the flame out of the roof vent flared when the flame puffed out of the door vent. The charging and discharging phases continue with a reasonable constant pulsing frequency during the course of the fire.

Figure 10.1 shows the schematic charging and discharging action described above. Figure 10.2 shows the photographs of the fireball at the door opening and Figure 10.3 is the sequential photo shots of the pulsing action taken during the experiment, showing the simultaneous flares at the flame jet out of the roof vent when flame puffs out of the door vent.

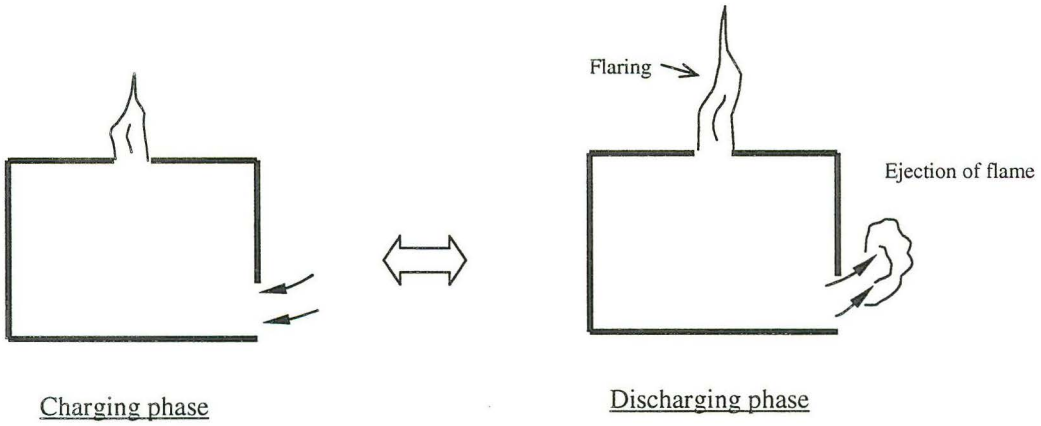

Figure 10.1 Schematic representation of the pulsating action.

(a) Discharging (b) Charging (c) Discharging

Figure 10.2 Photos for the periodic charging and discharging action at the door vent.

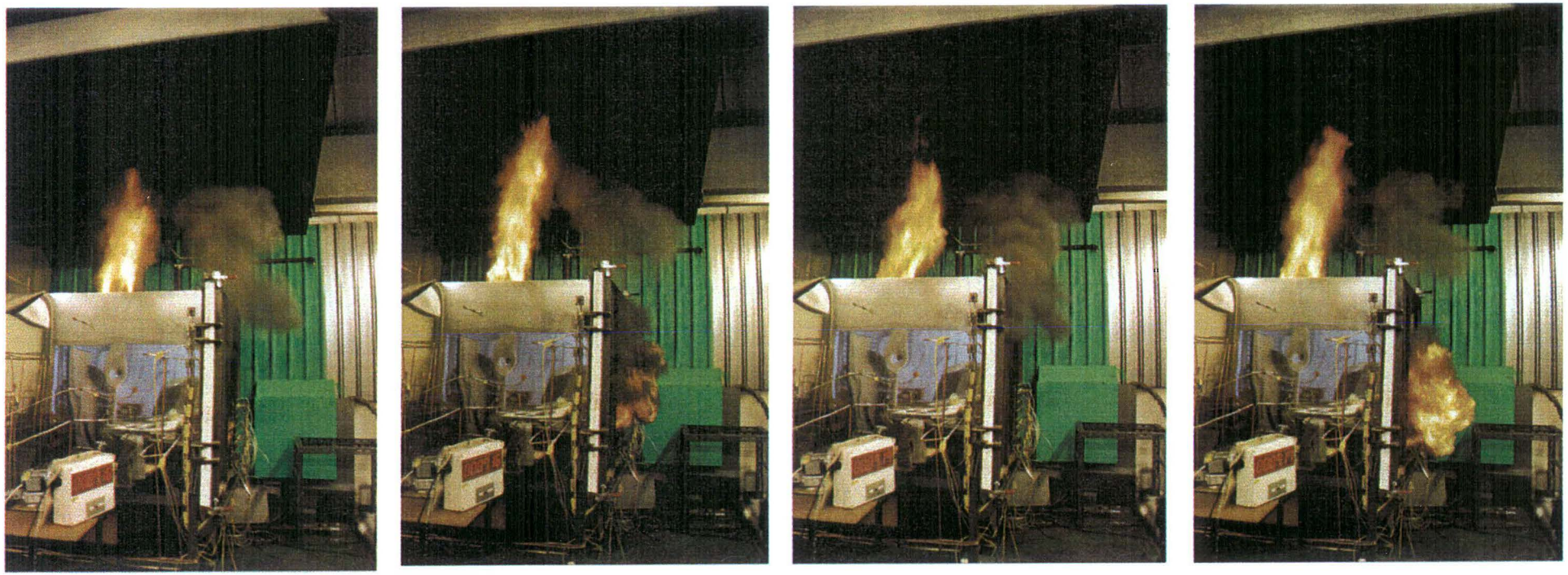

(a) Charging phase (b) Discharging phase (c) Charging phase (d) Discharging phase

Figure 10.3 Photos for the sequence of events during the charging and discharging action.

Similar observations were made for experiments D2R300, D3R250 and D3R300 except that during the initial stage, there was no outflow of smoke at the door vent. A black smoke layer was seen to reach close to the floor level and, until it got to orange red colour, flame puffed out of the door vent triggering the pulsing action. For the D3R300 experiment, the pulsing was not as obvious with the discharge at the door mostly consisting of black smoke and occasional flame. For the D3R350 experiment, no pulsing was observed with air flowing into the compartment via the door opening and out through the roof opening.

10.3 QUALITATIVE CONSIDERATIONS FOR PULSING

10.3.1 Triggering mechanisms for pulsing

Examining the video footage taken during the experiments revealed a consistent pattern in the sequence of event leading to the initiation of pulsing. From the observations through the door opening, the layer close to the floor level was initially black in colour. As the fire progressed, its colour changed from black to red and to orange red before flame exited the door vent, triggering the pulsing.

The colour change in the layer close to the floor level observed just before the initiation of the discharge phase suggests that layer ignition could be the triggering mechanism for the pulsing. Table 10.1 presents the initial conditions just before the pulsing. Two temperature values just before the pulsing are presented in the table. The first is the average temperature inside the compartment obtained by averaging all the 30 thermocouple-measurements inside the compartment. The second is the average temperature of the smoke layer close to the floor level. For the Door 2 opening, this temperature is represented by averaging the bottom three thermocouple-measurements of the second thermocouple tree. For the Door 3 opening, because of its lower opening height compared to Door 2, the average temperature measured from the bottom two thermocouples of the second thermocouple tree is taken to represent the layer temperature at the floor level. This temperature value is slightly lower than the average compartment temperature as the bottom thermocouples in the second

thermocouple-tree are located in the path of air inflow between the fuel pan and the door vent. It is noted that this temperature should be regarded as an indicative value because the bare-bead thermocouples could well experience radiation effects from the surroundings. The air mass inflow rate and the fuel mass loss rate just prior to the pulsing are also given in the table. The air mass flow rate given is the time-average value 30 seconds prior to the pulsing; and the fuel mass loss rate is the average value taken over the period from the start (time zero) up to the pulsing. The calculated equivalence ratio, Φ, inside the compartment for each test is presented with Φ defined as:

$$\Phi = \frac{\dot{m}_{fuel} \cdot r}{\dot{m}_{in}}$$

where r is the stoichiometric air to fuel mass ratio, and for heptane, r=15.1.

Table 10.1 Conditions prior to the pulsing.

		Conditions just before the pulsing action				
Test#	Time to pulse (min)	Averaged gas temperature in room (°C)	Layer temp near floor (°C)	Air mass inflow rate (kg/s)	Fuel mass loss rate (kg/s)	Calculated equivalence ratio, Φ
D2R150	5.0	644	535	0.009	0.003	5.0
D2R250	3.0	726	509	0.060	0.010	2.5
D2R300	3.0	726	512	0.070	0.006	1.3
D3R250	3.0	802	713	0.040	0.006	2.3
D3R300	4.5	780	575	0.060	0.007	1.8

From Table 10.1, it can be seen that just before the initiation of the pulsing, the environment is fuel-rich with Φ>1, and the layer temperature is above 500°C. Beyler (1984) has deduced a model that identifies the ignition criterion for the burning of a layer of incomplete combustion products that are remote from the plume flame, which acts as a pilot. The ignition criterion is represented by the ignition index, which is the left hand side term in Equation (10.1):

$$\frac{1-1/\Phi}{1+1/r}\cdot\frac{\Delta h_{c,O2}Y_{O2}}{c_p\left(T_{SL}-T_{layer}\right)}\geq 1 \qquad \textbf{(10.1)}$$

where Φ is the equivalence ratio, r is the stoichiometric air to fuel mass ratio, c_p is the average heat capacity of the products of complete combustion, $\Delta h_{c,O2}$ is the average heat of reaction of oxygen, Y_{O2} is the oxygen mass fraction in the supply air, T_{SL} is the adiabatic flame temperature (K) and T_{layer} is the layer temperature (K).

For heptane, C_7H_{16}, the stoichiometric air to fuel mass ratio, r, is 15.1. Using typical values suggested by Beyler (1984), c_p =1.1kJ/kg-K, T_{SL} =1700K (for total hydrocarbons), Y_{O2} =0.233 and $\Delta h_{c,O2}$ =13400kJ/kg, the potential of the layer ignition can be estimated.

Figure 10.4 plots the layer temperature versus the equivalence ratio required for igniting the layer according to Equation (10.1). The plot shows that, the lower the equivalence ratio, the greater the required temperature to ignite the layer. This behaviour matches well with the observation made during the experiment, where the layer close to the floor has to reach a higher temperature, as indicated by the change of colour from black to orange red, before the layer ignited, with flame appearing out of the door vent. The condition for each experiment just before pulsing presented in Table 10.1 is plotted on Figure 10.4. All the data points are all above the ignition index defined by Equation (10.1), except the D2R300 experiment which is slightly lower. The comparison between the data and the ignition index suggests that the layer involved was ignited prior to the pulsing. The data point for the D2R150 experiment is ignored in the plot as it has an estimated equivalence ratio of 5 which is considered too high. From Table 10.1, the air mass inflow rate for the D1R150 experiment seems to be too low. This suggests that the flow measurements at the door for this particular experiment could be in error.

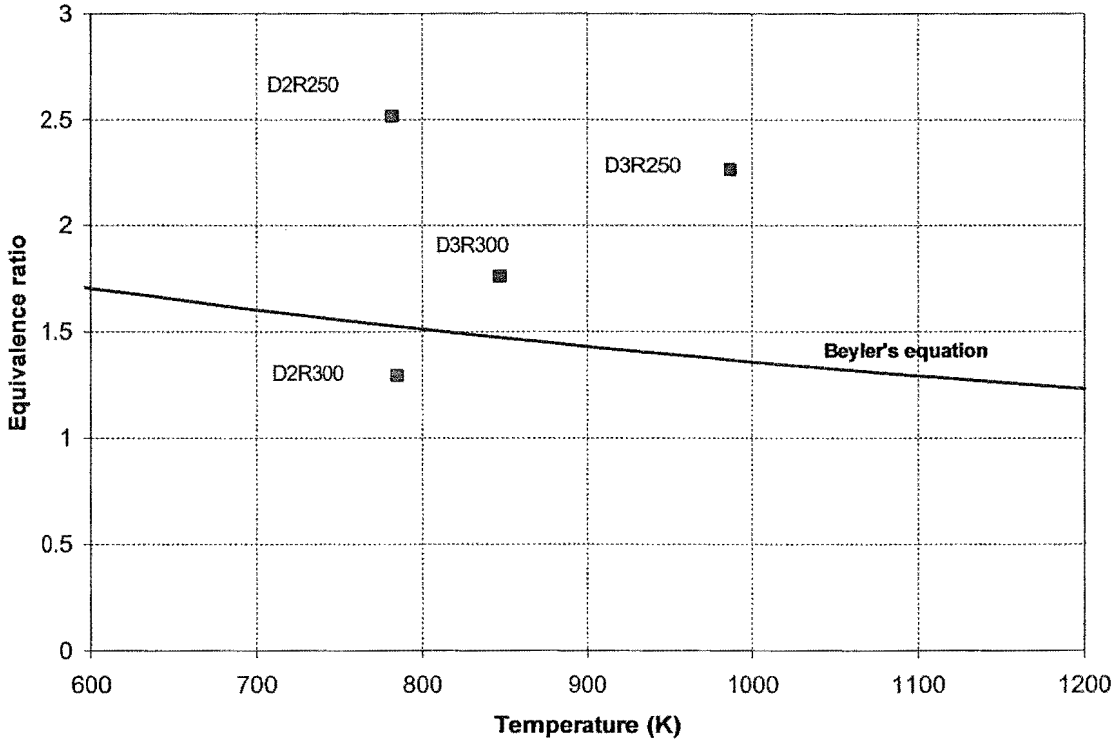

Figure 10.4 Ignition index of the layer.

The ignition of the layer by itself is not enough to initiate the pulsing. It has to take place in a compartment where the vent opening sizes are not excessive. In order to better understand the role of the layer ignition that leads to pulsing, it is useful to consider the whole compartment as a control volume. From the First Law of Thermodynamics, ignoring the kinetic and potential energy terms and the pressure work at the control surface, the conservation of energy can be expressed as follows:

$$\frac{d}{dt}\iiint_{CV}\rho u dV = \dot{q} + \sum \dot{m}_i \cdot h_i - \sum \dot{m}_e \cdot h_e \qquad (10.2)$$

where the net increase in the internal energy in the control volume is equal to the net heat added to the control volume, plus the net enthalpy flow into the control volume through the vent openings.

Using the definition of the total internal energy per unit mass, u, which is the product of the specific heat at constant volume, c_v, and the gas temperature, T, in Kelvin,

$u=c_v T$

and the ideal gas behaviour with

$$\rho = \frac{P}{RT}$$

where P is the pressure, T is the temperature and R is the gas constant.

For constant volume, V, that is independent of time, substituting the expressions for the total internal energy and the gas density in Equation (10.2), gives

$$\frac{c_v \cdot V}{R}\frac{dP}{dt} = \dot{q} + \sum \dot{m}_i \cdot h_i - \sum \dot{m}_e \cdot h_e \qquad \textbf{(10.3)}$$

Equation (10.3) provides a useful platform to discuss the role of the layer ignition that leads to the pulsing. The ignition of the layer would result in a sudden increase in the $\dot{q}$ term. Whether this perturbation is significant enough to increase the pressure inside the compartment would depend on the relative magnitudes of the increase in the $\dot{q}$ term and the enthalpy outflow. In the case where the vent opening is large and therefore there is a large convective heat loss through the outflow, a slight increase in the $\dot{q}$ term from the layer ignition would not be enough to cause a significant increase in compartment pressure. On the other hand, for the case where the vent opening is small with a small heat loss in the outflow, a sudden increase in the energy release would lead to instability in the system by increasing the compartment pressure. Gases would be forced out through the available openings as the system tries to relieve the pressure, triggering the initiation of the pulsing action.

10.3.2 Sustaining mechanism for pulsing

The ignition of the layer in a volume with a small opening increases the pressure inside the compartment. This results in hot gases being pushed out of both the roof vent and the door vent. During the discharge, the compartment as a system loses mass due to the outflows, and the pressure inside decreases. This can be shown by

considering the compartment as a whole with m, P, T and ρ representing the mass, pressure, temperature and density respectively, of gas inside the compartment at any instant t. Let V represent the volume of the compartment and use the subscript 0 to indicate the initial condition at the beginning of the discharge, i.e. after the ignition of the layer, and assuming the expansion inside the compartment during the discharging process follows the isentropic pressure temperature relationship, such as that typically used in jet propulsion cycle analysis, (see Loh, 1968) gives:

Mass inside the compartment

$$m = V\rho$$

Isentropic relationship for ideal gas, where $\beta = c_p/c_v$,

$$\frac{P}{\rho^{\beta}} = \frac{P_0}{\rho_0^{\beta}} = const = c$$

Then

$$\rho = \left(\frac{P}{c}\right)^{\frac{1}{\beta}}$$

Substituting into the mass equation gives:

$$m = V\left(\frac{P}{c}\right)^{\frac{1}{\beta}}$$

or in differential form of time, using the chain rule gives:

$$\frac{dm}{dt} = \frac{V}{\beta c^{\frac{1}{\beta}}} P^{\left(\frac{1-\beta}{\beta}\right)} \frac{dP}{dt} \qquad \textbf{(10.4)}$$

Equation (10.4) shows that, during the discharge period, the compartment is losing mass and subsequently the pressure inside the compartment decreases. When the inside pressure reduces to atmospheric pressure or even slightly below atmospheric pressure, fresh air inflow is sucked in via the entire door vent as the system tries to counter the mass losses. This starts the charging phase as air enters the compartment in the form of a gravity current. Experimental observations found that the air current entering the compartment punches through the fire environment creating mixing around its edges. The front of the current would also experience mixing. Because the fire environment at this stage is fuel-rich, the mixing at the front and around the edges of the air current can result in a flammable mixture. When the front of the air current reaches the fuel pan with a visible plume flame, it is ignited. This ignition is indicated by the flash observed at the edge of the fuel pan. A turbulent flame front propagating along the interface toward the opening follows after the ignition. The burning at the interface of the gravity current adds heat to the system, causing an increase in pressure inside the compartment. This initiates the discharge phase, with some of the unburned fuel being pushed out of the door opening and consumed in the form of fireball, and some extra unburned fuel being pushed out from the reservoir through the roof vent giving a longer flame jet.

Figure 10.5 (a), (b) and (c) are a series of frontal photos shot at the door opening representing the sequence of events. Figure (a) is the stage where the air current reaches the fuel pan. Note that the air inflow current appears to have roughly a cross section of the door opening flowing towards the pan, with mixing occurring at the top and at the sides. Figure (b) shows the flame burning along the interface of the mixed region as shown in (a). Figure (c) shows the unburned pyrolysates being forced out of the vent and burning as a fireball.

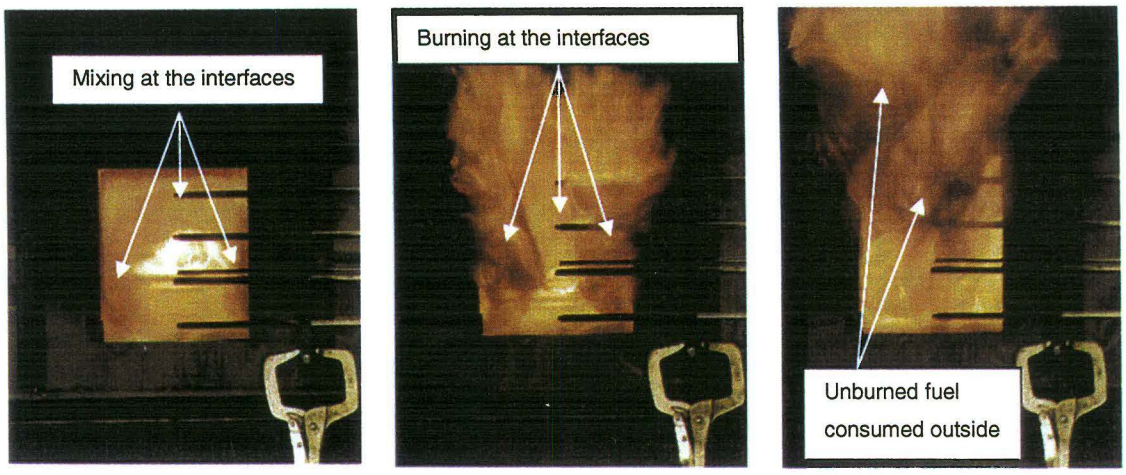

Mixing at the interface Flame at the interface Fireball

Figure 10.5 Frontal sequential photo shots showing: (a) the entering of air current; (b) the burning at the interface; and (c) the fireball.

After the discharge, the pressure in the compartment is expected to drop, and air flowing into the compartment through the door opening. This results in the charging phase. When the flammable mixture that rides on the air current reaches the fuel pan and is ignited, the burning along the interface of the gravity current initiates the discharge, completing the cycle. Once the pulsing starts, its frequency is reasonably constant throughout the entire test.

Table 10.2 shows the maximum charging and discharging velocity at the openings, weighted over the opening area during the continuous pulsing at the period of 20 to 30 minutes after ignition. The respective pulsing frequency for each test obtained from the video footage is also shown. The average compartment temperature (based on the measurements made by the three bare-bead wire thermocouple trees) and the average fuel mass loss rate over this period are also given.

Table 10.2 Velocities and frequency data for D2 and D3 experimental series averaged over 20 to 30 minute period.

			Velocities weighted over the door opening area (m/s)		
Test#	T_g (°C)	$\dot{m}_p$ (kg/s)	Charging Phase	Discharging Phase	Freq Pulse/min
D2R150*	880	0.0062	1.4	-2.4	46
D2R250	1031	0.0103	3.1	-2.4	54
D2R300	1064	0.0113	3.2	-2.6	55
D3R250	964	0.0089	3.3	-2.0	63
D3R300	1008	0.0103	2.4	-0.35	60

*Note: The data given for the D2R150 experiment are averaged over 15 to 20 minute period as the test was stopped after 25 minutes.

It is interesting to note that the pulsing frequency can be estimated by dividing the distance between the door opening and the edge of the pan (~1.2m) by the charging and discharging velocities at the door, such that

Frequency per minute=(1.2m/charging velocity + 1.2m/discharging velocity)$^{-1}$×60

This may mean that the location of the fuel pan plays a part in determining the pulsing frequency.

10.4 REMARKS

The continuous pulsing phenomenon observed in both the Door 2 and Door 3 experimental series was an unexpected event. The transient behaviour associated with the pulsing is likely to involve the change in compartment pressure due to small openings. The experiments showed that a steady but unstable state of pulsing could exist in a compartment having both horizontal and vertical openings. This finding therefore provides a new impetus for compartment system analysis in the future. It also exposes the limitations of the single zone fire model where the potential transient

dynamics have not been considered, subsequently leading to the prediction of erratic fire behaviours.

The analysis presented in the above sections provides qualitative considerations to the pulsing actions observed in the Door 2 and the Door 3 experimental series. No quantitative analysis has been made to analyse this pulsing behaviour as this is outside the scope of the study. Further research on this phenomenon is needed to quantify the parameters that are influential to the pulsing action and the limits to prevent the occurrence of the pulsing. The result would be useful to provide a bound for single zone fire model applications.

Chapter 11 PROPOSED SINGLE ZONE FIRE MODEL-CFIRE

This chapter describes the single zone fire model-CFIRE that has been developed utilising the results from the analysis performed in the previous chapters. Verification of the model is performed by comparing the simulated results with the experimental results.

11.1 INTRODUCTION

A fire in a building becomes a threat to a structure when it reaches flashover stage. For the purpose of structural fire designs, the post-flashover fire time-temperature history is required as a design input. Therefore it is highly desirable to have computer programs that calculate the expected fire gas temperature history inside the compartment. There are various post-flashover fire models which have been developed, and these were reviewed and described in Chapter 2. The review and analysis has shown that the current state of post-flashover fire models has the following limitations:

- only one type of fuel, be it either wood or pool, is allowed for each fire simulation;
- all the wood fuels involved inside the compartment are collectively described as plane (1-D), or stick or cylinder (2-D), or cube or sphere (3-D);
- the theory used for vertical window vent flows is only suitable for small size openings; and
- there is no allowance for roof vent opening.

The proposed computer program, CFIRE, has incorporated new advances to these limitations. These advances include:

1. Allowing two types of fuel, namely wood and liquid pool, to coexist inside the same compartment, burning either successively or simultaneously.
2. Creating a library of mass loss rate histories for typical furniture items using real furniture geometry. These mass loss rate profiles can be called upon if encountering furniture with a similar geometry instead of trying to describe all of the furniture items collectively as having a single geometry.
3. Vent flow equations are modified using a correction factor deduced from the line-plume analogy to account for the less well-mixed fire environment in a compartment with a full frontal wall opening.
4. Roof vent openings are accommodated in the model.
5. Allowing up to six different types of enclosure boundaries each with different properties to be specified during the description of the compartment. Two of the six can used to describe a two-layer composite boundary. However, cavity walls are not included.

Of course, CFIRE has not eliminated the many other limitations to existing post-flashover fire models including multiple openings, cross flow, wind effects and progressive burning behaviour. Future studies on these aspects are needed.

11.2 THEORY

The CFIRE model treats the entire fire compartment as a single zone and assumes that it behaves as a well-stirred reactor. The assumptions made are similar to COMPF2. These assumptions are given as follows:

- the gas temperature inside the compartment is uniform, as the spatial temperature variation of the fire gases inside the compartment and the thermal discontinuity close to the floor level are ignored;

- the gas flows across a single vertical window/door opening with/without a horizontal roof vent opening are buoyancy driven due to the temperature difference between the inside compartment and outside ambient environment;
- the reaction is infinitely fast, and the fire heat release rate inside the compartment is limited by the available ventilation rate or the fuel release rate;
- the fire environment is quasi-steady. The time variations in the fuel release rate and the heat losses through the homogenous solid enclosure boundaries with finite thickness are included; and
- the transient terms with regard to the rate of change in the gas phase mass and energy are dropped, as they are negligible under quasi-steady conditions.

The two principal equations for the single zone model are the heat and mass balance equations. These equations are presented as follows:

Heat balance equation

$$\dot{Q}_{FIRE} = \dot{Q}_L + \dot{Q}_R + \dot{Q}_W + \dot{Q}_{FB} \qquad \textbf{(11.1)}$$

where $\dot{Q}_{FIRE}$ is the fire heat release rate inside the compartment, $\dot{Q}_L$ is the heat loss from the convective gas flow, $\dot{Q}_R$ is the radiative losses via the opening, $\dot{Q}_W$ is the convective and radiative heat loss to the enclosing boundaries and $\dot{Q}_{FB}$ is the heat feedback vaporising the fuel.

Mass balance equation

$$\dot{m}_{in} + \dot{m}_p = \dot{m}_{out} + \dot{m}_{roof} \qquad \textbf{(11.2)}$$

where $\dot{m}_{in}$ and $\dot{m}_{out}$ are the mass flow rate of outside ambient air into the compartment and mass flow rate of hot gases out of the compartment via the vertical vent opening, respectively; $\dot{m}_{roof}$ is the mass outflow from the roof opening (zero if there is no roof vent opening); $\dot{m}_p$ is the mass loss rate of the fuel inside the compartment.

The mathematical expressions used to describe the individual terms in both the heat and mass balance equations are described in the following sections.

11.3 VENTILATION

For a fire compartment in which only natural convection conditions prevail, the flows between the compartment and its immediate ambient surrounding through a vent opening are driven by the pressure difference arising from the temperature or density difference between the two quiescent environments. Assuming the fire compartment is well-mixed with a uniform gas temperature (one of the assumptions made in the single zone compartment fire theory), the vent flow equations for a compartment with/without a roof vent opening are given as follows:

11.3.1 No roof vent opening

For a compartment with a vertical wall opening such as a door or a window, having no roof vent opening, the vent flows are described using the following equations (i.e. Equations (3.42) and (3.43) in Chapter 3).

Inflow:

$$\dot{m}_{in} = \frac{2}{3} \cdot \Lambda \cdot C_d \cdot W_v \cdot \rho_0 \cdot \sqrt{2g\left(1 - \frac{\rho_g}{\rho_0}\right)} \cdot (Z_n - \delta)^{3/2} \qquad (11.3)$$

Outflow:

$$\dot{m}_{out} = \frac{2}{3} \cdot \Lambda \cdot C_d \cdot W_v \cdot \rho_g \cdot \sqrt{2g\left(\frac{\rho_0}{\rho_g} - 1\right)} \cdot (H_s - Z_n)^{3/2} \qquad (11.4)$$

where the correction factor, Λ, of 0.6 deduced using the wall line-plume analogy is introduced to account for the less well-mixed environment encountered in a full wall

opening, A_v/A_w =1, such that Λ=1 for A_v/A_w <1, and Λ=0.6 for A_v/A_w =1. Note that the transitional opening fraction, A_v/A_w, is not given. As discussed in Chapter 3, further analysis with reference to experimental fires is necessary to deduce practical correction factors for the various opening geometries.

11.3.2 With roof vent opening

In the case where a compartment has a vertical wall vent and a horizontal roof vent openings, it has been shown that the mathematical vertical vent flow model described above can be extended to describe an additional horizontal roof vent opening. Provided the roof vent is not excessively large and the outflow is unidirectional, the vent flows across the vertical wall opening and the horizontal roof opening can be described using the following equations (Equations (7.3), (7.4) and (7.5) in Chapter 7):

Inflow through vertical wall opening:

$$\dot{m}_{in} = \frac{2}{3} \cdot \Lambda \cdot C_d \cdot W_v \cdot \rho_0 \cdot \sqrt{2g\left(1 - \frac{\rho_g}{\rho_0}\right)} \cdot (Z_n - \delta)^{\frac{3}{2}} \qquad \textbf{(11.5)}$$

Outflow through vertical wall opening:

$$\dot{m}_{out} = \frac{2}{3} \cdot \Lambda \cdot C_d \cdot W_v \cdot \rho_g \cdot \sqrt{2g\left(\frac{\rho_0}{\rho_g} - 1\right)} \cdot (H_s - Z_n)^{\frac{3}{2}} \qquad \textbf{(11.6)}$$

Outflow through horizontal roof opening:

$$\dot{m}_{roof} = C_{d,roofv} \cdot \rho_g \cdot A_{v,roof} \cdot \sqrt{2g\left(\frac{\rho_0}{\rho_g} - 1\right)} \cdot (H_c - Z_n)^{\frac{1}{2}} \qquad \textbf{(11.7)}$$

The mathematical model shows that, provided the gas temperature inside the compartment stays uniform, increasing the roof vent opening will increase the overall

mass outflow. To maintain the mass balance inside the compartment, the neutral-plane will rise allowing more air inflow through the vertical opening. It will reach a point where the neutral-plane is at the same height as the soffit of the vertical opening, and all the air flows into the compartment through the vertical vent and out through the horizontal vent. This condition is reached when

$$H_v = (H_c - \delta) - \left[\left(\frac{2}{3}\right)^2 \cdot \left(\frac{\Lambda C_d}{C_{d,roof}}\right)^2 \cdot \left(\frac{A_v\sqrt{H_v}}{A_{v,roof}}\right)^2 \cdot \frac{\rho_0}{\rho_g} \cdot \left(1 + \frac{\dot{m}_{fuel}}{\dot{m}_{in}}\right)^2 \right] \qquad \textbf{(11.8)}$$

Mathematically, the neutral-plane rises beyond the soffit of the vertical opening when

$$H_v \le (H_c - \delta) - \left[\left(\frac{2}{3}\right)^2 \cdot \left(\frac{\Lambda C_d}{C_{d,roof}}\right)^2 \cdot \left(\frac{A_v\sqrt{H_v}}{A_{v,roof}}\right)^2 \cdot \frac{\rho_0}{\rho_g} \cdot \left(1 + \frac{\dot{m}_{fuel}}{\dot{m}_{in}}\right)^2 \right] \qquad \textbf{(11.9)}$$

In this case, the air inflow through the vertical vent is estimated as

$$\dot{m}_{in} = \frac{2}{3} \cdot \Lambda \cdot C_d \cdot W_v \cdot \rho_0 \cdot \sqrt{2g\left(1 - \frac{\rho_g}{\rho_0}\right)} \cdot \left\{ (Z_n - \delta)^{3/2} - \left[(Z_n - \delta) - H_v \right]^{3/2} \right\} \qquad \textbf{(11.10)}$$

It should be noted that Equation (11.10) has not been experimentally verified. Caution should be exercised when encountering the case where the neutral-plane height is above the soffit of the vertical vent. Such a scenario is likely to occur in a compartment having a roof vent and a small wall opening.

The gas density in the vent flow equations is related to the compartment fire gas temperature using Equation (11.11) assuming ideal gas behaviour.

$$\rho = 353 / T \ \ (in\ Kelvin) \qquad \textbf{(11.11)}$$

It has been noted in Chapter 7 that there exists a limit for which the assumption of unidirectional flow across the horizontal roof vent opening is applicable. This limit is characterised by the critical Froude number as shown in Equation (7.11). Beyond this

limit, bi-directional flow across the roof vent opening can occur. However, neither this limit nor the bi-directional flow behaviour is imposed and accounted for in this program. This is because the critical Froude number given by Yamada (1997) is deduced from experiments with gas temperatures (<300°C) much lower than the typical post-flashover fires. Extrapolation to high temperature is not warranted until further study is conducted. Note that the correction factor, Λ, has been included in conjunction with the roof vent flow calculation. For a compartment having a roof vent opening with a large wall opening, caution should be exercised, as this condition has not yet been thoroughly examined.

11.4 FIRE HEAT RELEASE RATE

The heat release rate from the fire inside the compartment depends on the mass loss rate of the fuel and the air inflow rate into the compartment. The fire environment inside the compartment could either be fuel-rich or fuel-lean, and the corresponding fire heat release rate would be ventilation limited or fuel limited respectively. The status of the fire inside a compartment is described using the global equivalence ratio, Φ, defined as

$$\Phi = \frac{r \cdot \dot{m}_p}{\dot{m}_{in}} \qquad (11.12)$$

where r is the stoichiometric air to fuel mass ratio, $\dot{m}_p$ is the fuel release rate, and $\dot{m}_{in}$ is the ventilating air inflow rate into the compartment. With this definition, the fuel-rich case is indicated by Φ greater than 1, where the amount of fuel being released is greater than the amount that can be completely combusted for the given ventilating air flow rate; for the fuel-lean case, Φ is less than 1, there is sufficient amount of air to completely combust the fuel.

The heat release rate during the fuel lean case is limited by the fuel release rate, whereas during the fuel-rich case, it is limited by the ventilating air inflow rate into

the compartment. Since the combustion reaction inside the compartment is assumed to be infinitely fast, the expressions for the fire heat release rate inside the compartment are described as follows:

For $\Phi<1$ (fuel-lean):

$$\dot{Q}_{fire} = b_p \times \dot{m}_p \times \Delta h_{c,net} \tag{11.13}$$

For $\Phi>1$ (fuel-rich):

$$\dot{Q}_{fire} = b_p \times \frac{\dot{m}_{in}}{r} \times \Delta h_{c,net} = b_p \times \frac{1}{\Phi} \times \dot{m}_p \times \Delta h_{c,net} \tag{11.14}$$

where the net calorific value of the fuel is $\Delta h_{c,net}$ and r is the stoichiometric air to fuel mass ratio. The factor b_p (<1.0), is used to account for mixing inefficiency during combustion. This factor is difficult to quantify and generally has a value ranging between 0.5 and 0.9 (Babrauskas, 1981).

11.5 CONVECTIVE HEAT LOSS

The convective heat loss in the gases flowing out of the compartment window is calculated as the product of the mass flow rate and the enthalpy gained by the gas species due to the increased temperature. This is shown in Equation (11.15) where Y_i is the species mass fraction per unit mass of the mass outflow and h_i is the enthalpy gained by each species due to the temperature increase.

$$\dot{Q}_L = \dot{m}_{out} \times \sum_i Y_i \cdot h_i \tag{11.15}$$

By definition, under constant pressure and ideal gas behaviour, the change of enthalpy for each species is given by Equation (11.16) where c_{pi} is the specific heat of the

individual gas species. The gas species are determined from the chemical equilibrium equation and the temperature dependence of specific heat for each species follows that given in Van Wylen et al (1994).

$$h_i = \int_{T_0}^{T} c_{p_i} \cdot dT \qquad \textbf{(11.16)}$$

The species considered include carbon dioxide (CO_2), water vapour (H_2O), nitrogen gas (N_2), and unburned fuel. The production of these gas species is estimated using chemical equilibrium equations (Equations (4.4) and (4.5)). The existence of other incomplete combustion species such as carbon monoxide (CO), hydrogen (H_2) and soot (C) are neglected for simplicity.

11.6 RADIATIVE HEAT LOSS

The radiative heat loss from the vent opening, $\dot{Q}_R$, is simply represented by a blackbody radiation at gas temperature, T_g. According to the CIB data (Thomas and Heselden, 1972), such a treatment is a reasonable approximation to the radiation flux from the vent opening. The expression for this radiative heat loss term is given in Equation (11.17),

$$\dot{Q}_R = A_v \cdot \sigma \cdot \left(T_g^4 - T_0^4\right) \qquad \textbf{(11.17)}$$

where A_v is the vent opening area, σ is the Stefan-Boltzmann constant, T_g is the gas temperature and T_0 is the temperature of the outside ambient air.

11.7 WALL HEAT LOSS

The term "wall" refers to the enclosure boundaries that include ceiling, walls and floor. These enclosure boundaries are treated as homogeneous solids with constant thermal properties. The heat transfer across the wall is considered to be one-dimensional. For a finite thickness, assuming no internal heat generation, the transient conduction through walls is given by Equation (11.18),

$$\frac{\partial^2 T}{\partial x^2} = \frac{1}{\varphi} \cdot \frac{\partial T}{\partial t} \tag{11.18}$$

where φ is the thermal diffusivity and is defined as

$$\varphi = \left. \frac{k}{\rho \cdot c_p} \right|_{solid}$$

The convective and radiative heat transfer for both the inner and the outer wall surfaces are accounted for and the boundary conditions for each side of the wall are given in Equations (11.19) and (11.20) respectively.

Fire side:

$$-k\left(\frac{\partial T}{\partial x}\right)_{solid,fire} = h_{fire} \cdot \left(T_g - T_{wi}\right) + \sigma \cdot \varepsilon_{res} \cdot \left(T_g^4 - T_{wi}^4\right) \tag{11.19}$$

Ambient side:

$$-k\left(\frac{\partial T}{\partial x}\right)_{solid,amb} = h_{amb} \cdot \left(T_{wo} - T_0\right) + \sigma \cdot \varepsilon_w \cdot \left(T_{wo}^4 - T_0^4\right) \tag{11.20}$$

where the convective heat transfer coefficient for the fire side, h_{fire}, is taken as 25W/m^2-K and 10W/m^2-K for the ambient side, h_{amb}; and ε_{res} is the resultant emissivity between the hot gases and the wall surfaces defined as

$$\varepsilon_{res} = \frac{1}{1/\varepsilon_g + 1/\varepsilon_w - 1} \tag{11.21}$$

The transient heat transfer across the wall is solved using the finite difference method. In the CFIRE model, each wall is divided into 10 layers of equal thickness giving 9 internal nodal points and 2 external boundary nodal points. The nodal heat transfer expression can be obtained by applying the heat balance method on each node, which consists of the temperature term of the two adjacent nodes, with the exception of the expressions for the two boundary nodes that are subjected to both the convective and the radiative boundary conditions. The Crank-Nicolson method is used instead of the implicit or the explicit method, because it has the advantage of numerical stability for all of the Fourier numbers or Δt and the least accumulated truncation error for the numerical system (Croft and Lilley (1977)). These nodal expressions can be arranged in the form of a matrix and solved simultaneously at each time interval. For a two-layer composite wall, with each having different thermal properties, the treatment is similar to the single homogeneous solid wall, such that each layer is divided into 10 slices of equal thickness. The interface node is modified to account for the different thickness and thermal properties between the two adjacent slices. Details of the nodal equations expressed using the Crank-Nicolson method are presented in Appendix E.

The heat transfer and hence the temperature profile across the wall is solved at successive time-step as the fire progresses. The CFIRE model allows the specification of up to six different types of enclosure boundaries. The total heat losses from these enclosing walls are estimated as:

$$\dot{Q}_W = \sum_j A_{t,j} \cdot h_{fire} \cdot \left(T_g - T_{wi,j}\right) + A_{t,j} \cdot \sigma \cdot \varepsilon_{res} \cdot \left(T_g^4 - T_{wi,j}^4\right) \tag{11.22}$$

where $A_{t,j}$ and $T_{wi,j}$ are the area (m^2) and the inside wall surface temperature (K) of the j-th wall of the compartment respectively.

11.8 FEEDBACK TERM

This is the heat required to vaporise the unburned fuel. The feedback term is evaluated as

$$\dot{Q}_{FB} = \left(\dot{m}_p - \dot{Q}_{FIRE} / \Delta h_{c,net}\right) \times L_g \qquad \textbf{(11.23)}$$

The bracketed term refers to the amount of fuel that has not been burned. By definition, the energy feedback required to vaporise the liquid or solid fuel has been included in the value of net heat of combustion, $\Delta h_{c,net}$. Therefore, the feedback term is to account for the fuel that has been released but is not participating in the combustion.

11.9 FUEL MASS LOSS RATE MODELS

Two general types of fuel are considered: (1) cellulosic or wood-based fuel; and (2) non-charring pool-like fuel. Both of these fuels exhibit very different burning behaviours. The mass loss rate models for each fuel type are presented as follows.

11.9.1 Wood

For wood fuels burning inside a post-flashover compartment, there exist three possible burning regimes, namely fuel surface controlled, porosity controlled and ventilation controlled. In each regime, the fuel mass loss rate is estimated using a characteristic parameter. These three regimes are briefly described as follows.

11.9.1.1 Fuel surface controlled

During the fuel surface controlled regime, the fuel mass loss rate is determined by the exposed fuel surface area and a prescribed regression rate. Ödeen's method (as Equation (6.5)) has been used to describe the fuel mass loss rate at this regime.

$$\frac{\dot{m}_p}{M_0} = \frac{F}{D/2v_p} \cdot \left(\frac{m(t)}{M_0}\right)^{1-\frac{1}{F}} \quad \textbf{(11.24)}$$

This method describes the mass loss rate based on the change in surface area of a simple geometrical shape with a characteristic dimension, D, over time, at a constant regression rate. Alternatively, Equation (11.24) can be expressed as

$$\dot{m}_p = v_p \times \rho_{wood} \times A_{exposed}(t) \quad \textbf{(11.25)}$$

where the mass loss rate is the product of the regression rate, v_p, the density of the fuel, ρ_{wood} and the remaining exposed surface area of the fuel at time t, $A_{exposed}(t)$. The total exposed surface area depends on the initial shape of the fuel as well as the total amount of fuel. As the burning progresses, as described by the regression rate, v_p, the remaining fuel surface area will decrease with time due to the burning away of the fuel items.

In the CFIRE model, a catalogue of individual mass loss history of furniture items is stored in the program. The mass loss rate history for each furniture item is deduced from Equation (11.25) using detailed geometrical measurement made on each furniture item with a constant regression rate of 0.011mm/s (Yii, 2000).

User can select the furniture items by their code name as the fuel load for fire simulation purposes. The geometries of the furniture items, their respective code names and their mass loss histories are presented in Appendix B.

11.9.1.2 Porosity controlled

For fuel that is densely packed together, such as in the form of densely packed wood cribs, the mass loss rate is dependent on the vertical shaft area inside the fuel. This is known as a porosity controlled burning regime. The mass loss rate is characterised by the stick clear spacing to crib height ratio, S/h_{crib}, such that,

$$\dot{m}_p = 4.4\times10^{-4}\left(\frac{S}{h_{crib}}\right)\frac{M_o}{D} \qquad \textbf{(11.26)}$$

It should be noted that the above equation is deduced from densely packed wood cribs. For this reason, its application is restricted to modelling wood cribs. With regard to wooden furniture, this regime is not considered.

11.9.1.3 Ventilation controlled

Ventilation controlled burning regime occurs when there is not enough oxygen to burn all the exposed fuel surfaces. This is the maximum mass loss rate for wood fuels, such that an increase in fuel surface area would not result in an increase in the mass loss rate. The ventilation controlled mass loss rate has been estimated by using the equivalence ratio expression (Equation (11.12)) which links the mass loss rate with the ventilation.

From the ventilation analysis presented in Chapter 9, for a compartment with both horizontal and vertical openings, provided the neutral-plane height is at or below the vertical wall vent opening, the air inflow into the compartment via the wall vent opening can be approximated as follows (i.e. Equation (9.14) in Chapter 9):

$$\dot{m}_{in} \approx 0.45A_v\sqrt{H_v} + 0.91A_{v,roof}\sqrt{H_c-(H_v+\delta)} \qquad \textbf{(11.27)}$$

And in the case where the wall opening has no downstand, i.e. soffit at the roof level, the air inflow into the compartment via the wall vent opening is approximated as (i.e. Equation (9.18) in Chapter 9):

$$\dot{m}_{in} \approx 0.5A_v\sqrt{H_v}\cdot\left(1+\left(A_{v,roof}/A_v\right)-0.1\left(A_{v,roof}/A_v\right)^2\right) \qquad \textbf{(11.28)}$$

Babrauskas (1995) suggested that wood crib fires inside a compartment can burn in a slightly fuel-rich environment but no greater than 35% fuel-rich, i.e. a maximum of Φ=1.35. This is a useful upper limit for describing the ventilation controlled burning regime. Given that the stoichiometric air to fuel mass ratio for wood, r,

($CH_{1.455}O_{0.645}$•$0.18H_2O$) is 5.3, setting Φ=1.35 and substituting the appropriate expressions for the air inflow rate (Equations (11.27) and (11.28)) into the equivalence ratio equation (Equation (11.12)), the respective ventilation controlled mass loss rate expressions are deduced:

For wall opening having a finite downstand depth, $(H_c-(H_v+\delta)) >0$,

$$\dot{m}_p \approx 0.12 A_v \sqrt{H_v} + 0.23 A_{v,roof} \sqrt{H_c - (H_v + \delta)} \qquad \textbf{(11.29)}$$

For wall opening having no downstand, $(H_c-(H_v+\delta)) =0$,

$$\dot{m}_p \approx 0.12 A_v \sqrt{H_v} \cdot \left(1 + \left(A_{v,roof}/A_v\right) - 0.1\left(A_{v,roof}/A_v\right)^2\right) \qquad \textbf{(11.30)}$$

The full frontal wall opening effect is only considered when no roof vent opening is involved. As shown in Equation (6.14b), the ventilation controlled mass loss rate in a compartment with a full frontal opening is estimated as:

$$\dot{m}_p \approx 0.07 A_v \sqrt{H_v} \qquad \textbf{(11.31)}$$

Note that for a compartment without a roof vent opening, the mass loss rate expressions given in Equations (11.29) and (11.30) are the same as given by Babrauskas (1981 and 1995).

11.9.1.4 Application and actual mass loss rate

In the CFIRE program, the user can select relevant furniture items, with their individual mass loss rate histories catalogued in the program. Ödeen's model, Equation (11.24), and the crib porosity model, Equation (11.26) are also provided to model the burning of wood crib. The mass loss rate history for the specified wood crib is sorted by using the minimum rate calculated between these two equations over time. After specifying the fuels, the individual mass loss rates from these items are summed to give the overall fuel controlled mass loss rate. If the overall fuel controlled

mass loss rate is greater than the ventilation controlled rate, the actual mass loss rate will be at the rate controlled by the ventilation (Equations (11.29), (11.30) or (11.31)), until the fuel surface area diminishes to a level that gives a mass loss rate less than the ventilation controlled rate. After that, the fire is fuel controlled. However, in the case where the overall fuel mass loss rate is less than the ventilation controlled rate, the fire will be fuel controlled over the entire duration. This has been schematically shown in Figure 6.13 in Chapter 6. The essence of this treatment is to allow the burning of fuel to switch from ventilation controlled to fuel controlled burning over the fire duration. A t-squared growth fire (Buchanan, 2002) as given in Equation (11.32) at a user specified rate is added at the front of the actual mass loss rate history to include the growth phase.

$$\dot{Q}_{growth} = \dot{m}_p \cdot \Delta h_{c,net} = \left(t/k_{growth}\right)^2 \qquad (MW) \qquad \textbf{(11.32)}$$

or

$$\dot{m}_p = \left(t/k_{growth}\right)^2 / \Delta h_{c,net} \qquad (kg/s)$$

where $\dot{Q}_{growth}$ is the t-squared heat release rate (MW), t is the time (s), and k_{growth} is the growth constant ($s/\sqrt{MW}$), with k_{growth} =600 for slow growth rate, 300 for medium growth rate, 150 for fast growth rate and 75 for ultra-fast growth rate. Note that converting the t-squared heat release rate, $\dot{Q}_{growth}$ (MW), to fuel mass loss rate, $\dot{m}_p$ (kg/s), would require the division by the fuel heat of combustion, $\Delta h_{c,net}$, in the form of MJ/kg.

The t-squared fire grows until the mass loss rate reaches the onset of the actual mass loss rate history. The t-squared growth and the actual mass loss rate curve inside the compartment are then used in the fire gas temperature calculation.

11.9.2 Pool

The pool fire analysis performed in Chapter 5, showed that in a fuel-rich environment, Φ>1, the fuel vaporisation rate is dominated by the radiation from the surrounding hot environment. Assuming that the pool burning inside a compartment is receiving

radiation directly from the hot gases and the view factor between the pool and the room is 1.0, the mass loss rate of the pool is given as follows:

$$\dot{m}_p = A_{pool} \frac{\alpha \varepsilon_g \sigma T_g^4 - \sigma T_v^4}{L_g} \tag{11.33}$$

where A_{pool} is the area of the pool, ε_g is the gas emissivity, σ is the Stefan-Boltzmann constant, T_g is the compartment gas temperature, T_v is the fuel boiling temperature, and L_g is the heat of gasification of the liquid fuel. The term, α, is the attenuation factor, having a value less than or equal to unity. A value of 0.65 is taken as typical from the heptane fire analysis performed in Chapter 5. Note that if α is set as 1.0, it assumes there is no attenuation by the fire plume and the vaporising fuel above the pool and the radiation heat flux from the surrounding hot gases is fully imposed on the fuel surface.

11.9.2.1 Fire growth phase

Since the fire model has been developed to investigate a post-flashover fire, the pool burning behaviour before flashover is not explicitly modelled. The growth stage is simply modelled using a t-squared fire growth at a user specified rate given in Equation (11.32). The "switch-over" from the t-squared mass loss rate to that of a radiation driven mass loss rate (Equation (11.33)) is determined by the gas temperature inside the compartment, such that a high enough gas temperature has to be reached before producing a fuel-rich environment (i.e. Φ>1). This "switch-over" temperature is given in Equation (11.34) by substituting Equation (11.33) into the expression for equivalence ratio, Equation (11.12), with Φ set to be greater than 1.

$$T_g > \left\{ \left[\left(\frac{\dot{m}_{in}}{A_{pool}} \cdot \frac{L_g}{r} \right) + \sigma T_v^4 \right] \Big/ \left(\alpha \varepsilon_g \sigma \right) \right\}^{1/4} \tag{11.34}$$

Note that during the growth phase, should the t-square mass loss rate exceed the stoichiometric mass loss rate ($\dot{m}_{in}/r$) for the given ventilation, the stoichiometric mass loss rate is used until the gas temperature inside the compartment has reached

the "switch-over" temperature defined by Equation (11.34). After the "switch-over" temperature has been reached, the pool mass loss rate is described using Equation (11.33).

11.10 BURNING OPTIONS FOR MIXED FUEL TYPES

One of the advancements made in the CFIRE program is that of allowing the coexistence of wood and pool fuels inside a single compartment. For compartments consisting of both wood-based fuels and liquid/thermoplastics fuels, two burning options are available for modelling. Option (1) is the successive burning option that assumes the pool fuel to burn first, followed by the wood. This option allows the pool fire to burn at a mass loss rate prescribed by Equation (11.33) until close to exhaustion, defined by the remaining fuel mass in the pool specified by the user. This is followed by the burning of the wood fuels with the mass loss rate subjected to either fuel surface or ventilation control. Option (2) is the simultaneous burning option that assumes the pool and the wood burn together after flashover. This option sets the wood fuel to ignite and burn first with a t-squared growth rate, then after the inside compartment gas temperature reaches the "flashover" temperature (set as 500°C in the model), the mass loss rate of the pool (evaluated using Equation (11.33)) is added on top of the mass loss rate of wood. Note that in the simultaneous burning option, the effective stoichiometric air to fuel mass ratio and the combined heat release rate from the two sources, both in term of unit mass of total fuel released, are calculated over time. Depending on the ventilation conditions, the eventual fire heat release rate inside the compartment is evaluated using Equations (11.13) or (11.14).

11.11 CALCULATING FIRE GAS TEMPERATURE

The fire gas temperature calculation involves estimating an initial fire gas temperature, followed by the calculation of the equivalence ratio from the mass loss rate of the fuel and the air inflow rate. The equivalence ratio is used to determine the fire heat release rate, the combustion species production and hence the convective heat loss. Together with the heat loss terms for vent radiation and wall heat losses, the fire heat release rate is compared with the total heat loss, i.e. the heat balance equation. If the equation is not in balance, a new temperature is tried until it is balanced. The calculated fire gas temperature is stored and the wall temperature profile is updated over the single time step. The operation then moves to the next time step until the duration specified by the user is reached.

11.12 OPERATING ALGORITHM

The computer program called the CFIRE is written in MATLAB. The operating algorithm is presented as follow.

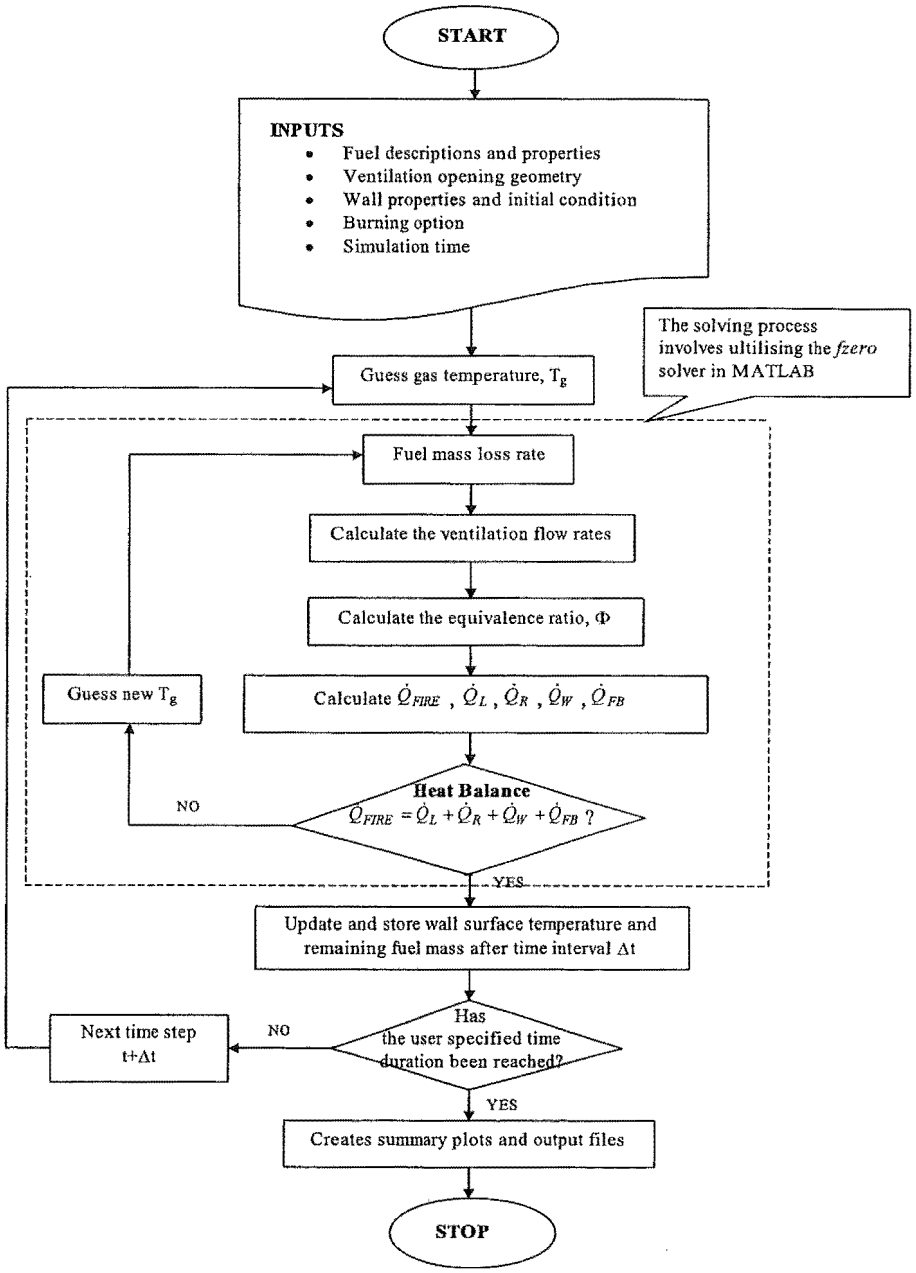

Figure 11.1 Operating algorithm for the CFIRE computer program.

11.13 VERIFICATION OF FIRE MODEL

The objective of a mathematical fire model is to predict the outcome of real fires. Its adequacy for predicting the expected fire is determined by comparing the simulated results against experimental results. There are numerous post-flashover compartment fire experiments being reported around the world. The type of fuel used in these experiments range from wood cribs, to thermoplastics or liquid pool, to real furniture items. The instrumentation and hence measurements made between experiments also varies. The measurements range from simply measuring the gas temperature inside the compartment with the overall fuel mass loss history, to including vent flow measurements. Subjected to the availability of data, only a selection of experiments were used to verify the CFIRE program. These fires are described below.

11.13.1 NFSC Fires

Numerous compartment fire tests were carried out at the Centre Technique Industriel de la Construction Métallique (CTICM) in France as part of the NFSC (Natural Safety Fire Concept) programme in Europe. These tests are reported in considerable detail by Arnault et al (1973 and 1974) and Roy (1993a, 1993b, 1993c). The test data is available in the form of electronic spreadsheet files.

Most of these tests involved wood fires, but some involved a fuel load consisting of combinations of real furniture, paper and wood. The measurements provided include the fuel mass loss history. Also recorded are the mean temperature, and maximum and minimum temperatures histories inside the compartment. Feasey (1999) indicated that these temperatures were taken by ten thermocouple recordings inside the compartment, with five located 700mm below ceiling level and five 1050mm above the floor level. The maximum and minimum temperature histories presented in the data are actually the maximum and minimum temperature measured respectively at any thermocouple at the particular time step.

The fuel mass loss rate data and the fire gas temperature history from these tests present an opportunity to test the adequacy of the CFIRE program. The

experimentally measured fuel mass loss rate history is used as the input in the following verification exercise. This would reveal the adequacy of applying the single zone theory to describe the fire temperature history inside a post-flashover compartment. In this verification exercise, only a selection of wood fire tests is presented for illustrative purposes. These tests are selected to represent a wide range of vent opening geometries. The attributes of these tests are summarised in Table 11.1.

Table 11.1 NFSC experimental fires.

NFSC No.	Room height (m)	Room width (m)	Room depth (m)	Vent height (m)	Vent width (m)	$A_v\sqrt{H_v}$ ($m^{2.5}$)	A_v/A_w (–)	Compartment lining
19	3.13	3.38	3.68	2.18	1.18	3.8	0.24	N / A
33	3.13	3.38	3.68	2.18	1.18	3.8	0.24	INSULATED
47	3.13	3.38	3.68	2.18	1.18	3.8	0.24	INSULATED
40	3.13	3.38	3.68	2.18	1.95	6.3	0.40	INSULATED
41	3.13	3.38	3.68	2.18	1.95	6.3	0.40	INSULATED
42	3.13	3.38	3.68	2.18	1.95	6.3	0.40	INSULATED
79	3.13	3.10	3.60	2.00	3.00	8.5	0.62	N / A
80	3.13	3.10	3.60	2.00	3.00	8.5	0.62	N / A
81	3.13	3.10	3.60	2.00	3.00	8.5	0.62	N / A
44	3.13	3.38	3.68	2.92	2.18	10.9	0.60	INSULATED
45	3.13	3.38	3.68	2.92	2.18	10.9	0.60	INSULATED
46	3.13	3.38	3.68	2.92	2.18	10.9	0.60	INSULATED

The test compartment walls were constructed of 16cm of hard brick (fire side) and 11.5cm of normal brick (ambient side); the ceiling and the wall that contained the vent were constructed of 17.5cm of lightweight concrete. The floor was constructed of refractory concrete. In the cases indicated as INSULATED in the table, the ceiling and the walls were insulated using 2.5cm vermiculite insulation. The material properties used in the simulation for these boundaries are listed in Table 11.2. In the cases with vermiculite insulation, the walls were modelled using the two-layer composite wall with the vermiculite layer at the fire side and the combined hard and normal brick on the adjacent layer at ambient side using the mean weighted properties. In the cases without vermiculite insulation, the hard brick and normal brick

were separate entries modelled as a two-layer composite wall. It should be noted that in these simulations, the heat loss from the floor was not accounted for, as it was assumed that the floor was covered by the fuel inside the compartment.

Table 11.2 Wall properties used in fire modelling for NFSC fires.

Material	Thickness (m)	k (W / m K)	ρ (kg / m^3)	c_p (J / kg K)	ε_w
Vermiculite	0.025	0.2	200	1850	0.9
Light weight concrete	0.175	0.75	1800	840	0.9
Hard brick	0.160	1.32	2000	840	0.9
Normal brick	0.115	0.69	1600	840	0.9
Mean weighted normal and hard brick	0.275	1.06	1833	840	0.9

The cellulosic fuel properties used for the simulations are listed in Table 11.3.

Table 11.3 Fuel properties and modelling parameters used in fire modelling for NFSC fires.

Fuel composition	$CH_{1.455}O_{0.645} \bullet 0.18\ H_2O$
Net heat of combustion, $\Delta h_{c,net}$	15100 kJ/kg
Heat of gasification, L_g	4000 kJ/kg
Stoichiometric air to fuel mass ratio, r	5.3
Modelling Parameters	
Combustion mixing factor, b_p	0.95
Emissivity of fire gas, ε_g	0.9

Note: The emissivity of fire gas from wood fuel is taken as 0.9 for full-size compartments with sizes greater than 2-3m (Babrauskas and Williamson, 1978).

Figure 11.2 presents the simulation results for the above fires compared with the respective mean fire temperature measured during the experiments. It can be seen that the simulations compare favourably with the experimental fire temperature.

It is noted that the model predicts a slightly lower gas temperature at large openings, and a faster decay rate compared to the experiments. Because the temperature is evaluated using the fire heat release rate inside the compartment, which is the product between the fuel mass loss rate and the fuel heat of combustion, given the fuel mass loss rate history is an input, the low heat release rate is due to the low heat of combustion value being used in the model. In the model, the heat of combustion for wood is taken as 15.1MJ/kg, which accounts for 12% moisture content by weight (c.f. ~18.8MJ/kg for dry wood). For wood having lower moisture contents than 12% will have heat of combustion values greater than 15.1MJ/kg. It should be noted that since the model used a single heat of combustion value for the entire burning duration for wood, this treatment does not accommodate the oxidation of char. The heat of combustion for char is approximately 33MJ/kg (Harmathy, 1972), about two times the heat of combustion value of wood used in the model. When the burning of char dominates, particularly at the later stage of the burning, the resulting heat release rate inside the compartment could be larger than predicted. Since the CFIRE model uses a single constant heat of combustion of wood to model the entire duration of the burning, such a treatment is one of the limitations associated with the model.

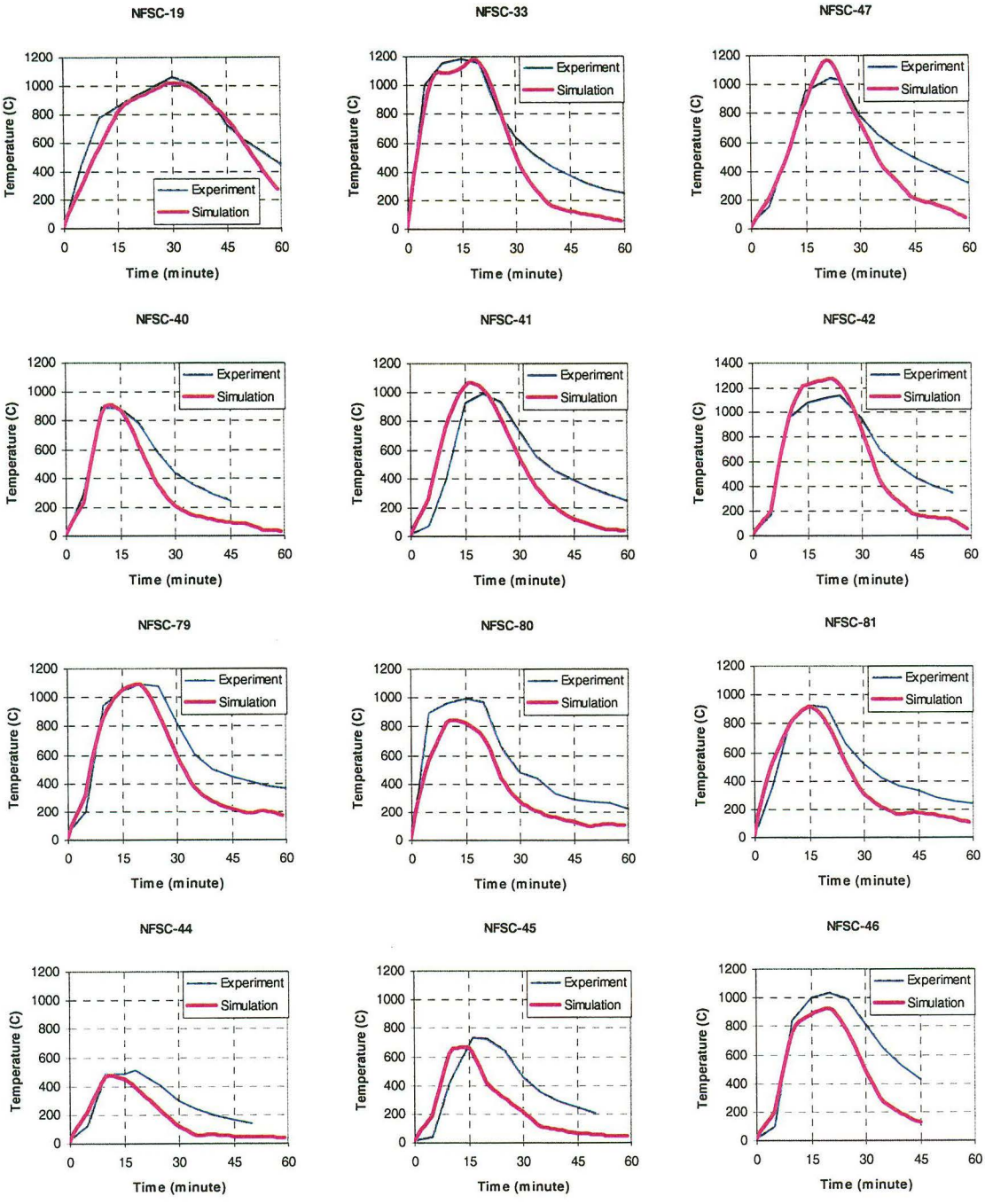

Figure 11.2 Comparison between simulated and experimental temperature results for NFSC wood fires.

From the comparisons between the simulated and the experimentally measured temperature results, it can be seen that the CFIRE program is adequate for modelling the post-flashover compartment fires. However, the fuel mass loss rate history inside the compartment needs to be known.

This is echoed in the post-flashover fires study by Feasey (1999) and Feasey and Buchanan (2002) who provided a method to describe the fuel mass loss rate history utilising the mass loss rate routines in COMPF2. It is to produce a representative mass loss rate history that describes the burning of wood for the particular fuel load and ventilation opening, thereby producing a representative fire gas time-temperature history.

With regard to the furniture mass loss rate models in the CFIRE program, no verification was made, as no corresponding data is available.

11.13.2 Parkes (1996) compartment pool fires

Parkes (1996) conducted a series of small-scale post-flashover compartment fires using liquid heptane in the form of pool. His experiments have been described in Chapter 5. The measurements made include the temperature inside the compartment and the fuel mass loss rate. His data is used to test the pool fire model (Equation (11.33)) in the CFIRE program. Table 11.4 tabulates the experiments performed by Parkes (1996).

Table 11.4 Summary of the test matrix from Parkes (1996) fire experiments.

Experiment Test #	H_v (m)	W_v (m)	A_v (m^2)	$A_vH_v^{0.5}$ ($m^{2.5}$)
1	0.5	0.125	0.0625	0.0442
2	0.5	0.0625	0.0163	0.0221
3	0.5	0.03125	0.0156	0.0110
4	0.375	0.125	0.0469	0.0287
5	0.375	0.0625	0.0234	0.0144
7	0.25	0.125	0.0313	0.0156
8	0.25	0.0625	0.0156	0.0078
11	0.25	0.125	0.0313	0.0156
12	0.5	0.03125	0.0156	0.0110
13	0.375	0.03125	0.0117	0.0072
14	0.5	0.125	0.0625	0.0442

Note: Tests 9 and 10 not included as fire self extinguished. Test 6 is not included as the data were not recorded.

The walls of the test compartment were composite, lined with layers of different materials, including calcium silicate and gypsum plaster boards. The wall properties used in the fire modelling are tabulated in Table 11.5. The total area for ceiling, side-walls and back-wall is $5.2m^2$, the area for the floor is $1.37m^2$ (neglecting the pool area) and the area for the wall that contains the vent is $0.926m^2$ minus the vent opening area.

Note that since the CFIRE program could only model the wall up to two layers of composite, these walls are modelled as kaowool layer on top of a combined layer defined by the mean weight average of the calcium silicate and gypsum plaster boards.

Table 11.5 Wall properties used in fire modelling for Parkes (1996) experiments.

Wall	Type	Thickness (m)	Conductivity (W / m K)	Density (kg / m^3)	Heat capacity (J / kg K)	Emissivity
Ceiling, side-walls and back-wall	Kaowool blanket	0.075	0.04	160	1000	0.9
	Calcium silicate	0.020	0.23	900	1293	0.9
	Gypsum plaster	0.020	0.48	1440	840	0.9
	Weighted average gypsum + calcium silicate	0.040	0.36	1170	1067	0.9
Floor	Kaowool blanket	0.025	0.04	160	1000	0.9
	Calcium silicate	0.040	0.23	900	1293	0.9
	Gypsum plaster	0.020	0.48	1440	840	0.9
	Weighted average gypsum + calcium silicate	0.060	0.31	1080	1142	0.9
Vent wall	Calcium silicate	0.020	0.23	900	1293	0.9

The fuel properties and modelling parameters used are presented in the Table 11.6.

Table 11.6 Fuel properties and modelling parameters used in the fire modelling for Parkes (1996) experiments.

Fuel composition	C_7H_{16}
Net heat of combustion, $\Delta h_{c,net}$	44500 kJ/kg
Heat of gasification, L_g	500 kJ/kg
Stoichiometric air to fuel mass ratio, r	15.1
Modelling Parameters	
Combustion mixing factor, b_p	0.7
Emissivity of fire gas, ε_g	0.7
Attenuation factor, α	0.65
Pool area	$0.031m^2$

Note: Because the absorption coefficient for heptane fire is unknown, the emissivity of heptane fire gas is estimated as 0.7 due to the small size of the compartment involved (see Chapter 5).

In the modelling exercises performed, the fuel mass loss rate for each test was not an input but was calculated using the pool model in the CFIRE program.

Figure 11.3 compares the time-average temperature history measured from the two thermocouple-trees inside the compartment during the experiment with the temperature history calculated from the CFIRE program for each test. The agreement between the simulations results from the CFIRE program and the experimental measurements is good.

Figure 11.4 compares the simulated mass loss rate of fuel from the model to that measured during the experiment. It can be seen that the pool model produces satisfactory mass loss rate results compared to the measurements made during the experiments.

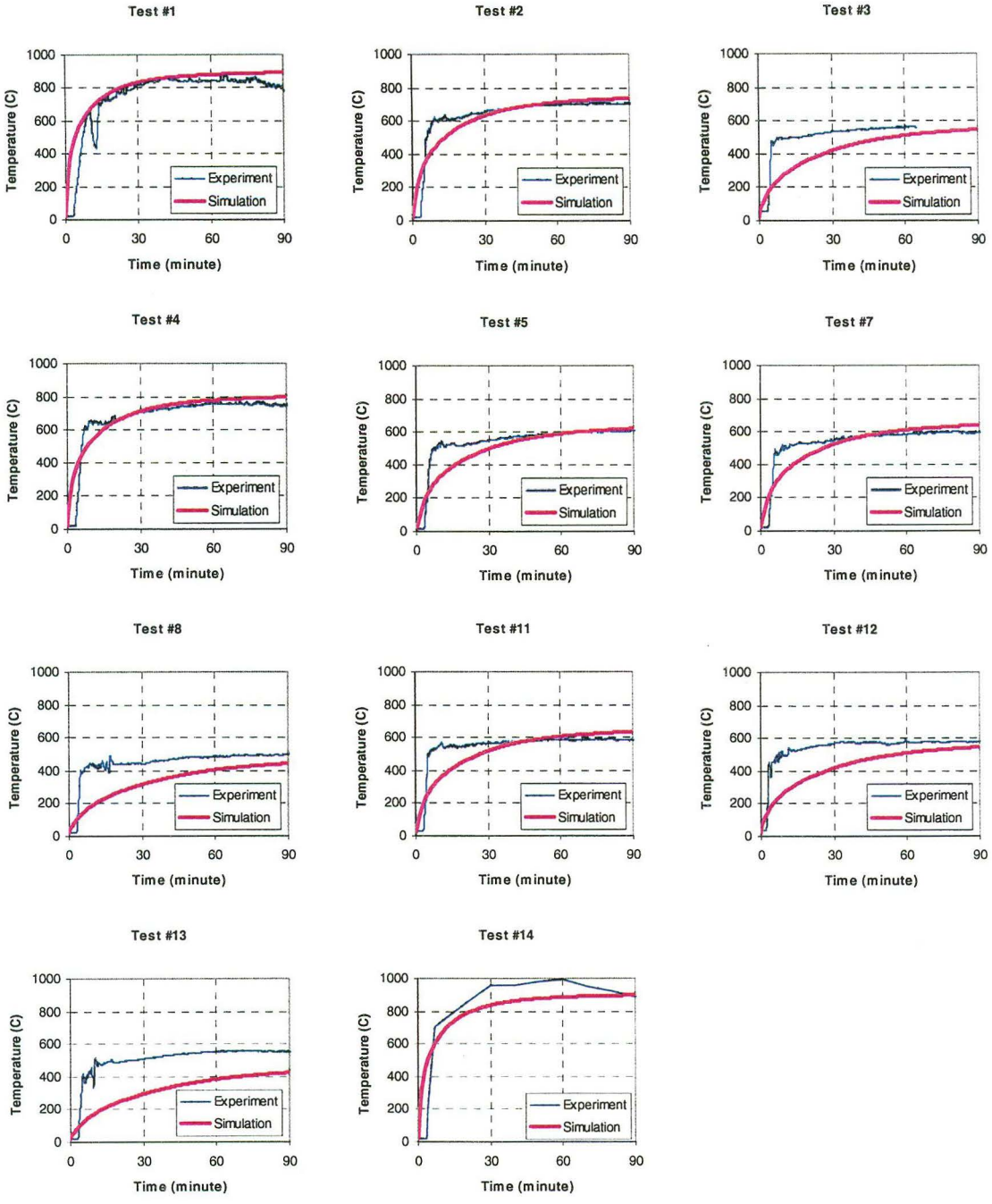

Figure 11.3 Comparison between the simulated and experimental temperature results for heptane pool fires from Parkes (1996) experiments.

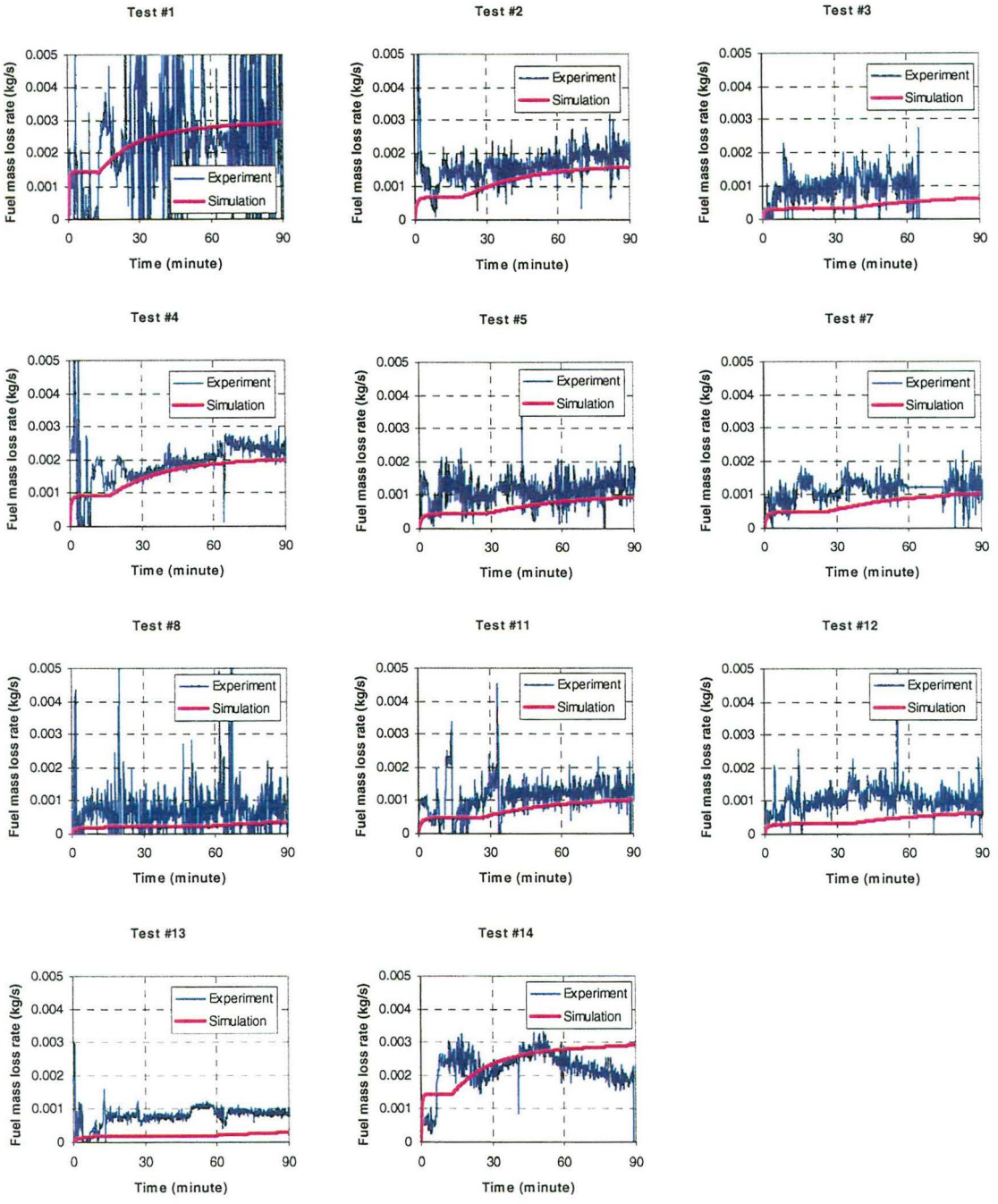

Figure 11.4 Comparison between the simulated and experimental fuel mass loss rate results for heptane pool fires from Parkes (1996) experiments.

11.13.3 Yii (author) compartment pool fires

The author conducted a series of small-scale compartment fire experiments with roof and door vent openings. The compartment had an internal dimension of 1m high by 1m wide by 1.5m deep lined with kaowool ceramic fibre insulating boards. A heptane

pool of 0.3m in diameter was used as the fire source. Details of the experiments have been reported in Chapter 8. In the experimental series, apart from measuring the gas temperature inside the compartment and the fuel mass loss rate, the gas flow rates across the door opening were also measured. Therefore this provides an opportunity to verify the vent flow models used in the CFIRE program. Table 11.7 provides the summary of the test matrix for the Door 1 experimental series.

The wall properties and fuel properties used in the fire modelling for the author's experiments are presented in Table 11.8 and Table 11.9 respectively. In these modelling exercises, the fuel mass loss rate for each test was not an input but was calculated using the pool model in the CFIRE program.

Table 11.7 Summary test matrix for the Door 1 experimental series.

Test	Sill (m)	H_v (m)	W_v (m)	$A_v\sqrt{H_v}$ ($m^{2.5}$)	H_c (m)	$A_{v,roof}$ (m^2)	$A_{v,roof}\sqrt{(H_c-H_v)}$
D1R0	0	0.45	0.25	0.075	1.0	0	0
D1R150	0	0.45	0.25	0.075	1.0	0.018	0.013
D1R250	0	0.45	0.25	0.075	1.0	0.049	0.036
D1R300	0	0.45	0.25	0.075	1.0	0.071	0.053

Table 11.8 Wall properties used in the fire modelling for Yii's experiments.

Wall	Type	Thickness (m)	Conductivity (W / m K)	Density (kg / m^3)	Heat capacity (J / kg K)	Emissivity
Ceiling, side-walls and back-wall	Kaowool vacuum board	0.025	0.15	250	1000	0.9
	Kaowool blanket	0.050	0.04	160	1000	0.9
Floor and front wall	Kaowool vacuum board	0.050	0.15	250	1000	0.9

Table 11.9 Fuel properties and modelling parameters used in the fire modelling for Yii's experiments.

Fuel composition	C_7H_{16}
Net heat of combustion, $\Delta h_{c,net}$	44500 kJ/kg
Heat of vaporisation, L_g	500 kJ/kg
Stoichiometric air to fuel mass ratio, r	15.1
Modelling Parameters	
Combustion mixing factor, b_p	0.7
Emissivity of fire gas, ε_g	0.7
Attenuation factor, α	0.65
Pool area	$0.071m^2$

Note: Because the absorption coefficient for heptane fire is unknown, the emissivity of heptane fire gas is estimated as 0.7 due to the small size of the compartment involved (see Chapter 5).

Figure 11.5 to Figure 11.8 present the comparisons between the experimentally measured results and the simulation results from CFIRE. The results compared are: (a) the average gas temperature inside the compartment; (b) the mass flow rates across the door vent, (c) the fuel mass loss rate; and (d) the neutral-plane height at the door. It can be seen that overall CFIRE produced satisfactory predictions to these attributes. The vent flow predictions compare well with the experimental measurements. Note that the decrease in the experimentally measured mass flow rate of air and the neutral plane height over time observed in the plot is due to the effect of soot build-up on the velocity probes as discussed in Chapter 9. The satisfactory comparison made between the experimental and simulation results suggested that CFIRE can be used to model post-flashover fires inside a compartment with both horizontal and vertical openings. However, it should be noted that the vent flow model has not been tested under the condition at which the neutral-plane height is above the soffit height of the door opening. This is because the tests designed to investigate this condition, i.e. the Door 2 and Door 3 series, had produced an unexpected pulsing behaviours as described in Chapter 9. The pulsing phenomenon observed in both the Door 2 and Door 3 series also highlights the inadequacy of the CFIRE model as it fails to describe these transient dynamic behaviours.

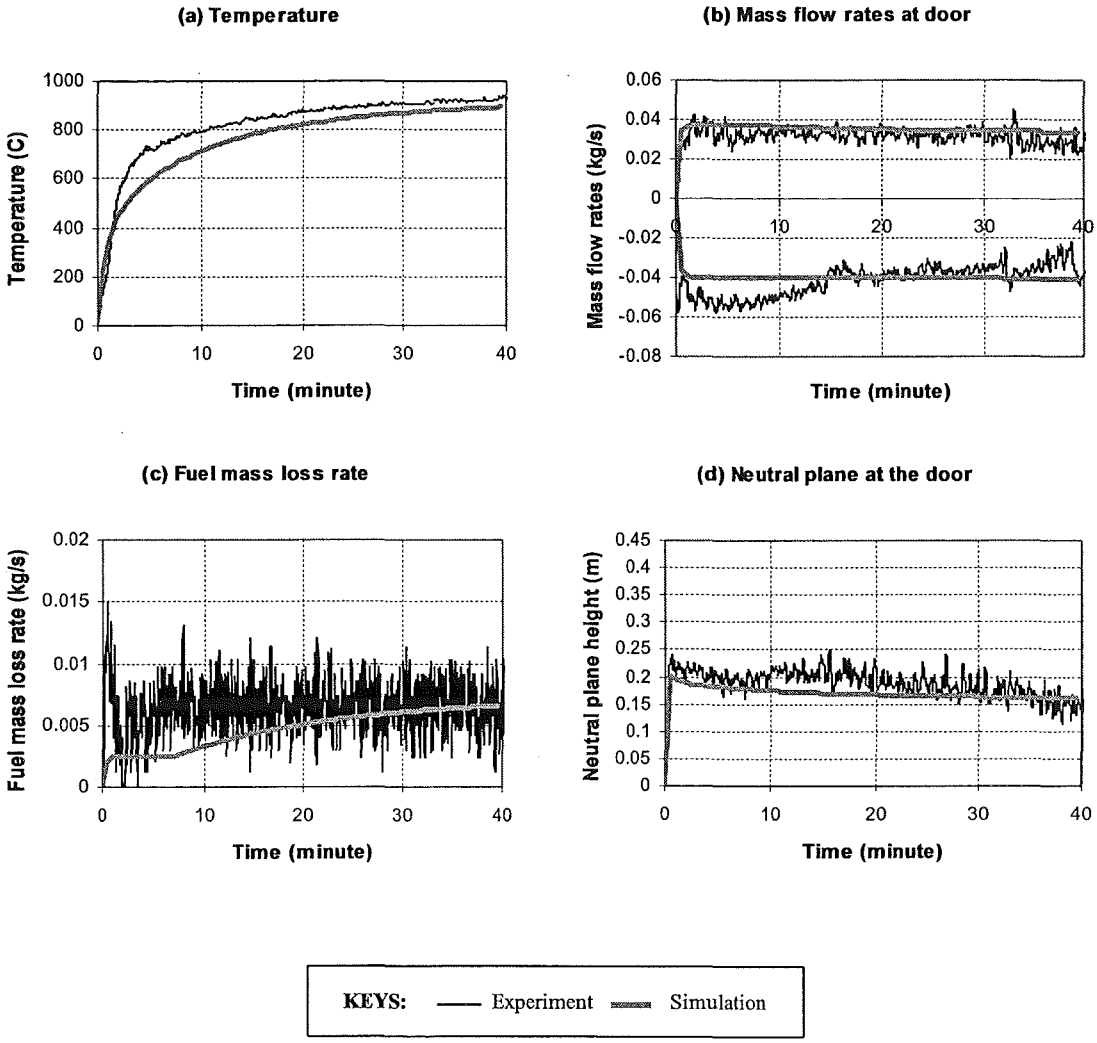

Figure 11.5 **Comparisons between the experimentally measured results and simulations results from the CFIRE program for D1R0 experiment.**

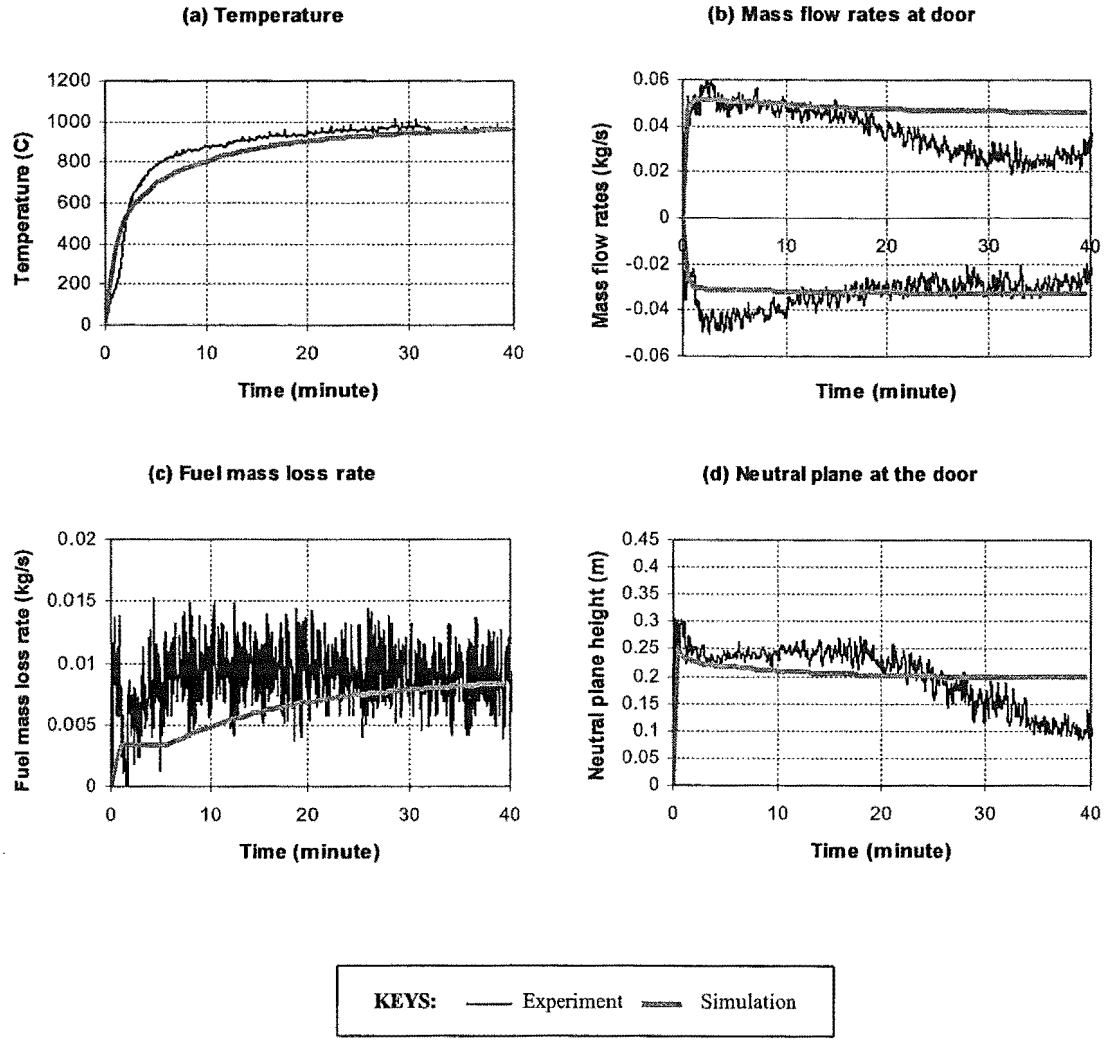

Figure 11.6 Comparisons between the experimentally measured results and simulations results from the CFIRE program for D1R150 experiment.

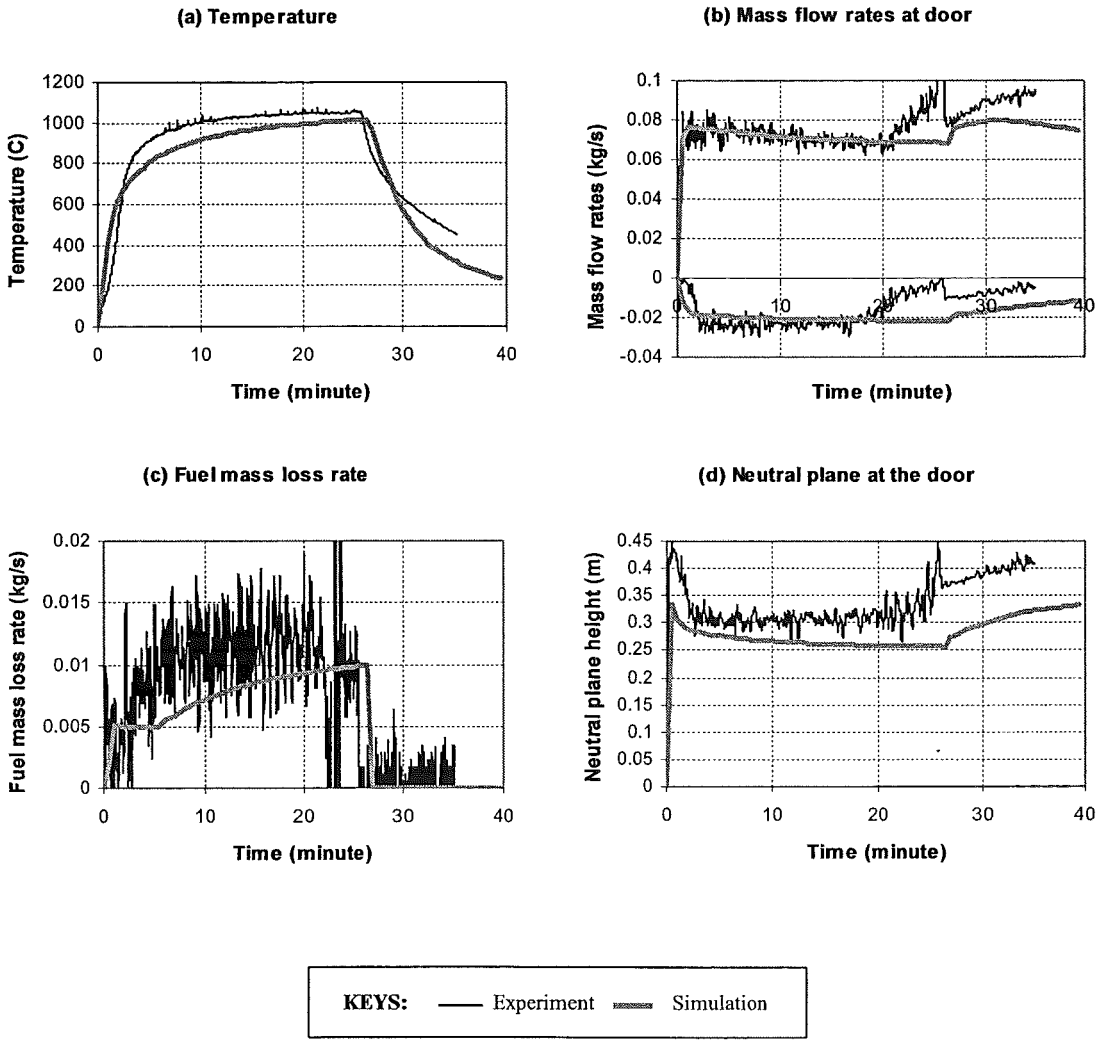

Figure 11.7 Comparisons between the experimentally measured results and simulations results from the CFIRE program for D1R250 experiment.

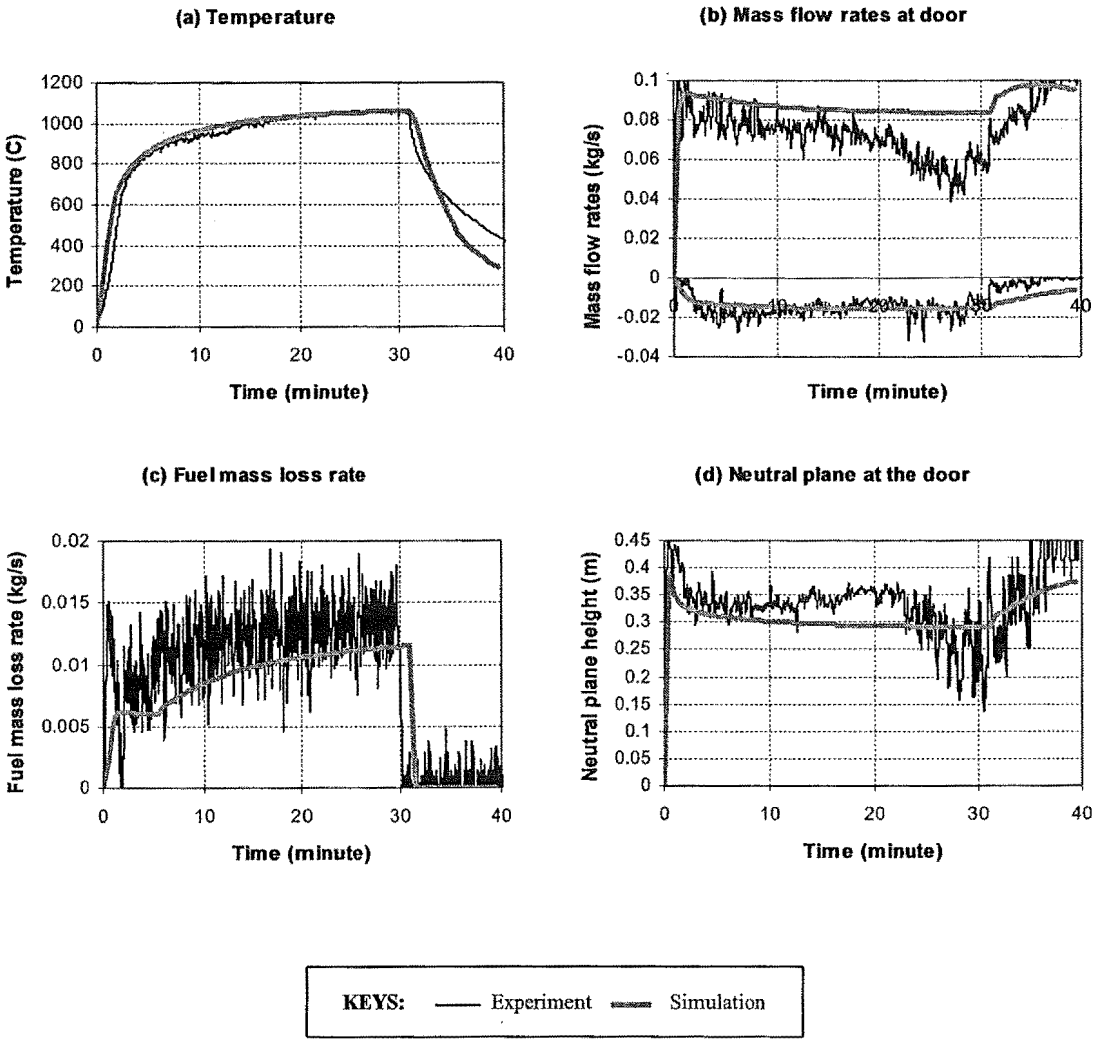

Figure 11.8 Comparisons between the experimentally measured results and simulations results from the CFIRE program for D1R300 experiment.

11.14 REMARKS

The verification exercises performed have shown that the CFIRE computer program can produce satisfactory estimations compared to experimental results. However, it should be mentioned that not all the features provided in the CFIRE program have been tested. These not yet verified features include:

- The furniture mass loss rate model;
- The vent flow model for a very large door opening such as a full wall opening with/without roof vent opening;
- The vent flow model for the condition at which the neutral-plane is above the soffit of the door;
- The fuel mass loss rate in a compartment with a wood fuel load with both horizontal and vertical openings during the ventilation controlled burning regime (Equations (11.29) and (11.30)).

Caution should be exercised when the above scenarios are encountered. Further research and study are required of these areas. The pulsing phenomenon observed in the Door 2 and Door 3 experiments by the author also exposed a limitation of the CFIRE program. Future research is necessary to perform in-depth study of the cause of this pulsing dynamic and to establish bounds for applying the CFIRE program.

Chapter 12 FIRE SIMULATION STUDIES

This chapter uses the CFIRE computer program to simulate the fire time-temperature curves inside a compartment with different types of fuel at different ventilation openings. A steady-state analysis is also performed. The studies highlight the importance of identifying the types of fuel involved, whether the fuel is wood or thermoplastic/liquid pool, and the respective fuel surface area. It is shown that fuel with different physical and burning characteristics result in very different fires in terms of the temperature and duration, even with the same total amount of fuel load.

12.1 INTRODUCTION

Experimental test fires usually use wood cribs as the fuel. The fuel load is often reported as the fuel mass per unit floor area, and the surface area of the fuel is seldom reported. In such cases, if only one form of fuel is involved, the fuel mass indirectly represents the available fuel surface. According to Ödeen's model (Equation (6.5)), wood fuel with a greater surface area would release a greater amount of fuel than similar wood fuel with less surface area, with the same regression rate. The increase in the release rate of available fuel would in turn increase the heat release rate of the fire inside the compartment. Hence, for a single form of fuel such as wood cribs, increasing the fuel load would inevitably increase the total available fuel surface and result in a more severe fire than the lower fuel load case. Design fires such as that proposed by Magnusson and Thelandersson (1970) are largely based upon wood crib test fires. For the aforementioned reason, these fires are characterised using the fire load per unit area. The use of the fire load per unit area as a characteristic parameter has perhaps resulted in fuel load surveys which only report the fuel mass or heat content per unit floor area, without any useful descriptions being given about the characteristics of the fuels involved.

Fire loads in typical residential and commercial occupancies are likely to include wooden items such as bookshelves, desks, tables and chairs. Each of these wooden furniture items has a different exposed surface area and mass; furniture can be considered "thick" when its exposed surface area is small compared to its overall mass, e.g. a fully packed bookshelf, or "thin" with a large surface area compared to its mass, e.g. desk, table. Apart from wooden furniture, realistic occupancies also consist of thermoplastic materials such as mattresses and upholstered furniture that have pool-like burning behaviour. These vastly different fuel characteristics will produce different fires inside a compartment.

In this chapter, simulation studies are performed using the CFIRE program to investigate the possibilities of different fire time-temperature histories resulting from different types of fuel, even with the same fuel load. The importance of fuel surface area on the potential resulting fire temperature is also highlighted.

12.2 SCENARIOS

In order to study the effects of fuel types on the resultant fires, six fuel scenarios are considered. These fuel scenarios are:

1. 100% thick wood-based furniture;
2. 100% thin wood-based furniture;
3. 100% thermoplastic fuel;
4. 50% thick wood-based furniture and 50% thin wood-based furniture;
5. 50% thick wood-based furniture and 50% thermoplastic fuel;
6. 50% thin wood-based furniture and 50% thermoplastic fuel.

The "thick" wood based furniture refers to a selection of furniture items with a small surface area to mass ratio; whereas the "thin" furniture refers to a selection of items with a large surface area to mass ratio. The furniture items involved are given in Appendix B. In this study, the thick fuels are represented by using a mixture of

bookshelves completely full and bookshelves 50% full of books, and the thin fuels are represented using a mixture of desks, tables and chairs. Thermoplastic fuel is represented by a large slab of polyurethane foam with an area equal to the floor area of the compartment.

For all scenarios, a fire load density of 800MJ/m^2 (floor area) is used, to represent a typical office fire hazard (BIA, 1992). The compartment considered is 3m high by 5m wide by 5m deep, lined with gypsum plasterboard 38mm thick. This is schematically shown in Figure 12.1. Four different ventilation openings are considered, as shown in Table 12.1. The fuel properties are given in Table 12.2. A t-squared fire given in Equation (11.32) with a fast growth rate, i.e. k_{growth} =150 ($s/\sqrt{MW}$) is used to represent the growth phase of the aforementioned fire scenarios.

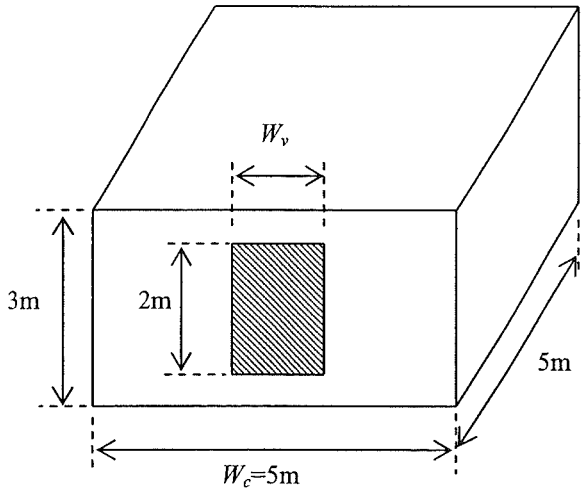

Figure 12.1 Schematic representation of the compartment used in the analysis.

Table 12.1 Compartment specifications used in the fire simulations.

Compartment size	5.0m × 5.0m × 3.0m high
Internal bounding surface area, A_T	110m^2
Ventilation opening height, H_v	2.0m
Ventilation opening width, W_v	0.76m, 1.56m, 3.11m, 4.67m
Ventilation parameter, $A_vH_v^{0.5}$	2.15, 4.40, 8.80, 13.20 m$^{2.5}$
Ventilation factor, $F_v = A_vH_v^{0.5}/A_T$	0.02, 0.04, 0.08, 0.12 m$^{0.5}$
Enclosing boundary	Density, ρ = 720 kg/m^3 Specific heat, c_p = 1130 J/kg K Thermal conductivity, k = 0.2 W/m K Thickness, L = 0.038 m Emissivity, ε_w = 0.9
Modelling Parameters used	
Exposed wall area for heat transfer, A_t	85 m^2 minus the vent opening area
Combustion mixing factor, b_p	0.9
Gas emissivity, ε_g	0.9

Table 12.2 Fuel properties used in the fire simulations.

	Wood	Polyurethane foam
Fuel composition	$CH_{1.455}O_{0.645} \bullet 0.18\ H_2O$	$CH_{1.91}O_{0.263}N_{0.055}$
Net heat of combustion, Δh_c	15,100 kJ/kg	28,700 kJ/kg
Heat of gasification, L_g	4,000 kJ/kg	2,700 kJ/kg
Vaporisation temperature, T_v	N/A	600 K
Stoichiometric air to fuel mass ratio, r	5.3	9.8
Attenuation factor, α	N/A	0.65

Note: The chemical formula for polyurethane foam ($CH_{1.91}O_{0.263}N_{0.055}$) used in this analysis is the same as used by Takeda and Yung (1992) in their modelling of polyurethane fires inside a compartment.

For fuel load scenarios that consist of both wood-based products and thermoplastic fuels (scenarios 5 and 6), there are two burning options available in the CFIRE computer program. These options are: (1) a successive burning option that assumes the pool to burn first and the wood fire to continue after the pool burns off; and (2) a simultaneous burning option that assumes pool and wood burn together after flashover (set as 500°C). In the comparative study between different fuel scenarios,

the successive burning option was chosen to simulate the fire for scenarios 5 and 6. In doing so, these scenarios are conditional on the assumption that the thermoplastic fuel burns first, followed by the wood fuel. This assumption is not necessarily an indication of what will actually happen in a real fire, but it is used as a first approximation to show the capability of the CFIRE computer program.

12.3 FIRE SIMULATION RESULTS

12.3.1 Effects of fuel types

Figure 12.2 shows the simulated fire gas time-temperature histories inside the compartment for the six fuel scenarios at different ventilation openings. Note that each scenario has the same fire load (800MJ/m^2 floor area). The simulation results show that the gas temperatures inside the compartment are dependent on the type of fuel involved.

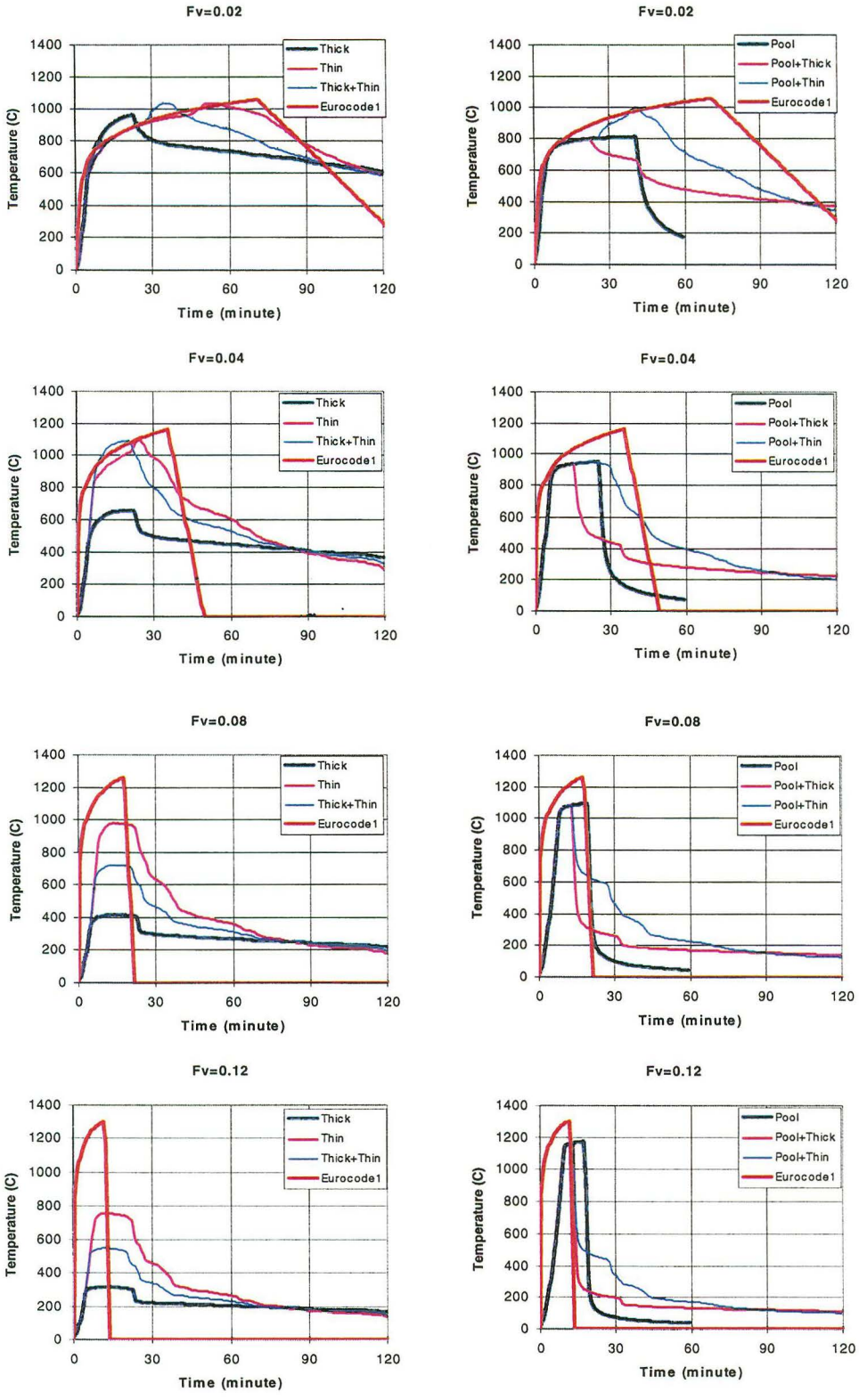

Figure 12.2 **Simulation results giving fire gas temperatures for different types of fuel and different sizes of window opening, compared with Eurocode parametric fire curves (Fuel load of 800MJ/m^2 floor area).**

Considering the left hand graphs of Figure 12.2, the results show that thin wood-based fuel items give higher fire gas temperatures than thick fuel items. This is because thin fuel has more surface area than thick fuel for a given mass, therefore a higher mass loss rate. At small openings, F_V=0.02 and 0.04, there is generally enough fuel surface area for thin fuel to produce a mass loss rate at the ventilation limit $0.12 A_v \sqrt{H_v}$ (Equation (11.29)). This results in a ventilation controlled fire where the heat release rate is close to the maximum for the given vent opening, i.e. combustion using nearly all the available incoming air from the opening, producing a high gas temperature. Note that for small opening (F_V=0.02), the temperature in the room with thick fuel climbs faster than that with thin fuel. Reviewing the mass loss rate history for thick fuel, its mass loss rate is found to be lower than the thin fuel counterpart that burns at the maximum rate of $0.12 A_v \sqrt{H_v}$. This lower mass loss rate is due to thick fuel having less surface area compared to thin fuel. Since the maximum mass loss rate, $0.12 A_v \sqrt{H_v}$, corresponds to a slightly fuel-rich burning with an equivalence ratio of approximately 1.35, by burning at a rate slightly less than the maximum rate, the burning of thick fuel will be closer to stoichiometry, resulting a hotter gas temperature due to lower convective heat loss.

For larger openings, F_V=0.08 and 0.12, there is not enough fuel surface available, even for thin fuel to produce a ventilation controlled fire. The fire environment inside the compartment is therefore fuel-lean and the heat release rate depends on the mass loss rate controlled by the fuel surface. The resulting temperatures are less than for the small openings because the mass loss rate is low compared with the available air supply. The decay rate for the thin wood is faster than for the thick wood. The fire continues until all fuels are exhausted. For combined thick and thin wood-based fuel, the fire gas temperature is between the thick case and thin case as expected. For thick fuel and large openings, the calculated temperatures using the assumed fuel mass loss rate are unrealistically low for post-flashover fires, but they have been included to show the full range of output from the model. Note that at large openings with F_V= 0.12, the thick fuel and thin fuel scenarios are seen to have decay periods starting at the same time. This rather unexpected result happens because at this large opening, the burning is fuel-surface controlled from the beginning. The thick fuel items such as

50% filled bookshelves also consist of some thin components the same thickness as in the thin fuel items, and the decay phase starts when the thin components in the furniture items are exhausted. For example, for plane components 25mm thick, with a constant regression rate of 0.011mm/s from both sides, it takes approximately 20 minutes to burn away these thin components, at which time the decay phase starts. For thick fuel, the entire decay period is much longer and the fire heat release rate is much lower compared to thin fuel, due to the thick components involved.

Fuel load consisting of polyurethane foam is represented by a pool fire with an area equal to the floor area of the compartment of $25m^2$. This fire could also represent a fire where thermoplastic items melt and form a pool over the whole floor area. The relative size of the ventilation opening to the pool area has an important effect on the temperature generated inside the compartment, shown by the heavy lines on the right hand graphs of Figure 12.2. For a small opening, F_V=0.02, although the fire condition is fuel-rich and consuming nearly all the incoming oxygen, the fire gas temperature inside the room is not as high as that in the thin wood scenario. This is due to far more fuel being vaporised from the pool than can be burned with the available air. The unburned fuel is discharged from the compartment along with the hot gases. With this large extra mass in the discharge, the convective heat loss is greatly increased. This reduces the fire gas temperature generated inside the compartment. As the ventilation increases, the pool burns more efficiently therefore producing higher temperatures.

The results for the coexistence of both pool and wood fuels (scenarios 5 and 6) are very interesting. Note that the successive burning option has been used in the modelling which assumed that all the liquid fuel is burned before the wood begins to burn. For small openings, F_V=0.02, the fuel-rich pool fire produces very low temperatures. Once the pool has burned away, the wood fuel fire depends on the available surface area of wood. The thin wood fuel has sufficient area to produce a ventilation controlled fire, and since the convective heat loss is not as large as that cause by the pool, this produces an increasing temperature. For the thick fuel, however, due to less surface area being available, the fire becomes fuel surface controlled with slowly dropping temperature.

As the window size is increased, it can be seen that the pool fire becomes hotter, but once the pool has burned away, the temperatures drop rapidly because the wood items have insufficient area to achieve ventilation controlled burning, regardless of whether they are thick or thin. For all opening sizes, the mass of wood fuel in the right hand graphs is only half of that in the left hand graphs, so the wood surface area is also only half, leading to the fire being severely fuel controlled when the openings are large.

The corresponding Eurocode parametric fire curves for a fuel load of 800MJ/m^2 floor area (or 182MJ/m^2 total area) with enclosing boundaries properties of $\sqrt{(k\rho c)}$ =400 Ws$^{0.5}$/m^2-K are superimposed on the individual plots in Figure 12.2. The formula for Eurocode parametric fire curves are shown as follows (EC1, 1994)

The Eurocode equation for temperature T (°C) is

$$T = 1325\left(1 - 0.324e^{-0.2t^*} - 0.204e^{-1.7t^*} - 0.472e^{-19t^*}\right) \quad \textbf{(12.1)}$$

where t^* is the fictitious time (in hours) given by

$$t^* = \Gamma t \quad \textbf{(12.2)}$$

and t is the time (in hours) and

$$\Gamma = \frac{(F_v/0.04)^2}{(\sqrt{k\rho c}/1160)^2} \quad \textbf{(12.3)}$$

and F_v is the ventilation factor defined as

$$F_v = A_v\sqrt{H_v} / A_T \quad \textbf{(12.4)}$$

where A_T is the total internal bounding surface area (including opening) (m^2).

The equation for the duration of the burning period, t_d (in hours), is given as (Buchanan, 2002)

$$t_d = 0.00013 e_t / F_v = \frac{0.00013E}{A_v\sqrt{H_v}} \quad \textbf{(12.5)}$$

where e_t is the fuel load (MJ/m^2 total surface area), and E is the total energy content of the fuel (MJ).

The Eurocode uses a reference decay rate $(dT/dt)_{ref}$ equal to 625°C per hour for a fire burning duration less than 30 minutes and decreasing linearly to 250°C per hour for a fire burning duration greater than 2 hours. The actual decay rate is given by

$$dT / dt = (dT / dt)_{ref} \Gamma \quad \textbf{(12.6)}$$

It can be seen that in general, in term of maximum temperature, the Eurocode parametric fires compare well with thin wood scenarios at small openings, at F_v=0.02 and 0.04. At large openings, where F_v=0.08 and 0.12, the parametric fires have a maximum temperature much greater than all the wood fires simulated. This is expected because the parametric fires are deduced from Magnusson and Thelandersson's (1970) design fire curves. These design fires are based on wood fires with the assumption that the fire is ventilation controlled at every opening condition regardless of fuel load (Magnusson and Thelandersson, 1974). The close similarity between the parametric fires and the simulated thin wood furniture fires at small openings is due to the fact that the thin wood furniture has sufficient fuel surface area to achieve ventilation controlled burning. This corresponds to the underlying assumption made during the generation of Magnusson and Thelandersson's design fires, and hence the parametric fires. However, at large openings, the fuels involved in the simulations do not have sufficient surface area to achieve ventilation controlled burning. Therefore, the simulated temperatures are lower than the parametric fires. Comparing the parametric fires with the thermoplastic pool fire simulations, the parametric fire has a longer fully developed phase, i.e. the period between flashover to the onset of decay. This is because the thermoplastic pool fires burn in a fuel-rich

environment with the excess vaporised fuel burning outside the compartment. However, it is noted that the Eurocode parametric fires have fast decay rates compared to the simulated fires for large openings in particular. Such behaviour has been reported by Feasey and Buchanan (2002), where they found that the Eurocode equations often predict temperatures which are too low and give extremely fast decay rates for large openings in poorly insulated compartments and extremely slow decay rates for small openings in well insulated compartment. They suggested a modified modification factor, Γ_{DESIGN}, for the fully developed phase to obtain a higher temperature; a separate modification factor for the decay phase, Γ_{DECAY}, to produce a more realistic decay rates. These modification factors are given as follows

$$\Gamma_{DESIGN} = \frac{(F_v/0.04)^2}{(\sqrt{k\rho c}/1900)^2} \quad \textbf{(12.7)}$$

$$\Gamma_{DECAY} = \frac{\sqrt{F_v/0.04}}{\sqrt{\sqrt{k\rho c}/1900}} \quad \textbf{(12.8)}$$

The fictitious time, t^*, and the decay rate, dT/dt, are given as

$$t^* = \Gamma_{DESIGN} t \quad \textbf{(12.9)}$$

$$dT/dt = (dT/dt)_{ref} \Gamma_{DECAY} \quad \textbf{(12.10)}$$

Figure 12.3 shows the modified parametric fire curves plotted on top of the same simulation results as presented in Figure 12.2. It can be seen that in general, the modified parametric fires provide envelopes for the simulated fire curves, with more realistic decay rates than in Figure 12.2. Therefore, they represents a family of conservative fire curves for the given fuel load, ventilation opening and the type of enclosure. The comparison made between the parametric fires and the simulation results shows that these parametric fires can be seen as a family of useful fire curves for the purpose of structural fire designs. They do not in any way describe the fire behaviour of realistic furnishing inside an occupancy.

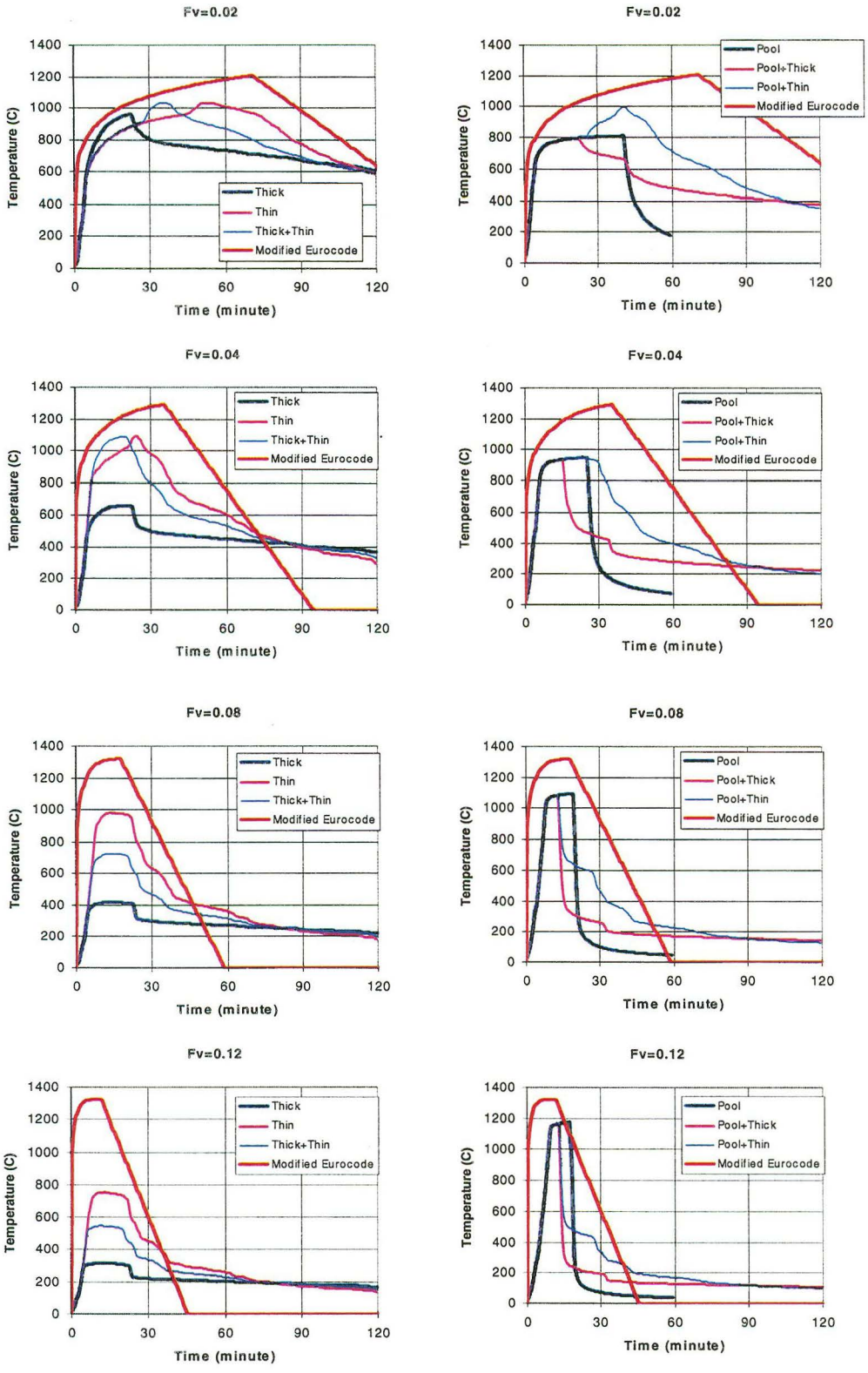

Figure 12.3 Comparison of modified parametric fires with the simulation results for different types of fuel and different sizes of window opening with a total fuel load of 800MJ/m^2 floor area.

12.4 ANALYTICAL STUDY ON THE EFFECTS OF FUEL SURFACE AREA TO VENT OPENINGS

The simulation results presented in Figure 12.2 have indicated that both the fuel types ("wood" and "pool") and their surface area strongly affect the resultant fire characteristics at various opening geometries. As noted in the previous chapters (Chapters 5 and 6) these two fuel types each has different burning behaviour to each other. The "wood" refers to wood fuels where the mass loss rate is restricted by either the ventilation or the fuel surface area. In the case of fuel surface controlled, the mass loss rate is prescribed by a constant regression-burning rate from the surface. This is the burning model used to model wooden furniture in the previous section, which assumes that the fuel mass loss rate is not affected by the imposed radiation. The "pool" refers to thermoplastic or liquid fuels where the mass loss rate is driven by the imposed radiation from the surrounding hot environment.

The analysis performed in this study is to investigate the important parameters that affect the fire temperature and the fuel mass lass rate for these two fuel types each with different burning behaviour.

This analysis is based on the single zone compartment fire theory as used in the CFIRE program, with some simplifications. The simplifications are made on the air inflow rate term by using the approximated equation ($\dot{m}_{in} \approx C \cdot A_v \sqrt{H_v}$ (Equation (3.8)), and the use of a mean specific heat for the hot gases, c_p, to estimate the convective heat loss. This will facilitate a presentation on all the important parameters on the heat balance equation, which will be the focus of the analysis. In the analysis, fuel with a fixed surface area is considered and the resultant fire gas temperature and the fuel mass flux inside the compartment are evaluated at the steady-state condition.

The formulations used in this analysis are given in the following section.

12.4.1 Formulations

For a compartment having only a vertical wall opening, assuming the compartment behaves as a single zone well-stirred reactor with infinitely fast reactions, the conservation of energy and mass equations give

$$\dot{Q}_{FIRE} = \dot{Q}_L + \dot{Q}_R + \dot{Q}_W + \dot{Q}_{FB} \tag{12.11}$$

$$\dot{m}_{in} + \dot{m}_p = \dot{m}_{out} \tag{12.12}$$

The expression for each individual heat term in the energy balance equation is given as follows.

Convective heat loss term

Taking the mean specific heat of the out going hot gases, c_p, as 1150J/kg-K (Janssens, 1992), and approximating the air inflow into the compartment as in Equation (3.8), the convective heat loss term can be written in the following form:

$$\begin{aligned} \dot{Q}_L &= c_p\left(T_g - T_0\right)\cdot\left(\dot{m}_p + \dot{m}_{in}\right) \\ &\approx c_p\left(T_g - T_0\right)\cdot\left(A_F\dot{m}_p'' + C\cdot A_v\sqrt{H_v}\right) \end{aligned} \tag{12.13}$$

where the fuel rate, $\dot{m}_p$ (kg/s), is expressed as the product between the fuel surface area, A_F (m^2), and the fuel mass flux per unit fuel surface area, $\dot{m}_p''$ ($kg\ s^{-1}m^{-2}$).

Radiation heat loss from vent opening

The radiation heat flux from the vent opening is represented as a blackbody at temperature T_g, with the expression given as

$$\dot{Q}_R = A_v\cdot\sigma\cdot\left(T_g^4 - T_0^4\right) \tag{12.14}$$

where A_v is the vent opening area, σ is the Stefan-Boltzmann constant, T_g is the gas temperature and T_0 is taken as the temperature of the outside ambient air.

Heat loss through the enclosing boundaries

In this analysis, only the steady-state solution is considered. The general form of wall heat loss term is given as follows

$$\dot{Q}_W = A_t \cdot \dot{q}''_w \tag{12.15}$$

where $\dot{q}''_w$ is the heat loss per unit area of the enclosing boundaries. Note that A_t is the surface area of the enclosing boundaries subjected to heat transfer. This will have a value lower than the total internal surface area, A_T, as the floor area is generally not included in the heat transfer calculation assuming that the fuel packages cover all of the floor area. At steady-state, $\dot{q}''_w$ is expressed as follows,

$$\dot{q}''_w = h'_{fire}\left(T_g - T_{wi}\right) = \frac{k}{L}\left(T_{wi} - T_{wo}\right) = h'_{amb}\left(T_{wo} - T_0\right) \tag{12.16}$$
$$= \frac{T_g - T_0}{\frac{1}{h'_{fire}} + \frac{L}{k} + \frac{1}{h'_{amb}}}$$

where L is the wall thickness and k is its conductivity. The terms h'_{fire} and h'_{amb} are the "lumped" convective heat transfer coefficient at the hot fire side and the cold ambient side of the wall respectively. These coefficients include both convective and radiative heat loss components such that

$$h'_{fire} = h_{fire} + \varepsilon_{res}\sigma\left(T_g^3 + T_g^2 T_{wi} + T_g T_{wi}^2 + T_{wi}^3\right) \tag{12.17}$$

and

$$h'_{amb} = h_{amb} + \varepsilon_{res}\sigma\left(T_{wo}^3 + T_{wo}^2 T_0 + T_{wo} T_0^2 + T_0^3\right) \tag{12.18}$$

The convective heat transfer coefficients, h_{fire} and h_{amb}, are taken as 25W/m^2-K and 10W/m^2-K respectively. Both the inside and outside wall surface temperature, T_{wi} and

T_{wo}, are solved for the given L/k and the convective and radiative boundary conditions.

Feedback term

This is the heat required to vaporise the unburned fuel. The feedback term is evaluated as

$$\dot{Q}_{FB} = \left(\dot{m}_p - \dot{Q}_{FIRE} / \Delta h_{c,net}\right) / L_g \qquad \textbf{(12.19)}$$

where L_g is the heat of gasification.

Fire heat release rate

The fire heat release rate depends on whether the fire environment is fuel rich or fuel lean. For simplicity, the mixing between fuel and air is assumed to be perfect, i.e. b_p=1, such that

For fuel-rich condition

$$\begin{aligned} \dot{Q}_{FIRE} &= \dot{m}_{in} \cdot \Delta h_{c,net} / r \\ &\approx C \cdot A_v \sqrt{H_v} \cdot \Delta h_{c,net} / r \end{aligned} \qquad \textbf{(12.20)}$$

For fuel-lean condition

$$\begin{aligned} \dot{Q}_{FIRE} &= \dot{m}_p \cdot \Delta h_{c,net} \\ &= A_F \dot{m}_p'' \cdot \Delta h_{c,net} \end{aligned} \qquad \textbf{(12.21)}$$

By substituting these individual heat terms into the conservation of energy equation (Equation (12.11)), the expressions for both the fuel-rich and the fuel-lean conditions are obtained. Following Quintiere's (2002) treatment, the term, $\frac{A_F}{A_v\sqrt{H_v}}$, is expressed as the product between $\frac{A_t}{A_v\sqrt{H_v}}$ and $\frac{A_F}{A_t}$.

Fuel-rich

$$C \cdot \frac{\Delta h_{c,net}}{r} = c_p\left(T_g - T_0\right) \cdot \left(\frac{A_t}{A_v\sqrt{H_v}} \cdot \frac{A_F}{A_t} \cdot \dot{m}_p'' + C \right) + \frac{\sigma\left(T_g^4 - T_0^4\right)}{\sqrt{H_v}} \qquad \textbf{(12.22)}$$

$$+ \left(\frac{A_t}{A_v\sqrt{H_v}} \right) \cdot \dot{q}_w'' + \left(\frac{A_t}{A_v\sqrt{H_v}} \cdot \frac{A_F}{A_t} \cdot \dot{m}_p'' - \frac{C}{r} \right) \cdot L_g$$

where $\dot{m}_p''$ the fuel mass loss rate per unit fuel area is

"Pool"
$$\dot{m}_p'' = \frac{\alpha\varepsilon_g\sigma T_g^4 - \sigma T_v^4}{L_g} \qquad \textbf{(12.23)}$$

"Wood"
$$\dot{m}_p'' = \frac{C \cdot A_v\sqrt{H_v}}{r} \cdot \frac{1}{A_F} \qquad \textbf{(12.24)}$$
$$= \frac{C/r}{\left(\frac{A_t}{A_v\sqrt{H_v}} \cdot \frac{A_F}{A_t} \right)}$$

Fuel-lean

$$\left(\frac{A_t}{A_v\sqrt{H_v}} \cdot \frac{A_F}{A_t} \cdot \dot{m}_p'' \right) \cdot \Delta h_{c,net} = c_p\left(T_g - T_0\right) \cdot \left(\frac{A_t}{A_v\sqrt{H_v}} \cdot \frac{A_F}{A_t} \cdot \dot{m}_p'' + C \right) \qquad \textbf{(12.25)}$$

$$+ \frac{\sigma\left(T_g^4 - T_0^4\right)}{\sqrt{H_v}} + \left(\frac{A_t}{A_v\sqrt{H_v}} \right) \cdot \dot{q}_w''$$

where $\dot{m}_p''$ is taken as the free burning mass flux.

The switch from the fuel-rich to the fuel lean condition is determined using the equivalence ratio, Φ, defined as

$$\Phi = \frac{r \cdot \dot{m}_p}{\dot{m}_{in}} \approx \frac{r \cdot A_F \cdot \dot{m}''_p}{C \cdot A_v \sqrt{H_v}} \tag{12.26}$$

The stoichiometric condition occurs when Φ=1. By substituting the mass loss rate expressions for "pool" given in Equations (12.24) into Equation (12.26) with equivalence ratio set as greater than unity, i.e. Φ>1, the conditions necessary to achieve fuel-rich condition is given as follows:

For "pool":

$$\frac{A_F}{A_v \sqrt{H_v}} > \frac{C}{r} \cdot \frac{L_g}{\alpha \varepsilon_g \sigma T_g^4 - \sigma T_v^4} \tag{12.27}$$

or in other word, the fire gas temperature, T_g, must be high enough to impose sufficient heat flux on the pool to create a fuel-rich environment, such that

$$T_g > \left\{ \left[\frac{L_g}{r} \cdot \frac{C A_v \sqrt{H_v}}{A_F} + \sigma T_v^4 \right] \Big/ (\alpha \varepsilon_g \sigma) \right\}^{\frac{1}{4}} \tag{12.28}$$

For "wood", the $\dot{m}''_p$ involved simply has to be

$$\dot{m}''_p \geq \frac{A_v \sqrt{H_v}}{A_F} \cdot \frac{C}{r} \tag{12.29}$$

If these conditions are not met, the fire becomes fuel-lean.

Two dominant geometrical parameters can be seen in both Equations (12.22) and (12.25). These parameters are $A_t / A_v \sqrt{H_v}$ and $A_F / A_v \sqrt{H_v}$. The former relates to the heat losses through the enclosing boundaries, whereas the later relates to the fuel mass loss rate. Note that these two parameters are not totally independent as they are

related by A_F / A_t. Apart from these two parameters, it is apparent that for the "pool" type of fuel, the $(\Delta h_{c,net}/r)/L_g$ ratio would be influential over the fuel mass loss rate, where $(\Delta h_{c,net}/r)$ is the heat of combustion of air for the fuel. It can be seen from Equation (12.22) that high $(\Delta h_{c,net}/r)$ will result in a greater fire heat release rate, hence high resulting gas temperature and fuel mass loss rate; and a low L_g represents a fuel that is easily vaporised.

12.4.2 Analysis

In order to study these parameters, a compartment 5m wide by 5m deep by 3m high as used in the previous analysis (shown in Figure 12.1) is considered. It has a wall opening with a height of 2m at one end of the compartment, and the opening width will be varied from W_v/W_c=0.02 up to 1.0, thereby varying the vent parameter, $A_v\sqrt{H_v}$. The properties of the enclosing boundaries used in the analysis are given in Table 12.1.

The two main fuel types, i.e. "wood" and "pool", each with different burning characteristics are analysed. Of the "pool" fuels, three fuels with different $(\Delta h_{c,net}/r)/L_g$ ratios are tested to investigate the effect of the $(\Delta h_{c,net}/r)/L_g$ ratio on the resultant fire gas temperature and fuel mass loss rate. The properties of the fuel involved are presented in Table 12.3. The fuel surface area is described using the parameter, A_F/A_t. The value of A_F/A_t for each fuel is chosen such that it gives the entire burning spectrum from fuel-rich to fuel-lean over the geometry of the vent openings considered.

Table 12.3 Fuel properties.

	"Wood"	"Pool"		
Fuel	Wood	Heptane	Polyethylene	Polyurethane
Composition	$CH_{1.455}O_{0.645} \bullet 0.18H_2O$	C_7H_{16}	$(C_2H_4)_n$	$CH_{1.91}O_{0.263}N_{0.055}$
r	5.3	15.1	14.76	9.8
$\Delta h_{c,net}$ (kJ/kg)	15,100	44,500	43,300	28,700
L_g (kJ/kg)	N/A	500	2,400	2,700
$(\Delta h_{c,net}/r)/L_g$	N/A	5.89	1.22	1.08
T_v (K)	N/A	371	663	600
$\dot{m}''_{p,freeburn}$ (kg s^{-1} m^{-2})	0.005*	0.065	0.026	0.021
α	N/A	0.65	0.65	0.65
A_F/A_t	0.6	0.005	0.025	0.05

*Note: The free burning mass flux for wood is taken as 0.005kg $s^{-1}m^{-2}$ corresponding to a regression rate of 0.011mm/s and a wood density of 450kg/m^3.

12.4.3 Results

The steady-state solutions are calculated using the equations given in Section 12.4.1. Figure 12.4 plots $\dot{m}_p / A_F$ versus $A_v\sqrt{H_v} / A_F$ for the fuel types considered. The "wood" model produces the ventilation controlled and fuel surface controlled burning regimes as shown by Harmathy (1972). The slope of the "wood" model in the ventilation controlled burning regime is *C/r*, approximately 0.09, i.e. the Kawagoe correlation. The point of transition from ventilation controlled to fuel surface controlled is when the free burn mass flux, $\dot{m}''_{p,freeburn}$, equals $C \cdot A_v\sqrt{H_v} / r / A_F$. For $\dot{m}''_{p,freeburn}$ less than $C \cdot A_v\sqrt{H_v} / r / A_F$, the fire becomes fuel surface controlled.

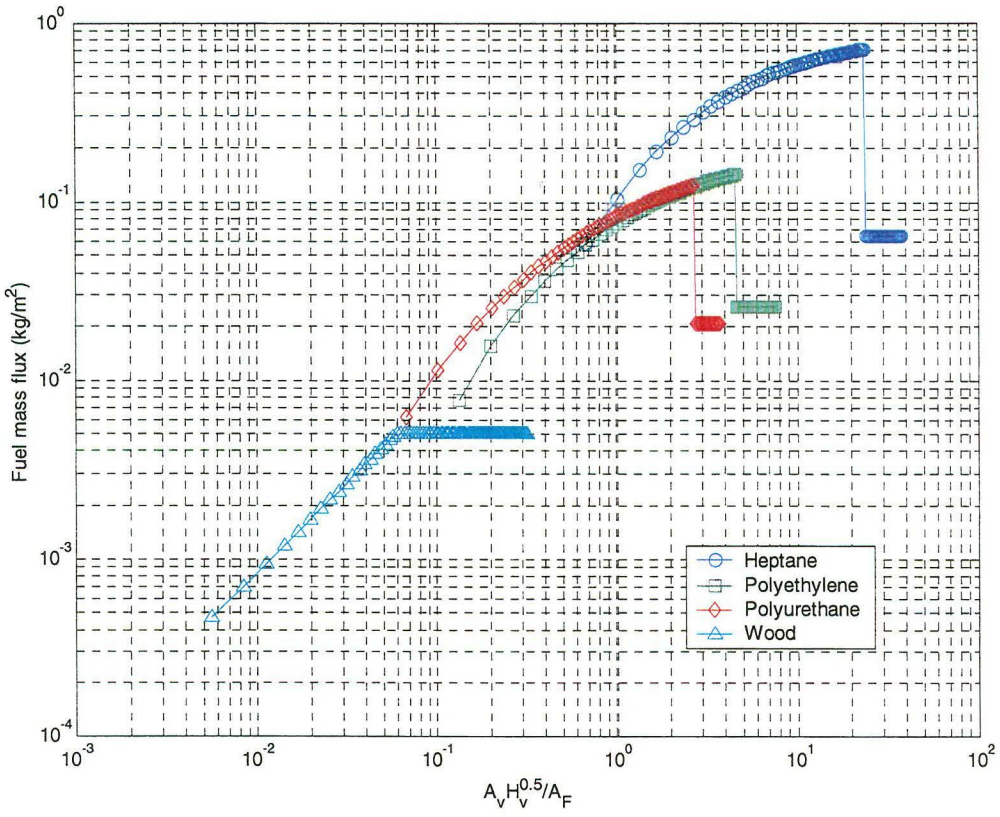

Figure 12.4 Fuel mass flux versus $A_v\sqrt{H_v}/A_F$ for different types of fuel.

For "pool" fires, it can be seen that the fuel mass flux, $\dot{m}_p / A_F$, increases with the ventilation term, $A_v\sqrt{H_v}/A_F$, indicating a fuel-rich burning where the fire heat release rate is limited by the available ventilation. An increase in $A_v\sqrt{H_v}/A_F$ will mean a greater ventilation, resulting a greater heat release rate and hence temperature, leading to an increase in the pool fuel mass flux. From the plots, it can also be seen that for "pool" fires, the relationship between the fuel mass loss rate, $\dot{m}_p$, and the vent parameter, $A_v\sqrt{H_v}$, is not constant with a large deviation occurring especially at large openings. This is consistent with the study by Bullen (1976).

The increase of the fuel mass flux from a "pool" fire ceases at a point where the ventilation opening is too large with respect to the fuel surface area, such that the heat losses are too great for the compartment to sustain a high enough temperature to vaporise enough fuel from the available fuel surface to achieve fuel-rich burning. In

such a condition, the pool fire would be a localised fuel-lean fire with a low compartment temperature. Such behaviour has been noticed by Babrauskas and Wickström (1979) in their study of pool fires inside a compartment. In reality, the switch from fuel-rich to fuel-lean may not be as abrupt as shown in Figure 12.4. Quintiere (2002) has performed a similar analysis, but includes both the vitiation and the radiation effects in the modelling of the "pool" mass loss rate in the fuel-lean condition (c.f. the use of the free burning rate for fuel-lean condition in this analysis). His results have shown a gradual decrease in the mass flux when switching from the ventilation controlled to the fuel controlled regime. From the plot of Figure 12.4, it can be seen that the critical threshold of $A_v\sqrt{H_v}/A_F$, between the fuel-rich and the fuel-lean condition, increases for a pool with a lower heat of gasification. This is understandable because a pool with a low heat of gasification can be readily vaporised, so less fuel surface area is required to achieve a fuel-rich burning for a given ventilation opening compared to fuels with higher heat of gasification.

Comparing the fuel mass loss behaviours between the "pool" fire and the "wood" fire, it is clear that the "pool" fire could achieve a fuel-rich condition, i.e. a ventilation limited fire heat release rate, at a much smaller fuel surface area for a given ventilation opening than a "wood" fire. This is consistent with the findings by Bullen and Thomas (1978) and Böhm and Hadvig (1982). The required pool surface area to achieve fuel-rich burning decreases for pools with a high $(\Delta h_{c,net}/r)/L_g$ ratio.

Figure 12.5 presents the corresponding compartment fire temperature versus $A_v\sqrt{H_v}/A_F$ for the fuels considered. The very low temperatures associated with localised pool fires and wood fires burning at a free burning rate at large openings are presented for completeness. It can be seen that at small $A_v\sqrt{H_v}/A_F$ ratio, the pool fires, especially those with high $(\Delta h_{c,net}/r)/L_g$ ratios, produce a lower compartment temperature than wood fires. This is expected because the wood fire burns closer to stoichiometry according to Equation (12.24), whereas the pool fire burns in a highly fuel-rich environment releasing more fuel than could be burned with the available air. These unburned fuels are discharged outside the compartment, which in turn increases the convective heat loss term. This results in lower temperatures inside the

compartment but would increase the hazard due to external flaming. At large $A_v\sqrt{H_v}/A_F$ ratio, pool fires could produce temperatures much higher than wood fires as the wood fuel does not have a sufficient fuel surface area to produce ventilation controlled burning.

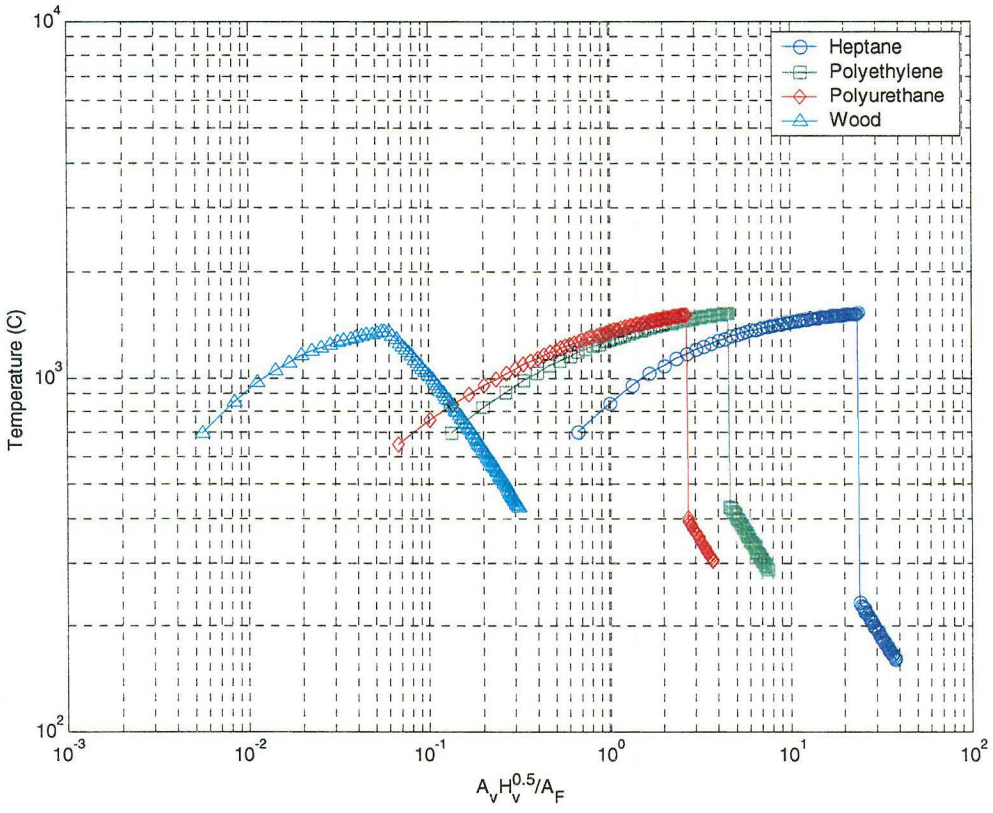

Figure 12.5 **Compartment fire gas temperature versus $A_v\sqrt{H_v}/A_F$ for different types of fuel.**

It should be noted that the above plots for the thermoplastic pool fires (Figures 12.4 and 12.5) are specific to the modelling parameters used, notably the enclosure surface area, A_t/A_F, the enclosure properties, L/k, and the vent opening height, H_v. As shown in Equation (12.22), both the A_t/A_F and L/k terms are associated with the enclosure boundaries heat loss; where the H_v term is associated with the radiative heat loss through opening. Because these terms are involved in the energy balance equation, they are influential over the resulting gas temperature and hence the fuel mass flux. For a given $A_v\sqrt{H_v}/A_F$, the enclosure boundary heat loss increases with a large

enclosure area, A_t/A_F, as well as a large heat loss per unit area of the enclosing boundaries, $\dot{q}''_w$, which is a function of L/k during steady-state heat transfer (Equation (12.16)); whereas the radiative heat loss through the opening increases with a low opening height, H_v, as a low H_v means a large opening area, A_v, for a given $A_v\sqrt{H_v}$. High heat loss terms would mean a low gas temperature and hence a low fuel mass flux. The transition point, $A_v\sqrt{H_v}/A_F$, between fuel-rich burning and fuel-lean burning, depends on both the fuel heat of gasification, L_g, and the temperature inside the compartment, as shown in Equation (12.27). The compartment needs to sustain a high enough gas temperature given the losses to vaporise enough fuel from the available fuel surface to achieve fuel-rich burning. By having greater heat losses, such as compartment boundaries with high thermal inertia, hence large $\dot{q}''_w$, the transition point is expect to be at a lower $A_v\sqrt{H_v}/A_F$ than those with a low thermal inertia having the same heat transfer surface area and opening geometry.

12.5 DISCUSSION AND SUMMARY

The above study has shown that different types of fuel can result in markedly different fires due to the different burning characteristics. Wooden furniture items are modelled so as to have the burning characteristics of "wood" such that the fuel mass loss rate is either controlled by the available ventilation or by the fuel surface area. According to Ödeen's model, a single large cube would have a lower mass loss rate than multiple smaller cubes with the same total mass at the same regression rate. This is simply because the large cube has a small surface area for the given mass. The single large cube and multiple small cubes could be used to resemble "thick" and "thin" furniture scenarios respectively. The thick furniture would have a smaller fuel surface area than the thin furniture for the same mass or fuel load. This means that the mass loss rate and hence the fire heat release rate for thick furniture would be lower compared to thin furniture, resulting in a less severe fire even with the same fuel load. This effect can be seen in the fire time-temperature histories presented in Figure 12.2. The available fuel surfaces and the ventilation opening size are important in determining

whether the fire will be ventilation controlled. This is characterised using the $A_v\sqrt{H_v}/A_F$ ratio and the requirement for ventilation controlled burning as given in Equation (12.29). From the simulation results for large openings with F_v=0.08 and 0.12, even thin furniture with a large exposed surface area does not produce a ventilation controlled fire. The temperature is therefore lower than predicted by the Eurocode parametric fires, derived by assuming ventilation controlled burning. Note that a typical office might have a large amount of loose paper which would act like "very thin" fuel, leading to hotter ventilation controlled burning in the early stages of a post-flashover fire.

With regard to the decay phase, since thin furniture usually consists of thin panels with a large surface area and small thickness, once these surfaces have burned off, the remaining total fuel surface is reduced significantly. This results in an abrupt increment in the $A_v\sqrt{H_v}/A_F$ ratio. As shown in Figure 12.5, this would result in a rapid drop in the temperature constituting a fast decay rate. For thick furniture, the change of the $A_v\sqrt{H_v}/A_F$ ratio over the fire duration is not as large as that of thin furniture. Therefore, the change in temperature is more gradual hence giving a slower decay rate.

It has been conceived that the existence of thermoplastic fuel inside a compartment can be beneficial for the structures inside the fire compartment, on the assumption that thermoplastics are vaporised easily under the radiation and discharged outside the compartment (Harmathy, 1979). However, through the present analysis, this is only partially true. As shown in Figure 12.4 and Figure 12.5, at small $A_v\sqrt{H_v}/A_F$ ratios, the pool fire has a greater mass loss rate per unit area and a lower fire gas temperature compared to the wood fire. In such conditions, the existence of pool could be beneficial to the fire compartment itself as a large amount of fuel is discharged outside the compartment, at the same time lowering the inside compartment temperature. This effect could be seen in the simulation results for small openings such as F_v=0.02 in Figure 12.2. However, at a large opening, the pool requires less fuel surface area to achieve a ventilation limited fire than wood fuel as shown in Figure 12.4. In this case, the thermoplastic fuel acts to increase the maximum fire gas

temperature, which would otherwise not be achievable if wood fuels were the sole fuel load inside the compartment. This can be seen in the simulated results for F_v=0.08 and 0.12. For a compartment having both thermoplastics and woods as fuels, the maximum fire gas temperature can be much higher than for a compartment with only wood fuels.

The above analyses highlight the importance of identifying the types of fuel and the fuel surface area, i.e. $A_v\sqrt{H_v}/A_F$ and A_F/A_t terms, involved in a fire compartment. Often these parameters are ignored and substituted by a single parameter, the total fuel load per floor area of the compartment. There exist a lot of possibilities to achieve the same fuel load per square metre with different combinations of fuels that could result in vastly different fires. Therefore, it is important that future fire load surveys include not only the mass of fuel, but also the fuel type and the exposed fuel surface area and thickness. This will allow the development of design fires for different categories of occupancies based on the fuel types, characteristics and properties involved.

It is acknowledged that the analyses performed ignore the preferential burning behaviours observed in a long deep compartment by Thomas and Bennetts (1999) and Kirby et al (1999). In such scenarios, the temperature inside the compartment is not uniform and the fuel surface area involved in the vaporising process might not be the same as the total available fuel surface area inside the compartment. The CFIRE computer program is not expected to produce an adequate simulation for such conditions. More research is needed on the topic of preferential burning, in particular the ignition and burning criteria for individual fuels at the back of the compartment. This would assist future model development for describing preferential burning behaviour.

Chapter 13 CONCLUSIONS AND RECOMMENDATIONS

This chapter concludes the thesis and summarises the major findings. Recommendations for future research on the area of post-flashover fires studies are given.

13.1 Existing fire models

The following points describe the characteristics of most existing post-flashover fire models:

- The post-flashover compartment is modelled using the single zone compartment fire theory, such that the entire compartment is treated as a well-stirred reactor.
- The associated vent flow theory applied in the models is based upon the orifice analogy that is only applicable for small wall openings.
- Combustion inside the compartment is assumed to be infinitely fast. The existence of incomplete combustion products, hence the combustion efficiency, is crudely estimated or ignored.
- In the case of modelling the mass loss rate of cellulosic fuels, fuel characteristics such as surface area and thickness are either not considered or collectively described as plane (one-dimensional), or stick or cylinder (two-dimensional), or cube or sphere (three-dimensional). Two burning regimes are generally used, namely the ventilation controlled regime and the fuel surface controlled regime. The mass loss rate during the ventilation controlled regime is assumed to be a result of a gas phase reaction whereas the mass loss rate during the fuel surface controlled is modelled using a prescribed regression

rate on the available fuel surface. For densely packed wood cribs, there is another burning regime known as the crib porosity controlled regime, which is accounted for in some models.

- The existing single zone fire models are restricted to modelling a single fuel type, either a cellulosic fire or a pool fire, but cannot model the coexistence of both fuel types inside the same compartment.
- Neither roof vent openings nor wind effects are considered.

13.2 FINDINGS

13.2.1 Compartment with large wall vent openings

Based on the analytical vent flow studies using the line-plume analogy, the following findings have been made in this study:

- The orifice analogy typically used to describe compartment vent flow should be restricted to small wall opening applications.
- For large wall openings such as a full wall opening, the fire environment inside a compartment is going to be less uniform than with a small wall opening; in such a case, the mass flow rate of air into the compartment is dictated by the plume entrainment.
- Depending on the plume entrainment constant, the flow rate due to entrainment could be as low as ~60% of the flow rate estimated from the orifice theory (the Kawagoe method).

13.2.2 Compartment with both horizontal and vertical vent openings

Based on the experimental vent flow studies on a compartment with a horizontal roof opening and a vertical door opening, it is found that:

- For a compartment with a small roof vent, and a large door opening with a small downstand, stable vent flows across the openings was observed. The neutral-plane was below the soffit of the door opening with inflow and outflow through the door and outflow through the roof opening.
- For a compartment with a small roof vent, and a small door opening with a large downstand, a sustained pulsing phenomenon was observed. The pulsing consists of charging and discharging phases; with air being sucked into the compartment via the entire door vent during the charging phase, and hot gases and unburned fuel being pushed out of the roof and door vents during the discharging phase.

From the analytical study, for a compartment with a small roof vent, and a large wall opening with a small downstand, where the neutral-plane is below the soffit of the wall opening:

- The flows can be described using an extended form of vent flow formulation that includes the roof vent opening.
- It is shown that in such circumstances, the area of the roof vent and the depth of the downstand between the ceiling and the soffit of the wall opening are significant in determining the extra air inflow due to the existence of the roof vent opening. These effects can be described using a single parameter, $A_{v,roof}\sqrt{H_c-(H_v+\delta)}$.

13.2.3 Analytical study of different fuels

- From the steady-state analytical studies of cellulosic and pool fires burning inside a compartment, the ventilation to the fuel surface ratio, $A_v\sqrt{H_v}/A_F$, the fuel surface to enclosure area ratio, A_F/A_t, and in the case for pool fires, the ratio between the heat of combustion of air for the fuel and the heat of gasification of the fuel, $(\Delta h_{c,net}/r)/L_g$, are found to be influential in determining the resulting compartment fire temperature and fuel mass loss rate.
- It is shown that the pool fires, with low heat of gasification, L_g, generally require less fuel surface area to achieve fuel-rich (ventilation controlled) burning than the wood fires.

13.3 CFIRE

The proposed post-flashover fire computer program, CFIRE, has incorporated these findings. The improvements of CFIRE compared with earlier models include the following:

- The vent flow formulations are modified to account for a full-wall size opening and to include a roof vent opening;
- Two types of fuel, wood and liquid pool, may be considered to coexist inside the same compartment, burning either successively or simultaneously;
- A library of mass loss rate histories for typical furniture items has been derived using real furniture geometry. This library can be called upon if encountering furniture with similar geometry instead of trying to describe all of the furniture items collectively as having a single geometry.

These represent the new advances of the modelling capabilities compared to existing fire models. The modelling capabilities of the CFIRE program have been verified in part with available test fire data and shown to produce satisfactory results.

13.4 SIMULATION STUDIES

Based on the simulation studies using the CFIRE program, the following findings are made:

- For wood fires, the fire time-temperature histories are highly dependent on the remaining fuel surface area at various times during the fire.
- Thin wood tends to result in a shorter and hotter fire as it has a greater surface area than thick wood, even with the same fuel load.
- For a small ventilation opening, a pool fire inside a fire compartment is less severe than a wood fire because the thermoplastic fuel is vaporised easily under the radiation, resulting in a large amount of excess fuel been discharged outside the compartment.
- In the case of large openings, pool fires are more likely to produce a hotter fire in the compartment than wood fires, because wood fuel would not have sufficient fuel surface area to achieve ventilation controlled burning.
- Comparing these simulated fires with the Eurocode parametric fires, the Eurocode parametric fires do not provide realistic decay rates. The modified parametric fires are conservative as they provide envelopes for the simulated fire curves, including the decay phase. However, parametric fires do not clearly describe the fire behaviour of realistic furnishing inside the fire compartment.

13.5 FUTURE RESEARCH

This thesis has covered a wide scope of topics involving compartment fire modelling. There are areas that require further research in order to improve the understanding of post-flashover compartment fires. Filling the gaps in knowledge of these currently unknown fire behaviours could lead to a fire model capable of modelling a wider range of practical scenarios. The areas that need further research are:

13.5.1 Vent flows

- Vent flows in compartments with high ceilings;
- The unstable bi-directional flow across large roof openings;
- Vent flows in compartments with large wall openings and roof vent openings;
- Effects of wind on vent flows.

13.5.2 Deep compartments

- The progressive burning behaviour of discrete fuel packages from the vent opening towards the inside of deep compartments, notably the conditions necessary to ignite and burn those fuel packages at the back of the compartment.

13.5.3 Fuels

- Verification and calibration of the wooden furniture model;
- Estimation of the equivalent pool area of upholstered furniture inside a post-flashover compartment;
- The burning behaviour of fuels during the aforementioned (§13.5.1) vent opening conditions; and
- Details of fuel load surveys in real occupancies that differentiate between the fuel types, and including the respective exposed fuel surface area and thickness.

13.5.4 Unstable conditions

- Identify the parameters and conditions that cause pulsing to occur in compartments with both horizontal and vertical vent openings.

13.5.5 Experimental technique

- An improved experimental technique for measuring the velocity and mass flow through vent openings is needed to obtain accurate data for analytical studies.

REFERENCES

Arnault, P., Ehm, H. and Kruppa, J. (1973) *Rapport Expérimental sur Les Essais Avec des Feux Naturels Exécutés Dans La Petite Installation de Maiziéres-lés-Metz*, Centre Technique Industriel de la Construction Métallique Report No. CECM 3/73-11-F.

Arnault, P., Ehm, H. and Kruppa, J. (1974) *Incendies Naturels avec des Meubles et du Papier*, Centre Technique Industriel de la Construction Métallique Report No. 2.10.20-3.

ASTM (1988) Standard test methods for fire tests of building construction and materials. *E119-88*. American Society for Testing and Materials.

ASTM Standard E 603-98, 1998 Annual book of ASTM standards, vol.04.07.West Conshohocken, Pennsylvania: American Society for Testing and Materials, p.512.

Babrauskas, V. (1976) Fire Endurance in Buildings. Ph.D Dissertation, University of California, Berkeley, *Report No. UCB FRG 76-16.*

Babrauskas, V. and Williamson, R.B. (1978) Post-Flashover Compartment Fires: Basis of a Theoretical Model. *Fire and Materials*, **2**, (2), 39-53.

Babrauskas, V. and Williamson, R.B. (1979) Post-Flashover Compartment Fires: Application of a Theoretical Model. *Fire and Materials*, **3**, (1), 1-7.

Babrauskas, V. (1979) COMPF2-A Program for Calculating Post-Flashover Fire Temperatures. National Bureau of Standards, *NBS Technical Note 991.*

Babrauskas, V. and Wickström, U.G. (1979) Thermoplastic Pool Compartment Fires. *Combustion and Flame*, **34**, 195-202.

Babrauskas, V. (1981) A Closed-form Approximation for Post-Flashover Compartment Fire Temperatures. *Fire Safety Journal*, **4**, 63-73.

Babrauskas, V. (1992a) "Chapter 7 Simple Cases of Heat Release Rates- (b) Pools". In: *Heat Release In Fires*. Eds: V. Babrauskas and S.J. Grayson. Elsevier Applied Science, London. pp. 201-206.

Babrauskas, V. (1992b) "Chapter 8 Related Quantities- (a) Heat of Combustion and Potential Heat". In: *Heat Release In Fires*. Eds: V. Babrauskas and S.J. Grayson. Elsevier Applied Science, London. pp. 207-223.

Babrauskas, V. (1995) Burning Rates, Chapter 3-1. SFPE Handbook of Fire Protection Engineering, 2nd Edition, Society of Fire Protection Engineers, Bethesda, MD, pp. **3**-1-**3**-15.

Beyler, C.L. (1984) Ignition and Burning of a Layer of Incomplete Combustion Products. *Combustion Science and Technology*, **39**, 287-303.

Beyler, C.L. (1986) Major Species Production by Diffusion Flames in a Two-Layer Compartment Fire Environment. *Fire Safety Journal*, **10**, 47-56.

BIA (1992) *New Zealand Building Code and Approved Documents*. New Zealand Building Industry Authority, Wellington, New Zealand.

Blevins, L.G. and Pitts, W.M. (1999) Modelling of bare and aspirated thermocouples in compartment fires. *Fire Safety Journal*, **33**, 239-259.

Böhm, B. and Hadvig, S. (1982) Non-conventional Fully Developed Polyethylene and Wood Compartment Fires. *Combustion and Flame*, **44**, 201-221.

Brosmer, M.A. and Tien, C.L. (1987) Radiative Energy Blockage in Large Pool Fires. *Combust. Sci. and Tech.*, Vol. **51**, pp 21-37.

Buchanan, A.H. (1998) Modelling Post-Flashover Fires with FASTLite. *J. of Fire Prot. Engr.*, **9**, (3), 1-11.

Buchanan, A.H. (2001) *Structural Design for Fire*, John Wiley and Sons, Chichester.

Bullen, M.L. (1976) A Combined Overall and Surface Energy Balance for Fully Developed Ventilation Controlled Liquid Fuel Fires in Compartments. *Fire Research Note No.1051*, Fire Research Station.

Bullen, M.L. and Thomas, P.H. (1978) Compartment Fires with Non-Cellulosic Fuels. Seventeenth Symposium (International) on Combustion, *The Combustion Institute*, pp. 1139-1148.

Cadorin, J.F. and Franssen, J.M. (1999) The One Zone Model Ozone- Description and Validation Based on 54 Experimental Fire Tests. Rapport interne SPEC/99_05, Dpt "Mécanique des Matériaux et Structures", University of Liège.

Childs, P.R.N. (2001) *Practical Temperature Measurement*. Butterworth-Heinemann, Oxford.

Cox, G. (1995) "Compartment Fire Modelling". In: *Combustion Fundamentals of Fire*. Ed: G. Cox. Academic Press, London. pp. 329-404.

Croft, D.R. and Lilley, D.G. (1977) *Heat Transfer Calculations Using Finite Difference Equations*. Applied Science Publishers Ltd, London.

Deal, S. (1994) Technical Reference Guide for FPETool Version 3.2, *Nat. Inst. Stand. Tech.* (U.S.), NISTIR 5486, Gaitherburg, MD 20899.

Denize, H.R. (2000) The Combustion Behaviour of Upholstered Furniture Materials in New Zealand. *Fire Engineering Research Report 00/4*, University of Canterbury, New Zealand.

Drysdale, D.D. (1985) *An Introduction to Fire Dynamics*. John Wiley & Sons, New York.

EC1 (1994) *Eurocode 1: Basis of Design and Design Actions on Structures. Part 2-2: Actions on Structures Exposed to Fire. ENV 1991-2-2*. European Committee for Standardisation, Brussels, Belgium.

Emmons, H.W. (1997) A Universal Vent Flow Formula. In: *Thirteenth Meeting of the UJNR Panel on Fire Research and Safety, March 13-20, 1996, Volume 1*. Ed: K.A. Beall, National Institute of Technology, NISTIR 6030. pp. 229-236.

Enright, P.A. (1999) Heat release and the combustion behaviour of upholstered furniture. *Fire Engineering Research Report 99/17*, University of Canterbury, New Zealand.

Feasey, R. (1999) Post-Flashover Design Fires. *Fire Engineering Research Report 99/6*, University of Canterbury, New Zealand.

Feasey, R. and Buchanan, A.H. (2002) Post-Flashover fires for structural design. *Fire Safety Journal*, **37**, 83-105.

Fleischmann, C.M. and Parkes, A.R. (1997) Effects of Ventilation on the Compartment Enhanced Mass Loss Rate. *Fire Safety Science- Proceedings of the Fifth International Symposium*, pp. 415-426.

Franssen, J.M. (1999) Improvement of the Parametric Fire of Eurocode 1 based on Experimental Test Results. *Fire Safety Science- Proceedings of the Sixth International Symposium*, pp. 927-938.

Goodger, E.M. (1977) *Combustion Calculations- Theory, worked examples and problems*. The MacMillan Press Ltd., London.

Gottuk, D.T., Roby, R.J., Peatross, M.J. and Beyler, C.L. (1992) Carbon-Monoxide Production in Compartment Fires. *J. of Fire Prot. Engr.*, **4**, (4), 133-150.

Grella, J.J. and Faeth, G.M. (1975) Measurements in two-dimensional thermal plume along a vertical adiabatic wall. *J. Fluid Mech.*, **71**, (4), 701-710.

Griffiths, D.V. and Smith, I.M. (1991) *Numerical methods for engineers: a programming approach.* Blackwell Scientific Publications, Oxford.

Gritzo, L.A., Gill, W. and Nicolette, V.F. (1998) Estimates of the Extent and Character of the Oxygen-Starved Interior in Large Pool Fires. *Very Large-Scale Fires, ASTM STP 1336*, Eds. N.R. Keltner, N.J. Alvares and S.J. Grayson. American Society for Testing and Materials.

Gross, D. and Robertson, A.F. (1965) Experimental Fires in Enclosures. Tenth Symposium (International) on Combustion, *The Combustion Institute*, 931-942.

Harmathy, T.Z. (1972) A New Look at Compartment Fires, Part I. *Fire Technology*, **8**, (3), 196-217.

Harmathy, T.Z. (1978) Mechanism of Burning of Fully-Developed Compartment Fires. *Combustion and Flame*, **31**, 265-273.

Harmathy, T.Z. (1979) Effect of the Nature of Fuel on the Characteristics of Fully Developed Compartment Fires. *Fire and Materials*, **3**, (1), 49-60.

Harmathy, T.Z. and Meheffrey, J.R. (1983) Post-flashover Compartment Fires. *Fire and Materials*, **7**, (2), 49-61.

Heselden, A.J.M., Thomas, P.H. and Law, M. (1970) Burning Rate of Ventilation Controlled Fires in Compartments. *Fire Technology*, **6**, (2), 123-125.

Inberg, S.H. (1928) Test of Severity of Building Fires. *National Fire Protection Quarterly*, **22**, (1) 43-61.

Incropera, F.P. and DeWitt, D.P. (2001) *Fundamentals of heat and mass transfer.* 5th Edition, John Wiley & Sons, New York.

Iqbal, N. and Quintiere, J.G. (1994) Flame Heat Fluxes in PMMA Pool Fires. *J. of Fire Prot Engr.*, **6**, (4), pp 153-162.

ISO (1975) Fire resistance tests- elements of building construction. *ISO 834-1975.* International Organisation for Standardisation.

Janssens, M. (1992) "Room Fire Models-General". In: *Heat Release In Fires*. Eds: V. Babrauskas and S.J. Grayson. Elsevier Applied Science, London. pp 113-157.

Kanury, A.M. (1992) "Chapter 7 Simple Cases of Heat Release Rates- (a) Burning of Liquid Fuel Surfaces". In: *Heat Release In Fires*. Eds: V. Babrauskas and S.J. Grayson. Elsevier Applied Science, London. pp. 175-200.

Kawagoe, K. (1958) Fire Behaviour in Rooms. Building Research Institute, Report No. 27, Japan.

Kawagoe, K. and Sekine, T. (1963) Estimation of Fire Temperature-Time Curve in Rooms. Building Research Institute, *BRI Occasional Report No. 11.*

Kawagoe, K. (1967) Estimation of Fire Temperature-Time Curve in Rooms-Third Report. Building Research Institute, *BRI Research Paper No. 29.*

Kawagoe, K., Thomas, P.H. and Pickard, R. (1972) "C. Preliminary experiments for the CIB Programme- Analysis of Rate of Burning". In: *Supplementary reports of work for the CIB International Co-operative Research Programme on Fully Developed Fires*, Ed: A.J.M. Heselden. Fire Research Station Note: FRN 923/72.

Kirby, B.R., Wainman, D.E., Tomlinson, L.N., Kay, T.R. and Peacock, B.N. (1999) Natural Fires in Large Scale Compartments. *International Journal on Engineering Performance-Based Fire Codes*, **1**, (2), pp. 43-58.

Law, M. (1983) A Basis for the Design of Fire Protection of Building Structures. *The Structural Engineer*, **61A**, (1).

Lee, S.L. and Emmons, H.W. (1961) A study of natural convection above a line fire. *J. Fluid Mech.*, **11**, 353-369.

Lin, E.C.Y. and Mehaffey, J.R. (1997) Modelling the Fire Resistance of Wood-Frame Office Buildings. *J. of Fire Sciences*, **15**, 308-338.

Loh, W.H.T. (1968) "Chapter 2 Thermodynamic Cycle Analysis of Gas Turbine and Air-breathing Propulsion Systems". In: *Jet, Rocket, Nuclear, Ion and Electric Propulsion: Theory and Design*. Ed: W.H.T. Loh. Springer-Verlag New York Inc., New York. pp. 119-206.

Magnusson, S.E. and Thelandersson, S. (1970) Temperature-Time Curves of Complete Process of Fire Development. A Theoretical Study of Wood Fuel Fires in Enclosed Spaces. Acta Polytechnica Scandinavica, Civil Engineering and Building Construction Series, No. 65, CIB/CTF/72/46, Stockholm.

Magnusson, S.E. and Thelandersson, S. (1974) A Discussion of Compartment Fires. *Fire Technology*, **10**, 228-246.

McCaffrey, B.J. and Heskestad, G. (1976) A Robust Bidirectional Low-Velocity Probe for Flame and Fire Application. *Combustion and Flame*, **26**, 125-127.

Massey, B.S. (1989) *Mechanics of Fluids,* Sixth Edition. Chapman & Hall, London.

Mitler, H.E. (1978) The Physical Basis for The Harvard Computer Fire Code. Division of Applied Sciences, *Home Fire Project Technical Report No. 34*, Harvard University.

Mulholland, G., Yusa, S., Janssens, M., Twilley, W. and Babrauskas, V. (1992) The Effect of Oxygen Concentration on CO and Smoke Produced by Flames. *Fire Safety Science- Proceedings of the Third International Symposium*, pp. 585-594.

Nakaya, I., Tanaka, T. and Yoshida, M. (1986) Doorway Flow Induced by a Propane Fire.. *Fire Safety Journal*, **10**, 185-195.

Nilsson, L. (1971) The Effect of the Porosity and Air Flow Factor on the Rate of Burning for Fire in Enclosed Space. Swedish National Building Research Institute Report R22, Stockholm.

Ödeen, K. (1963) Theorectical Study of Fire Characteristics in Enclosed Spaces (Bulletin 10). Div. of Bldg. Constr., Royal Inst. of Tech., Stockholm.

Parker, W.J. (1988) Prediction of the Heat Release Rate of Wood. Doctor of Science Dissertation, The George Washington University.

Parker, W.J. (1992) "Prediction of Heat Release Rate from Basic Measurements". In: *Heat Release In Fires*. Eds: V. Babrauskas and S.J. Grayson. Elsevier Applied Science, London. pp 333-356.

Parkes, A.R. (1996) Under-Ventilated Compartment Fires- A Precursor to Smoke Explosions. *Fire Engineering Report 96/5*, University of Canterbury.

Parkes, A.R. (2002) PhD Thesis, University of Canterbury, New Zealand. Under preparation.

Pettersson, O. (1996) The Parametric Temperature-Time Curves According to ENV 1991-2-2: 1995E- A Summary Evaluation. *International Organisation for Standardisation*, ISO/TC92/SC2/WG2, N261.

Pitts, W.M., Braun, E., Peacock, R.D., Mitler, H.E., Johnsson, E.L., Reneke, P.A. and Blevins, L.G. (1998) Temperature Uncertainties for Bare-Bead and Aspirated Thermocouple Measurements in Fire Environments. In: *Annual Conference on Fire Research, November 2-5, 1998*. Ed: K.A. Beall, National Institute of Technology, NISTIR 6242. pp. 15-16.

Prahl, J. and Emmons, H.W. (1975) Fire Induced Flow Through an Opening, *Combustion and Flame*, **25**, 369-385.

Quintiere, J.G. and DenBraven, K. (1978) Some Theoretical Aspects of Fire Induced Flows Through Doorways In A Room-Corridor Scale Model. National Bureau of Standards, *NBSIR 78-1512.*

Quintiere, J.G. (1984) A Perspective on Compartment Fire Growth. *Combustion Science and Technology*, **39**, pp. 11-54.

Quintiere, J.G. (1992) A Semi-Quantitative Model for the Burning Rate of Solid Materials. National Institute of Standards and Technology, NISTIR 4840, Gaithersburg, MD.

Quintiere, J.G. (1997) *Principles of Fire Behaviour*. Delmar Publishers, New York.

Quintiere, J.G. (2002) Fire Behaviour in Building Compartment. *Personal Communication.*

Rockett, J.A. (1976) Fire Induced Gas Flow in an Enclosure. *Combustion Science and Technology*, **12**, 165-175.

Roy, F. (1993a) *Essais d'Incendies Naturels avec Profilés en Acier Nus et Protégés.* Centre Technique Industriel de la Construction Métallique Report No. 92-E-080.

Roy, F. (1993b) *Essais d'Incendies Naturels avec Profilés en Acier Nus et Protégés.* Centre Technique Industriel de la Construction Métallique Report No. 92-E-093.

Roy, F. (1993c) *Essais d'Incendies Naturels avec Profilés en Acier Nus et Protégés.* Centre Technique Industriel de la Construction Métallique Report No. 92-E-094.

Santo, G. and Tamanini, F. (1981) Influence of Oxygen Depletion on the Radiative Properties of PMMA Flames. Eighteenth Symposium (International) on Combustion, *The Combustion Institute*, pp. 619-631.

Schaffer, E.L. (1966) *Review of Information Related to the Charring of Wood.* Research Note FPL-145, USDA Forest Prods. Lab., Madison.

Schaffer, E.L. (1967) *Charring Rate of Selected Woods- Transverse to Grain.* Research Paper FPL 69, USDA Forest Prods. Lab., Madison.

Schneider, U., Kersken-Bradley, M. and Max, U. (1990) *Neuberechnung der Wärmeabzugsfaktoren w für die DIN V 18230 Teil 1-Baulicher Brandschutz im industribau* [in German]. Arbeitsgemeinschaft Brandsicherheit Munchen/Kassel.

Spearpoint, M.J. (1999) Predicting the ignition and burning rate of wood in the cone-calorimeter using an integral model. *NIST-GCR-99-775.*

Spearpoint, M.J. and Quintiere, J.G. (2000) Predicting the Burning of Wood Using an Integral Model. *Combustion and Flame*, **123**, 308-324.

Steckler, K.D., Baum, H.R. and Quintiere, J.G. (1984) Fire Induced Flows Through Room Openings- Flow Coefficients. Twentieth Symposium (International) on Combustion, *The Combustion Institute*, pp 1591-1600.

Stull, D.R. and Prophet, H. (1971) *JANAF Thermodynamical Tables*, National Bureau of Standards, Washington, D.C.

Takeda, H. and Akita, K. (1982) New Modelling of Liquid or Thermoplastic Pool Fires in Compartment. Nineteenth Symposium (International) on Combustion, *The Combustion Institute*, pp 897-904.

Takeda, H. (1983) Mixing Effect and Combustion Efficiency in Compartment Fires. *Fire Safety Journal*, **5**, 199-204.

Takeda, H. and Yung, D. (1992) Simplified Fire Growth Models for Risk-Cost Assessment in Apartment Buildings. *J. of Fire Prot. Engr.*, **4**, (2), 53-66.

Tanaka, T. and Yamada, S. (1994) An Empirical Model of the Yield of Carbon Monoxide in Fires. *Fire Science and Technology*, **14**, (1 & 2), 19-29.

Tewarson, A., Lee, J.L. and Pion, R.F. (1981) The Influence of Oxygen Concentration on Fuel Parameters for Fire Modelling. Eightteenth Symposium (International) on Combustion, *The Combustion Institute*, pp. 563-570.

Tewarson, A. (1995) Generation of Heat and Chemical Compounds in Fires, Chapter 3-4. SFPE Handbook of Fire Protection Engineering, 2nd Edition, Society of Fire Protection Engineers, Bethesda, MD, pp. **3**-53-**3**-124.

Thomas, I.R. (1999a) CIB Tests of Fire Severity in Single Vent Enclosures with Uniform Fire Load- Paper 1. *Personal Communication.*

Thomas, I.R. (1999b) The Severity of Fires in Enclosures- Paper 5. *Personal Communication.*

Thomas, I.R. and Bennetts, I.D. (1999) Fires in Enclosures with Single Ventilation Openings- Comparison of Long and Wide Enclosures. *Fire Safety Science-Proceeding of the Sixth International Symposium*, pp. 941-952.

Thomas, P.H., Hinkley, P.L., Theobald, C.R. and Simms, D.L. (1963) Investigations into the flow of hot gases in roof venting, *Fire Research Technical Report No.7.*

Thomas, P.H. and Heselden, A.J.M. (1972) Fully developed fires in single compartments. A cooperative research programme of the Conseil Internationale du Batiment. Conseil Internationale du Batiment Report No. 20, *Fire Research Note No. 923.*

Thomas, P.H. (1974) "Fires in Enclosure". In: *Heat Transfer in Fires: Thermophysics, social aspects, economic impact.* Ed: P.L. Blackshear. John Wiley & Sons, New York. pp. 73-94

Thomas, P.H. (1992) Two-Dimensional Smoke Flows from Fires in Compartments: Some Engineering Relationships. *Fire Safety Journal*, **18**, 125-137.

Thomas, P.H. (1995) "The Growth of Fire- Ignition to Full Involvement". In: *Combustion Fundamentals of Fire*. Ed: G. Cox. Academic Press, London. pp. 275-328.

Tien, C.L., Lee, K.Y. and Stretton, A.J. (1995) Radiation Heat Transfer, Chapter 4-1. SFPE Handbook of Fire Protection Engineering, 2nd Edition, Society of Fire Protection Engineers, Bethesda, MD, pp. **1**-65-**1**-79.

Tran, H.C. (1992) "Experimental Data on Wood Materials". In: *Heat Release In Fires*. Eds: V. Babrauskas and S.J. Grayson. Elsevier Applied Science, London. pp. 357-372.

Tsuchiya, Y. and Sumi, K. (1971) Computation of the Behaviour of Fire in an Enclosure. *Combustion and Flame*, **16**, 131-139.

Van Wylen, G.J., Sonntag, R.E. and Borgnakke, C. (1994) *Fundamentals of Classical Thermodynamics*. 4th Edition, John Wiley & Sons, Inc., New York.

Ward, C. (1995) Post-Flashover Fire Models-A Review. Centre for Fire Safety Studies, Worcester Polytechnic Institute, *FPE 520 Term Paper*.

Yamada, S. and Tanaka, T. (1994) A Model for Predicting Concentrations of Carbon Monoxide in Building Fires. *Fire Safety Science- Proceedings of the Fourth International Symposium*, pp. 539-550.

Yamada T. (1997) Experimental Study of the Exchange Flow through a Horizontal Ceiling Vent in Atrium Fires- Criteria of Supply Air and Pressure necessary for Uni-directional Flow. In: *Thirteenth Meeting of the UJNR Panel on Fire Research and Safety, March 13-20, 1996, Volume 2*. Ed: K.A. Beall, National Institute of Technology, NISTIR 6030. pp. 21-29.

Yii, H.W. (2000) Effect of Surface Area and Thickness on Fire Loads. *Fire Engineering Research Report 00/13*, University of Canterbury, New Zealand.

Yii, E.H. (2002) Exploratory Roof Vent Fire Experiment. *Fire Engineering Research Report*, University of Canterbury, New Zealand, under preparation.

Zukoski E.E. (1995) "Properties of Fire Plumes". In: *Combustion Fundamentals of Fire*. Ed: G. Cox. Academic Press, London. pp. 101-219.

Appendix A Vitiation and radiation effects on pool fires

Appendix A presents the small-scale mass loss rate data obtained from the literature and compares it with the calculations made using Quintiere's model.

A.1 SMALL-SCALE MASS LOSS RATE DATA UNDER VITIATION AND RADIATION EFFECTS

The data presented here are the test data from Tewarson et al (1981), Santo and Tamanini (1981) and Mulholland et al (1992). These data have been published in the respective literature. For the tests by Tewarson et al (1981) and Santo and Tamanini (1981), no external irradiance heat flux was imposed upon the burning fuels, only the oxygen concentration in the supply air stream was changed. For the tests by Mulholland et al (1992), both oxygen concentration and irradiance heat flux were varied.

These data sets are to be compared with the prediction made by the Quintiere's model, given as follows.

$$\dot{m}''_p = \dot{m}''_{freeburn}\left(\frac{Y_{ox}}{0.233}\right) + \frac{\dot{q}''_{rad}}{L_g} \qquad \textbf{(A.1)}$$

Table A.1 presents the data for Tewarson et al (1981) and Santo and Tamanini (1981) tests. Both the testing oxygen concentration and the respective mass loss rate per unit area of fuel measured are presented. The calculated mass loss rates presented are

evaluated using Equation (A.1) with the radiation term, $\dot{q}''_{rad} / L_g$, set to zero, as there was no external irradiance heat flux imposed on the burning samples during the tests.

Table A.1 Summary of experimental mass loss data sets under the influence of oxygen vitiated conditions found in literature.

		Experimental measurements		Model calculation
Source	Fuel	O_2 (by wt)	$\dot{m}''_{p,\exp}$	$\dot{m}''_{p,calc}$
Tewarson et al (1981)	PMMA (ϕ=0.1m)	0.233	0.0115	Free-burn
		0.207	0.0077	0.0102
		0.195	0.0076	0.0096
		0.183	0.0059	0.0090
	PMMA (ϕ=0.3m)	0.233	0.0129	Free-burn
		0.223	0.0121	0.0123
		0.212	0.0106	0.0117
		0.200	0.0092	0.0111
	Heptane(ϕ=0.1m)	0.233	0.0356	Free-burn
		0.223	0.0291	0.0341
		0.212	0.0253	0.0324
		0.190	0.0183	0.0290
		0.178	0.0174	0.0272
		0.173	0.0170	0.0264
	PP (ϕ=0.1m)	0.233	0.0065	Free-burn
		0.208	0.0053	0.0058
		0.196	0.0022	0.0055
Santo and Tamanini (1981)	PMMA (ϕ=0.3m)	0.233	0.0129	Free-burn
		0.221	0.0123	0.0122
		0.211	0.0108	0.0117
		0.201	0.0092	0.0111

In the tests by Mulholland et al (1992), both oxygen concentration and irradiance heat flux were varied. However, no free-burn case has been reported, as irradiance heating was involved in all their tests, so a base case scenario for each material (PMMA and

PE) has to be chosen. The base case chosen are presented in the Table A.2. They represent the value closest to the free-burn case.

Table A.2 Base case scenarios for Mulholland et al (1992) PMMA and PE data sets.

Material	Oxygen concentration (by weight)	Irradiance heat flux (kW/m^2)	Mass loss rate (kg/m^2 s)	Heat of gasification (kJ/kg)
PMMA	0.233	15	0.021	2200
PE	0.233	25	0.008	2700

In order to calculate the mass loss rate of fuel under vitiated conditions and irradiance heat flux, both the vitiation and radiation terms are calculated relative to the base case scenario. For example, for PMMA fuel under an oxygen concentration (by weight) of 0.169 and an irradiance heat flux of 30 kW/m^2, the vitiation term is calculated as follow with $\dot{m}''_{freeburn} = 0.021$ (kg/m^2 s) as in the base case where

$$\dot{m}''_{freeburn}\left(\frac{Y_{ox}}{0.233}\right) = 0.021 \times \left(\frac{0.169}{0.233}\right)$$
$$= 0.015 \quad kg/m^2 s$$

As for the radiation term, since the irradiation flux is 15 kW/m^2 different to the base case, i.e. 30 kW/m^2 c.f. 15 kW/m^2 in the base case, using the heat of gasification property for PMMA (2200 kJ/kg), it is calculated as

$$\frac{\Delta\dot{q}''}{L_g} = \frac{15}{2200}$$
$$= 0.007 \; kg/m^2 s$$

Hence the mass loss rate of the fuel under these conditions is evaluated as:

$$\dot{m}''_p = \dot{m}''_{freeburn}\left(\frac{Y_{ox}}{0.233}\right) + \frac{\Delta\dot{q}''}{L_g}$$
$$= 0.015 + 0.007$$
$$= 0.022 \; kg/m^2 s$$

The experiment data from Mulholland et al (1992) tests and the corresponding mass loss rate calculated are presented in the Table A.3.

Table A.3 Summary of Mulholland et al (1992) PMMA and PE data sets.

	Experimental measurements			Model calculation
Material	O_2 (by wt)	$\dot{q}''_{irrd}$ (kW/m^2)	$\dot{m}''_{p,exp}$ (kg/m^{2}s)	$\dot{m}''_{p,calc}$ (kg/m^{2}s)
PMMA	0.191	15	0.015	0.017
PMMA	0.179	15	0.013	0.016
PMMA	0.169	15	0.011	0.015
PMMA	0.233	30	0.025	0.028
PMMA	0.191	30	0.021	0.024
PMMA	0.169	30	0.019	0.022
PMMA	0.155	30	0.015	0.021
PE	0.190	25	0.006	0.007
PE	0.170	25	0.004	0.006
PE	0.233	40	0.010	0.014
PE	0.190	40	0.008	0.012
PE	0.157	40	0.007	0.011

These values presented Table A.1 and Table A.3 were use to plot Figure 5.3 in Chapter 5.

Appendix B Mass loss rate histories of furniture

Appendix B reproduces the mass loss rate histories of the wooden furniture surveyed by Yii (2000). These plots are presented for the completeness of this thesis.

B.1 OVERVIEW

Yii (2000) surveyed and measured the geometry of typical furniture items including bookshelves, cupboards, desks, tables and chairs. Each furniture item was divided into individual components of different geometrical shapes. Applying a regression rate of 0.011mm/s on all the exposed surface areas, the change of the remaining surface area of the furniture over time is manually evaluated by summing the remaining surface area of each component over time. The mass loss rate history of the furniture item over time due to surface regression is therefore obtained via Equation (6.6), i.e. by multiplying the regression rate (0.011mm/s), the density of wood (450 kg/m^3) and the remaining fuel surface area, $A_F(t)$.

It is found that there are different behaviours between different types of wooden furniture items, and so they are classified into two categories, namely (1) "thick" and (2) "thin". This classification is arbitrary and is based upon the furniture respective mass loss rate curve. Wood-based furniture items that present a rapid drop in mass loss rate during the first 30 minutes, and burn away completely in less than three hours, are classified as "thin". Wood-based furniture items that do not exhibit any rapid drop in the mass loss rate, or burn for three hours or more are classified as "thick".

Table B.1 categorised the furniture items surveyed and measured by Yii (2000). The estimated mass of each furniture item is also given.

Table B.1 Groupings for typical furniture.

Classification	Furniture item
Group 1- "Thick" furniture	Bookshelf (I) 50% (51kg)
	Bookshelf (I) 75% (70kg)
	Bookshelf (I) 100% (86kg)
	Bookshelf (II) 50% (144kg)
	Bookshelf (II) 75% (197kg)
	Bookshelf (II) 100% (243kg)
	Bookshelf (III) 100% filled (444kg)
	Cupboard (I) 100% filled (149kg)
	Small cabinet 100% filled (29kg)
Group 2- "Thin" furniture	Bookshelf (I) 25% filled (31kg)
	Bookshelf (II) 25% filled (92kg)
	Cupboard (I) empty (65kg)
	Small cabinet empty (15kg)
	Desk (I) (48kg)
	Desk (II) (12.5kg)
	Desk (III) (67kg)
	Table (I) (18kg)
	Table (II) (25kg)
	Stool (1kg)
	Chair (I) (10kg)
	Chair (II) (4.5kg)

B.2 MASS LOSS RATE HISTORIES OF FURNITURE

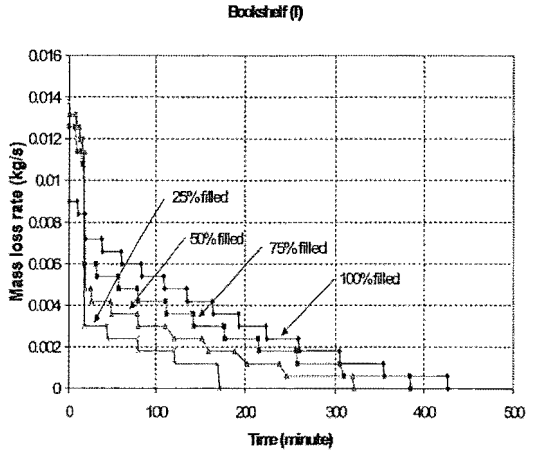

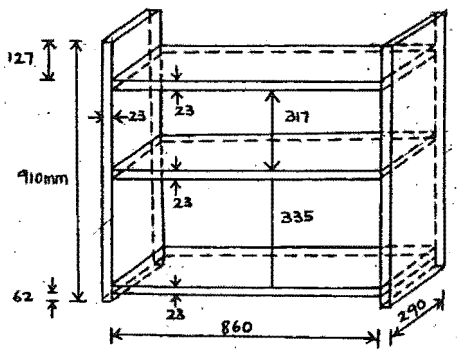

Figure B.1 Bookshelf (I)

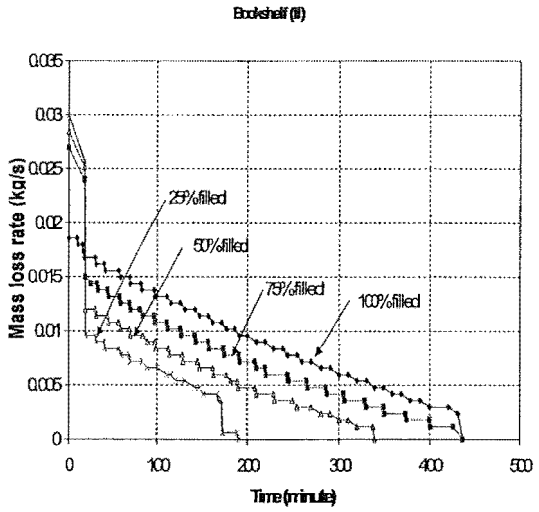

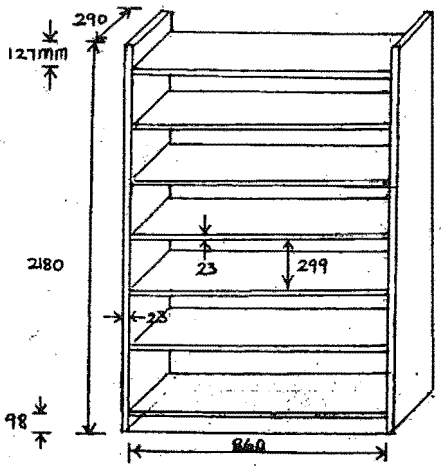

Figure B.2 Bookshelf (II)

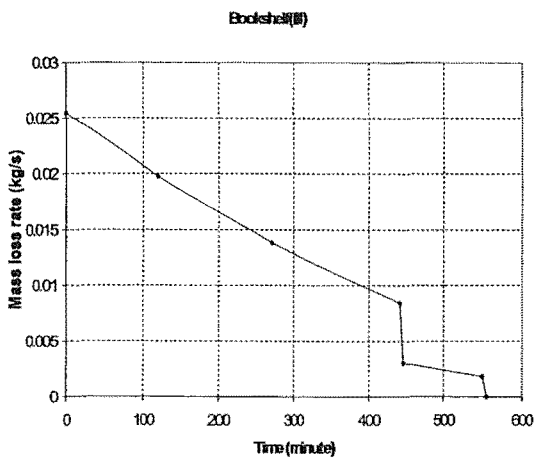

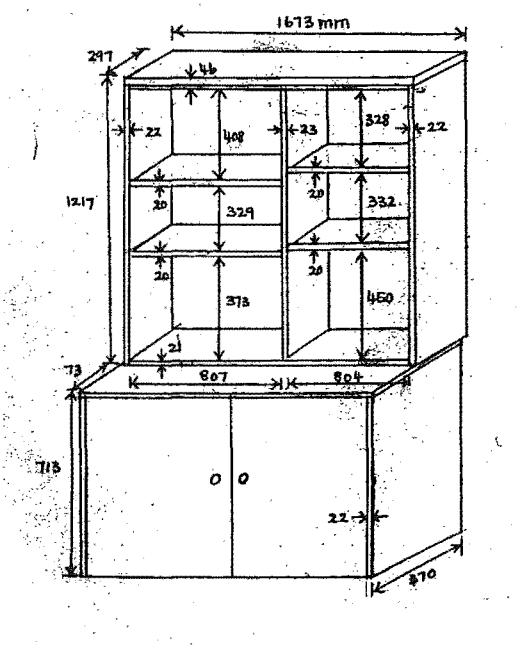

Figure B.3 Bookshelf (III)

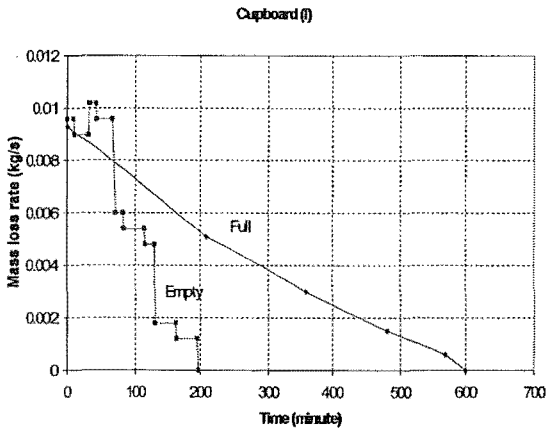

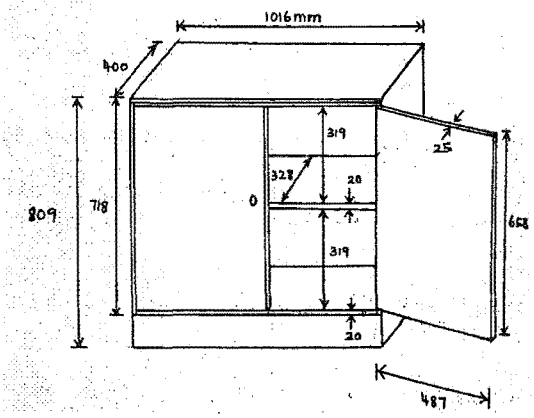

Figure B.4 Cupboard (I)

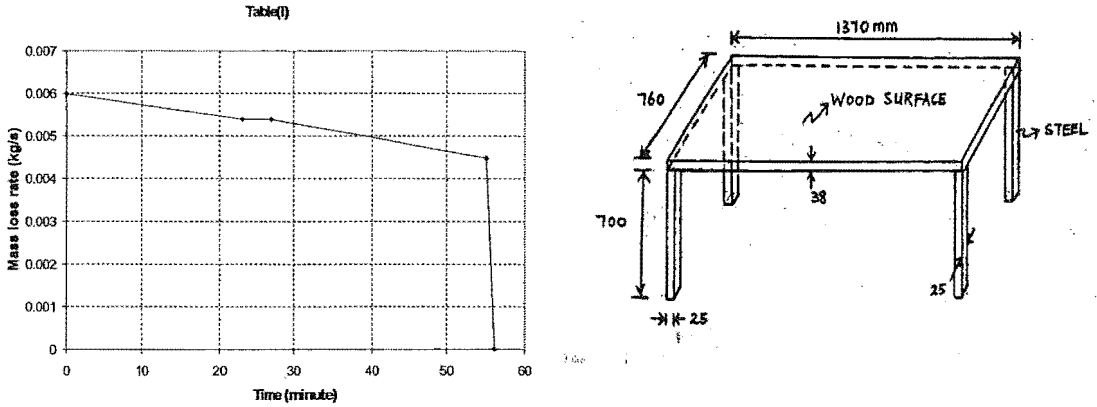

Figure B.5 Table (I)

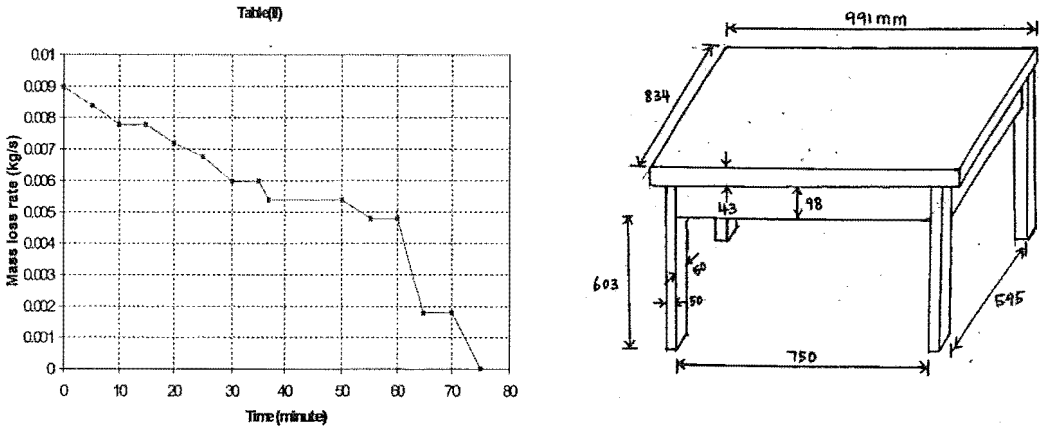

Figure B.6 Table (II)

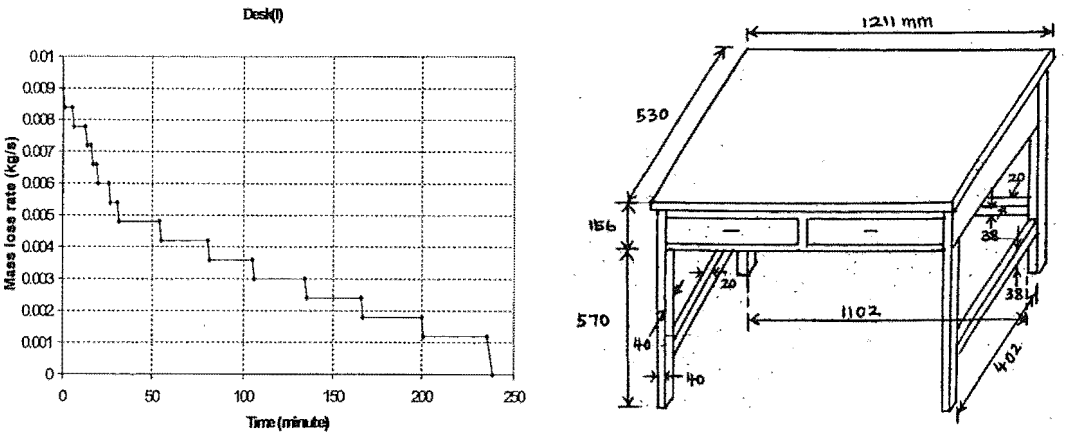

Figure B.7 Desk (I)

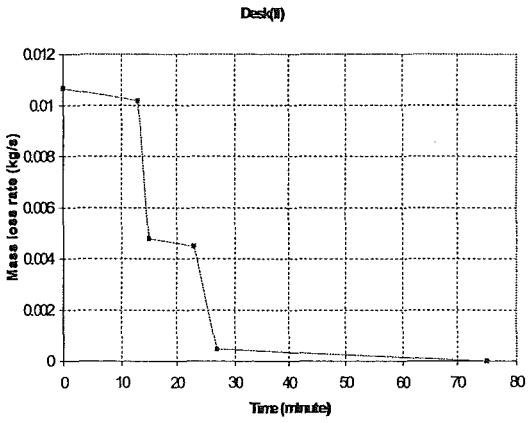

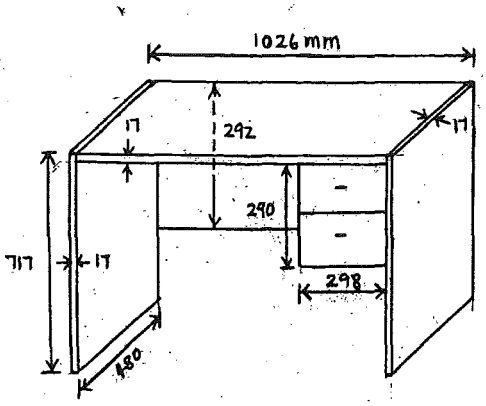

Figure B.8 Desk (II)

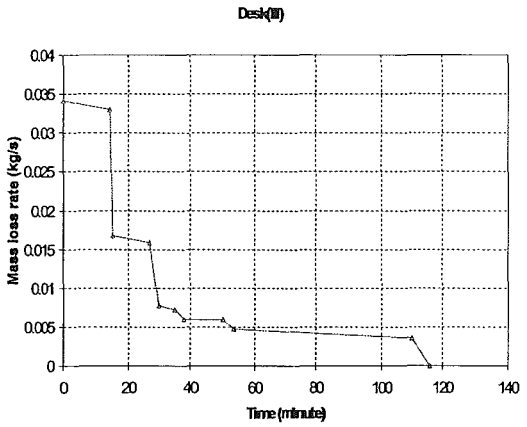

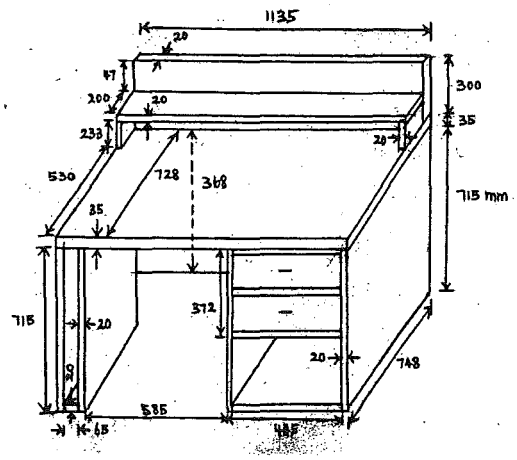

Figure B.9 Desk (III)

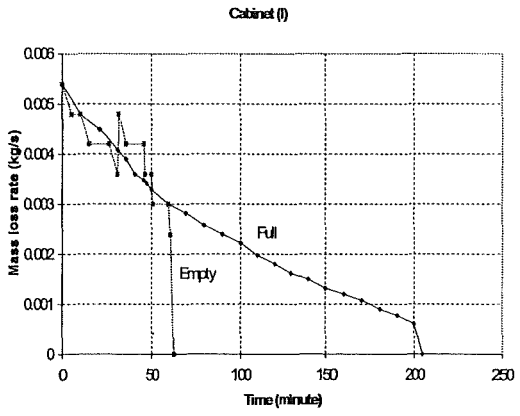

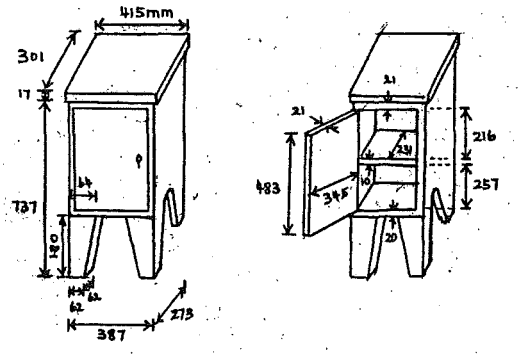

Figure B.10 Small cabinet

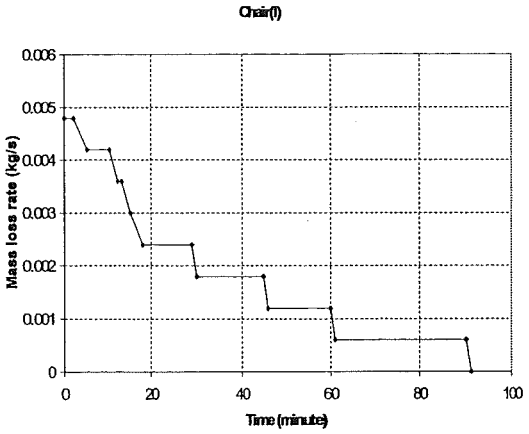

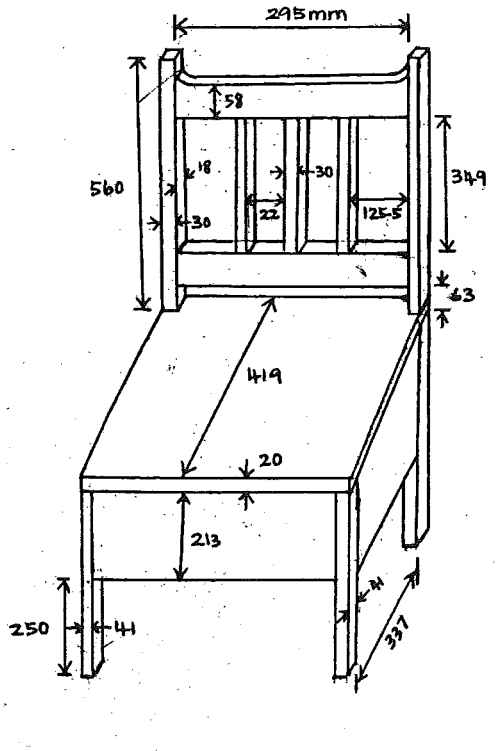

Figure B.11 Chair (I)

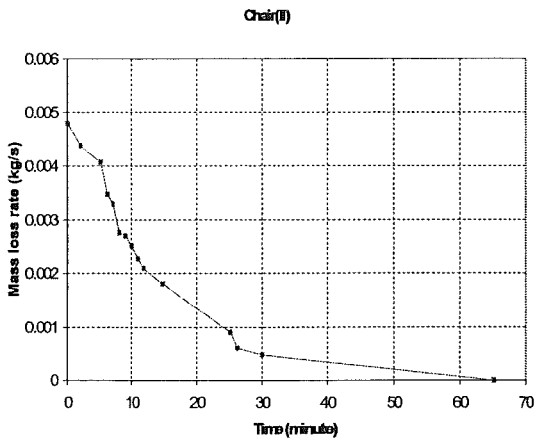

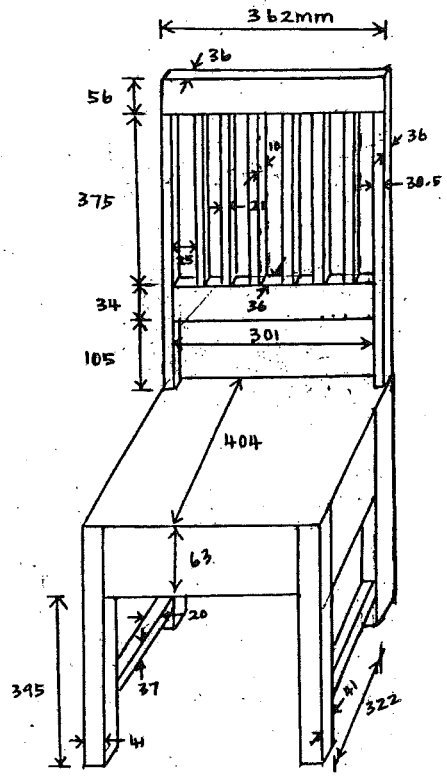

Figure B.12 Chair (II)

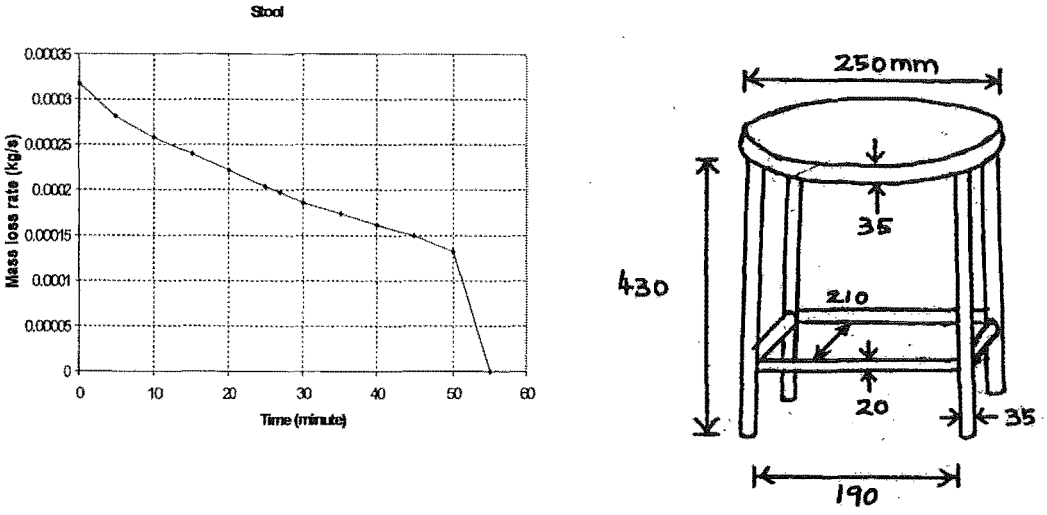

Figure B.13 Stool

Appendix C Velocity probe for reduced scale fire experiment

Appendix C presents the calibration results for the Type-S pitot tube tested using the wind tunnel facility.

C.1 INTRODUCTION

Vent flow is an important aspect in compartment fire dynamics. To measure vent flow experimentally, the bi-directional probe developed by McCaffrey and Heskestad (1976) is often used. The probe consists of a short piece of stainless steel tube with a diaphragm in the middle. Two pressure taps are drilled on either side of the diaphragm where the support tubes are attached. The probe itself has a diameter of 22.2mm (or 7/8″); its fabrication details are shown in Figure C.1.

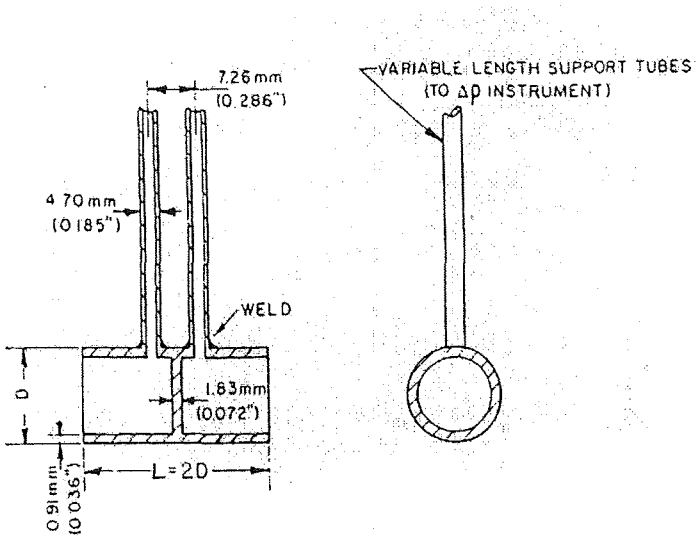

Figure C.1 Fabrication details of McCaffrey and Heskestad bi-directional probe.

For the purpose of measuring the vent flows in the scaled down fire compartment, the standard McCaffrey and Heskestad (1976) bi-directional probe was considered too big and could interfere with the actual flow when multiple probes are positioned at the vent openings. Scaling down the standard bi-directional probe would involve labour intensive work in manufacturing, such as welding the joint between the supporting tubes and the pressure taps on the sensing tubes. The joint would also have to be reasonably clean of burr to ensure minimal disturbance in the pressure differential measurements.

The type-S pitot tube is a type of velocity probe that has been used in stack gas velocity measurement in duct system. It consists of two stainless steel tubes with impact or sensing holes orientated at 180° angles to one another. Its basic operating principal is similar to the bi-directional probe, having a sensing hole facing upstream measuring the stagnation pressure and a sensing hole facing downstream measuring the static pressure. However, the manufacturing of the type-S pitot tube is more straightforward than the bi-directional probe, as the type-S pitot tube does not require wielding between the support tubes and the sensing tube. Rather, the end edges of support tubes are bent such that they form pressure taps themselves. The manufacturing specifications for the type-S pitot tube allow a minimum external tube diameter down to 3/16 inch or 4.8mm which is much smaller than the standard bi-directional probe. With these attributes, the type-S pitot tube presents an attractive alternative for reduced-scale compartment fire applications.

In this appendix, the calibration results for the type-S pitot are reported. The calibration was carried out using the wind tunnel facility in the Mechanical Engineering Department at the University of Canterbury.

C.2 APPARATUS

C.2.1 Type-S pitot tube

The type-S pitot tube used in this experiment was fabricated using a 1/4 inch or 6.35mm external diameter stainless steel tube as shown in Figure C.2. The distance between the tips of the two opposite outward facing impact holes was cut and ground to 18.5mm.

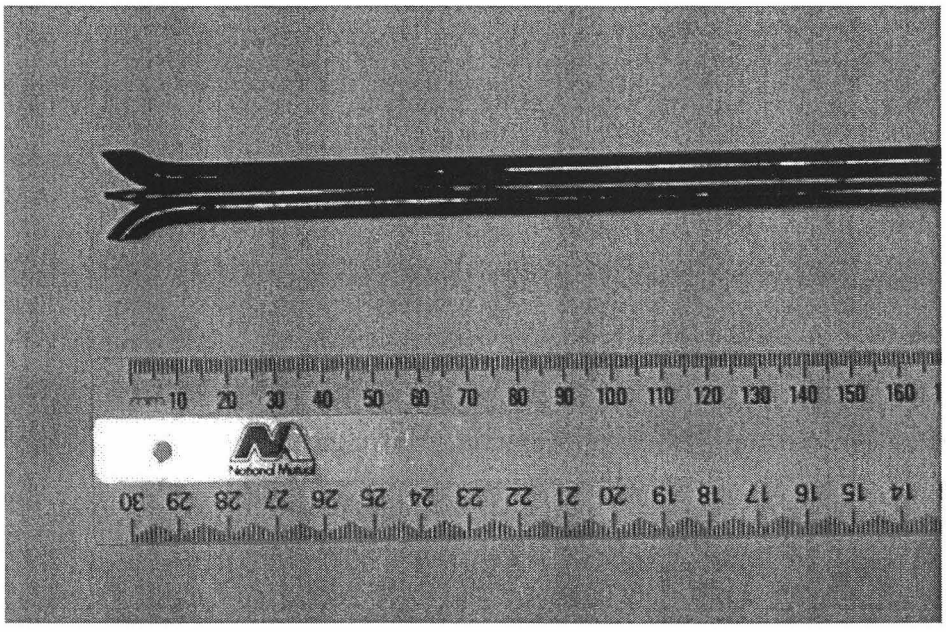

Figure C.2 A type-S pitot tube.

The manufacturing specification for the type-S pitot tube can be found from the Emission Measurement Center- Codes of Federal Regulations (EMC-CFR) promulgated test methods for type-S pitot tube on the United States Environmental Protection Agency (USEPA) website: http://www.epa.gov/ttn/emc/tmethods.html, and is shown in Figure C.3.

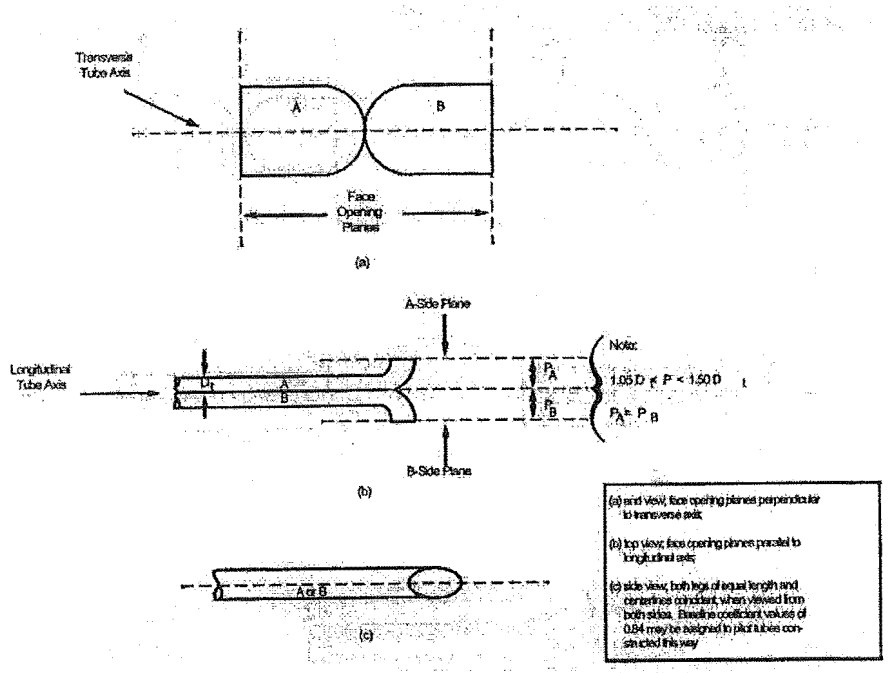

Figure C.3 Recommendation for properly constructed Type-S pitot tube (USEPA).

Two thermocouples were mounted on the probe by tacking 3mm diameter hollow tubes between the upper and lower sides of the two support tubes, which thermocouple wires were run through and correctly located at the sensing point. This is schematically presented in Figure C.4 showing the cross section of the probe.

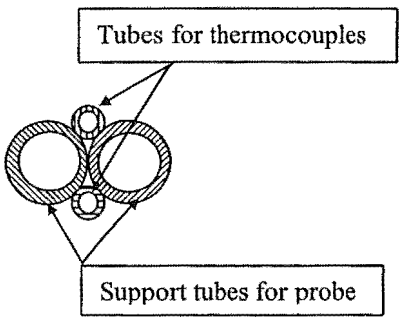

Figure C.4 Schematic representation of the cross section of a type-S pitot tube.

C.2.2 Wind tunnels

High-speed and low-speed wind tunnels were used to test the type-S pitot tube under a wide range of air speeds.

The high-speed wind tunnel was a fan-driven sub-sonic wind tunnel. It had a test section of 1.5m by 1.5m cross section and 2m in length where the velocity of airflow was uniform. The velocity of the wind tunnel in the test section was monitored using a standard pitot-static tube connected to a water manometer with reading accuracy within 0.1mm H_2O, and a digital thermometer was used to monitor the airflow temperature inside the wind tunnel. The ambient atmospheric pressure was also monitored. The velocity of airflow in the high-speed wind tunnel was evaluated as:

$$v_{airflow} = \sqrt{2 \cdot \Delta P_{ps} \cdot \frac{R_{air}}{C_{ps}} \cdot \frac{T_{airflow}}{P_{atm}}} \qquad \textbf{(C.1)}$$

where

$v_{airflow}$ -Air flow velocity (m/s)

ΔP_{ps} -Pressure differential of the pitot-static tube (Pa) measured using a water manometer ($\rho_w g h_w$)

$T_{airflow}$ -Air flow temperature (K)

P_{atm} -Ambient atmospheric pressure (Pa)

R_{air} -Specific gas constant for air 287 J/kgK

C_{ps} -Pitot-static tube instrument calibration coefficient (0.997)

The low-speed wind tunnel was driven by compressed air. The compressed air was directed to enter the high-speed end of the tunnel via a flowmeter. The flowmeter is attached to a water manometer for monitoring the entering flow. It is then passed through a gradual expanded chute of 1.5m in length to smooth out the turbulence and slow down the air speed. The diameter of the exit opening is 99mm. It operates at a velocity range lower than 1.5m/s. The air speed at the exit was evaluated as:

$$v_{airflow} = \frac{1}{A_{exit}} \sqrt{C_{flowmeter} \cdot \frac{\rho_w}{\rho_{air}} \cdot h_{w\,flowmeter}} \qquad \textbf{(C.2)}$$

where

A_{exit} -Opening area at the exit of the wind tunnel (m^2)
In this particular wind tunnel, $=7.698\times10^{-3}$ m^2

$C_{flowmeter}$ -Calibration constant for the flowmeter, 480.85×10^{-12}

ρ_w -Density of water in the manometer, $1000 kg/m^3$

ρ_{air} -Density of air in the airflow, calculated using the Ideal Gas Law ($\rho=P/RT$) (kg/m^3)

h_w -Water head measured in the water manometer off the flowmeter (mm)

C.3 CALIBRATION

C.3.1 Background

The type-S pitot tube has the "total head" tube facing in the direction of the flow and the "static" tube facing backward into the wake behind the instrument. Based upon the Bernoulli equation:

$$P + \frac{1}{2}\rho v^2 + \rho g z = const \qquad \textbf{(C.3)}$$

At the stagnation point, i.e. at the tube facing into the flow direction, the flow along the streamline is brought to a standstill. From the Bernoulli equation (Equation (C.3)), the pressure has to increase from P to $(P + \rho v^2/2)$. The quantity $(P + \rho v^2/2)$ is known as the stagnation pressure of that streamline (Massey, 1989). Knowing the static pressure, the velocity of the flow can be calculated. For an instrument such as the type-S pitot tube, because the static tube is in the wake region, it will be measuring a

pressure slightly less than the undisturbed static pressure. A correction factor C_{calib}, obtained from calibration is required to correct for this difference such that

$$\Delta P = C_{calib} \times \frac{\rho v^2}{2} \qquad \textbf{(C.4)}$$

where ΔP is the pressure differential measured between the stagnation and static pressure measured by the probe, and ρ and v are the density and velocity of the flow.

C.3.2 Testing programme

The type-S pitot tube was subjected to two test programmes. The first test programme involved testing at different flow velocities. Given the wind tunnel facility available, the type-S pitot tube was tested in the range between 0.5 and 4.0 m/s under ambient conditions. Both the forward and reversed positions of the probe were tested, to check the bi-directional capability. The second test programme involved testing at different flow angles. This was to investigate the probe responses to flows at various angles. In the angle-testing programme, the velocity probes were tested with flow angles ranging between ±40° in the plane normal to the axes of the support tubes, at an increment of 10°. Figure C.5 shows the definition of the flow angles.

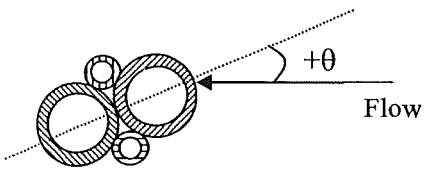

Figure C.5 Definition of the flow angle.

Four type-S pitot tubes were tested to gauge the consistency in the manufacturing.

C.3.3 Method

The high-speed wind tunnel was used to calibrate the type-S pitot tube over the velocity range of 2m/s to 4m/s. The type-S pitot tube was held from outside the tunnel test section on a test platform, and placed some distance (~150mm) below the standard pitot-static tube used for monitoring the velocity inside the wind tunnel. The type-S pitot tube was connected to a MKS Baratron Type 223B bi-directional pressure transducer and the signal was logged via a data logger. An averaged pressure transducer reading over a one-minute duration was taken at each flow velocity. The temperature of the wind tunnel airflow was measured using a digital thermometer. The atmospheric pressure was measured using a barometer. Similar procedures were performed in the low-speed wind tunnel where the type-S pitot tube was placed in the centre at the exit of the wind tunnel. Four type-S pitot tubes were tested.

The angle-testing programme was carried out in the high-speed wind tunnel at a flow velocity of 2.8m/s. Four wooden wedges of 10°, 20°, 30° and 40° inclinations on the test platform were used in turn to position the probe at each desirable angle. While maintaining the same flow velocity inside the wind tunnel, an averaged pressure transducer signal over a one-minute duration was taken at each inclination.

C.4 RESULTS

C.4.1 Velocity testing

From the velocity testing, the calibration factor, C_{calib}, for the type-S pitot tube was found by plotting the term, $\rho v^2/2$, against the pressure differential measured at the probe, ΔP. Figure C.6 presents the calibration plot at the low speed regime where the Reynolds number (based on the probe diameter) is less than 700. The expression for the Reynolds number is given in Equation (C.5).

$$\mathrm{Re} = \frac{\rho u D}{\mu} = \frac{u D}{\nu} \qquad \textbf{(C.5)}$$

where D is the diameter of the probe, ρ is the density (kg/m^3), μ is the dynamic viscosity (kg m^{-1} s^{-1}) and ν is the kinematic viscosity (m^2/s)

By fitting a linear regression line through the origin, the calibration factor, C_{calib}, for the type-S pitot tube is approximately 1.59.

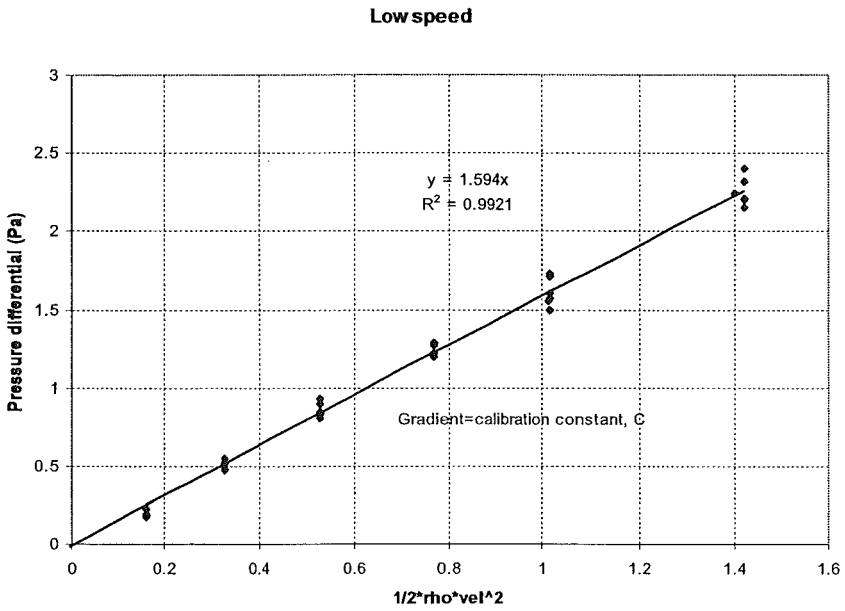

Figure C.6 Calibration plot at the low speed regime (Re<700).

Figure C.7 presents the calibration plot at the high-speed regime where the Reynolds number (based on the probe diameter) is greater than 900. The calibration factor, C_{calib}, is found to be approximately 1.90.

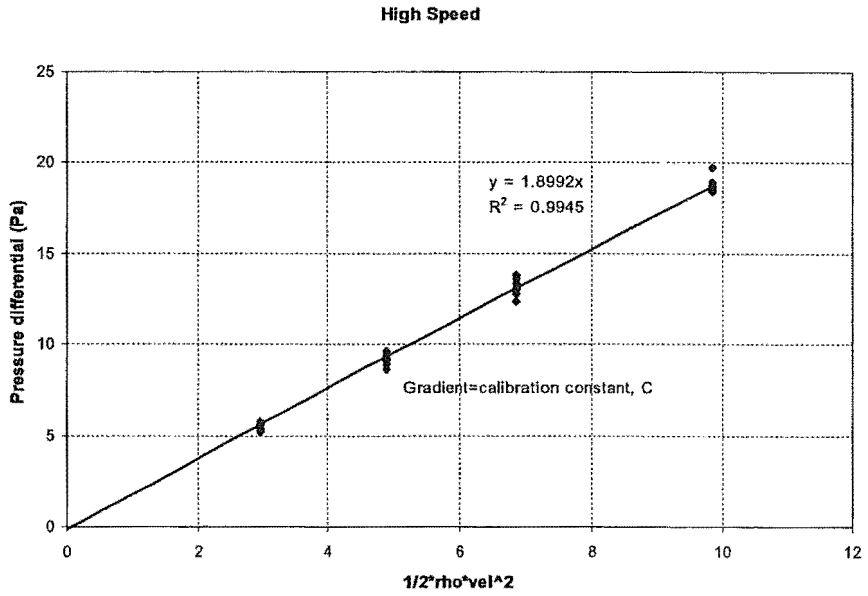

Figure C.7 Calibration plot at the high speed regime (Re>900).

Figure C.8 plots the square-root of the calibration factor, $C_{calib}^{1/2}$ (defined in Equation (C.6)) against the Reynolds number (defined in Equation (C.5)), for the four type-S pitot tubes tested.

$$C_{calib}^{1/2} = \frac{(2\Delta P/\rho)^{1/2}}{v} \qquad \textbf{(C.6)}$$

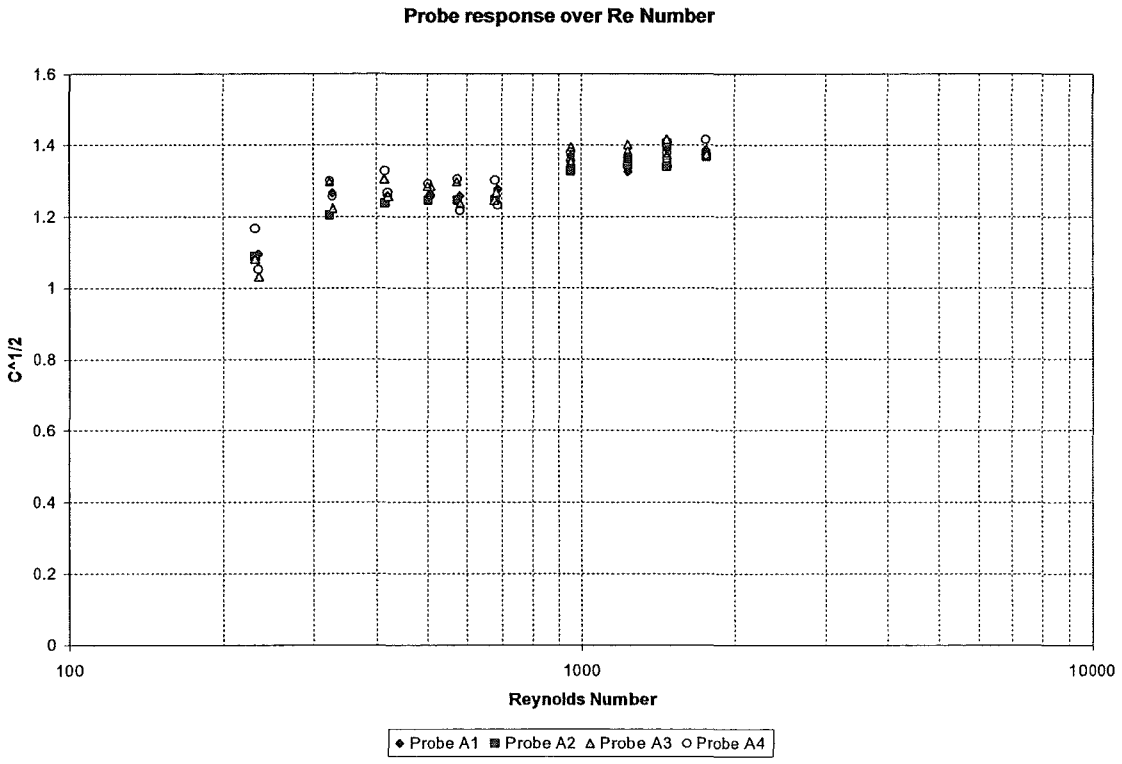

Figure C.8 Probe response versus Reynolds number.

From Figure C.8, the results show that the four probes tested were reasonably consistence with one another. This indicates the type-S pitot tubes can be manufactured consistently. It also shows that the calibration factor is not constant over the entire range of the Reynolds number tested. Hence, separate calibration constants should be used for different regimes, such that for Re<700, C_{calib}=1.59, and for Re>900, C_{calib}=1.90.

C.4.2 Angle testing

Figure C.9 shows the probe responses for the four type-S pitot tubes tested in both directions, forward and reversed, at different flow angles. The response was represented using the velocity ratio defined as the ratio of velocity measured at test angle to the velocity at zero angle, i.e. $v(\theta)/v(\theta=0)$. These angle tests were performed at a flow velocity of 2.85m/s, by setting the pressure differential of the pitot-static tube that monitored the tunnel flow to 0.5mm H_2O. However, the exact flow velocity in each test session for each probe varied slightly subjected to the atmospheric

pressure and temperature change between days of testing. The test velocity for probes A1 and A4 was 2.84m/s; and for probes A2 and A3, the test velocity was 2.85m/s.

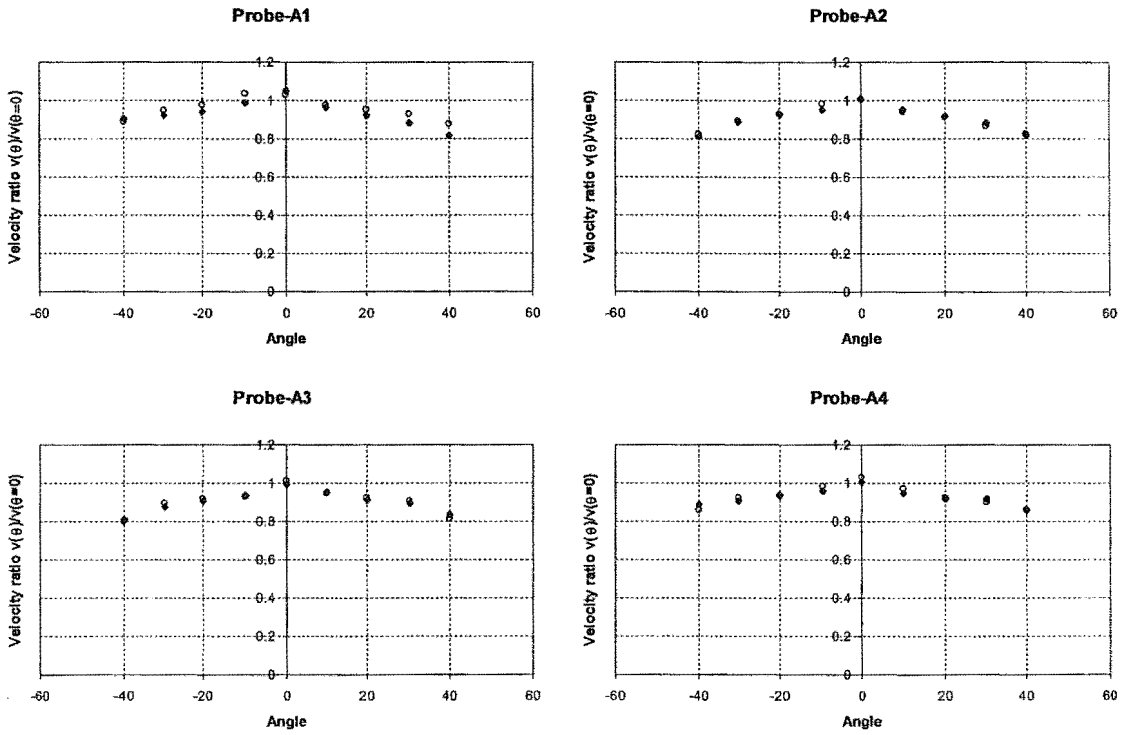

Figure C.9 Angle-test results for type-S pitot tube.

From the Figure C.9, it can be seen that the type-S pitot tubes exhibit a symmetric behaviour. Again, all the four probes tested show consistence responses. The type-S pitot tubes are found to underestimate the flow velocity as the flow angle increased. Within a ±30° flow angle range; the probe underestimates the velocity by approximately 10%. At 40°, the probe could underestimate the flow velocity by up to 20%.

C.5 CONCLUSION

The testing programmes showed that the type-S pitot tube can be manufactured consistently. The type-S pitot tubes were found to have a different response at the low speed regime (Re<700) compared to the high speed regime (Re>900). The calibration factor, C_{calib}, is approximately 1.59 for Re<700 and 1.90 for Re>900. From the angle tests, it was found that, for flow angle ranging from +30° to -30° in the plane normal to the axes of the support tubes, the type-S pitot tube could underestimate the velocity by 10%. However, at a 40° flow angle, the accuracy of the type-S pitot tube deteriorated and it could underestimate the flow velocity by up to 20%.

Appendix D Measuring probe placement

Appendix D presents the locations of the velocity probes at the openings for during the experimental series.

D.1 DOOR VENT

D.1.1 Door 1

Door 1 is a vertical door opening of 450mm high by 250mm wide flush with the floor level.

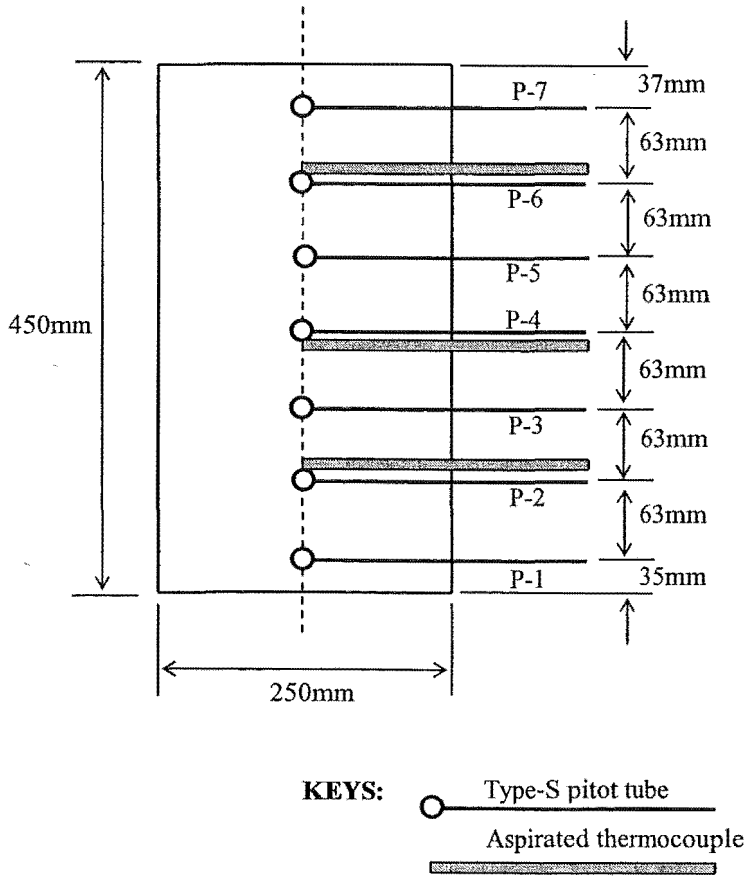

D.1.2 Door 2

Door 2 is a vertical door opening of 250mm high by 250mm wide flush with the floor level.

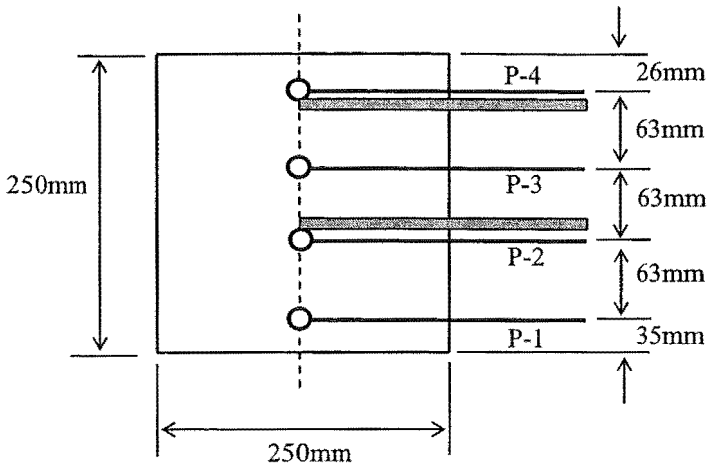

D.1.3 Door 3

Door 3 is a vertical door opening of 125mm high by 250mm wide flush with the floor level.

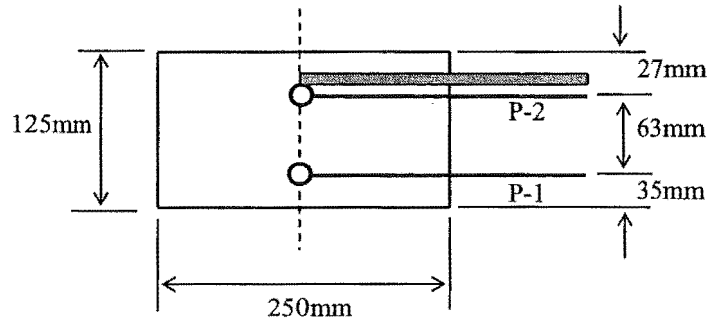

D.2 ROOF VENT

D.2.1 Roof 150mm in diameter

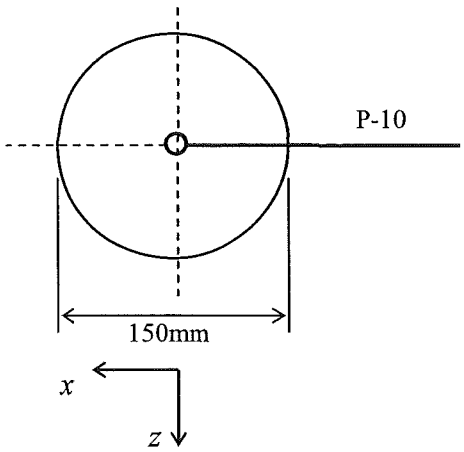

D.2.2 Roof 250mm in diameter

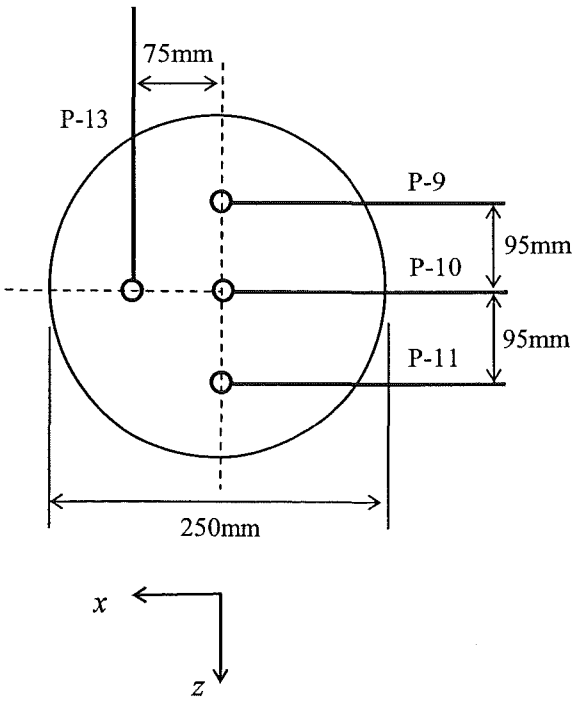

D.2.3 Roof 300mm in diameter

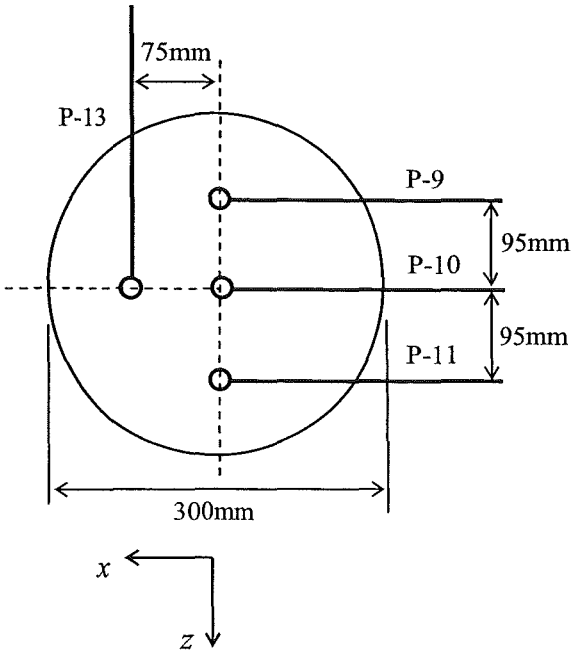

D.2.4 Roof 350mm in diameter

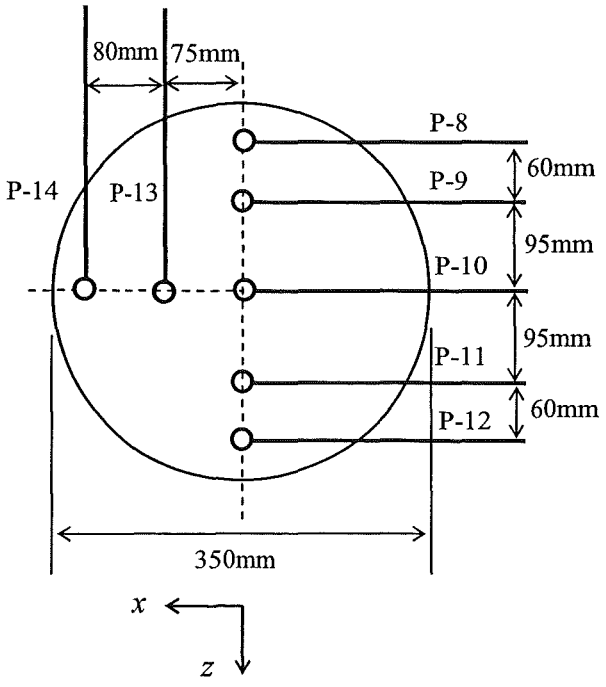

D.2.5 Roof 400mm in diameter

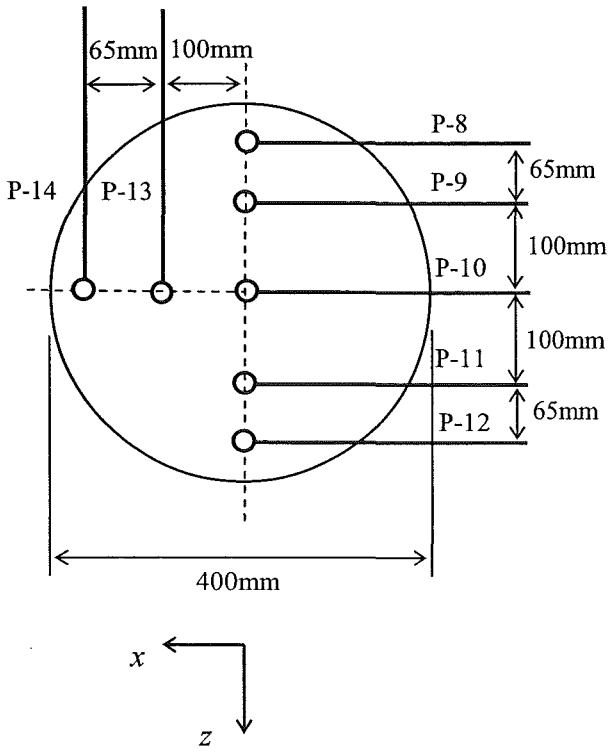

Appendix E Wall heat transfer calculations

Appendix E details the finite difference method used in the CFIRE program for calculating the heat transfer across the enclosure wall.

E.1 INTRODUCTION

The term "wall" refers to the enclosure boundaries that include ceiling, walls and floor. These enclosure boundaries are treated as homogeneous solids with constant thermal properties. The heat transfer across the wall is considered to be one-dimensional. For a finite thickness, assuming no internal heat generation, the transient conduction through the walls is given by Equation (E.1),

$$\frac{\partial^2 T}{\partial x^2} = \frac{1}{\varphi} \cdot \frac{\partial T}{\partial t} \qquad \textbf{(E.1)}$$

where φ is the thermal diffusivity and is defined as

$$\varphi = \left. \frac{k}{\rho \cdot c_p} \right|_{solid}$$

where k is the thermal conductivity, ρ is the density and c_p is the specific heat of the solid.

The second derivative, $\frac{\partial^2 T}{\partial x^2}$, can be written in weighted average form (Croft and Lilley, 1977), as

$$\frac{\partial^2 T}{\partial x^2} = \lambda \cdot \left.\frac{\partial^2 T}{\partial x^2}\right|_{j+1} + (1-\lambda) \cdot \left.\frac{\partial^2 T}{\partial x^2}\right|_{j} \qquad \textbf{(E.2)}$$

where j is the time interval, and λ is the weighting parameter.

Hence Equation (E.1) becomes

$$\frac{\partial^2 T}{\partial x^2} = \lambda \cdot \left.\frac{\partial^2 T}{\partial x^2}\right|_{j+1} + (1-\lambda) \cdot \left.\frac{\partial^2 T}{\partial x^2}\right|_{j} = \frac{1}{\varphi} \cdot \frac{\partial T}{\partial t} \qquad \textbf{(E.3)}$$

E.2 FINITE DIFFERENCE METHOD

The finite difference method is a numerical technique. It has the advantage of implementing complicated boundary conditions that have precluded the use of analytical techniques. The finite difference method solves the temperature at discrete points in the medium of interest. These points are term as *nodes* and the aggregate of nodes is termed as a *nodal network.* The heat transfer through the enclosing boundaries during a fire is considered as one-dimensional. A series of nodes is assigned along the wall thickness forming a nodal network as shown in Figure E.1.

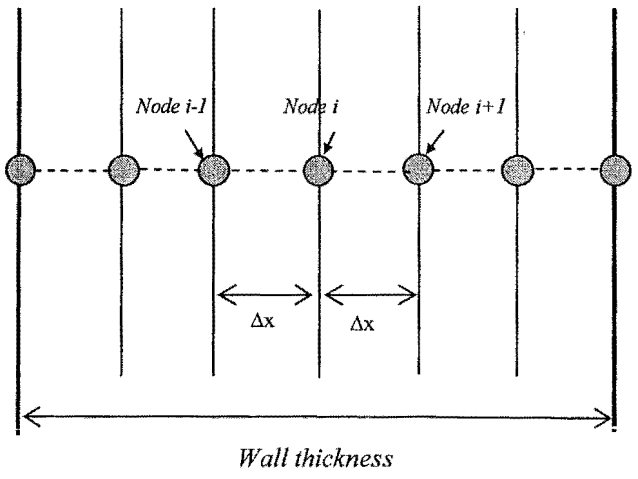

Figure E.1 One-dimensional conduction nodal network

In order to apply the finite difference method to solve the heat transfer through the wall, the derivative terms in the differential equation are replaced by their "finite difference" equivalents. The Central Difference Scheme is used, as it is likely to be the most accurate, being the average of the forward and the backward difference versions (Griffiths and Smith, 1991). The finite difference equations (FDE) for the derivative terms are as follows:

$$\frac{\partial^2 T}{\partial x^2} = \frac{T_{i-1} - 2T_i + T_{i+1}}{(\Delta x)^2} \quad and \quad \frac{\partial T}{\partial t} = \frac{T_{i,j+1} - T_{i,j}}{\Delta t}$$

Substituting these FDEs into Equation (E.3), the governing equation for transient conduction through a solid in finite difference form is given in Equation (E.4).

$$\begin{aligned} &- Fo\lambda \cdot T_{i-1,j+1} + (1 + 2Fo\lambda) \cdot T_{i,j+1} - Fo\lambda \cdot T_{i+1,j+1} \\ &\quad = Fo(1-\lambda) \cdot T_{i-1,j} + [1 - 2Fo(1-\lambda)] \cdot T_{i,j} + Fo(1-\lambda) \cdot T_{i+1,j} \end{aligned} \qquad \textbf{(E.4)}$$

Where Fo is the Fourier number, given as

$$Fo = \frac{\varphi \cdot \Delta t}{(\Delta x)^2} = \frac{k}{\rho c_p} \cdot \frac{\Delta t}{(\Delta x)^2}$$

and the λ is the weighting parameter. Setting λ=0, 1, 0.5 retrieves the explicit, fully implicit and the Crank-Nicolson mid-difference schemes respectively (Croft and Lilley, 1977). In the CFIRE program, the Crank-Nicolson method is used as it has the advantage of numerical stability for all Fourier number or Δt and the least accumulated truncation error for the system. Hence substituting λ=0.5 into Equation (E.4) gives the finite difference equation based on the Crank-Nicolson method.

$$\begin{aligned} &- \frac{Fo}{2} T_{i-1,j+1} + (1 + Fo) T_{i,j+1} - \frac{Fo}{2} T_{i+1,j+1} \\ &\quad = \frac{Fo}{2} T_{i-1,j} + (1 - Fo) T_{i,j} + \frac{Fo}{2} T_{i+1,j} \end{aligned} \qquad \textbf{(E.5)}$$

In the CFIRE program, each wall is divided into 10 slices of equal thickness giving 9 internal nodal points and 2 external boundary nodal points. This is shown in Figure E.2. These nodal points describe the temperature profile of the wall across its thickness. The hot fire gas with temperature T_{gas} ($>T_{amb}$) on the fire side is the source that initiates the heat transfer across the wall.

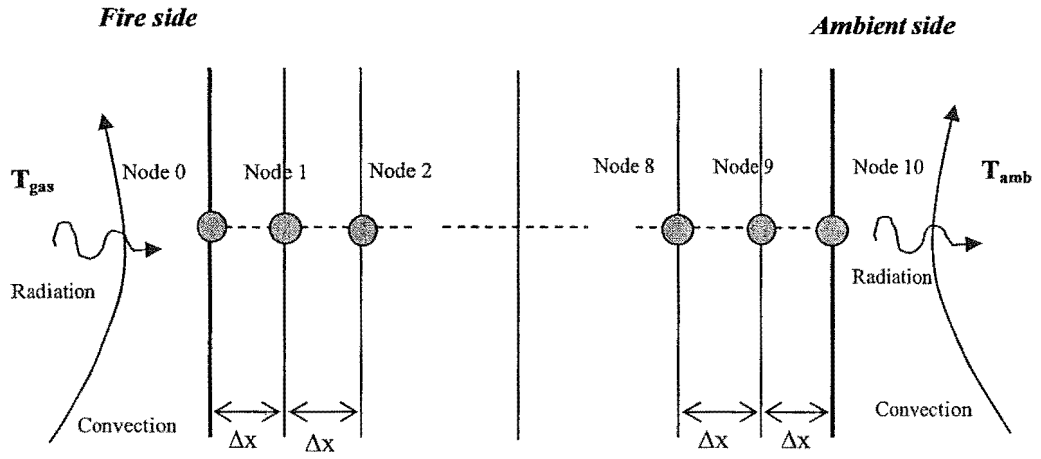

Figure E.2 Temperature nodes along the wall thickness.

E.2.1 Boundary conditions

Equation (E.5) is only applicable for the internal nodes (Node 1 to 9). At the boundaries, the two external nodes (Node 0 and 10) are subjected to both convective and radiative heat transfer. The boundary conditions at these two nodes are given in Equations (E.6) and (E.7) respectively

Fire side (Node 0):

$$-k\left(\frac{\partial T}{\partial x}\right)_{0,j+1} = h_{fire}\cdot\left(T_{gas}-T_{0,j+1}\right)+\sigma\cdot\varepsilon_{res}\cdot\left(T_{gas}^4-T_{0,j+1}^4\right) \qquad \textbf{(E.6)}$$

Ambient side (Node 10):

$$-k\left(\frac{\partial T}{\partial x}\right)_{10,j+1} = h_{amb}\cdot\left(T_{10,j+1}-T_{amb}\right)+\sigma\cdot\varepsilon_{w}\cdot\left(T_{10,j+1}^4-T_{amb}^4\right) \qquad \textbf{(E.7)}$$

where the convective heat transfer coefficient for the fire side, h_{fire}, is taken as 25W/m^{2}K and 10W/m^{2}K for the ambient side, h_{amb}; and ε_{res} is the resultant emissivity between the hot gases and the wall surfaces defined as

$$\varepsilon_{res} = \frac{1}{1/\varepsilon_g + 1/\varepsilon_w - 1} \qquad \textbf{(E.8)}$$

Since the solution involves solving for the wall temperature at time interval j+1, i.e. $T_{0,j+1}$, where it is raised to the fourth power to account for radiation effect, it needs to be linearised before the calculation can proceed. Using the method suggested by Croft and Lilley (1977), taking ϕ=T^4 will generate the approximation

$$\phi \approx \phi_0 + \left.\frac{\partial \phi}{\partial T}\right|_0 \cdot \Delta T$$

so that

$$\begin{aligned} T_{0,j+1}^4 &\approx T_{0,j}^4 + 4T_{0,j}^3\left(T_{0,j+1} - T_{0,j}\right) \\ &= 4T_{0,j}^3 \cdot T_{0,j+1} - 3T_{0,j}^4 \end{aligned} \qquad \textbf{(E.9)}$$

which is linear in $T_{0,j+1}$ and uses the "old" value at node 0, $T_{0,j}$, as a coefficient together with a constant.

The boundary conditions could be accounted by the PDE (Partial Differential Equation) replacement method. Consider the boundary node, 0, and assume there is a fictitious node, F, in front of node 0 spaced Δx apart. The derivative term, $\left(\frac{\partial T}{\partial x}\right)_{0,j+1}$ in Equation (E.6) could be expressed as

$$\left(\frac{\partial T}{\partial x}\right)_{0,j+1} = \frac{T_{1,j+1} - T_{F,j+1}}{2\Delta x} \qquad \textbf{(E.10)}$$

Substituting Equations (E.9) and (E.10) into the boundary condition (Equation (E.6)) gives a temperature expression for the fictitious node F, i.e. $T_{F,j+1}$. This expression is substituted into Equation (E.5) applied on Node 0. This gives the expression for $T_{0,j+1}$, subjected to the convective and radiative boundary conditions shown in Equation (E.11).

$$T_{0,j+1}\cdot\left[\frac{Fo\cdot\Delta x\cdot h_{fire}}{k}+\frac{4Fo\cdot\Delta x\cdot\sigma\cdot\varepsilon_{res}}{k}T_{0,j}^{3}+(1+Fo)\right]+T_{1,j+1}\cdot[-Fo] \qquad \textbf{(E.11)}$$
$$=Fo\cdot T_{1,j}+\frac{Fo\cdot\Delta x\cdot h_{fire}}{k}\cdot(2T_{gas}-T_{0,j})$$
$$+\frac{Fo\cdot\Delta x\cdot\sigma\cdot\varepsilon_{res}}{k}\cdot(2T_{gas}^{4}+2T_{0,j}^{4})+(1-Fo)\cdot T_{0,j}$$

Similarly, for the boundary node, 10, at ambient side

$$T_{9,j+1}\cdot[-Fo]+T_{10,j+1}\cdot\left[\frac{Fo\cdot\Delta x\cdot h_{amb}}{k}+\frac{4Fo\cdot\Delta x\cdot\sigma\cdot\varepsilon}{k}T_{10,j}^{3}+(1+Fo)\right] \qquad \textbf{(E.12)}$$
$$=Fo\cdot T_{9,j}+\frac{Fo\cdot\Delta x\cdot h_{amb}}{k}\cdot(2T_{amb}-T_{10,j})$$
$$+\frac{Fo\cdot\Delta x\cdot\sigma\cdot\varepsilon}{k}\cdot(2T_{amb}^{4}+2T_{10,j}^{4})+(1-Fo)\cdot T_{10,j}$$

By applying Equation (E.5) to each individual internal node (Node 1 to 9), together with Equations (E.11) and (E.12), the temperature of the eleven nodes at the time interval j+1 are solved simultaneously in the form of matrix.

E.2.2 Composite wall

For a composite wall made of two different homogeneous solid materials with a perfect contact at the interface, a finite difference equation at the interface node, I, is needed. Figure E.3 shows schematically the interface node between two slices of different materials with different thickness.

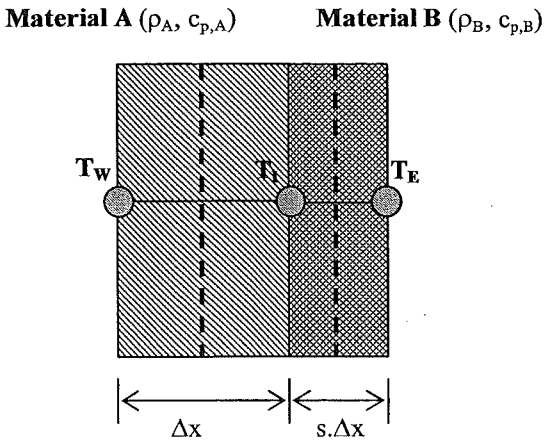

Figure E.3 Interface node T_I

The transient finite difference equation (FDE) at the interface could be obtained by applying energy balance to a control volume about the interface node I, where the energy balance equation is given in Equation (E.13).

$$\dot{E}_{in} + \dot{E}_g = \dot{E}_{store} \qquad \textbf{(E.13)}$$

By assuming heat flow is *into* the node, and there is no internal heat generation,

$$\dot{E}_{in} = Ak_A \frac{(T_W - T_I)}{\Delta x} + Ak_B \frac{(T_E - T_I)}{s \cdot \Delta x}$$

$$\dot{E}_g = 0$$

$$\dot{E}_{store} = A\frac{\Delta x}{2}\left(\rho_A \cdot c_{p,A} + s \cdot \rho_B \cdot c_{p,B}\right)\frac{\Delta T_I}{\Delta t}$$

where A is the area of the wall into the page. Substituting the above expressions into Equation (E.13), gives

$$k_A\left(T_{W,j} - T_{I,j}\right) + \frac{k_B}{s}\left(T_{E,j} - T_{I,j}\right) = G\left(T_{I,j+1} - T_{I,j}\right) \qquad \textbf{(E.14)}$$

where

$$G = \frac{0.5 \times \left(\rho_A \cdot c_{p,A} + s \cdot \rho_B \cdot c_{p,B}\right) \cdot (\Delta x)^2}{\Delta t}$$

The choice of time-level at which the left-hand side in Equation (E.14) is evaluated is such that (Croft and Lilley, 1977)

$$\lambda(value\ at\ t + \Delta t) + (1 - \lambda)(value\ at\ t)$$

To be consistence with the Crank-Nicolson scheme used before, putting λ=0.5 gives

$$\begin{aligned} &0.5k_A\left(T_{W,j+1} - T_{I,j+1}\right) + 0.5\frac{k_B}{s}\left(T_{E,j+1} - T_{I,j+1}\right) \\ &+ 0.5k_A\left(T_{W,j} - T_{I,j}\right) + 0.5\frac{k_B}{s}\left(T_{E,j} - T_{I,j}\right) = G\left(T_{I,j+1} - T_{I,j}\right) \end{aligned} \quad \textbf{(E.15)}$$

or in the form consistent with Equation (E.5), Equation (E.15) is rewritten as

$$\begin{aligned} &0.5k_A T_{W,j+1} - \left[0.5 \cdot \left(k_A + \frac{k_B}{s}\right) + G\right] \cdot T_{I,j+1} + 0.5\frac{k_B}{s} T_{E,j+1} \\ &= -0.5k_A T_W + \left[0.5 \cdot \left(k_A + \frac{k_B}{s}\right) - G\right] \cdot T_I - 0.5\frac{k_B}{s} T_E \end{aligned} \quad \textbf{(E.16)}$$

In the CFIRE program, each of the two composite layers is divided into 10 slices. The solving method is the same as in a single homogeneous solid wall except Equation (E.16) is used for the interface node. The temperatures of the nodes at time interval j+1 are solved simultaneously in the form of matrix.